L'ornementation des os dermiques des pseudosuchiens : morphologie, évolution, fonction

François Clarac

ED 398: Géosciences Ressources Naturelles Environnements Soutenue publiquement le: 15/09/2017

Thèse pour l'obtention du grade de docteur de l'Université Pierre et Marie Curie-Sorbonne Universités

Spécialité: B*iologie de l'*Évolution et Paléontologie

François CLARAC

L'ORNEMENTATION DES OS DERMIQUES DES PSEUDOSUCHIENS: MORPHOLOGIE, EVOLUTION, FONCTION

Directeurs : Jorge Cubo & Vivian de Buffrénil

Melanosuchus niger (Caïman noir)
Pierrelatte, 2015

COMPOSITION DU JURY

- **Dr. Tortsen Scheyer** (Paläontologisches Institut und Museum, Zürich): Rapporteur
- **Dr. Angela Delgado Buscalioni** (Universidad Autonoma de Madrid): Rapporteur
- **Prof. Martin Sander** (Universität Bonn): Examinateur
- **Dr. Alexandra Houssaye** (Muséum National d'Histoire Naturelle): Examinateur
- **Dr. Damien Germain** (Muséum National d'Histoire Naturelle): Examinateur
- **Prof. Loïc Villier** (Université Pierre et Marie Curie): Examinateur
- **Prof. Armand de Ricqlès** (Université Pierre et Marie Curie): Invité
- **Dr. Vivian de Buffrénil** (Muséum National d'Histoire Naturelle): Directeur
- **Prof. Jorge Cubo** (Université Pierre et Marie Curie): Directeur

UMR 7193: Institut des Sciences de la Terre de Paris
Équipe: Biominéralisation et environnements sédimentaires

UMR 7207: Centre de Recherche sur la Paléobiodiversité et les Paléoenvironnements
Équipe: Formes et fonctions

REMERCIEMENTS

"It ain't about how hard you hit but about how hard you can get hit and keep moving forward… how much you can take and keep moving forward. That's how winning is done"

Sylvester Stallone (Rocky Balboa, 2006)

Mes premiers remerciements s'adressent sans détour à mes deux directeurs de thèse: Vivian de Buffrénil qui m'a encadré continuellement depuis mon stage de Master 1 et Jorge Cubo qui a pris en main la direction cette thèse au sein de l'Université Pierre et Marie Curie. Je remercie chaleureusement Nicolas Rabet et Fabienne Audebert qui m'ont permis de découvrir le milieu de la recherche en acceptant de m'encadrer en tant que stagiaire volontaire au cours ma licence de biologie à l'UPMC. Mes pensées se dirigent également envers les collaborateurs qui sont intervenus au cours de mon stage de Master 2 puis pendant ma thèse et qui m'ont ainsi permis de progresser par leur important apport technique et pédagogique: Thibaud Souter et Raphaël Cornette (plateforme de morphométrie), Vittorio Sansalone (Laboratoire Modélisation et Simulation Multi Echelle, UPEC Paris 12) et Florent Goussard (responsable de la plateforme 3D du CR2P). Je remercie également les chargés de collections et les directeurs de parc zoologiques qui m'ont permis d'accéder aux spécimens requis à la réalisation de mon travail: Salvador Bailon (collections d'anatomie comparée, MNHN), Ronan Allain, Noureddine Jalil, Gaël Clément, Damien Germain, Jean-Sébastien Steyer (collections de paléontologie, MNHN), Philippe Béarez (collection d' archéozoologie, MNHN), Carl Mehling, Mark Norell (collections de Paléontologie, AMNH), Michael Brett-Surman (collections de paléontologie, Smithsonian Institution), Jeremy F. Jacobs (collections d'anatomie comparée, Smithsonian Institution), Samuel Martin (directeur de la Ferme aux Crocodiles) et bien sûr Fabrice Thete (directeur de la Planète des Crocodiles) pour qui mes pensées les plus sincères s'adressent directement à ses proches. J'adresse un grand remerciement à Alexandra Quilhac pour son énorme investissement dans mon travail d'analyse histologique ainsi que pour sa participation active aux prélèvements sur des spécimens vivants. Au même titre, en vue des risques que représente la manipulation de crocodiliens adultes, je remercie également les employés de la Planète des Crocodiles (Geoffrey Fomel et Cédric Goetgheluck) qui m'ont apporté leur aide pour la capture des caïmans dans leur enclos. De même, je salue chaleureusement Hayat Lamrous et Marie-Claire Lajarille pour leur intervention capitale dans la réalisation des coupes histologiques. Évidemment, je n'oublie pas mes différents recruteurs et responsables de formation qui m'ont permis d'accéder aux différentes étapes de mon parcours: Régine Vigne-Lebbe, Véronique Barriel, Pascal Tassy, François Baudin et le comité de l'école doctorale 398. Je remercie également les membres de mon jury de thèse pour leur présence et leur travail d'évaluation. J'adresse également un clin d'œil à l'ensemble de mes collègues de l'UMR pour les moments de convivialité passés ensembles; sans oublier le groupe du "baby" et les « FT ». Enfin, je remercie mes différents entraineurs de boxe (et autres disciplines pugilistiques): Jean-Louis Annaloro, Tahar Mahtallah, Cyrille Parzy, Wilfrid Hembert et Didier Guillon dont l'enseignement m'a permis de remporter le championnat de France universitaire de Kickboxing quelques mois avant de rendre ce présent manuscrit.

SOMMAIRE

INTRODUCTION

Les os dermiques des vertébrés proviennent d'une ossification membranaire ayant lieu au cours des stades embryonnaires à l'image de la formation du toit crânien (Morriss-Kay, 2001; Abzhanov, 2007) ou lors des premiers stades post-embryonnaires à l'image de la mise en place des ostéodermes chez les crocodiliens (Gilbert et al., 2001; Vickaryous and Hall, 2008; Vickaryous and Sire, 2009). Ces os disposent souvent d'une structure en diploë qui se caractérise par la superposition successive de trois couches: une couche basale constituée d'os compact (souvent lamellaire), une couche intermédiaire composée d'os spongieux qui présente souvent du remaniement (résorption puis dépôt secondaire; remaniement haversien), une couche apicale composée à nouveaux d'os compact (souvent à fibres parallèles). Au sein de nombreux groupes de vertébrés comme les placodermes (Downs and Donoghue, 2009), squamates (Zylberberg et Castanet, 1985), « tétrapodomorphes ichtyens » (Zylberberg et al, 2010), cette strate apicale peut présenter une ornementation qui se définit par la présence d'un motif répété à la surface du cortex externe. Ces motifs peuvent avoir une forme tuberculaire ou vermiculaire mais ils présentent le plus souvent un réseau de cupules et de sillons séparés par des crêtes (Bystrow, 1947; Witzman, 2009). Ce dernier cas de figure est notamment observable chez les « stégocéphales » et les pseudosuchiens (Fig. 1). Cependant, au sein de ces deux derniers groupes, l'ornementation se met en place via deux mécanismes histologiques distincts: une croissance par apposition préférentielle formant un relief vallonné comme chez les « stégocéphales » ou de la résorption superficielle excavant les cupules comme chez les pseudosuchiens (Buffrénil, 1982; Buffrénil et al., 2015; Buffrénil et al., 2016; Fig. 2). Ces deux différents mécanismes conduisent donc le développement de l'ornementation qui évolue au cours de l'ontogénie chez ces deux groupes de vertébrés à croissance cyclique et continue (Hutton, 1986 ; Steyer et al, 2004). Chez les « stégocéphales », les strates entre les lignes d'arrêt de croissance du cortex externe sont déposées suivant une apposition différentielle homothétique ou non-homothétique dans le cas où la croissance varie de façon relative au sein de la couche apicale. Chez les pseudosuchiens, les cupules se creusent par résorption puis sont partiellement ou complètement comblées par un dépôt osseux secondaire tout en subissant parallèlement une dérive liée à des mécanismes de croissance transversale ou longitudinale. Les deux processus qui permettent la mise en place de l'ornementation (résorption puis dépôt secondaire ou croissance par apposition différentielle) étant différents au sein de ces deux taxons phylogénétiquement séparés, il est de ce fait évident que l'ornementation est un caractère homoplasique.

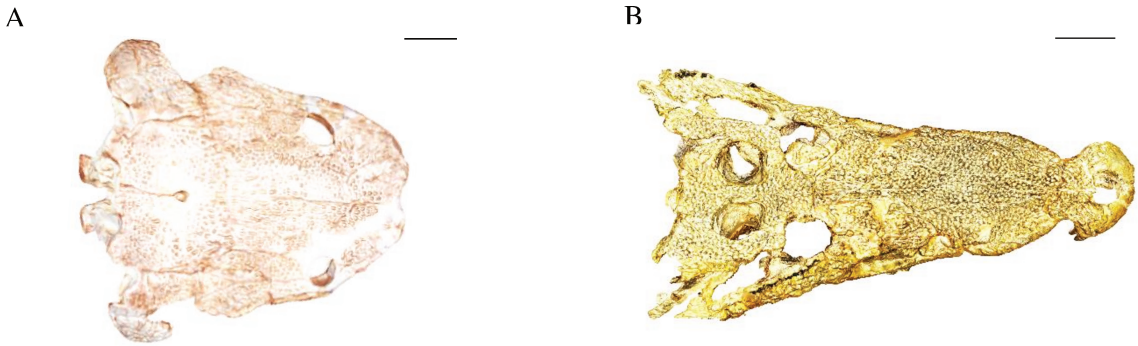

Figure 1. A: vue dorsale d'un crâne de Metoposaurus azerouali (Scan surfacique 3D; temnospondyle du Trias, Bassin d'Argana, Maroc). Barre d'échelle: 7cm. B: vue dorsale d'un crâne d'Amphicotylus lucasii (Reconstruction par photogrammétrie; crocodyliforme du Jurassique inférieur, Colorado, Etats-Unis). Barre d'échelle: 5cm.

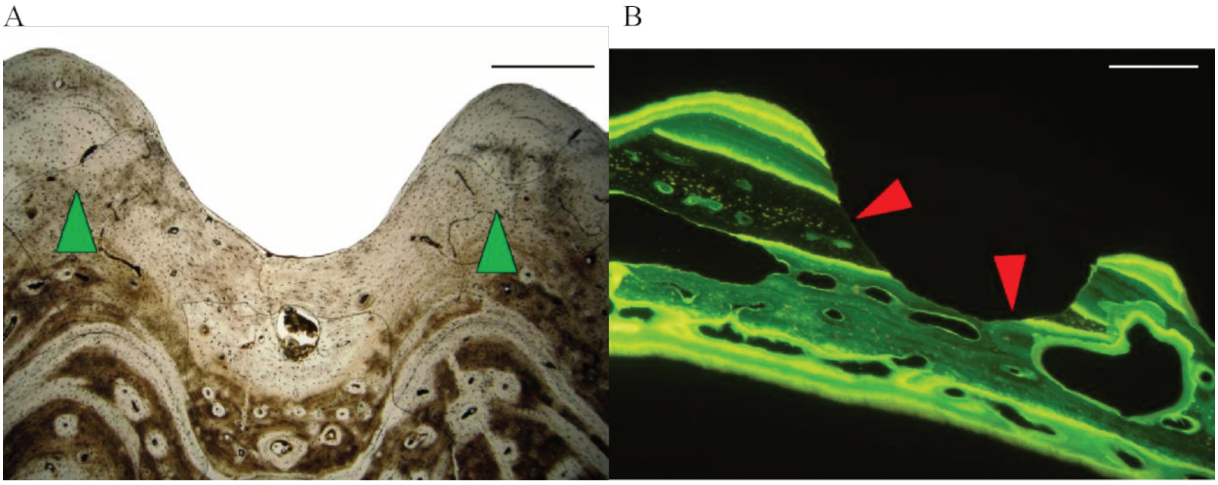

Figure 2. A: Coupe d'os dermique crânien de Plagiosternum sp. (Temnospondyli; Trias moyen) observé au microscope photonique. Flèches vertes: croissance par apposition différentielle. Barre d'échelle: 5 mm. B: Coupe d'ostéoderme dorsal de Caiman crocodilus (Alligatoridae; actuel) observé au microscope sous lampe à UV après marquage in vivo. Flèches rouges: activité de résorption. Barre d'échelle: 6 mm.

Malgré la différence dans l'histogénèse de l'ornementation entre « stégocéphales » et pseudosuchiens, on observe dans les deux cas des pertuis vasculaires au fond des cupules qui relient l'espace intra osseux et la superficie de l'os (Fig. 3). Cette caractéristique commune dénote donc l'existence d'un réseau vasculaire péri-osseux qui serait mis en relation avec un réseau vasculaire intra-osseux lui-même relié à la circulation sanguine générale via des canaux qui traversent la couche basale de l'os (foramens; Witzmann et al., 2010). La convergence de caractéristiques morphologiques composant l'ornementation au travers de différentes lignées évolutives tels que le réseau de cupules et sillons traversé de canaux ont par conséquent amené divers auteurs à émettre des hypothèses visant à expliquer un possible rôle fonctionnel. Ces implications hypothétiques concernent notamment les transferts de chaleur chez les vertébrés ectothermes (Seidel, 1979; Farlow et al., 2010) ou l'augmentation de la résistance mécanique osseuse (Coldiron,1974).

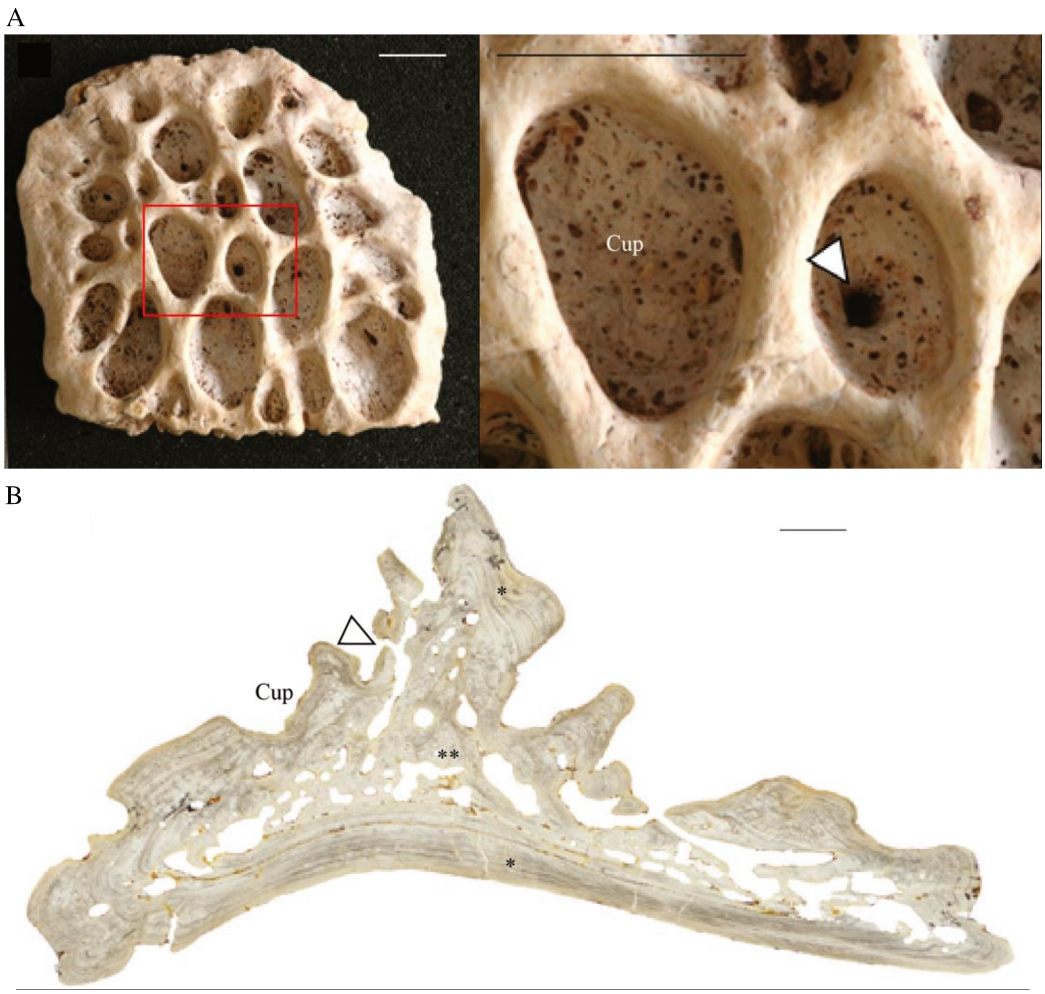

Figure 3. A: Plan rapproché sur l'ornementation d'un ostéoderme de Sarcosuchus imperator (Pholidosauridae, Cretacé inférieur). Barre d'échelle: 1cm. Cup: Cupule. La flèche blanche pointe un canal centro-cupulaire. B: Coupe histologique d'un ostéoderme de Diplocynodon remensis (Alligatoroidea, Paleocène supérieur); * os compact à fibres parallèles; ** Os spongieux; Cup: cupule; La flèche blanche pointe un canal centro-cupulaire. Barre d'échelle: 8mm.

Sachant qu'aucune de ces hypothèses n'est appuyée par des arguments avérés, le but de cette thèse est donc de les tester en se focalisant sur l'étude d'un groupe encore représenté dans la nature actuelle: les pseudosuchiens. Pour cela, il a tout d'abord été nécessaire de développer une méthode permettant de quantifier l'ornementation afin de l'appliquer a posteriori sur un échantillon représentatif de la diversité écologique et phylogénétique des pseudosuchiens depuis le Trias (250Ma; Fig. 4). Le suivi de l'expression de ce caractère sur l'ensemble de la lignée me permettra, grâce à des analyses phylogénétiques comparées, de discuter les patrons d'expression de l'ornementation au travers de l'évolution des différents modes de vie des pseudosuchiens. Ainsi, je testerai l'influence de la phylogénie sur l'expression de l'ornementation des os dermiques pseudosuchiens afin d'extraire cette composante a posteriori pour tester la corrélation entre le degré d'expression de l'ornementation osseuse et le mode de vie adopté par les pseudosuchiens au cours de l'évolution (terrestre, amphibie, pélagique; Fig.

4). D'autre part, l'utilisation de techniques de morphométrie géométrique appliquées à la morphologie crânienne m'amènera à illustrer l'existence de contraintes développementales qui tempèrent l'expression de l'ornementation au niveau crânien. Ainsi ayant défini le contexte d'expression de l'ornementation osseuse chez les pseudosuchiens, dans la seconde partie de ma thèse, je chercherai à définir les implications morpho-fonctionnelles liées à son développement grâce des simulations se basant sur la modélisation 3D d'ostéodermes ornementés (analyses en éléments finis). Ces analyses viseront à quantifier l'influence de l'ornementation sur les propriétés mécaniques et thermiques des os dermiques des pseudosuchiens. Enfin, dans l'objectif de pouvoir mettre en évidence les possibles implications physiologiques de l'ornementation osseuse (transferts de chaleur, Seidel, 1979, Farlow et al., 2010; tampon de l'acidité sanguine en phase anoxique; Jackson et al., 2003 Janis et al., 2012), j'identifierai la circulation sanguine intra-osseuse et péri-osseuse des ostéodermes grâce à des prélèvements in vivo combinés à des techniques de marquage histologique.

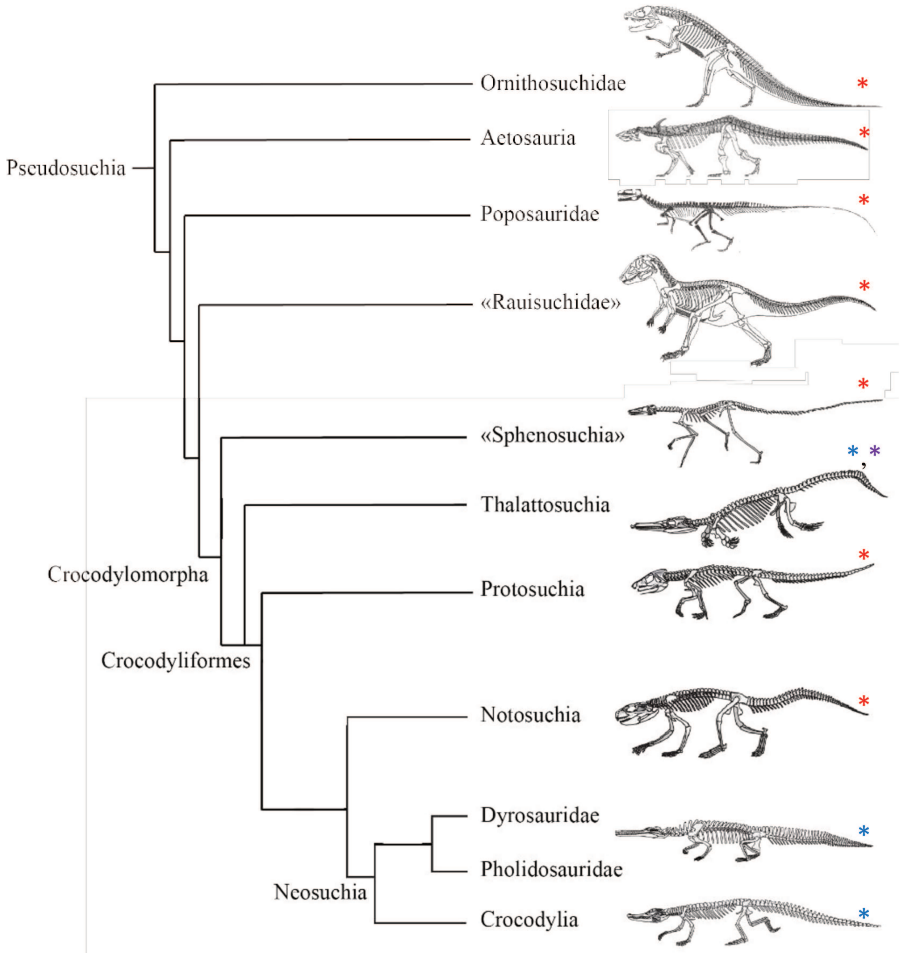

Figure 4. Phylogénie des pseudosuchiens, d'après Nesbitt (2011) et Wilberg (2015);

Reconstitutions: Crocodylomorpha, d'après Wilberg (2012); « Rauisuchidae », d'après Chatterjee (1985); Poposauridae, d'après Gauthier et al.(2011); Aetosauria d'après Parker (2008), Ornithosuchidae d'après Walker (1964).

*: mode de vie terrestre
*: mode de vie amphibie
*: mode de vie pélagique

Références

Abzhanov A, Rodda SJ, McMahon AP, Tabin CJ. 2007. Regulation of skeletogenic differentiation in cranial dermal bone. Development 134: 3133-3144.

Buffrénil Vde. 1982. Morphogenesis of bone ornamentation in extant and extinct crocodilians. Zoomorphology 99: 155–166.

Buffrénil Vde, Clarac F, Fau M, Martin S, Martin B, Pellé E, Laurin M. 2015. Differentiation and growth of bone ornamentation in vertebrates: A comparative histological study among the Crocodylomorpha. J Morphol 21: 1–21. (Article en annexe).

Buffrénil Vde, Clarac F, Canoville A, Laurin M. 2016. Comparative data on the differentiation and growth of bone ornamentation in Gnathostomes (Chordata: Vertebrata). J Morphol 277: 634-670. (Article en annexe).

Bystrow A. 1947. Hydrophilous and Xerophilous Labyrinthodonts. Acta Zool 28: 137–164.

Chatterjee S. 1985. Postosuchus, a new thecodontian reptile from the Triassic of Texas and the origin of tyrannosaurs. Philos Trans R Soc London Ser B 309: 395–460.

Coldiron RW. 1974. Possible function of ornament in labyrinthodont amphibians. Occ Pap Mus Nat Hist Univ Kansas 33: 1-19.

Downs JP, Donoghue PCJ. 2009. Skeletal histology of Bothriolepis canadensis (Placodermi, Antiarchi) and evolution of the skeleton at the origin of jawed vertebrates. J Morphol 270: 1364–1380.

Farlow JO, Hayashi S, Tattersall GJ. 2010. Internal vascularity of the dermal plates of Stegosaurus (Ornithischia, Thyreophora). Swiss J Geosci 103: 173–185.

Gauthier JA, Nesbitt SJ, Schachner ER, Bever GS, Joyce WG. 2011 The bipedal stem crocodilian Poposaurus gracilis: Inferring function in fossils and innovation in archosaur locomotion. Bull Peab Mus of Nat Hist 52(1): 107-126

Gilbert SF, Loredo GA, Brukman A, Burke AC. 2001. Morphogenesis of the turtle shell : the development of a novel structure in tetrapod evolution. Evol Dev 3: 47–58.

Hutton JM. 1986. Age Determination of living Nile crocodiles from the cortical stratification of bone. Copeia 2: 332-341.

Jackson DC, Andrade D, Abe AS. 2003. Lactate sequestration by osteoderms of the broad-nose caiman, Caiman latirostris, following capture and forced submergence. J Exp Biol 206: 3601–3606.

Janis CM, Devlin K, Warren DE, Witzmann F. 2012. Dermal bone in early tetrapods: A palaeophysiological hypothesis of adaptation for terrestrial acidosis. Proc Biol Sci 279:3035–3040.

Morriss-Kay GM. 2001. Derivation of the mammalian skull vault. J Anat 199: 143-151.

Nesbitt SJ. 2011. The early evolution of archosaurs: relationships and the origin of major clades. Bull Am Mus Nat Hist 352: 1–292.

Parker WG. 2008. Description of new material of the aetosaur Desmatosuchus spurensis (Archosauria: Suchia) from the Chinle Formation of Arizona and a revision of the genus Desmatosuchus. PaleoBios 28: 281–40.

Seidel MR. 1979. The osteoderms of the American alligator and their functional significance. Herpetol'Leag 35: 375-380.

Steyer JS, Laurin M, Castanet J, Ricqlès Ade. 2004. First histological and skeletochronological data on temnospondyl growth: palaeoecological and palaeoclimatological implications. Palaeogeogr Palaeoclimatol Palaeoecol 206: 193–201.

Vickaryous MK, Hall BK. 2008. Development of the dermal skeleton in Alligator mississippiensis (Archosauria, Crocodylia) with comments on the homology of osteoderms. J Morphol 269: 398-422.

Vickaryous MK, Sire JY. 2009. The integumentary skeleton of tetrapods: origin, evolution and development. J Anat 214: 441–464.

Walker AD. 1964. Triassic reptiles from the elgin area: Ornithosuchus and the origin of carnosaurs. Philos Trans R Soc London Ser B 248: 54-134

Wilberg EW. 2015. What's in an outgroup? The impact of outgroup choice on the phylogenetic position of Thalattosuchia (Crocodylomorpha) and the origin of Crocodyliformes. Sys Biol 64: 621–637.

Witzman F. 2009. Comparative histology of sculptured dermal bones in basal tetrapods, and the implications for the soft tissue dermis. Palaeodiversity 2: 233–270.

Witzmann F, Scholz H, Müller J, Kardjilov N. 2010. Sculpture and vascularization of dermal bones, and the implications for the physiology of basal tetrapods. Zool J Linn Soc 160: 302–340.

Young GC. 2009. An Ordovician vertebrate from western New South Wales, with comments on Cambro-Ordovician vertebrate distribution patterns. Alcheringa 33: 79–89.

Zylberberg L, Castanet J. 1985. New data on the structure and the growth of the osteoderms in the reptile Anguis fragilis (Anguidae, Squamata). J Morphol 186: 327–342.

Zylberberg L, Meunier FJ, Laurin M. 2010. A microanatomical and histological study of the postcranial dermal skeleton in the Devonian sarcopterygian Eusthenopteron foordi. Acta Palaeont Pol 55: 459–470.

PARTIE 1: PATRONS D'EXPRESSION DE L'ORNEMENTATION OSSEUSE CHEZ LES PSEUDOSUCHIENS.

Protosuchus richardsoni (Jurassique inférieur)

Sebecus icaeorhinus (Eocène)

Voay robustus (Quaternaire)

Diplocynodon hantoniensis (Paléogène)

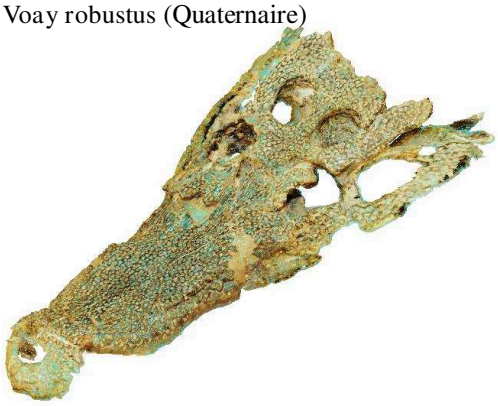

Amphicotylus lucasii (Jurassique inférieur)

Sarcosuchus imperator (Crétacé inférieur)

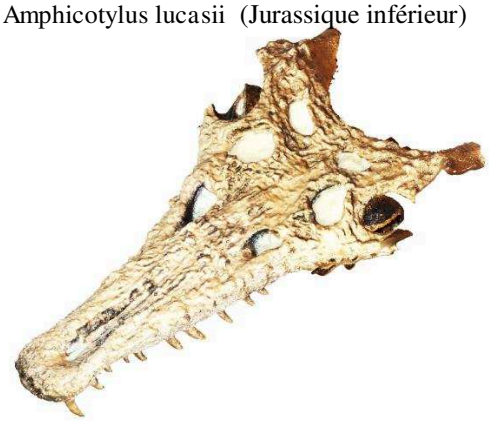

Proterochampsa barrionuevoi (Trias supérieur)

Araripesuchus wegeneri (Crétacé inférieur)

CHAPITRE 1: QUANTIFICATION DE L'ORNEMENTATION OSSEUSE CHEZ LES CROCODILIENS

Caiman yacare

(Espèce actuelle, Amérique du sud, reconstruction surfacique 3D par photogrammétrie)

A Quantitative Assessment of Bone Area Increase Due to Ornamentation in the Crocodylia

François Clarac,[1,2,3]* Thibaud Souter,[4] Raphaël Cornette,[5] Jorge Cubo,[1,2] and Vivian de Buffrénil[3]

[1]*Sorbonne Universités, Université Pierre et Marie Curie (UPMC), UPMC Univ Paris 06, UMR 7193, Institut Des Sciences De La Terre Paris (ISTeP), 4 Place Jussieu, BC 19, Paris F-75005, France*
[2]*CNRS, UMR 7193, Institut Des Sciences De La Terre Paris (ISTeP), 4 Place Jussieu, BC 19, Paris F-75005, France*
[3]*Département Histoire De La Terre, Museum National D'histoire Naturelle, UMR 7207 (CR2P), Sorbonne Universités, Muséum National d'Histoire Naturelle (MNHN)/CNRS/UPMC, Bâtiment De Géologie Paris Cedex 05 F-75231, France*
[4]*Plateforme De Morphométrie Du MNHN -UMS 2700 Outils Et Méthodes De La Systématique Intégrative, 55 Rue Buffon, Paris 75005, France*
[5]*Institut De Systématique, Evolution, Biodiversité, ISYEB, UMR 7205, CNRS, MNHN, UPMC, EPHE, Muséum National D'histoire Naturelle, Sorbonne Universités, 57 Rue Cuvier 75005 Paris, France*

ABSTRACT Bone ornamentation, in the form of highly repetitive motives created by pits and ridges, is a frequent feature on vertebrate skull roofs and osteoderms. The functional significance of this character remains a matter of controversy and speculation. The many diverging hypotheses proposed to explain it all share a common logical prerequisite: bone ornamentation should increase significantly the surface area of the bones that bear it. In order to test this assumption in the Crocodylia, we developed a method for quantifying the gain in area due to ornamentation using a three-dimensional-surface scanner. On crocodylian osteoderms, the gain in area can be up to 40%, and on the cranial table, it ranges between 10 and 32% in adult specimens (in both cases, it shows substantial differences between the adults of the various species included in the sample). Area gain on the snout is lesser (0–20% in adults), and more variable between species. In general, bone ornamentation is less pronounced, and results in fewer area gains in juvenile specimens. The main morphometric results yielded by this study are discussed in reference to the few comparative data available hitherto, and to the functional interpretations proposed by previous authors. J. Morphol. 276:1183–1192, 2015. © 2015 Wiley Periodicals, Inc.

KEY WORDS: thermoregulation; osteoderms; dermal bones; pits; gain in area

INTRODUCTION

Bone ornamentation, also referred to as bone sculpture, frequently occurs on dermal bones in many vertebrate taxa, especially those having an aquatic or amphibious lifestyle (Downs and Donoghue, 2009; Witzmann et al., 2010;). The most common (though nonunique) form of bone ornamentation consists of pits and interconnected ridges that are distinguishable from « simple » vascular imprints because they occur only on the outer surface of the bones, and tend to constitute a highly repetitive, nonrandom geometrical pattern. The Crocodylia (Buffrénil, 1982), together with several temnospondyls (Bystrow, 1935; Witzmann and Soler-Gijon, 2010), turtles (Scheyer et al., 2007) or actinopterygians (Lundberg and Aguilera, 2003), are typical examples of the pit and ridge form of bone ornamentation. However, despite its frequency, the functional significance of this feature is poorly understood. Several hypotheses have been proposed to answer that question: better resistance to mechanical stress (Coldiron, 1974); augmenting bone-dermis contact and thus improving skin anchorage (Romer, 1947; Witzmann et al., 2010); facilitating cutaneous respiration (Bystrow, 1947); increasing basking efficiency in ectothermic vertebrates (Seidel, 1979), or contributing to buffer respiratory acidosis in early land-dwelling vertebrates and, more generally, semiaquatic tetrapods (Janis et al., 2012). The last two hypotheses are supported by the occurrence of a rich vascular supply topographically related to bone ornamentation (Witzmann et al., 2010). All these interpretations have at least one common point: they implicitly rely on the assumption that bone ornamentation increases the area available to skin anchorage or to gas or heat exchanges of the body with the environment. A recent study by Rinehart and Lucas (2013) addressed this question in temnospondyls

Contract grant sponsor: Sorbonne Université (Doctoral fellowship).

*Correspondence to: F. Clarac; Département Histoire de la Terre, Museum National d'Histoire Naturelle, UMR 7207 (CR2P), Bâtiment de Géologie Paris Cedex 05 F-75231, France.
E-mail: fclarac@mnhn.fr

Received 6 March 2015; Revised 16 April 2015;
Accepted 30 April 2015.

Published online 30 June 2015 in
Wiley Online Library (wileyonlinelibrary.com).
DOI 10.1002/jmor.20408

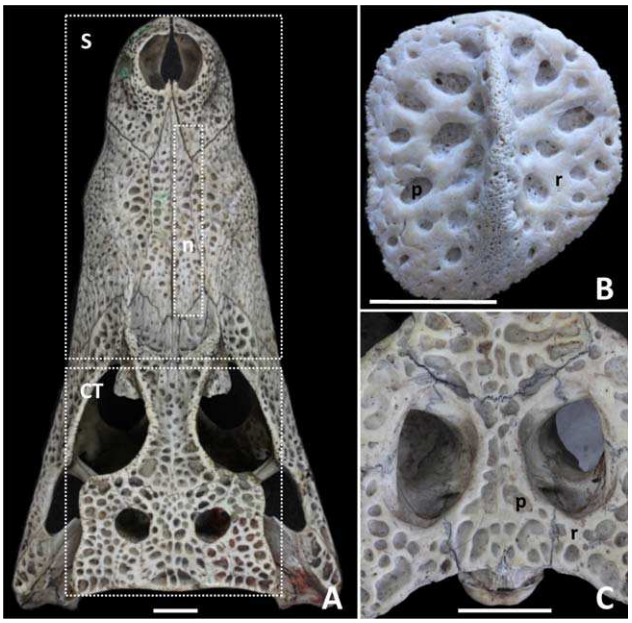

Fig. 1. Bone ornamentation on crocodylian skull and osteoderm. (**A**) General aspect of bone ornamentation on the CT and snout (S) of *C. crocodilus* skull 1. Scale bar: 16 mm. (**B**) Dorsal osteoderm of *C. acutus* (MNHN 1870-500; absent in our sample), letters "p" and "r," respectively, indicate a "pit" and a "ridge." Scale bar: 12.5 mm. (**C**) Cranial table of *C. acutus* (subadult), same abbreviations as (B). Scale bar: 25 mm. [Color figure can be viewed in the online issue, which is available at wileyonlinelibrary.com.]

with a relatively simple approach based on area assessments from bidimensional sections through bone reliefs. This study revealed that the area increase due to ornamentation is "relatively small" (ca. 10–20%). Until now, no attempt at quantifying this possible gain in area has been performed on the dermal skeleton of the Crocodylia, the vertebrate taxon that displays the most extensive and well-characterized ornamentation. The present study is aimed at performing such quantifications using a three-dimensional (3D) approach.

MATERIAL AND METHODS

Biological Material

The sample comprises clean, fat free dry calvaria, and osteoderms (Fig. 1) from 14 extant and 4 extinct crocodylian taxa belonging to the Neosuchia clade (sensu Bronzati et al., 2012; Table 1). Extant taxa represent all three living families (i.e., Crocodylidae, Alligatoridae, and Gavialidae; Fig. 2), all genera except *Tomistoma*, and two thirds of the species that compose the Crocodylia today. Of course, the four extinct taxa do not pretend to span the very rich fossil record of the Crocodylomorpha, but simply to show that the methods used for extant samples are also applicable to extinct ones. In addition to taxonomic diversity, this sample also displays ontogenetic variation, and includes juveniles, subadults and adults for various species. These three stages are not distinguishable in osteoderms, therefore, only two categories, juvenile and adult, are considered for them. For the detailed study of the influence of ornamentation characteristics on superficial bone area, two anatomical regions per calvarium were studied: the cranial table (CT), a region representing most of the postorbital part of the crocodylian skull, and the right nasal bone, that is considered here to represent the snout, that is the preorbital region (Fig. 1). The skull table is quite similar from one specimen to another whereas the nasal displays a fairly broad diversity in ornamental pattern related to ontogenetic growth stages and specific skull morphology (Iordansky, 1973; Langston, 1973).

Data Acquisition

The general methodological approach used in this study for quantifying the gain in area due to ornamentation basically involves measuring the real area, RA, of the ornamented surface of bones with all its deep (pits) and protruding reliefs (ridges), and compare it to a theoretical smooth area, SA, that would exist in the absence of ornamentation. This basic comparison reveals a gain in area, GA, attributable to ornamentation. It was conducted at two complementary levels: i) the level of the total ornamented face of bones (or CT). This level is designated by the suffix "tot" in measurements or indices; ii) the level of the pits themselves (the essential element of bone ornamentation in crocodylians) designated by the suffix "pit." Crocodylian ornamentation is mainly due to pit excavation (by resorption), the ridges being just a remnant of the original surface of the bones (Buffrénil, 1982; Buffrénil et al., 2014).

To this purpose, all sampled specimens were scanned with a Breuckmann StereoScan^{3D-} surface scanner, a device that reconstructs 3D topography using phase contrast. In brief, the surface of the bones is virtually reconstructed as a meshwork composed of polygons united by their edges, and folded according to bone reliefs inside a 3D environment. We used three scope ranges, depending on sample size, to obtain adequate mesh resolutions: small scope range (60 mm), resolution: 12 μm; medium scope range (250 mm), resolution: 18 μm; large scope range (720 mm), resolution: 22 μm. The 29 3D-objects thus obtained were exported in PLY-format. Imperfections of the mesh (noise, artefacts, self-interactions, etc.), when present, were corrected using Geomagic Studio 2012* cleaning tools (*Geomagic Worldwide Headquarters 430 Davis drive, Marisville, NC). At this initial stage, one important parameter was measured: the real area of the total bone surface, RAtot in mm^2, as defined above.

The bone surface was then made smooth. To this purpose, the polygons composing each pit were manually selected along the crest edges that define it, and suppressed. The resulting mesh was then only composed of the crest of which we could measure the area (CrA; Fig. 3A,B). After pit erasure, the openings generated inside the mesh were filled one by one, using dedicated tools for 3D-filling. Among the different options, which consider the orientation of the mesh surrounding the opening, the option generating the flattest surface was systematically selected (Fig. 3C). Finally, a noise reduction filter was applied on the entire resulting object (Fig. 3D) in order to suppress local geometrical kinks and smooth the mesh on the object. One more parameter was measured after the smoothing operation: SAtot in mm^2. At this stage, two descriptive parameters were derived from RAtot, SAtot and the area of the crests (CrA): the surface of the pits themselves, or RApit, that corresponds to the area of the walls and bottoms of the whole set of pits on the ornamented surface: RApit = RAtot–SAtot. We obtained the area of the pits in projection on the smooth surface of the bone (SApit) through the following operation: SApit = SAtot–CrA.

Quantifying the Gain in Area

The basic morphometrical parameters mentioned above allow the computation of the index, GAtot in %, that expresses the gain in area on the total ornamented surface of a bone or on a cranial region: GAtot = 100 (RApit/SAtot). This index was computed independently for the osteoderms ($GAtot_o$), the CT ($GAtot_t$), and the right nasal bone ($GAtot_n$).

Two additional indices were then established: i) the relative area of the whole set of pits (in projection on the smooth surface), as compared to the whole smooth area of a bone, OA_{relat}. This index is given by the equation: OA_{relat} = SApit/SAtot; ii)

*TABLE 1. Taxonomic description of our sample; the numbers (1; 2; 3) are referred in the text and in the figures when it is needed to designate one specific specimen among the same species. For reasons of clarity "C. crocodilus skull (1)" will be mentioned as "C. crocodilus skull" in all figures except Figure 4 as it is the only skull specimen of that species that has been used beside the repeatability test. Therefore, "C. crocodilus skull (2 and 3)" do not appear on Figure 2 as they have not been used in the core of the study. *Smith: Smithsonian collection specimen. The abbreviation "ost." is the short for "osteoderm"*

Genus	Species	Author	Period	Body part	Ontogenetic rank	MNHN Collection number
Gavialis	*gangeticus*	Gmelin (1789)	extant	skull	subadult	ZA-AC custom seizure n°1
Gavialis	*gangeticus*	Gmelin (1789)	extant	skull	Adult	1944-249
Osteolaemus	*tetraspis*	Cope (1861)	extant	ost.	Juvenile	AC.1991.4488a
Osteolaemus	*tetraspis*	Cope (1861)	extant	ost.	Juvenile	AC.1991.4488b
Osteolaemus	*tetraspis*	Cope (1861)	extant	skull	subadult	1931-45
Crocodylus	*niloticus*	Laurenti (1768)	extant	skull	Adult	A5307
Crocodylus	*moreletii*	Duméril & Bibron (1851)	extant	skull	Juvenile	ZA-AC custom seizure n°2
Crocodylus	*rhombifer*	Cuvier (1807)	extant	skull	Adult	1949-421
Crocodylus	*acutus*	Cuvier (1807)	extant	ost.	Juvenile	1909-275
Crocodylus	*acutus*	Cuvier (1807)	extant	ost.	juvenile	1909-274
Crocodylus	*acutus*	Cuvier (1807)	extant	skull	adult	1944-266
Crocodylus	*acutus*	Cuvier (1807)	extant	skull	subadult	ZA-AC custom seizure n°3
Crocodylus	*acutus*	Cuvier (1807)	extant	skull	juvenile	ZA-AC custom seizure n°4
Crocodylus	*intermedius*	Graves (1819)	extant	skull	adult	1885-489
Crocodylus	*porosus*	Schneider (1801)	extant	skull	adult	A5316
Crocodylus	*palustris*	Lesson (1831)	extant	skull	adult	1944-229
Mecistops	*cataphractus*	Gray (1847)	extant	skull	adult	1928-01
Alligator	*mississipiensis* (1)	Daudin (1802)	extant	ost.	juvenile	VdB/FCP/A.m.03a
Alligator	*mississipiensis* (2)	Daudin (1802)	extant	ost.	juvenile	VdB/FCP/A.m.03b
Alligator	*mississipiensis*	Daudin (1802)	extant	skull	adult	1919-127
Caiman	*Crocodilus* (1)	Linnaeus (1758)	extant	skull	subadult	1887-773
Caiman	*Crocodilus* (2)	Linnaeus (1758)	extant	skull	juvenile	ZA-AC custom seizure n°5
Caiman	*Crocodilus* (3)	Linnaeus (1758)	extant	skull	juvenile	ZA-AC custom seizure n°6
Caiman	*crocodilus*	Linnaeus (1758)	extant	ost.	adult	1989-6489
Caiman	*Crocodilus* (1)	Linnaeus (1758)	extant	ost.	juvenile	1986-0454
Caiman	*Crocodilus* (2)	Linnaeus (1758)	extant	ost.	juvenile	1986-0453
Melanosuchus	*niger*	Spix (1825)	extant	skull	adult	1900-112
Paleosuchus	*trigonatus*	Schneider (1801)	extant	skull	subadult	ZA-AC 2014-1
Sarcosuchus	*imperator*	Broin & Taquet (1866)	Cretaceous	ost.	adult	1966-15 Gad-4
Machimosaurus	*hugii*	Von meyer (1837)	Jurassic-Cretaceous	ost.	adult	SMNS 81608 (*Smith)
Diplocynodon	*sp.*	Pomel (1847)	Cretaceous-Miocene	ost.	adult	F.SG-676
Teleosauridae (family)	Indet.(1)	Geoffroy (1831)	Jurassic	ost.	adult	RNJ466
Teleosauridae (family)	Indet.(2)	Geoffroy (1831)	Jurassic	ost.	adult	RNJ465
Teleosauridae (family)	Indet.(3)	Geoffroy (1831)	Jurassic	ost.	adult	RNJ467

the local area gain at the level of the pits, GApit. This index involves the whole set of pits occurring on the surface of a bone. It is equivalent to a basic coefficient of local area enlargement due to pit concavity, as compared to the area of the pits in projection on the smooth surface of the bone:GApit = RApit/SApit. The meaning of this index is both relative to the depth of the pits, and to their actual form.

Testing Repeatability

Since the method used in this study is original, its repeatability had to be assessed. Therefore, the process described above was performed 20 consecutive times on the right half of the frontal of five specimens, three subadult *Caiman crocodilus* (Alligatoridae), one *Crocodylus moreletii* (Crocodylidae), and one *Gavialis gangeticus* (Gavialidae). The variability between repeated measures was tested at both intraspecific (*C. crocodilus*) and interspecific levels. The difference between the extreme values of GAtot (on each of the three skeletal regions considered) for each specimen after 20 repetitions gives an approximation of the error of this method (Fig. 4): Er (Error; %) = 100 (Max–Min)/Max (where Max is the highest value and Min the lowest value).

Statistical Analyses

In order to test the possible occurrence of a phylogenetic signal susceptible to interfere with statistical tests, phylogenetic signal tests were carried out using the "caper" package (Orme et al., 2012) of R (R Development Core Team, 2012), with reference to both the molecular and the morphological phylogenies (Piras et al., 2014) proposed for Crocodyliformes. To perform regression analysis in R, as most data did not follow a Brownian motion model of character evolution (tests were performed using the Phenotypic Diversity Analysis Program module (Midford et al., 2011) of Mesquite (Maddison and Maddison, 2011), we could not calculate independent contrasts and we had to apply the phylogenetic generalized least square (PGLS) method using the "caper" package (Orme et al., 2012) of R.

RESULTS

Repeatability

The 20 repetitions of GAtot measurement (Fig. 4) reveal that precision is more important for

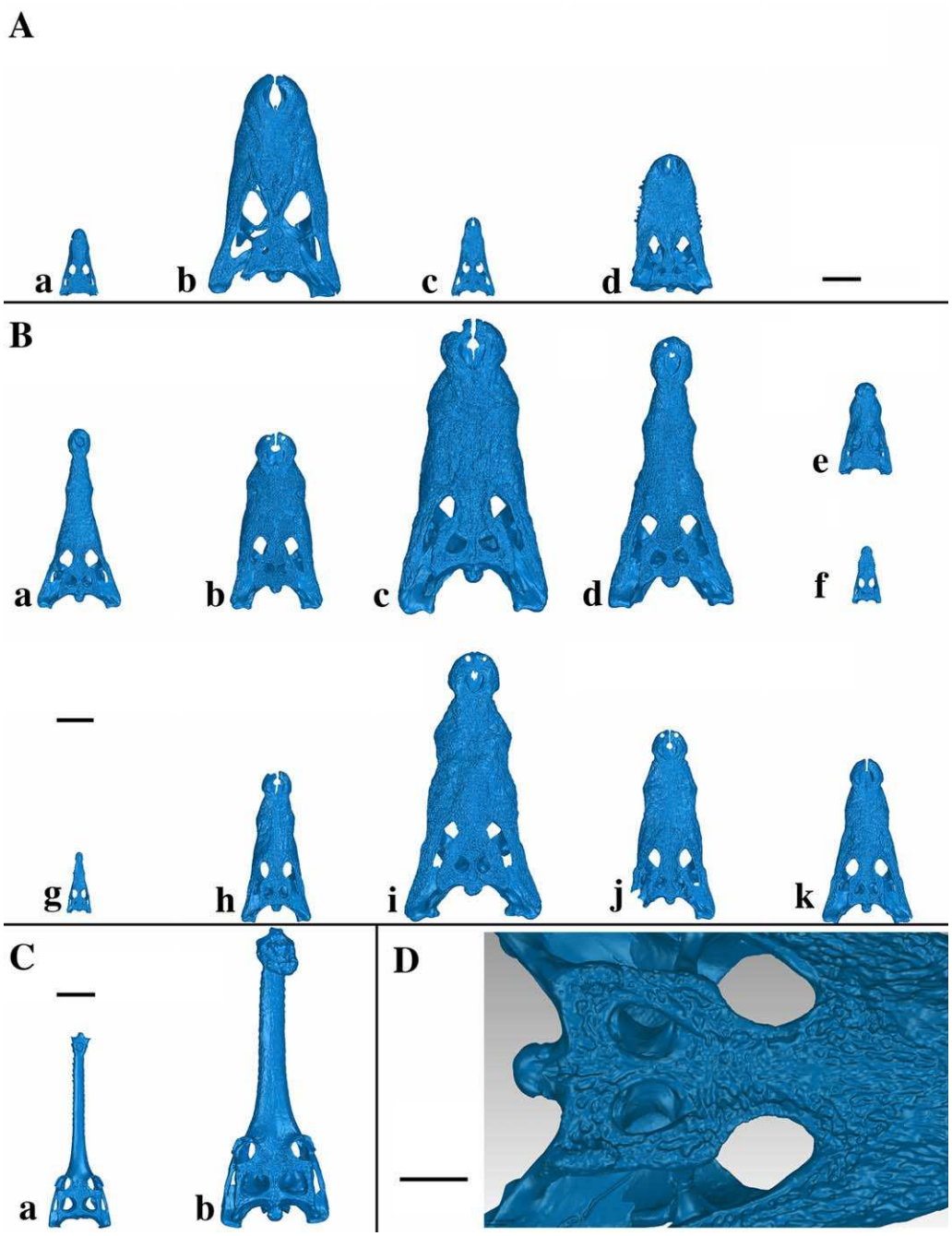

Fig. 2. General aspect of the crocodylians skulls resulting from the scanning process. **A**: Alligatoridae: **a**. *Paleosuchus trigonatus* subadult **b**. *M. niger* adult **c**. *C. crocodilus* subadult **d**. *A. mississipiensis* subadult. Scale bar: 100 mm **B**: Crocodylidae: **a**. *Mecistops cataphractus* adult **b**. *Crocodylus palustris* adult **c**. *C. porosus* adult **d**. *Crocodylus intermedius* adult **e**. *O. tetraspis* subadult **f**. *C. moreletii* juvenile **g**. *C. acutus* juvenile **h**. *C. acutus* subadult **i**. *C. acutus* adult **j**. *Crocodylus rhombifer* adult **k**. *Crocodylus niloticus* adult. Scale bar: 100 mm **C**: Gavialidae **a**. *G. gangeticus* subadult **b**. *G. gangeticus* adult male. Scale bar: 100 mm **D**: Close-up on the skull table of *C. niloticus*. Scale bar: 45 mm. [Color figure can be viewed in the online issue, which is available at wileyonlinelibrary.com.]

adults and subadults with a large size ($Er < 1\%$ in *G. gangeticus* subadult, *C. crocodilus* skull 1) than in juveniles and subadults of small size ($Er < 3\%$: *C. moreletii* skull, *C. crocodilus* skulls 2 and 3). Thus, the precision of the measures is related to the size of specimens, not their taxonomic position.

Gain in Area on Total Osteoderms and Skull Bones

The gain in area on the osteoderms (GA_o; Fig. 5A) varies between 0 and 5% for the juvenile *Alligator mississipiensis* and *Crocodylus acutus*. In *C. crocodilus*, GA_o is higher: 10–15% in juveniles and adults. Values in *Osteolaemus tetraspis* (juvenile)

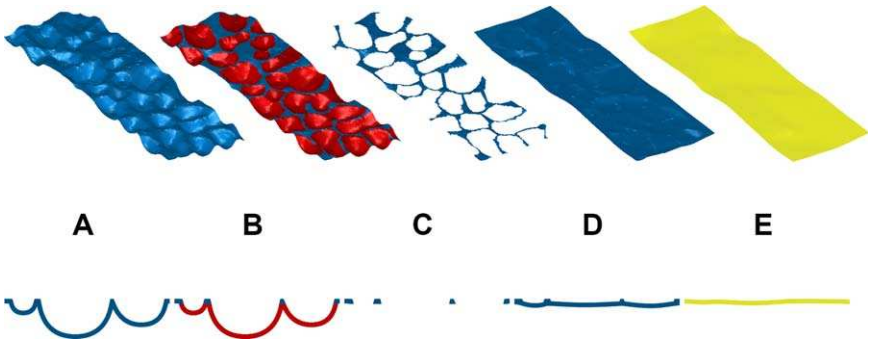

Fig. 3. Processing of the scan. **A**: Scan of the real ornamented surface. **B**: Selection of the mesh composing the pits (in red). **C**: Deletion of the pits. **D**: Filling the gaps by a smooth surface. **E**: Application of a noise reduction filter on the mesh to obtain a homogenous smooth surface.

are also of about 15%. Area gain on osteoderms is close to 20% in *Sarcosuchus imperator* and approaches 30% in *Diplocynodon sp*. (both adults). The highest levels of GA_o are encountered in the Teleosauridae, with values reaching 30% (*Machimosaurus hugii*: 33%) and 39% (undetermined Teleosauridae). Our data thus show that GA_o ranges from 5 to 40% and is influenced by both taxonomic frames and the ontogenetic developmental stages.

The gain in area on the skull table ($GAtot_t$; Fig. 5B) ranges from 7 to 20% in the Alligatoridae, and from 5 to 32% for the Crocodylidae, a subsample that, includes juveniles. For the Gavialidae $GAtot_t$ is much lower: some 10%, at most, for the adult specimen. Area gain on the nasal is homogenous among Alligatoridae ($GAtot_n = 5\%$; Fig. 5B) except for *Melanosuchus niger* ($GAtot_n = 12\%$). Six of the Crocodylidae have an area gain under 5% on the nasal, one has a gain under 10%, whereas the other four have a $GAtot_n$ of some 20%. As the snout displays no ornamentation in *G. gangeticus*, $GAtot_n$ is zero in both specimens of that species.

Different values of area gain were obtained for the CT and the snout, with $GAtot_n$ being generally much lower than $GAtot_t$. Therefore, we paid special attention to the ratio between $GAtot_n$ and $GAtot_t$ in order to check if the difference between these values is dependent on the anatomical regions. For this purpose, we considered an index of contrast in area gain, or CGA, between these two cranial territories: $CGA = (GAtot_n/GAtot_t) - 1$. If the gain in area is zero on the nasal and

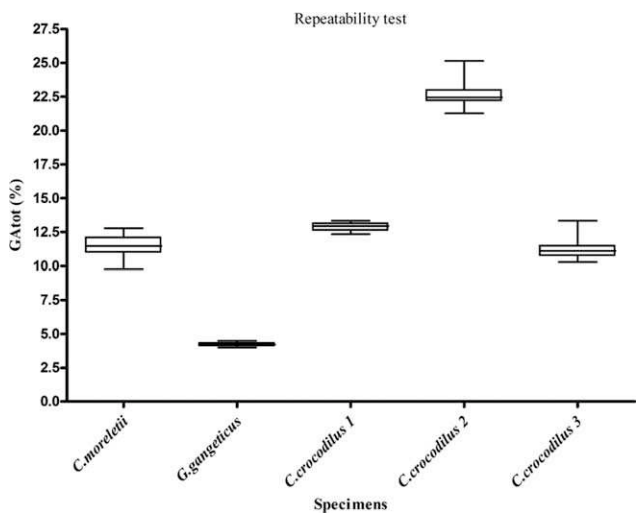

Fig. 4. Boxplot of the repeatability test after the 20 repetitions of the GAtot measure for each specimen. From left to right: *C. moreletii* skull; *G. gangeticus* skull subadult; *C. crocodilus* skull 1; *C. crocodilus* skull 2; *C. crocodilus* skull 3.

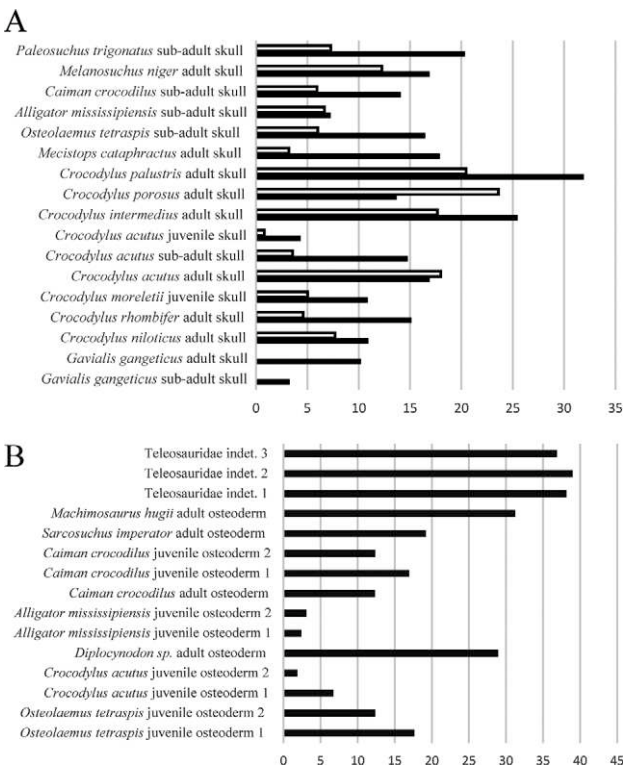

Fig. 5. **A:** $GAtot_t$ (%; in black): total gain in area on the skull table, $GAtot_n$ (%; in white) total gain in area on the nasal. Figure 5**B**: $GAtot_o$ (%): total gain in area on osteoderms.

TABLE 2. Contrast of gain in area between the nasal and the skull table (CGA; no unity)

Specimens	CGA
Gavialis gangeticus (subadult)	−1
Gavialis gangeticus (adult)	−1
Crocodylus niloticus	−0,297025562
Crocodylus rhombifer	−0,697152266
Crocodylus moreletii	−0,53714462
Crocodylus acutus (adult)	0,065172778
Crocodylus acutus (subadult)	−0,759005177
Crocodylus acutus (juvenile)	−0,814323732
Crocodylus intermedius	−0,305832096
Crocodylus porosus	0,724247768
Crocodylus palustris	−0,358984317
Mecistops cataphractus	−0,821109001
Osteolaemus tetraspis	−0,635470979
Alligator mississipiensis	−0,080619538
Caiman crocodilus	−0,578723852
Melanosuchus niger	−0,273817966
Paleosuchus trigonatus	−0,641870303

positive on the skull table, the ratio will reach −1. In the reverse situation, CGA could theorically tend to « $+\infty$ ». More generally, if $GAtot_n < GAtot_t$, then $CGA < 0$; if $GAtot_n > GAtot_t$, then $CGA > 0$; if $GAtot_n = GAtot_t$, then $CGA = 0$.

The contrast in area gain (Table 2) is negative for 15 out of the 17 specimens, which indicates that the gain in surface is higher on the CT than on the nasal. The lowest possible value of CGA (i.e., −1) is observed in *G. gangeticus* whose snouts bear no ornamentation. *Crocodylus porosus* shows the only highly positive value, CGA = 0.72; indicating that the gain in area is more than twice higher on the nasal than on the CT. The three specimens of *C. acutus* show an increasing value of CGA, in pace with their sizes.

Influence of Ontogeny and Phylogeny

In *C. acutus*, the value of $GAtot_t$ increases by a factor of 3 from the juvenile to the subadult ranks. On the nasal, the gain in area remains under 5% in juveniles and subadults; it is then multiplied by 3 in the adults.

Tests of phylogenetic signal (Blomberg's K and Pagel's lambda) show that the variable $GAtot_t$, OA_{relat}, $GApit_t$ are independent of phylogeny (Table 3) whereas $GAtot_n$ and $GApit_n$ show a phylogenetical signal.

TABLE 3. Phylogenetic signal in data, measured as Pagel's lambda

Anatomical region	Variables	Phylogenetical signal
Skull table	GAtot	Not significant
	GApit	Not significant
	OArelat	Not significant
Nasal	GAtot	Significant
	GApit	Significant
	OArelat	Not significant

*TABLE 4. Characteristics of the gain in area on the **skull table** (GAtot is in percentage; GApit and OArelat have no unity)*

	GAtot (%)	GApit	OArelat
Alligator mississipiensis	10,206849	1,1038	0,49501
Caiman crocodilus	14,082334	1,2244	0,5988958
Crocodylus acutus (adult)	16,88422	1,2659	0,5915347
Crocodylus acutus (juvenile)	4,3488101	1,0784	0,4130005
Crocodylus acutus (subadult)	14,760852	1,2081	0,6003417
Mecistops cataphractus	17,894057	1,2187	0,6404411
Crocodylus intermedius	25,456406	1,4981	0,4979489
Crocodylus moreletii	10,87426	1,2397	0,4478343
Crocodylus niloticus	10,929202	1,1893	0,4820772
Crocodylus palustris	31,901311	1,4759	0,6613389
Crocodylus porosus	13,685915	1,2259	0,5066751
Crocodylus rhombifer	15,135995	1,2623	0,4893289
Gavialis gangeticus (adult male)	10,206849	1,1051	0,4573896
Gavialis gangeticus (subadult)	3,2675138	1,0634	0,4214721
Melanosuchus niger	16,880454	1,2527	0,4924039
Osteolaemus tetraspis	16,465805	1,1897	0,6682581
Paleosuchus trigonatus	20,329926	1,235	0,6891942
Mean	**14,900633**	**1,2257**	**0,5384203**
Median	**14,760852**	**1,2244**	**0,4979489**
Standard deviation	**6,9557843**	**0,1176**	**0,0907715**
Max	**6,8501796**	**0,1133**	**0,090082**
Min	**3,2675138**	**1,0634**	**0,4130005**

Values of GA_{PIT} and OA_{RELAT}

The average $GAtot_t$ (14.9%) is almost twice as high as the average $GAtot_n$ [8.4%] (Tables 4 and 5). However, the average OA_{relat} is similar in both cases (around 0.53) whereas the average $GApit_t$ (1.23) is much higher than the average $GApit_n$ (1.02). These data suggest that the pits are more developed on the skull table than on the snout if we consider mean values.

Multivariate regressions (Table 6) show that the correlations between GAtot on the one hand and on the other hand GApit, and OA_{relat} are highly significant both for the skull table and for the nasal. However, it is noticeable that the correlation between GAtot and GApit is significant for both the skull table and the nasal, whereas the specific correlation between GAtot and OA_{relat} is significant only for the skull table.

DISCUSSION

Comparative Elements

The area gain observed in this study on crocodylian skulls, some 10–30% in adult specimens, is relatively close to that measured in temnospondyl amphibians (10–20%) by Rinehart and Lucas (2013). According to the results of the repeatability test, a possible error of 3%, at most, can be considered for our data. Both methods nevertheless rely on very distinct principles, and have different constraints and limitations. The methodology we propose here has some practical advantages because it necessitates very few manipulations of the

*TABLE 5. Characteristics of the gain in area on the **nasal** (GAtot is in percentage; GApit and OArelat have no unity)*

	GAtot (%)	GApit	OArelat
Alligator mississipiensis	6,66828151	1,14206864	0,55088995
Caiman crocodilus	5,93255139	1,09436717	0,53859678
Crocodylus acutus (adult)	17,9846117	1,27337308	0,68319236
Crocodylus acutus (juvenile)	0,80747082	1,00915936	0,41393773
Crocodylus acutus (subadult)	3,55728894	1,03740987	0,48024072
Mecistops cataphractus	3,20108568	1,05510411	0,6115329
Crocodylus intermedius	17,67102	1,29321244	0,66780248
Crocodylus moreletii	5,03320953	1,1106504	0,47745053
Crocodylus niloticus	7,68294935	1,14619902	0,64675186
Crocodylus palustris	20,4492406	1,31101699	0,68900064
Crocodylus porosus	23,5979076	1,35461338	0,72571896
Crocodylus rhombifer	4,58390179	1,09020492	0,56756289
Gavialis gangeticus (adult male)	0	0	0
Gavialis gangeticus (subadult)	0	0	0
Melanosuchus niger	12,2582825	1,22194614	0,60502508
Osteolaemus tetraspis	6,00226363	1,11199616	0,66749482
Paleosuchus trigonatus	7,28075035	1,01926818	0,62105969
Mean	**8,39475384**	**1,01591705**	**0,52625044**
Median	**6,00226363**	**1,1106504**	**0,60502508**
Standard deviation	**7,33404381**	**0,39658063**	**0,21525258**
Max	**7,32058372**	**0,39525062**	**0,21515923**
Min	**0**	**0**	**0**

biological (or paleontological) material, and can be applied to the total surface of large objects such as adult crocodylian skulls. Moreover, all the operations related to data acquisition and modeling processes can be saved to serve subsequently to other morphometric treatments.

Rinehart and Lucas' (2013) study concluded that, as compared to total body mass, bone area increase due to ornamentation on the skull roof of temnospondyls is of negligible importance and can neither improve thermoregulation significantly, nor increase skin breathing. Since bone sculpture on the skull roof of the Crocodylia yields a similar area gain, Rinehart and Lucas' conclusion stands also for this taxon, at least if the cranial region is considered exclusively. However, an important difference exists between the dermal skeleton of crocodylians and that of temnospondyls: the former have heavy, extensively developed osteoderm shields, whereas the latter are most often devoid of postcranial osteoderms (Schoch and Milner, 2000, 2014). In most crocodylian taxa, dermal shields composed of densely ornamented osteoderms cover the whole dorsal area of the body from snout tip to tail tip, and spread more or less extensively to the flanks and the ventral surface (Kälin, 1955; Wermuth and Fuchs, 1978; Brazaitis, 1987). Some taxa also display osteoderms on their limbs, so that their whole body is covered by a continuous shield (Hill, 2010). One of the results of this study is to show that area gain due to ornamentation is more pronounced on osteoderms (up to 40%) than on skull bones, especially the snout region. Considering the whole area in which ornamented dermal elements (bones or osteoderms) occur in the Crocodylia, the total gain in area due to ornamentation appears considerably higher in this taxon than in the temnospondyls. Therefore, Rinehart and Lucas's conclusion is likely to be irrelevant to the case of crocodylians if their dermal skeleton is taken into account. The estimations of area gain presented here should contribute to future efforts in the study of the possible contribution of ornamented dermal elements to the global exchange capacities (for e.g., heat or gas) of the crocodylian body.

Another important difference between bone ornamentation in crocodiles and temnospondyls involves the osteogenic processes that create pits and ridges. In temnospondyls, bone ornamentation results from preferential accretion on top of the ridges (Witzmann and Soler-Gijón, 2010 see also Vickaryous and Hall, 2008). In this situation, pits are a passive consequence of ridge elevation. Conversely, in crocodiles, ornamentation is mainly due to the excavation of pits through local resorption

TABLE 6. PGLS using morphological phylogeny. GAtot is the variable we aim to explain depending on GApit and OArelat; adjusted $R^2 = 0.9135$ (skull table); adjusted $R^2 = 0.9764$ (nasal)

Skull table	*P*-value	Correlation with GAtot
Intercept (GApit and OArelat)	2.145 e − 06	Significant
GApit	1.132 e − 06	Significant
OArelat	0.0006195	Significant
Nasal	*P*-value	Correlation with GAtot
Intercept (GApit and OArelat)	8.313 e − 09	Significant
GApit	3.490 e − 07	Significant
OArelat	0.1034	Not significant

of bone cortices; ridges are then a consequence of pit differentiation and their upward growth plays but a limited role, if any, in the constitution of ornamentation reliefs (Buffrénil et al., 2014). In addition, bone ornamentation in crocodylians is permanently remodeled and transformed through intense resorption and reconstruction of cortical surface. Pits and ridges can thus be continuously displaced, enlarged, reduced, eroded, or filled up during ontogeny. If osteogenic processes are taken into account, then the pit and ridge ornamentation of temnospondyls and crocodiles, beyond their total morphologic similarity, must be considered as homoplasic, not homologic. The present study reveals that total area gain, GAtot, on a bone is essentially determined by two basic factors: the relative extent of the set of pits, OArelat, and an index of local area enlargement, GApit that directly reflects the depth and shape of the pits. Bone area gain in temnospondyls and crocodylians necessarily depends on the same two factors. Therefore, the respective efficiency of ridge elevation (temnospondyls) or pit excavation and remodeling (crocodylians), for controlling GApit and OArelat, and thus influencing GAtot during ontogeny, is open to question. A precise model for explaining the growth of bone ornamentation in temnospondyls, and especially the relationship between the size of the pits and the overall size of the bones that bear them, remains to be done (see on this topic Witzmann and Soler-Gijón, 2010; Witzmann et al., 2010). However, it seems obvious that the mechanism involved in the crocodylians, a permanent and integral remodeling of bone surface through resorption and reconstruction, is more rapid, more flexible, and submitted to less geometrical constraints than the mechanism at work in the temnospondyls because it relies on two main complementary mechanisms, resorption and reconstruction, whereas one mechanism only, apposition of primary bone tissue, is available for the temnospondyls.

Functional Considerations

Before considering the contribution of our results to the assessment of the various hypotheses proposed to date for the functional significance of bone ornamentation, a basic question must be addressed: is there an actual functional role for this character, or does it present a neutral variation indicative of limited functional meaning? Our results show that GAtot and GApit on the CT are independent of phylogeny, whereas these indices on the snout region (nasal bone) show a significant phylogenetic signal. This result suggests that $GAtot_t$ and $GApit_t$ might have an implication in a functional or a structural role as they do not evolve randomly; conversely $GAtot_n$ and $GApit_n$ seem to have evolved following a Brownian motion model, with low selective pressure exerted on their variation.

As repeatedly pointed (Coldiron, 1974; Witzmann et al., 2010; Rinehart and Lucas, 2013; Buffrénil et al., 2014), the functional role of bone ornamentation remains obscure and controversial. The present study gives significant information relative to crocodylians: area gain due to ornamentation is unlikely to be negligible if it is considered on both the skull roof, and the extensive osteoderm shield displayed by these animals. Therefore, several of the hypotheses about the role of bone ornamentation that were rejected by previous authors (Rinehart and Lucas, 2013) cannot be merely discarded in the case of the Crocodylia because of the feeble area gain observed on skull bones; they must be reconsidered in a critical scope integrating the results of this study, along with the whole set of data available on the anatomy and histology of ornamented bone surfaces in this taxon. Five of the most common functional interpretations can thus be re-examined.

1. A contribution of bone ornamentation to transcutaneous gas exchanges (Bystrow, 1947) is conceivable in reference to area gain; however, it must be definitely discarded in the crocodylians because their skin, like that of other reptiles, is covered by a thick layer of keratin, impervious to gas exchanges (Bellairs, 1969; Landmann, 1986).
2. Similarly, the role of bone ornamentation for improving the attachment of the skin onto bone surface (Romer, 1947; Witzmann, 2009; Witzmann et al., 2010) could be considered possible with reference to area gain, but the intense remodeling process that occurs on the surface of crocodylian ornamented bones (be they skull bones or osteoderms) is in poor agreement with this hypothesis because the Sharpey's fibers that anchor the dermis onto the bone surface are repeatedly resorbed during this process. The relationship between ornamented bones and dermal tissues remain to be studied in detail (for crocodiles, specific studies on this topic are ancient and of relatively limited precision, e.g., Schmidt 1914). Complementary observations made on the sample of 32 extant and extinct pseudosuchian taxa already used by Buffrénil et al. (2014) for studying the mode of development of bone ornamentation in crocodiles show that Sharpey's fibers are characteristically lacking in the layers of secondary lamellar bone tissue that form the floors of the pits. This additional element tends to confirm that, in the Crocodylia (the situation may be different in temnospondyls or turtles), bone ornamentation is unlikely to reinforce bone anchorage into the dermis, but rather results in making it less tight.
3. The involvement of bone ornamentation in the mechanical reinforcement of the bones (Coldiron,

1974; Rinehart and Lucas, 2013) is not specifically addressed by the results of the present study, but is by no means incompatible with them. However, the higher level of GAtot observed on the osteoderms reflects a better differentiation of ornamental reliefs on these elements, a situation difficult to explain in the frame of a mechanical interpretation. The mechanical involvement of the osteoderms, if any, is necessarily different from, and most likely far less intense than, that prevailing on skull bones, where the harsh stresses due to prey catching are concentrated (Erickson et al., 2003, McHenry et al., 2006). It would then be paradoxical that the osteoderms be more ornamented than skull bones if ornamentation had a predominant protective role against mechanical damages.

4. Another functional hypothesis refers to a contribution of bone ornamentation in thermal exchanges (heat captation and dissipation, depending on the thermal requirements) between an animal's body and the surrounding milieu (Seidel, 1979; Farlow et al., 2010). Bone ornamentation in crocodiles seems very little perceptible on the surface of the entire living animals, the possible benefit of GA for heat exchange would then depend on other considerations. For instance, pits house a rich vascular supply (Seidel, 1979; Farlow et al., 2010; Witzmann et al., 2010) that would either accelerate blood heating by direct exposition to sun radiations through overlying cutaneous layers, or facilitate heat dissipation by increasing skin perfusion in cool water or shade (see also on this topic Johnson et al., 1976; Smith et al., 1978; Robertson and Smith, 1979; Smith, 1979; Seebacher and Franklin, 2007). Although the geometric organization of these vascular bundles remains to be established on detailed, 3D micro-angiographic studies, it can be hypothesized that, an increase in bone area through ornamentation should necessarily result in a proportional increase in the local amount of superficial blood vessels, and finally improve the efficiency of heat capitation.
5. The occurrence of extensive, superficial vascularization related to bone sculpturing could also be considered in light of Janis et al.'s (2012) hypothesis attributing to ornamentation, and to the blood vessels associated with it, a role in the control of the acidosis process supposed to have occurred in the blood of basal amniotes incipiently adapting to life on dry land. By extension, this hypothesis could involve also extant diving or aquatic tetrapods. The capacity of bone, and especially the osteoderms, to contribute buffering blood lactate in excess has indeed been experimentally demonstrated in turtles (Jackson et al., 2000) and crocodiles (Jackson et al., 2003). In this process, the degree of inner bone perfusion is a prominent element because it controls the intensity of exchanges between blood and bone. However, the actual role of the superficial, outer blood vessels topographically related to ornamentation, but in limited contact with subjacent bones, remains obscure and conjectural. For this reason, although Janis et al.'s (2012) hypothesis is not contradictory (but rather in agreement) with the results of the present study, it should be considered with some caution until further documented.

In conclusion, the thermal hypothesis is congruent with the results of the present study, and closely fits the details of GAtot values observed in the different skeletal regions that were sampled. This hypothesis indeed involves a higher area gain on the entire dorsal surface of the body, a region directly exposed to sun rays, especially in a crocodile floating a long time in ambush with either its entire dorsal surface, or just its CT and nostrils, emerging from water (respectively the "high float" and the "common float" described by Smith, 1979). Our observations show that GA values are actually maximal on the osteoderms and CT, the two regions most often exposed, as postulated by this hypothesis. Finally, the "thermal hypothesis" is the sole interpretation susceptible to explain in detail the actual distribution of bone area gain due to ornamentation. This conclusion cannot, of course, be taken as formal evidence for this hypothesis; it should nevertheless be considered in future studies about the functional role of bone sculpture, at least in the Crocodylia.

ACKNOWLEDGMENTS

We would like to thank Dr. Salvador Bailon and Dr. Ronan Allain for their help in selecting the specimens suitable for this study in the MNHN collections. Finally, we will thank the UMS 2700 (MNHN/CNRS) for the access to the 3D scanner.

AUTHORS CONTRIBUTIONS

François Clarac created the dataset by scanning all the specimens, analyzed the scans and synthetized all the results. Thibaud Souter and Raphaël Cornette were chiefly involved in the technical aspects of data acquisition and in the statistical processing morphometric measurements. Jorge Cubo contributed to phylogenetic analyses and final writing of the manuscript. The whole project was supervised by Vivian de Buffrénil.

LITERATURE CITED

Bellairs A. 1969. The life of Reptiles. London: Weidenfeld & Nicolson. 945p.

Brazaitis P. 1987. The identification of crocodilian skins and products. In: Webb JW, Manolis SC, Whitehead PJ editors. Wildlife Management; Crocodiles and Alligators. Chipping Norton, Australia: Surrey Beatty and Sons PTY Limited. pp 373–392.

Bronzati M, Chinaglia-Montefeltro F, Langer MC. 2012. A species level supertree of the crocodyliformes. Hist Biol 24:598–606.

Buffrénil Vd. 1982. Morphogenesis of bone ornamentation in extant and extinct crocodilians. Zoomorphology 99:155–166.

Buffrénil Vd, Clarac F, Fau M, Martin S, Martin B, Pellé E, Laurin M. 2014. Differentiation and growth of bone ornamentation in vertebrates: A comparative histological study among the crocodylomorpha. J Morphol 276:425–445.

Bystrow AP. 1935. Morphologische untersuchungen der deckknochen des schädels der stegocephalen. 1. Mitteilung. Schädel der stegocephalen. Acta Zool Stock 16:65–141.

Bystrow AP. 1947. Hydrophilous and xerophilous labyrinthodonts. Acta Zool Stock 28:137–164.

Coldiron RW. 1974. Possible functions of ornament in the labyrinthodont amphibians. Occasional papers of the Museum of Natural History, University of Kansas, Vol. 33. pp 1–19.

Downs JP, Donoghue PCJ. 2009. Skeletal histology of bothriolepis canadensis (placodermi, antiarchi) and evolution of the skeleton at the origin of jawed vertebrates. J Morphol 270: 1364–1380.

Erickson GM, Lappin AK, Vliet KA. 2003. The ontogeny of bite-force performance in american alligator (alligator mississippiensis). J Zool 260:317–327.

Farlow JO, Hayashi S, Tattersall GJ. 2010. Internal vascularity of the dermal plates of stegosaurus (ornithischia, tyreophora). Swiss J Geosci 103:173–185.

Hill RV. 2010. Osteoderms in simosuchus clarki (crocodyliformes: notosuchia) from the late cretaceous of madagascar. J Vertebr Paleontol 30(6):154–176.

Iordansky NN. 1973. The skull of the Crocodilia. In: Gans C, editor. Biology of the Reptilia, Vol. 4. London: Morphology D. Academic Press. pp 201–262.

Jackson DC, Crocker CE, Ultsch GR. 2000. Bone and shell contribution to lactic acid buffering of submerged turtles chrysemys picta bellii at 3°C. Am J Physiol Regul Integr Comp Physiol 278:r1964–1571.

Jackson DC, Andrade D, Abe AS. 2003. Lactate sequestration by osteoderms of the broad-nose caiman, caiman latirostris, following capture and forced submergence. J Exp Biol 206: 3601–3606.

Janis CM, Devlin K, Warren DE, Witzmann F. 2012. Dermal bone in early tetrapods: A palaeophysiological hypothesis of adaptation for terrestrial acidosis. Proc Biol Sci 279:3035–3040.

Johnson CR, Webb GJW, Tanner C. 1976. Thermoregulation in crocodilians—II. A telemetric study of body temperature in the australian crocodiles, crocodylus johnstoni and crocodylus porosus. Comp Biochem Physiol 53A:143–146.

Kälin J. 1955. Crocodilia. In: Piveteau J, editor. Traité de Paléontologie, Vol. 5. Paris: Masson et Cie. pp 695–784.

Landmann L. 1986. Epidermis and dermis. In: Bereiter-Hahn, J, Matoltsky AG, Richards KS, editors. Biology of the Integument, Vol. 2 Vertebrates. Part IV: The Skin of Reptiles. Berlin: Springer-Verlag. pp 150–187.

Langston W Jr. 1973. The crocodilian skull in historical perspective. In: Gans C, editor. Biology of the Reptilia, Vol. 4. London: Morphology D. Academic Press. pp 263–284.

Lundberg JG, Aguilera O. 2003. The late miocene phractocephalus catfish (siluriformes: pimelodidae) from urumaco, venezuela: Additional specimens and reinterpretation as a distinct species. Neotrop Ichthyol 1:97–109.

Maddison WP, Maddison DR. 2011. Mesquite: A modular system for evolutionary analysis. Version 2.75. Available at: http://mesquiteproject.org.

McHenry CR, Clausen PD, Daniel WJT, Meers MB, Pendharkar A. 2006. Biomechanics of the rostrum in crocodilians: A comparative analysis using finite-element modeling. Anat Rec 288A:827–849.

Midford P, Garland TJ, Maddison WP. 2011. PDAP Package for Mesquite. Version 1.16. Available at: http://mesquiteproject.org/pdap_mesquite/index.html.

Orme D, Freckleton R, Thomas G, Petzoldt T, Fritz S, Isaac N, Pearse W. 2012. The caper package: Comparative analysis of phylogenetics and evolution in R. R package version 0.5.2.

Piras P, Buscalioni AD, Teresi L, Raia P, Sansalone G, Kotsakis T, Cubo J. 2014. Morphological integration and functional modularity in the crocodilian skull. Integr Zool 9:498–516.

R Development Core Team. 2012. R: A language and environment for statistical computing. Vienna R Foundation for statistical Computing.

Rinehart LF, Lucas SG. 2013. The functional morphology of dermal bone ornamentation in temnospondyl amphibians. In: Tanner LH, Spielmann JA, Lucas, SG, editors. The Triassic System. Albuquerque: New Mexico Museum of Natural History and Science. 61: 524–532.

Robertson SL, Smith EN. 1979. Thermal indications of cutaneous blood flow in the American alligator. Comp Biochem Physiol 62A:569–572.

Romer AS. 1947. Review of the Labyrinthodontia. Bulletin of the Museum of Comparative Zoolology, Harvard University, Vol. 99. pp 1–368.

Scheyer TM, Sander PM, Joyce WG, Böhme W, Witzel U. 2007. A plywood structure in the shell of fossil and living soft-shelled turtles (trionychidae) and its evolutionary implications. Org Divers Evol 7:136–144.

Schoch RR, Milner AR. 2000. Stereospondyli. In: Wellnhofer P, editor. Encyclopedia of Paleoherpetology. Part 3B. München: Verlag Dr. Friedrich Pfeil. pp 1–164.

Schoch RR, Milner AR. 2014. Temnospondyli. In: Sues HD, editor. Handbook of Paleoherpetology. Part 3A2. München: Verlag Dr. Friedrich Pfeil. pp 1–126.

Seebacher F, Franklin CE. 2007. Redistribution of blood within the body is important for thermoregulation in an ectothermic vertebrate (crocodylus porosus). J Comp Physiol B 177:841–848.

Seidel MR. 1979. The osteoderms of the American alligator and their functional significance. Herpetologica 35:375–380.

Smith EN. 1979. Behavioral and physiological thermoregulation of crocodilians. Am Zool 19:239–247.

Smith EN, Robertson SL, Davies DG. 1978. Cutaneous blood flow during heating and cooling in the American alligator. Am J Physiol 235:160–167.

Vickaryous MK, Hall BK. 2008. Development of the dermal skeleton in alligator mississippiensis (archosauria, crocodilia) with comments on the homology of osteoderms. J Morphol 269:398–422.

Wermuth H, Fuchs K. 1978. Bestimmen von Krokodilen und ihrer Häute. Stuttgart, New-York: Gustav Fisher Verlag. 100p.

Witzmann F. 2009. Comparative histology of sculptured dermal bones in basal tetrapods, and the implications for the soft tissue dermis. Palaeodiversity 2:233–270.

Witzmann F, Soler-Gijón R. 2010. The bone histology of osteoderms in temnospondyl amphibians and in the chroniosuchian bystrowiella. Acta Zool Stockh 91:96–114.

Witzmann F, Scholz H, Müller J, Kardjilov M. 2010. Sculpture and vascularization of dermal bones, and the implication for the physiology of basal tetrapods. Zool J Linn Soc 160:302–340.

CHAPITRE 2: LES CONTRAINTES DEVELOPPEMENTALES EXERCEES PAR LA MORPHOLOGIE CRANIENNE SUR L'ORNEMENTATION

Gavialis gangeticus

(Espèce actuelle, Inde, reconstruction surfacique par scanner 3D)

Journal of Anatomy

J. Anat. (2016) **229**, pp292–301 doi: 10.1111/joa.12470

Does skull morphology constrain bone ornamentation? A morphometric analysis in the Crocodylia

F. Clarac,[1,2,3] T. Souter,[4] J. Cubo,[1,2] V. de Buffrénil,[3] C. Brochu[5] and R. Cornette[6]

[1]*UPMC Univ Paris 06, UMR 7193, Institut des Sciences de la Terre Paris (ISTeP), Sorbonne Universités, Paris, France*
[2]*CNRS, UMR 7193, Institut des Sciences de la Terre Paris (ISTeP), Paris, France*
[3]*Département Histoire de la Terre, Museum National d'Histoire Naturelle, UMR 7207 (CR2P), Sorbonne Universités, MNHN/CNRS/UPMC, Bâtiment de Géologie Paris Cedex 05, France*
[4]*Plateforme de morphométrie du MNHN -UMS 2700 Outils et Méthodes de la Systématique Intégrative, Paris, France*
[5]*Department of Earth and Environmental Sciences, University of Iowa, Iowa City, IA, USA*
[6]*Institut de Systématique, Evolution, Biodiversité – ISYEB – UMR 7205 – CNRS, MNHN, UPMC, EPHE – Muséum national d'histoire naturelle, Sorbonne Universités, Paris, France*

Abstract

Previous quantitative assessments of the crocodylians' dermal bone ornamentation (this ornamentation consists of pits and ridges) has shown that bone sculpture results in a gain in area that differs between anatomical regions: it tends to be higher on the skull table than on the snout. Therefore, a comparative phylogenetic analysis within 17 adult crocodylian specimens representative of the morphological diversity of the 24 extant species has been performed, in order to test if the gain in area due to ornamentation depends on the skull morphology, i.e. shape and size. Quantitative assessment of skull size and shape through geometric morphometrics, and of skull ornamentation through surface analyses, produced a dataset that was analyzed using phylogenetic least-squares regression. The analyses reveal that none of the variables that quantify ornamentation, be they on the snout or the skull table, is correlated with the size of the specimens. Conversely, there is more disparity in the relationships between skull conformations (longirostrine vs. brevirostrine) and ornamentation. Indeed, both parameters GApit (i.e. pit depth and shape) and OArelat (i.e. relative area of the pit set) are negatively correlated with snout elongation, whereas none of the values quantifying ornamentation on the skull table is correlated with skull conformation. It can be concluded that bone sculpture on the snout is influenced by different developmental constrains than on the skull table and is sensible to differences in the local growth 'context' (allometric processes) prevailing in distinct skull parts. Whatever the functional role of bone ornamentation on the skull, if any, it seems to be restricted to some anatomical regions at least for the longirostrine forms that tend to lose ornamentation on the snout.

Key words: 3D-geometrical morphometrics; bone sculpture; crocodylians; Phylogenetic comparative analysis; skull morphology.

Introduction

Like temnospondyls and some other vertebrates, crocodylians possess a particular type of dermal bone ornamentation (also referred to as 'bone sculpture') made of pits and/or grooves separated by ridges (Bystrow, 1935; Lundberg & Aguilera, 2003; Scheyer et al. 2007; Witzmann & Soler-Gijon, 2010). However, the functional significance(s) of ornamentation remain(s) controversial, and has been related to either increasing basking efficiency in ectothermic vertebrates (Seidel, 1979), increasing bone mechanical strength (Coldiron, 1974), improving cutaneous respiration (Bystrow, 1947) or buffering blood acidosis (Janis et al. 2012). All these hypotheses implicitly postulate that sculpture provides a local gain in area to the bones. This is why specific effort was recently paid to obtaining quantitative data on this topic. Two distinct approaches were used in this purpose: Rinehart & Lucas (2013) made surface measurements on bone cross-sections in temnospondyls; whereas Clarac et al. (2015) proceeded to 3D surface reconstructions in crocodylians with a surface scanner. Both studies show that the gain in area ranges between 10% and 20% in both groups, with values generally higher for the

Correspondence
F. Clarac, UPMC Univ Paris 06, UMR 7193, Institut des Sciences de la Terre Paris (ISTeP), Sorbonne Universités, 4 place Jussieu, BC 19, F-75005 Paris, France. E: fclarac@mnhn.fr

Accepted for publication *20 February 2016*
Article published online *7 April 2016*

cranial table than for the rostral region (snout) in crocodylians. On crocodylian osteoderms, area gain can reach a maximum value of 40% (Clarac et al. 2015). According to these data, area gain due to ornamentation appears uneven in the diverse skeletal sites where bone sculpturing occurs. Considering the pronounced variability that characterizes skull shape among the Crocodylia (Iordansky, 1973; Piras et al. 2009, 2010; Blanco et al. 2014, 2015; Watanabe & Slice, 2014; Foth et al. 2015), a correlation is susceptible to exist between, on the one hand, total area gain and, on the other hand, skull morphology in this taxon. Of course, if bone ornamentation plays an actual role, elucidating this relationship is a pre-requisite for a realistic assessment of its functional involvement. Indeed, variations of skull morphology among taxa could imply constrains, such as: size influence, allometric variations between the snout and skull table due to feeding adaptions, relative size of the upper temporal fenestra, etc. All these variations could possibly limit the development of ornamentation and thus its possible function. The aim of this work is to assess the influence of the skull morphology on the efficiency of the hypothetical functions of bone ornamentation.

Materials and methods

Biological sample

The sample comprises 17 clean, fat-free dry crania from adult specimens belonging to 17 extant crocodylian species. It represents all three living families (i.e. Crocodylidae, Alligatoridae and Gavialidae) and all genera (Table 1); thus this sample is considered to stand for the variability of skull morphology in the 24 extant species. All these crania were selected for belonging to specimens that had at least reached their sexual maturity size so that their comparison was not biased by ontogenetical variability. Fourteen of these specimens are from the collections of comparative anatomy of the Muséum National d'Histoire Naturelle (MNHN, Paris, France). Additionally, three other skulls were downloaded (*Tomistoma schelegelii* TMM M-6342, *Crocodylus johnstoni* TMM M-6807, *Crocodylus moreletii* TMM M-4980) in STL-format from the Digimorph data-base (http://digimorph.org) Rowe (2002). These three scans were made along the coronal axis by recombination of slices the thickness of which is under 0.5 mm for the two largest skulls (*T. schlegelii* and *C. moreletii*), and under 0.25 mm for *C. johnstoni*. Slice spacing is equal to slice thickness in each case. The resolution of these scans is sufficient for measuring the gain in area due to ornamentation. Because precise body lengths were not available in the collection databases, these data had to be estimated by measuring the dorsal cranial length of each cranium (DCL), and multiplying it by 7.5 (according to Schmidt, 1944; Wermuth, 1964; Bellairs, 1969), in order to assess the full size of the body. Then, estimated sizes were compared with acknowledged specific references (Schmidt & Inger, 1957; Trutnau & Sommerlad, 2006).

Data acquisition

Geometric morphometrics (GM)

In order to accurately capture skull morphology of each skull, 33 landmarks were set on each specimen. The authors referred to Pierce et al. (2008) to lay an initial set of 28 landmarks on the left half of skull roof, and this set was completed with an extra series of five landmarks on the left palatal surface, in order to obtain a 3D reconstruction (Fig. 1). For the 14 skulls that belong to the MNHN collections, the landmarks on the specimens were directly set using a Microscribe (MUS 5.1 Revware system). For the three virtual specimens, the 'landmark' software [landmark version 3.0.0.6 copyright © 2002–2005 by Institute for Data Analysis and Visualization (IDAV) all rights reserved David Wiley] was used to lay the 33 landmarks on the skulls.

Measuring the gain in area due to ornamentation

The 14 crania from the MNHN collections were scanned with a Breuckmann StereoScan 3D-surface scanner, a device that reconstructs 3D topography using phase contrast. The surface of the bones is virtually reconstructed as a meshwork of adjacent polygons, folded according to bone reliefs inside a 3D space. Three

Table 1 List and systematics of the specimens.

Family	Genus	Species	Author	Year	Collection number
Gavialidae	*Gavialis*	*gangeticus*	Gmelin	1789	MNHN-1944-249
Crocodylidae	*Crocodylus*	*niloticus*	Laurenti	1768	MNHN-A5307
Crocodylidae	*Crocodylus*	*moreletii*	Duméril& Bibron	1851	TMM M-4980
Crocodylidae	*Crocodylus*	*rhombifer*	Cuvier	1807	MNHN-1949-421
Crocodylidae	*Crocodylus*	*acutus*	Cuvier	1807	MNHN-1944-266
Crocodylidae	*Crocodylus*	*intermedius*	Graves	1819	MNHN-1885-489
Crocodylidae	*Crocodylus*	*johnstoni*	Krefft	1873	TMM M-6807
Crocodylidae	*Crocodylus*	*porosus*	Schneider	1801	MNHN-A5316
Crocodylidae	*Crocodylus*	*palustris*	Lesson	1831	MNHN-1944-229
Crocodylidae	*Mecistops*	*cataphractus*	Gray	1847	MNHN-1928-01
Crocodylidae	*Tomistoma*	*schlegelii*	Müller	1838	TMM M-6342
Alligatoridae	*Alligator*	*mississippiensis*	Daudin	1802	MNHN-1919-127
Alligatoridae	*Caiman*	*crocodilus*	Linnaeus	1758	MNHN-1887-773
Alligatoridae	*Caiman*	*latirostris*	Daudin	1802	MNHN-A5305
Alligatoridae	*Melanosuchus*	*niger*	Spix	1825	MNHN-1900-112
Alligatoridae	*Paleosuchus*	*trigonatus*	Schneider	1801	MNHN-ZA-AC 2014-1

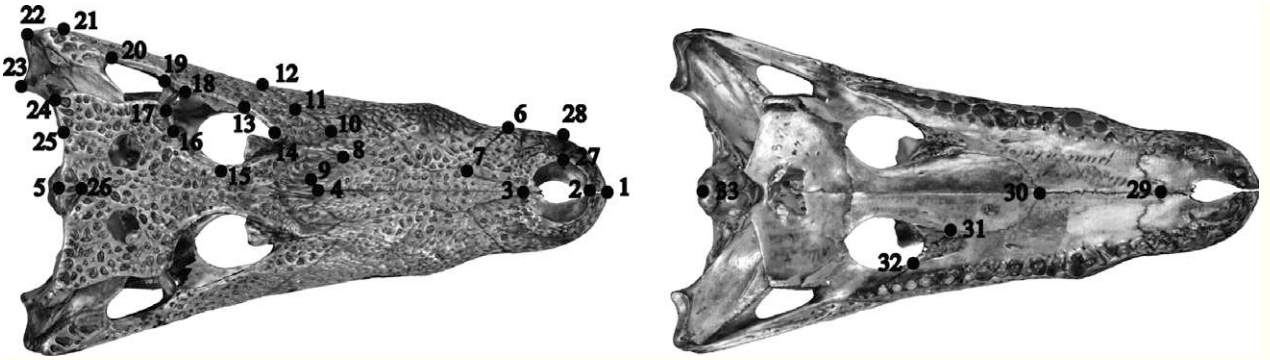

Fig. 1 Landmarks used in this analysis. 1: anterior tip of premaxillae contact; 2: posterior tip of premaxillae contact at the narial opening; 3: anterior tip of nasal bones (or contact of nasal-premaxilla); 4: nasal-nasal-frontal contact; 5: posterior midline of supraoccipital; 6: premaxilla-maxilla contact at lateral margin; 7: premaxilla-nasal-maxilla contact; 8: maxilla-nasal-prefrontal contact; 9: nasal-frontal-prefrontal contact; 10: maxilla-prefrontal-lachrymal contact; 11: maxilla-lachrymal-jugal contact; 12: maxilla-jugal contact along lateral margin; 13: jugal-lachrymal-orbit contact; 14: lachrymal-prefrontal contact at orbit; 15: prefrontal-frontal-orbit contact; 16: frontal-postorbital-orbit contact; 17: anterodorsal tip of postorbital bar; 18: anteroventral tip of postorbital bar; 19: posteroventral tip of postorbital bar; 20: jugal-quadratojugal-contact at infratemporal fenestra; 21: jugal-quadratojugal contact along lateral margin; 22: quadratojugal-quadrate contact along lateral margin; 23: medial condyle of quadrate; 24: posterolateral tip of squamosal (wing); 25: parietal-squamosal contact along posterior margin; 26: lateral contact of parietal-supraoccipital; 27: midlateral margin of external narial opening; 28: point on lateral margin of premaxilla corresponding to the mid-lateral margin of the external narial opening; 29: palatal contact of the premaxilla and the maxilla; 30: palatine-maxilla contact; 31: palatine-maxilla-palatine fenestra contact; 32: maxilla-ectopterygoid-palatine fenestra contact; 33: median posterior-most tip of the occipital condyle.

scope ranges were used, depending on sample size, to obtain adequate mesh resolutions: small scope range (60 mm), resolution: 12 μm; medium scope range (250 mm), resolution: 18 μm; large scope range (720 mm), resolution: 22 μm. The 14 3D-objects thus obtained were exported in PLY-format. Imperfections of the mesh (noise, artifacts, self-interactions, etc.), when present, were corrected using Geomagic Studio 2012* cleaning tools (*Geomagic Worldwide Headquarters 430 Davis drive, Marisville, NC 27560, USA).

Quantifying the gain in area due to ornamentation basically involves measuring the real area of the ornamented surface of bones with all its deep (pits) and protruding reliefs (ridges), and comparing it with a theoretical smooth area that would exist in the absence of ornamentation. Both these measurements were made with a dedicated tool in Geomagic studio 12, a software that was also used to obtain the smooth surface after converting the scans into PLY-format. The successive stages of this process have already been defined, tested and validated in a previous study (Clarac et al. 2015). This method was also applied to the scans downloaded from the Digimorph data-base. Finally, this surface analysis lead to the acquisition of three continuous variables that define the gain in area on the two anatomical regions of interest, i.e. skull table (representative of the orbital and postorbital part of the cranium) and right nasal (representative of the snout). These variables are as follows.

GAtot: the gain in area on the total surface of a bone (in percentage).
GApit: the local area gain at the level of the pits (i.e. the actual ornamented surface). It reflects the local basic enlargement of bone area due to pit concavity.
OArelat: the ratio of the area of the whole set of pits (in projection on the smooth surface), to the whole area of a bone after smoothing.

According to the location of the measurements, these variables have the indices 't', for cranial table, or 'n' for the right nasal (e.g. $GAtot_t$ ot $GAtot_n$, etc.).

Analyses

In order to test if the three variables that define the gain in area due to ornamentation (GAtot, GApit, OArelat) on both anatomical regions (skull table, snout) are correlated with skull morphology, a PGLS analysis was used (phylogenetic generalized least-squares; Grafen, 1989; R Development Core Team, 2012). This comparative phylogenetic analysis was set up using successively morphological and molecular time-scaled phylogenies of crown-Crocodylia (Brochu, 2003; Janke et al. 2006; McAliley et al. 2006; Oaks, 2011; Erickson et al. 2012; Piras et al. 2014). As GM dissociates *de facto* size from conformation, the correlation between the centroid size of the sampled specimens with the six variables that define ornamentation both on the skull table and on the snout ($GAtot_t$, $GAtot_n$, $GApit_t$, $GApit_n$, $OArelat_t$, $OArelat_n$) could be tested using the PGLS (Table 2). Then, in order to plot the diversity of skull conformations within the sample, a principal component analysis (PCA) was performed (Fig. 2). Thus, the correlation of the two main axes of the PCA (using their scores) with the six variables that define ornamentation could be tested. When the correlations between the PCA scores and the ornamentation variables were significant, a two-block partial least-squares (2B-PLS) was performed using these variables with the purpose of visualizing how ornamentation may covariate with the morphology of each region of the skull. Indeed, this approach finds the linear combinations that maximize the co-variation between the two sets of variables, here skull ornamentation and skull morphology in order to analyze the covariance between two data sets (Rohlf & Corti, 2000). Finally, in the purpose of picturing the evolution of these morphology-correlated variables that define ornamentation, they were mapped on the two phylogenies (both morphological and molecular data-based; Piras et al. 2014) that were previously used for the PGLS. In this purpose, Mesquite was used (Maddison & Maddison, 2011), a software that permits to optimize the features using the maximum of

Table 2 Correlation between the centroid size of the skulls and the variables that define ornamentation on the skull table and on the nasal using PGLS.

	Dependent (response) variable*	Phylogeny	Degrees of freedom	R^2	Intercept	Slope	*P*-value
Skull table	GAtot	Morphological	15	0.0187	13.647	0.0023	0.6007
		Molecular	15	0.0187	13.647	0.0023	0.6007
	GApit	Morphological	15	0.0005	1.284	−0.00001	0.9299
		Molecular	15	0.0009	1.286	0.00001	0.9081
	OArelat	Morphological	15	0.0644	0.588	−8.7e-05	0.3257
		Molecular	15	0.0644	0.588	−8.7e-05	0.3257
Nasal	GAtot	Morphological	15	0.1155	2.925	0.0071	0.1820
		Molecular	15	0.1155	2.924	0.0071	0.1820
	GApit	**Morphological**	15	0.5742	0.106	**0.0008**	**0.0004*****
		Molecular	15	0.2215	0.471	0.0005	0.0565
	OArelat	Morphological	15	1.9e-05	0.484	−3.2e-06	0.9867
		Molecular	15	1.9e-05	0.484	−3.2e-06	0.9867

*Independent (explanatory) variable: centroid size.
****P* value lower than 5% (significant).

parsimony (least-squares) in order to display the evolution of bone ornamentation on a phylogeny.

Results

The two combined main axes of PCA explain 60.82% of the variability of skull morphology. The first axis of the PCA (PC1: 51.72%) clearly stands for the elongation of the snout from the broader forms (*Caiman latirostris*) to the slender ones (*Gavialis gangeticus*) and represents the majority of the variability (among crocodylian skulls), whereas the second axis (PC2) explains only 9.1% of the variability and does not seem to correspond to any particular morphological pattern.

The only significant correlation between centroid size and ornamentation concerns $GApit_n$ and is obtained only when using the phylogeny based on morphological data, or PGLS (Table 2). The results of the PGLS analyses between skull morphology (PCA) and ornamentation ($GAtot_t$, $GApit_t$, $OArelat_t$, $GAtot_n$, $GApit_n$, $OArelat_n$) show that only two regressions were significant: $GApit_n$ and $OArelat_n$ to PC1 (whether the morphological or the molecular phylogeny were used; Fig. 3). Therefore the 2B-PLS was performed using only these two variables, the result of which outlined that both $GApit_n$ and $OArelat_n$ negatively covariate with PC1 (Fig. 4). This result means that snout elongation comes with a decrease of pits depth and ornamentation extend on bone surface in this anatomical region. Furthermore, the mapping and the optimizing of $GApit_n$ and $OArelat_n$ on the phylogeny of Crocodylia shows that ornamentation loss on the nasal is a homoplastic trait in longirostrines whether the morphological or molecular data-based phylogeny of Crocodylia was used (Fig. 5). Conversely, neither pit depth nor ornamentation extend are ever modified on the skull table when skull morphology varies.

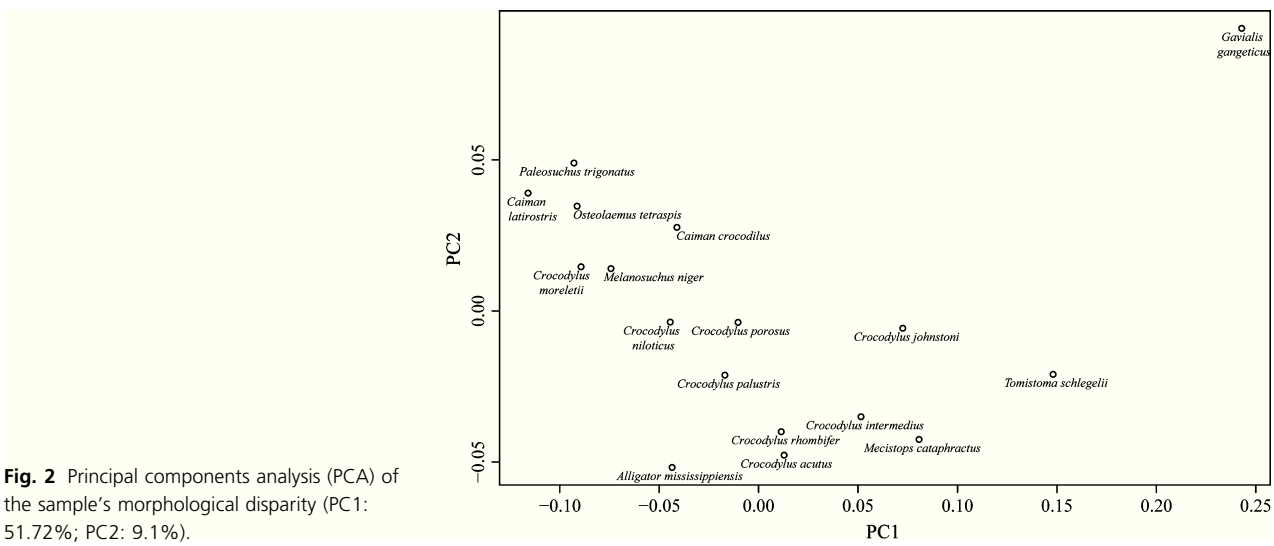

Fig. 2 Principal components analysis (PCA) of the sample's morphological disparity (PC1: 51.72%; PC2: 9.1%).

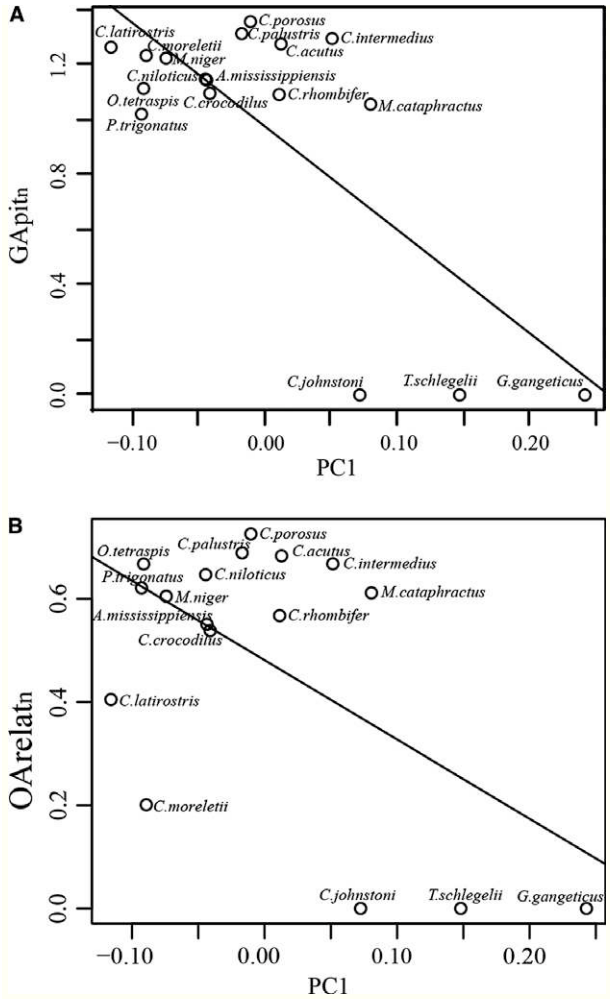

Fig. 3 Phylogenetic generalized least-square (PGLS). (A) $GApit_n$ is the variable that is aimed to be explained depending on PC1 using either molecular or morphological phylogeny (Piras et al. 2014). (B) $OArelat_n$ is the variable that is aimed to be explained depending on PC1 using either molecular or morphological phylogeny. The regression line is plotted on each figure.

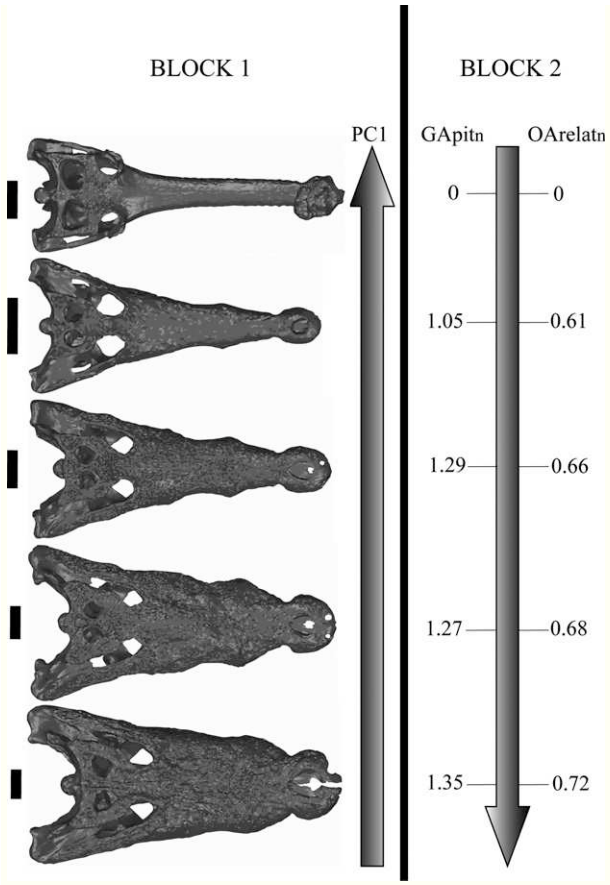

Fig. 4 Two-block partial least-squares (2B-PLS). Block 1 (on the left side): the skulls of specimens ranked along PC1 from the bottom to the top: *Crocodylus porosus*, *Crocodylus acutus*, *Crocodylus intermedius*, *Mecistops cataphractus*, *Gavialis gangeticus*; scale bar: 100 mm. Block 2 (on the right side): the values of $GApit_n$ and $OArelat_n$ that correspond to the skulls shown in Block 1 and that negatively covariate with PC1.

Discussion

A previous study assessing quantitatively the gain in area due to the ornamentation on the upper surface of dermal bones pointed out that: $GAtot_n$ and $GApit_n$ follow a Brownian motion (tests performed quantifying Pagel's Lambda), whereas all other variables do not (Clarac et al. 2015). This result means that only these two variables show a phylogenetic signal by evolving randomly, whereas the others remain stable and well maintained through natural selection. The same study also established that GAtot is strongly correlated to GApit and OArelat. Indeed, these last two variables directly influence GAtot as they represent, in general terms, the depth and form of the pits (GApit) and the relative area of the whole set of pits in projection on the whole smooth area of a bone (OArelat).

In this new study, $GApit_n$ is significantly correlated with the centroid size of the sampled skulls if the PGLS that is based on the morphological phylogeny is referred to. However, because the slope of the regression line is close to zero (slope: 0.0008; Table 2), it may be considered that the signification of this test is probably just an artifact. Indeed, all the other PGLS analyses give the same result whether the morphological or molecular data-based phylogeny is referred to. Therefore, it can be concluded that the size of the skull has no influence on the ornamentation in the Crocodylia.

Although the centroid size seems to have no influence on ornamentation, both $GApit_n$ and $OArelat_n$ appear to be correlated with snout shape. This result suggests that snout elongation influences both the depth (i.e. the excavation process) of the pits and the relative area that they occupy on snout bones, represented here by the nasal. Indeed, the 2B-PLS has shown that both these variables negatively covariate with PC1, which is the PC axis that stands for the

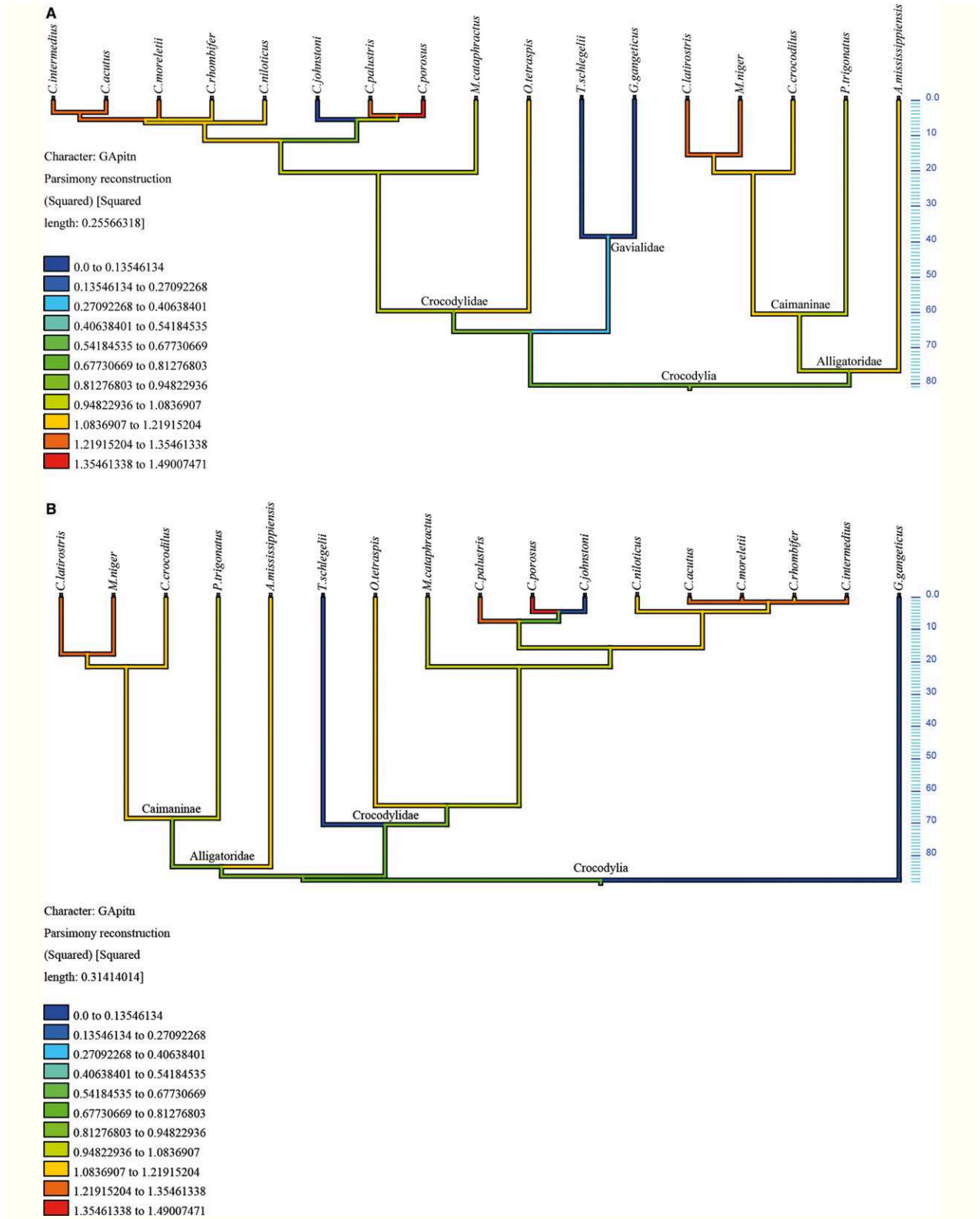

Fig. 5 Optimization of $GApit_n$ and $OArelat_n$ on the phylogeny of Crocodylia using parsimony reconstruction (least-squares). (A) Optimization of $GApit_n$ on a molecular phylogeny (Piras et al. 2014). (B) Optimization of $GApit_n$ on a morphological phylogeny (Piras et al. 2014). (C) Optimization of $OArelat_n$ on a molecular phylogeny. (D) Optimization of $OArelat_n$ on a morphological phylogeny. The molecular phylogeny used here is based on the one figured by Piras et al. (2014); the authors acknowledge that most molecular analyses support a closer relationship between *Osteolaemus* and *Mecistops* (McAliley et al. 2006; Oaks, 2011), but changing the tree to reflect this relationship does not change the overall results of the current study.

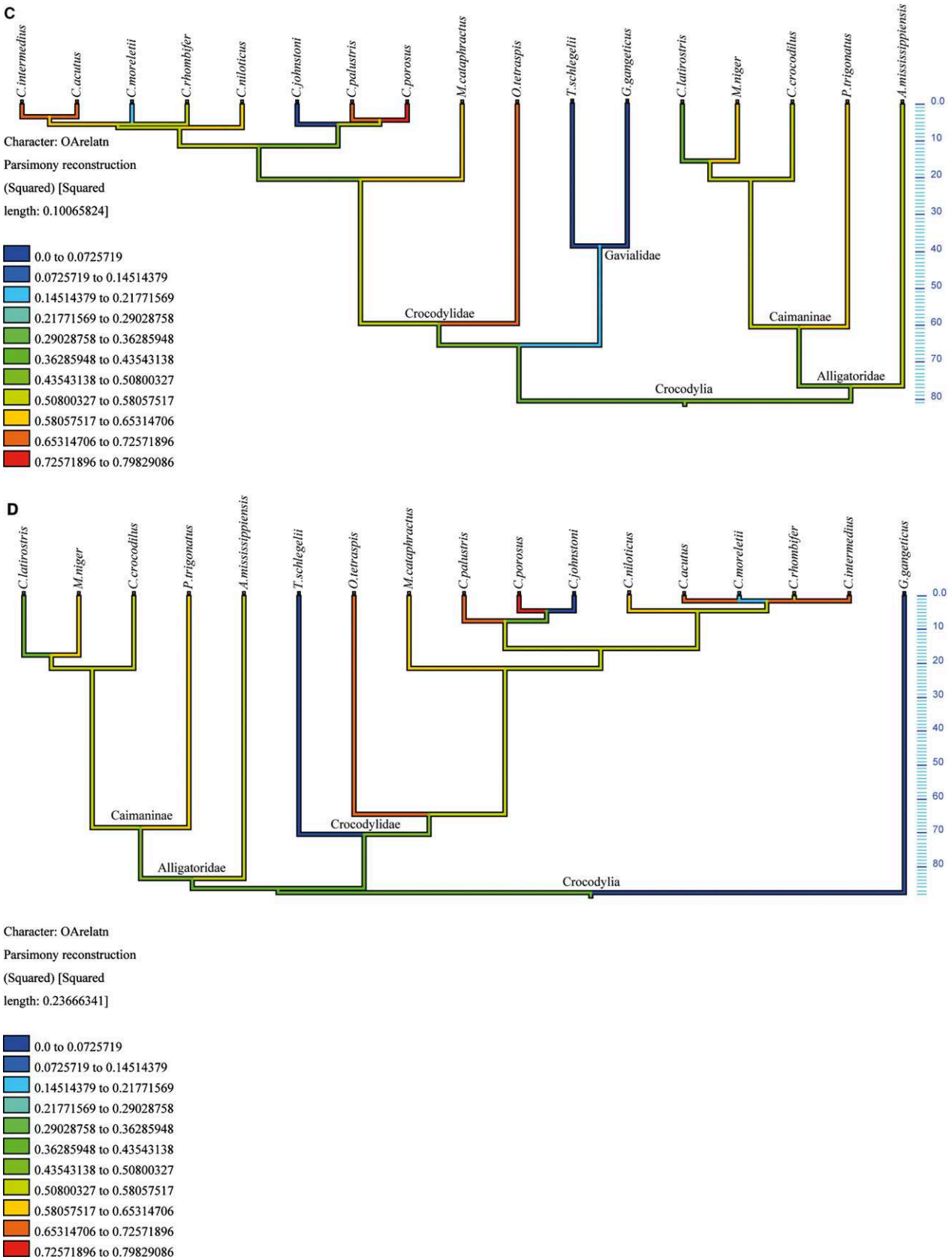

Fig. 5 Continued

elongation of the snout from the broadest forms (*Caiman latirostris*) to the most slender (*Gavialis gangeticus*). Even if $GAtot_n$ is not directly correlated with PC1, it is however obvious that it remains indirectly dependent on the elongation of the snout, as GAtot is strongly correlated with both GApit and OArelat (Clarac et al. 2015), two variables that are themselves correlated with PC1. For instance, $GAtot_n$ reaches zero in the typical slender-snouted forms (*Gavialis gangeticus*, *Tomistoma schlegelii*, *Crocodylus johnstoni*) as both $GApit_n$ and $OArelat_n$ are zero in the skulls displaying this morphology (Table 3).

Even if molecular phylogenies indicate that *Tomistoma schlegelii* and *Gavialis gangeticus* form a monophyletic taxon within the Crocodylia, it is nevertheless obvious that snout elongation is an homoplastic character not only within the Crocodylia (Fig. 5), but also within the Crocodylomorpha (Teleosauridae, Dyrosauridae, Pholidosauridae; Kälin, 1955) and probably the Archosauromorpha as a whole (assuming that Phytosauria is the sister group of Archosauria, according to Nesbitt, 2011). In the current data-set, $GApit_n$ is the only variable that is correlated to snout shape and that follows a Brownian motion (see also Clarac et al. 2015). Therefore, it can be assumed that pit depth on the snout evolved randomly while following a high rate of evolution and a low pressure of selection during crocodylian evolutionary history.

According to Iordansky (1973), long-snouted crocodylians are well adapted to fishing as the elongation of the snout would be an adaption for catching swimming-prey. Besides, as the functional role of bone ornamentation remains controversial and non-elucidated, it would be a significant advance to find out why long-snouted forms tend to lose ornamentation in the rostral part of their skulls whereas they keep it on the skull table. Nevertheless, in order to discuss this particularity, all extreme longirostrines must be considered for, like *Gavialis gangeticus* and most Teleosauridae (Hua, 1997; Pierce et al. 2009) that the surface of the skull table available to pit development is very low because the upper temporal fenestrae occupy the largest area thus limiting the ornamented bone expansion.

Long-snouted crocodylians withstand higher mechanical stress during feeding than short-snouted forms (Pierce et al. 2008). This mechanical stress is more pronounced in the anterior part of the snout of *Gavialis gangeticus*, opposite to the situation in all other species. It would therefore be quite surprising that the functional signification of ornamentation should be to increase bone strengthening (Coldiron, 1974). Conversely, the relative stability of bone ornamentation on the skull table in all taxa agrees with a possible role in thermoregulation, i.e. heat captation while basking (Seidel, 1979). Indeed, the skull table is more elevated than the snout and is thus more exposed to sun rays when crocodylians are partly submerged, because the development of postorbital bars lifted the skull table in modern semi-aquatic forms (Iordansky, 1973). Notwithstanding, in order to deal with this last functional assumption, the fact that the current results show that none of the variables defining area gain on both the skull table and the nasal is correlated to the size of the skull should be considered. Indeed, because heat exchange is based on the ratio

Table 3 List of the quantitative values for all specimens; Max: highest value; Min: lowest value.

Species	$GAtot_t$ (%)	$GApit_t$	$OArelat_t$	$GAtot_n$ (%)	$GApit_n$	$OArelat_n$
C.acutus	16.88	1.26	0.59	17.98	1.27	0.68
C.intermedius	25.45	1.49	0.49	17.67	1.29	0.66
C.johnstoni	6.58	1.52	0.39	0	0	0
C.moreletii	16.47	1.80	0.20	4.65	1.23	0.20
C.niloticus	10.92	1.18	0.48	7.68	1.14	0.64
C.palustris	31.90	1.47	0.66	20.44	1.31	0.68
C.porosus	13.68	1.22	0.50	23.59	1.35	0.72
C.rhombifer	15.13	1.26	0.48	4.58	1.09	0.56
M.cataphractus	17.89	1.21	0.64	3.20	1.05	0.61
O.tetraspis	16.46	1.18	0.66	6.00	1.11	0.66
T.schlegelii	11.59	1.22	0.51	0	0	0
G.gangeticus	10.20	1.10	0.45	0	0	0
A mississippiensis	10.20	1.10	0.49	6.66	1.14	0.55
C.crocodilus	14.08	1.22	0.59	5.93	1.09	0.53
C.latirostris	10.67	1.26	0.40	10.59	1.26	0.40
M.niger	16.88	1.25	0.49	12.25	1.22	0.60
P. trigonatus	20.32	1.23	0.68	7.28	1.01	0.62
Mean	14.22	1.26	0.50	7.52	0.94	0.45
Median	14.08	1.22	0.49	5.93	1.11	0.55
Max	31.90	1.80	0.68	23.59	1.35	0.72
Min	3.26	1.06	0.20	0	0	0

between the surface and the volume of the animal, the gain in area (GAtot) would be expected to be positively correlated to the size of the species. Thus, if ornamentation is involved in heat captation, it would likely be for providing a support to a vascular network on the surface of the outer cortex (Seidel, 1979; Farlow et al. 2010) than to directly increase the ratio between the surface and the volume of the whole body.

As the current results show that only $GApit_n$ and $OArelat_n$ are influenced by snout elongation, it is possible that the depth of the pits is antagonistic with the local growth rate of each bone. Indeed, pits are always drifted and remodeled during lifetime through a dynamic process of resorption followed by secondary reconstruction (de Buffrénil, 1982; de Buffrénil et al. 2015). This process might become extreme on the nasal of large long-snouted forms because this part of the skull has particularly high growth rates. Bone resorption would then be minor in regard to longitudinal drift and/or the secondary bone deposit in the pits. This local growth would then interfere with the basic functional role of ornamentation, whatever this role might be.

Conclusion

Although the functional signification of bone ornamentation remains a matter of conjecture, it is noticeable that its expression on the skull is never influenced by the size of the species. Conversely, skull shape influences the expression of its ornamentation, mainly on the rostral region. The expression of bone ornamentation on the skull table appears to be relatively stable and independent of phylogenetic frames and morphological disparity, whereas on the nasal it shows high plasticity in parallel with relative snout development. It can then be supposed that there may be a developmental constraint limiting the excavating of the pits on the snout of slender-snouted forms. The possible functional implication of bone ornamentation might consequently be restricted to some anatomical regions (skull table and osteoderms) at least among the longirostrine forms.

Acknowledgements

The authors thank the PPF UPMC-Biominéralisations for the acquisition of the Microscribe system (MUS 5.1 Revware system) used in this work to perform landmark acquisition. The authors would like to address their respectful acknowledgements to Jonathan R. Wagner (University of Texas) for providing information about the use of Digimorph. The authors also would like to thank Salvador Bailon for giving them access to the comparative anatomy collections of the MNHN. Finally, the authors would like to thank the UMS 2700 (MNHN/CNRS) for the access to the 3D scanner.

Authors' contributions

François Clarac created the dataset by scanning 14 specimens, analyzed all the scans, set the landmarks and synthesized all the results. Thibaud Souter and Raphaël Cornette were chiefly involved in the technical aspects of data acquisition and in the processing of morphometric analyses. Jorge Cubo contributed to PGLS analyses and final writing of the manuscript. Christopher Brochu provided three extra scanned specimens and brought his advice on crocodylians' phylogenetic nomenclature. The whole project was supervised by Vivian de Buffrénil.

References

Bellairs A (1969) The Life of Reptiles, Vol. 2. London: Weidenfeld G., Nicolson N.

Blanco RE, Jones WW, Villamil J (2014) The "death roll" of giant fossil crocodyliforms (Crocodylomorpha: Neosuchia): allometric and skull strength analysis. *Hist Biol* **2963**, 1–11.

Blanco MVF, Bona P, Olivares AI, Desojo JB (2015) Ontogenetic variation in the skulls of Caiman: Caiman latirostris and Caiman yacare (Alligatoridae, Caimainanae). *Herpetol J* **25**(2), 65–73.

Brochu CA (2003) Phylogenetic approaches toward crocodilian history. *Annu Rev Earth Planet Sci* **31**, 357–397.

de Buffrénil V (1982) Morphogenesis of bone ornamentation in extant and extinct crocodilians. *Zoomorphology* **99**, 155–166.

de Buffrénil V, Clarac F, Fau M, et al. (2015) Differentiation and growth of bone ornamentation in vertebrates: a comparative histological study among the Crocodylomorpha. *J Morphol* **276**, 425–445.

Bystrow AP (1935) Morphologische untersuchungen der deckknochendes schadels der stegocephalen. 1. Mitteilung. Schadel der stegocephalen. *Acta Zool* **16**, 65–141.

Bystrow AP (1947) Hydrophilous and xerophilous labyrinthodonts. *Acta Zool* **28**, 137–164.

Clarac F, Souter T, Cornette R, et al. (2015) A quantitative assessment of bone area increase due to ornamentation in the Crocodylia. *J Morphol* **276**, 1183–1192.

Coldiron RW (1974) Possible functions of ornament in the labyrinthodont amphibians. *Occ Pap Mus Nat Hist Kansas* **33**, 1–19.

Erickson GM, Gignac PM, Steppan SJ, et al. (2012) Insights into the ecology and evolutionary success of crocodilians revealed through bite-force and tooth-pressure experimentation. *PLoS ONE* **7**, e31781.

Farlow JO, Hayashi S, Tattersall GJ (2010) Internal vascularity of the dermal plates of *Stegosaurus* (Ornithischia, Tyreophora). *Swiss J Geosci* **103**, 173–185.

Fernandez Blanco MV, Bona P, Olivares AI, et al. (2015) Ontogenetic variation in the skulls of *Caiman*: the case of *Caiman latirostris* and *Caiman yacare* (Alligatoridae, Caimaninae). *Herpetol J* **25**, 65–73.

Foth C, Bona P, Desojo JB (2015) Intraspecific variation in the skull morphology of the black caiman *Melanosuchus niger* (Alligatoridae, Caimaninae). *Acta Zool* **96**, 1–13.

Grafen A (1989) The phylogenetic regression. *Proc R Soc Lond B Biol Sci* **205**, 581–598.

Hua S (1997) *Adaptations des crocodiliens Mesosuchiens au milieu marin*. Unpublished PhD thesis, Université Paris 6, Paris, France, 209 pp.

Iordansky NN (1973) The skull of the Crocodilia. In: *Biology of the Reptilia*, Vol. 4. (ed. Gans C), pp. 201–262. London: Morphology D. Academic Press.

Janis CM, Devlin K, Warren DE, et al. (2012) Dermal bone in early tetrapods: a palaeophysiological hypothesis of adaptation for terrestrial acidosis. *Proc Biol Sci* **279**, 3035–3040.

Janke A, Gullberg A, Hughes S, et al. (2006) Mitogenomic analyses place the gharial (*Gavialis gangeticus*) on the crocodile tree and pro-vide pre-K/T divergence times for most crocodilians. *J Mol Evol* **61**, 620–626.

Kälin J (1955) Crocodilia. In: *Traité de Paléontologie*, Vol. 5. (ed. Piveteau J), pp. 695–784. Paris: Masson et Cie.

Lundberg JG, Aguilera O (2003) The late Miocene *Phractocephalus* catfish (Siluriformes: Pimelodidae) from Urumaco, Venezuela: additional specimens and reinterpretation as a distinct species. *Neotrop Ichthyol* **1**, 97–109.

Maddison WP, Maddison DR (2011) Mesquite: a modular system for evolutionary analysis. Version 2.75. Available at: http://mesquiteproject.org.

McAliley LR, Willis RE, Ray DA, et al. (2006) Are crocodiles really monophyletic? Evidence for subdivisions from sequence and morphological data. *J Mol Evol* **39**, 16–32.

Nesbitt SJ (2011) The early evolution of archosaurs: relationships and the origin of major clades. *Bull Am Mus Nat Hist* **352**, 1–292.

Oaks JR (2011) A time-calibrated species tree of crocodylia reveals a recent radiation of the true crocodiles. *Evolution* **65**, 3285–3297.

Pierce SE, Angielczyk KD, Rayfield EJ (2008) Patterns of morphospace occupation and mechanical performance in extant crocodilian skulls: a combined geometric morphometric and finite element modeling approach. *J Morphol* **269**, 840–864.

Pierce SE, Angielczyk KD, Rayfield EJ (2009) Shape and mechanics in thalattosuchian (Crocodylomorpha) skulls: implications for feeding behaviour and niche partitioning. *J Anat* **215**, 555–576.

Piras P, Teresi L, Buscalioni AD, et al. (2009) The shadow of forgotten ancestors differently constrains the fate of Alligatoroidea and Crocodyloidea. *Glob Ecol Biogeogr* **18**, 30–40.

Piras P, Colangelo P, Adams DC, et al. (2010) The *Gavialis-Tomistoma* debate: the contribution of skull ontogenetic allometry and growth trajectories to the study of crocodylian relationships. *Evol Dev* **12**, 568–579.

Piras P, Buscalioni AD, Teresi L, et al. (2014) Morphological integration and functional modularity in the crocodilian skull. *Int Zool* **9**, 498–516.

R Development Core Team (2012) *R: A Language and Environment for Statistical Computing*. Vienna: R Foundation for Statistical Computing.

Rinehart LF, Lucas SG (2013) The functional morphology of dermal bone ornamentation in temnospondyl amphibians. In: *The Triassic System*. (eds Tanner LH, Spielmann JA, Lucas SG). Albuquerque: *New Mex Mus Nat Hist Sci Bull* **61**, 524–532.

Rohlf FJ, Corti M (2000) Use of the two-block partial least-squares to study covariation in shape. *Syst Biol* **49**, 1–368.

Rowe T (2002) Digimorph: A National Science Foundation Digital Library at the University of Texas at Austin. http//:digimorph.org.

Scheyer TM, Sander PM, Joyce WG, et al. (2007) A plywood structure in the shell of fossil and living softshelled turtles (Trionychidae) and its evolutionary implications. *Org Divers Evol* **7**, 136–144.

Schmidt KP (1944) Crocodiles. *Fauna* **6**, 67–72.

Schmidt KP, Inger F (1957) Knaurs Tierreich in Farben. *Reptilien*. 312 pp. München: Droemersche Verlagsanstalt.

Seidel MR (1979) The osteoderms of the American alligator and their functional significance. *Herpetologica* **35**, 375–380.

Trutnau L, Sommerlad R (2006) Behavior of crocodilians. In: *Crocodilians their Natural History and Captive Husbandry*. (ed. Chimaira B), pp. 143–156. Andreas S. Bram: Franckfurt am Main.

Watanabe A, Slice DE (2014) The utility of cranial ontogeny for phylogenetic inference: a case study in crocodylians using geometric morphometrics. *J Evol Biol* **27**, 1078–1092.

Wermuth H (1964) Das Verhältnis zwischen Kopf, Rumpf und Schwanzlänge bei den rezenten Krokodilen. *Senckenb Biol* **45**, 369–385.

Witzmann F, Soler-Gijon R (2010) The bone histology of osteoderms in temnospondyl amphibians and in the chroniosuchian *Bystrowiella*. *Acta Zool* **91**, 96–114.

CHAPITRE 3: L'EVOLUTION DE L'ORNEMENTATION CHEZ LES PSEUDOSUCHIENS: CONTRAINTES HISTORIQUES ET MORPHOLOGIQUES VERSUS ADAPTATIONS ECOLOGIQUES

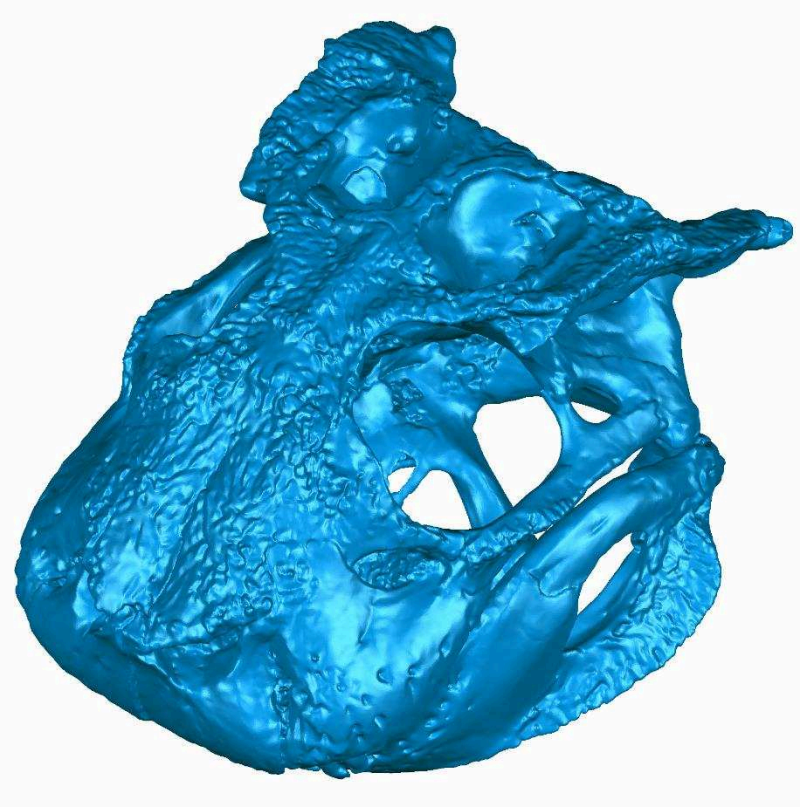

Simosuchus clarki

(Crétacé supérieur, Madagascar, reconstruction surfacique par tomographie 3D)

Biological Journal of the Linnean Society, 2017, **121**, 395–408. With 5 figures.

The evolution of bone ornamentation in Pseudosuchia: morphological constraints versus ecological adaptation

F. CLARAC[1–3*], V. DE BUFFRÉNIL[3], C. BROCHU[4] and J. CUBO[1,2]

[1]*Sorbonne Universités, UPMC Univ Paris 06, UMR 7193, Institut des Sciences de la Terre Paris (ISTeP), 4 place Jussieu, BC 19, F-75005 Paris, France*
[2]*CNRS, UMR 7193, Institut des Sciences de la Terre Paris (ISTeP), 4 place Jussieu, BC 19, F-75005 Paris, France*
[3]*Département Histoire de la Terre, Museum National d'Histoire Naturelle, UMR 7207 (CR2P), Sorbonne Universités, MNHN / CNRS / UPMC, Bâtiment de Géologie Paris Cedex 05, F-75231 Paris, France*
[4]*Department of Earth and Environmental Sciences, University of Iowa, Iowa City, IA 52242, USA*

Received 25 August 2016; revised 22 November 2016; accepted for publication 7 December 2016

Although frequent in vertebrates (e.g. crocodylians, stem-tetrapods, turtles), the adaptive significance of bone ornamentation, that is the honeycomb-like pattern of pits and ridges that occur on the surface of dermal bones, remains poorly understood. In order to help assess the evolutionary history and ecological correlates of this character, ornamentation was quantified in 69 extant and extinct Pseudosuchia (taxa more closely related to crocodiles than to birds). This variable was related to the dominant habitat (terrestrial, amphibious, pelagic) of these taxa within a phylogenetic framework covering more than 250 Myr of evolution. The phylogenetic analyses reveal a significant correlation between the degree of bone ornamentation on the skull roof with lifestyle (terrestrial, amphibious, pelagic). A straightforward adaptive interpretation of these results is to be avoided because skull morphology has recently been shown to strongly influence local development of bone ornamentation in Crocodylia. Indeed, ornamentation in long-snouted amphibious forms scores low or nil values on the skull roof while scoring very high values on osteoderms. Our results also show that amphibious forms, whether marine or fluvial, have a high degree of ornamentation, whereas terrestrial and pelagic forms are either not ornamented or have a low level of ornamentation. It is hypothesized that the high development of ornamentation among semi-aquatic pseudosuchians has been positively selected because it improves basking efficiency in semi-aquatic ambush (i.e. poorly active) predators. This process would have occurred at the Triassic-Jurassic boundary.

ADDITIONAL KEYWORDS: crocodylians – dermal bones – lifestyle – paleoecology – skull.

INTRODUCTION

Crocodylians display some of the best examples of pit-and-ridge bone ornamentation, a characteristic that also occurs on the dermal bones of numerous other extant and extinct vertebrates including stem tetrapods and turtles (Bystrow, 1935; Scheyer *et al.*, 2007; Witzmann & Soler-Gijon, 2010). Recently, three-dimensional analyses of bone surface showed that crocodylian ornamentation results in a gain in area due to both the depth of the pits and their relative extent over the cranial bones or osteoderms (Clarac *et al.*, 2015). Typically, this gain is higher on the skull table and osteoderms than on the nasal, where it is negatively influenced by the relative elongation of the snout (Clarac *et al.*, 2016).

Previous studies were mainly based on a sample of extant crocodylians which are all semi-aquatic and well ornamented (Iordansky, 1973). However, from the Triassic through the Eocene (Kälin, 1955), pseudosuchians were adapted to a broader range of habitat types and lifestyles that seem to have been correlated with distinct ornamentation patterns. For instance, the Mesozoic pelagic metriorhynchids had entirely lost the dermal shield and cranial ornamentation (Buffetaut, 1982). Similarly, ornamentation was faint and made of sparse and shallow pits on the skull and osteoderms of early terrestrial forms such as *Protosuchus*

*Corresponding author. E-mail: fclarac@mnhn.fr

richardsoni (Kälin, 1955) and later land-dwelling taxa such as the notosuchian *Simosuchus clarki* (Hill, 2010; Kley *et al.*, 2010a&b).

Although the functional significance of ornamentation remains to be ascertained, we aim to test in a phylogenetic context whether the morphological variables that define ornamentation on homologous anatomical regions, such as the skull table or the dorsal rostral surface, are correlated with pseudosuchian lifestyles over 250 million years of evolution. Correlations between bone ornamentation and ecology would give some insight on the possible adaptive (i.e. functional) significance of bone ornamentation and thus provide a basis for inferring the lifestyle of extinct pseudosuchians.

MATERIAL AND METHODS

Biological sample

Our total sample consists of the skulls of 69 adult and subadult pseudosuchians from 69 extant or extinct species, spanning in geological age from the Triassic to the present. First-hand quantifications of bone ornamentation, according to the methodology proposed by Clarac *et al.* (2015), were conducted on 42 ornamented skulls (Annex 1). We then added data for the remaining 27 skulls lacking ornamentation, using published references that describe specimens with a well-preserved dermatocranium (Annex 1, 2A). The institutions to which specimens belong are the following: MNHN: Muséum National d'Histoire Naturelle (Paris, France), AMNH: American Museum of Natural History (NY, USA), USNM: National Museum of Natural History Smithsonian Institution (Washington DC, USA), SAM: South-Africa Museum (Cape Town, South-Africa), NM: National Museum (Bloemfontein, South Africa), TMM: Texas Memorial Museum, University of Texas (Austin, USA), UA: University of Antananarivo (Madagascar).

Three-dimensional modelling

In our sample, the 16 modern skulls from the MNHN collections and *Araripesuchus wegeneri* (MNN GAD-19) were scanned with a Breuckmann StereoScan three dimensional (3D) surface scanner, which reconstructs three-dimensional topography using phase contrast. Bone surfaces are virtually reconstructed as a meshwork of adjacent polygons, folded according to bone reliefs inside a 3D space. We used two scope ranges, depending on sample size, to obtain adequate mesh resolutions: medium scope range (250 mm), with an 18 µm resolution, and large scope range (720 mm), with a 22 µm resolution. The 17 three-dimension objects thus obtained were exported in PLY-format. Imperfections of the mesh (noise, artefacts, self-interactions, etc.), when present, were corrected using Geomagic Studio 2012* cleaning tools (*Geomagic Worldwide Headquarters 430 Davis drive, Marisville, NC 27560, USA). We downloaded CT images for five additional skulls (*Tomistoma schelegelii* TMM M-6342, *Crocodylus johnstoni* TMM M-6807, *Crocodylus moreletii* TMM M-4980, *Calsoyasuchus valliceps* TMM 43631-1, *Simosuchus clarki* UA 8679) in STL-format from the Digimorph data base (http://digimorph.org; Rowe, 2002) to increase the above sample. These scans were made parallel to the coronal plane by reconstruction of slices with thicknesses less than 0.5 mm for the two largest skulls (*T. schleglii* and *C. moreletii*), less than 0.25 mm for *C. johnstoni*, less than 0.13 mm for *S. clarki* and less than 1 mm for *C. valliceps*. Slice spacing is equal to slice thickness in each case. Resolution of these scans was sufficient for measuring gain in area due to ornamentation. Finally, the skulls that belong neither to the MNHN collection nor to the Digimorph database were modelled through standardized three-dimensional photogrammetric reconstruction.

Because the Stereoscan equipment is heavy and requires a stable surface, specimens in some collections (e.g. AMNH and USNM) could not be scanned. For these, we used a portable device designed for taking a series of photographs of each skull under various, repeatable angles (Fig. 1). We used a Canon 60D camera equipped with a Canon 60 mm/2 macroobjective and Canon Speedlite 320EX flash. Camera sensitivity was set to 100 ISO, objective aperture set to 16, and exposure time set automatically by the camera in order to get clear shots. The goal was to let fix the camera in a position aimed at the object (target), which would rotate as if we used a Stereoscan 3D surface scanner (Fig. 1). Each skull was laid vertically on its occipital surface to align its sagittal axis with the centre of a rotating pad which was centred on an unmovable 360° graduated plastic sheet. Each specimen was then photographed every 10° while turning on itself along three separated 36 shot series: the first series was shot with the camera set at low vertical position on a tripod aimed at the skull table (Fig. 1A) and the two others were shot by lifting up the camera vertically into a higher position to point consecutively at the interorbital region (Fig. 1B) and the tip of the snout (Fig. 1C; pitch, roll and yaw of the shooting axis were nil in all series). In each case, the distance between the camera and object was set so that the region of interest took the full size of the field for better definition. Finally, we took a last series of 36 pictures of the entire skull by laying it on a side and by increasing the distance between the camera and the object (Fig. 1D). The purpose of this extra last shot series was to get a 3D reconstruction of one full skull per specimen after recombining all the pictures together. Indeed, the 3D model was generated automatically for each specimen after uploading the 144 pictures in jpeg format into Agisoft Photoscan Professional Version:

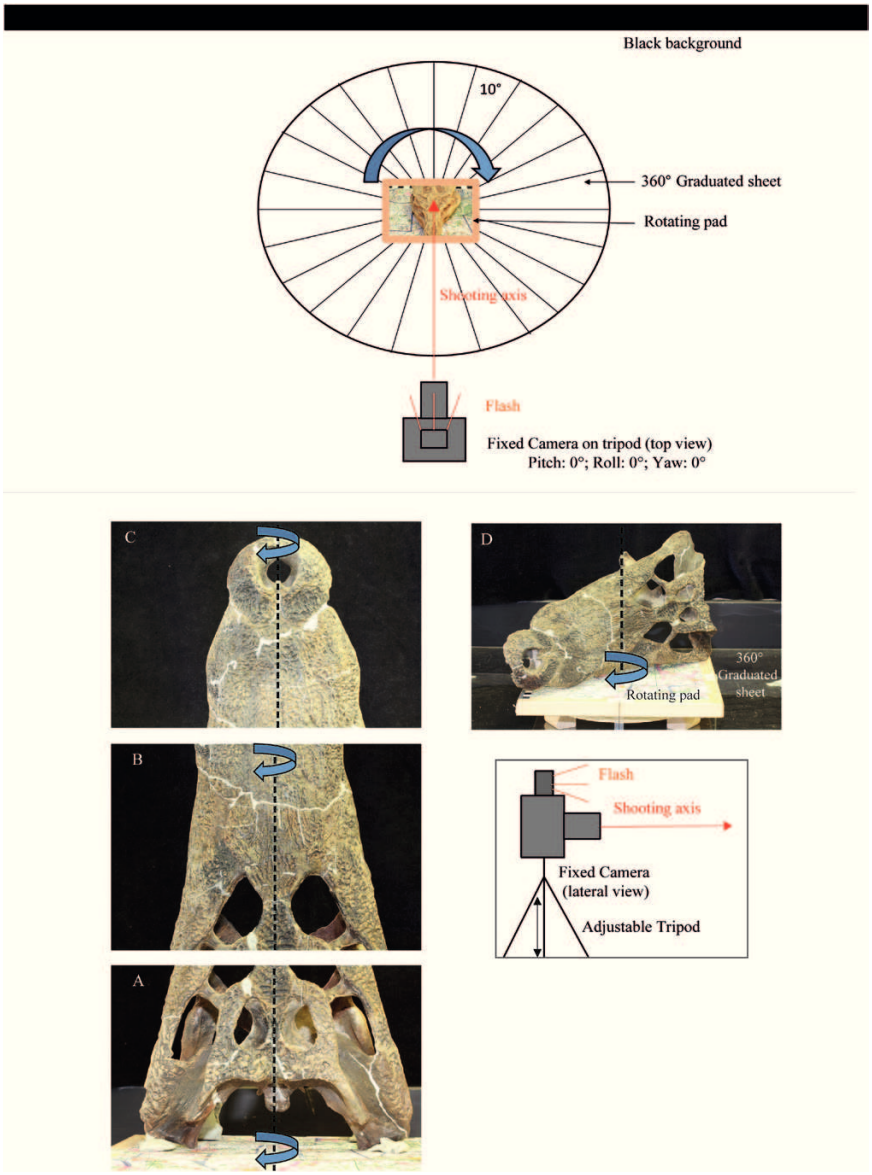

Figure 1. Photogrammetry technics. Each picture stands for the point of view from which each of the four shot-series has been taken. (A) targeting the skull table; (B): targeting the interorbital; (C): targeting the snout; (D): targeting the full skull. *When the specimen was too fragile to be layed vertically (for some fossils), we let it on the palatal side. We then pitched down the camera under an angle of 45° and we proceeded to the four series while setting the full skull (D) and each region of interest (A, B, C) at the center of the rotating pad.

1.1.4. This process involves four consecutive stages: aligning pictures, creating a dense cloud, meshworking and building a surface texture. Pictures partially blurred by short field depth were manually deleted as all pictures were previously checked one by one before the automatic alignment. Since this method had never been used previously for biological morphometry, we tested it on specimens that we had previously scanned with the Breuckmann Stereoscan 3D-surface scanner (*C. niloticus* and *Paleosuchus trigonatus*) and measured the ornamentation again (see below for methodology). The newly obtained values were similar within the experimental error. Thus, we can assume that the precision of this photogrammetry method is accurate enough.

Measuring the gain in area due to ornamentation

Quantifying the gain in area due to ornamentation involves comparing the measured area of the ornamented surface of bones, including deep (pits) and

protruding (ridges) relief, with a theoretical smooth area that would exist in the absence of ornamentation (Clarac *et al.*, 2015). This surface analysis results in the acquisition of three continuous variables that define the gain in area on the two anatomical regions of interest, that is skull table and right nasal (these two anatomical regions have been selected as they are, respectively, representative of the posterior and of the anterior part of the skull; Clarac *et al.*, 2015). The defined variables are:

- GAtot: gain in area, expressed in percent, on the total surface of an individual bone (nasal) or a bone region (cranial table) that is due to ornamentation.
- GApit: local area gain at the level of the pits themselves (i.e. the actual ornamented surface). It quantifies the basic enlargement of bone area that occurs locally due to pit concavity and results from a combination of the depth and three-dimensional shape of the pits.
- OArelat: relative area of the whole set of pits (in projection on the smooth surface) relative to the whole area of a bone after smoothing.

These variables have the indices t for cranial table or n for the right nasal (e.g. $GAtot_t$, $GAtot_n$).

Statistical analyses

We first tested whether the variables used to quantify ornamentation contain a significant phylogenetic signal. For this, we used Pagel's λ (Pagel, 1999) and Blomberg's *K* (Blomberg & Garland, 2002). Evolutionary patterns were then analysed by optimizing characters under analysis through least squared parsimony onto a phylogenetic tree. We included Ornithodira and a few basal archosauromorphs as outgroups. In order to test the relationships between GAtot, GApit and OArelat within Pseudosuchia, we performed regression analyses in R (R Development Core Team, 2012). We applied the phylogenetic generalized least square method (PGLS, Grafen, 1989), using the 'caper' package (Orme *et al.*, 2012) with reference to a morphology-based phylogeny of Pseudosuchia. This phylogeny was compiled in Mesquite (Maddison & Maddison, 2011), using published references for phylogenetic relationships and branch lengths. We referred to Nesbitt (2011) to assess the phylogenetic position of the Triassic archosauriforms, early pseudosuchians and early crocodylomorphs. We used Wilberg's (2015) phylogeny to set the position of Thalattosuchia (sister-taxon of Crocodyliformes) within which the phylogenetic relationships of the metriorhynchids were assessed according to Young (Young et al., 2009, 2010). Within the crocodyliforms, the phylogeny of the notosuchians was established after Pol *et al.* (2014) and the phyletic relationships of the neosuchians (including Crocodylia) were assessed according to the following authors: Brochu (2003, 2007), Brochu *et al.* (2012), Bronzati, Chinaglia-Montefeltro & Langer (2012) and Piras *et al.* (2014). When lacking information about the branch lengths (in million years), we used the date of first occurrence of each concerned species to assess its time of diversification with its corresponding sister taxon (Paleobiology Database; Behrensmeyer & Turner, 2013; http://fossilworks.org/?a=home). Moreover, in order to test if the variables used to quantify ornamentation are correlated with lifestyle, we performed a phylogenetic ANOVA (Garland *et al.*, 1993). For fossil taxa, lifestyle was inferred using morphological data from published references and summarized into three categories: terrestrial, amphibious and pelagic. These categories were assigned using published morphological data that concern the assessed locomotion (based on the limbs and scapular belt morphologies), the sensorial functions and the feeding strategies (based on the skull morphology: sight and nostrils orientations, anteroposterior position of the choanae, skull height, snout elongation; Annex 2B).

RESULTS

Phylogenetic signal and covariation analyses

All the variables used to quantify bone ornamentation, except GAtot in the nasal (i.e. GAtotn), contain a significant phylogenetic signal (Table 1A): both Pagel's λ and Blomberg's *K* are indeed significant. Regressions performed using PGLS show that GAtot is always correlated with GApit and OArelat regardless of the bone region (Table 1B, C). Phylogenetic ANOVA shows that all the variables defining ornamentation on pseudosuchian skulls (GAtott, GApitt, OArelatt, GAtotn, GApitn and OArelatn) are correlated with the lifestyle (terrestrial, semi-aquatic or pelagic; Table 2).

Patterns of character evolution

Optimization onto the phylogenetic tree using least squared parsimony (Figs 2, 3) shows that GAtot reaches high values only within Neosuchia (over 6%) and in one 'out-group' to Pseudosuchia: *Proterochampsa barrionuevoi* ($GAtot_t$ = 10%, $GAtot_n$ = 8%). In comparison with the neosuchian, these variables score low values in Notosuchia, *Protosuchus richardsoni*, teleosaurids and phytosaurs and are nil for the metriorhynchids and all Triassic terrestrial archosauriforms.

Paleoecology

Contrary to both the terrestrial and the pelagic forms, bone ornamentation in semi-aquatic forms usually

Table 1A. Phylogenetic signal test

	Variables	Pagel's λ		Blomberg's *K*	
		λ	*P*-value	*K*	*P*-value
Skull table	GAtot	0.664	5.38e-14***	0.264	0.002**
	GApit	0.940	1.55e-15***	0.416	0.001**
	OArelat	0.873	2.15e-11***	0.220	0.003**
Nasal	GAtot	0.366	9.66e-06***	0.052	0.793
	GApit	0.873	5.12e-12***	0.287	0.001**
	OArelat	0.733	6.69e-11***	0.139	0.030*

*significant

Table 1B. PGLS (Partial Generalized Least Squares): bivariate analyses

	Dependent (response) variable	Independent (explanatory) variable	Degrees of freedom	R^2	Intercept	Slope	*P*-value
Skull table	GAtot	GApit	63	0.444	0.043	5.975	1.39e-09***
	GAtot	OArelat	63	0.521	0.061	16.733	1.19e-11***
Nasal	GAtot	GApit	63	0.595	–0.107	5.583	5.78e-14***
	GAtot	OArelat	63	0.747	–0.129	14.992	<2.2e-16***

*significant

Table 1C. PGLS: Multivariate analyses

	Dependent (response) variable	Independent (explanatory) variables	Degrees of freedom	Adjusted R^2	*P*-value	Regression coefficient	*P*-value
Skull table	GAtot	GApit	62	0.519	5.28e-11***	1.723	0.249
		OArelat				12.995	0.001**
Nasal	GAtot	GApit	62	0.750	<2.2e-16***	–2.451	0.109
		OArelat				20.620	3.8e-07***

*significant

scores higher values on the skull table than on the nasal (Figs 2–4). Moreover, the dispersion of values for each variable (GAtot, GApit, OArelat) is wider in semi-aquatic forms than for the other two lifestyles (Fig. 4). In the case of pelagic forms, these values are nil, since metriorhynchids had completely lost bone ornamentation on the skull.

DISCUSSION

PHYLOGENETIC SIGNAL

Phylogenetic signal for continuous traits has been defined as the 'tendency for related species to resemble each other more than they resemble species drawn at random from the tree' (Blomberg & Garland, 2002: 905). Many parameters have been developed to quantify this signal; some of them, such as Blomberg's *K* and Pagel's λ, are based on a Brownian motion model of character evolution whereby character evolution follows a random walk along the branches of the phylogenetic tree, the variance of character distribution being directly proportional to branch length (Munkemuller *et al.*, 2012). Blomberg's *K* and Pagel's λ values close to zero mean that the data set is independent from phylogeny, whereas a value of one means that the character under analysis evolved following a Brownian motion model (i.e. it evolved in the absence of a significant action of natural selection). In our case study, Pagel's λ is significant for each variable. Blomberg's

K is also significant for each variable except $GAtot_n$. These results suggest that the expression of bone ornamentation follows a Brownian motion model of character evolution among basal pseudosuchian branches. However, Blomberg's K and Pagel's λ values are smaller than one. This means that the variation of bone ornamentation is also under the control of natural selection, the outcome of which disrupts Brownian motion-like mode of evolution. Therefore, adaptive and/or morphological constraints may also be involved in the evolution of the cranial ornamentation besides the influence of phylogeny. A good illustration of this conclusion is the sharp contrast between the low degree of ornamentation in *Calsoyasuchus valliceps* (semi-aquatic longirostrine goniopholid) and the high degree of ornamentation observed in its close relative, *Amphicotylus lucasi* (semi-aquatic mesorostrine goniopholid; Fig. 2).

Table 2. Phylogenetic ANOVA; testing the effect of lifestyle (terrestrial, amphibious, pelagic) on ornamentation parameters using phylogenetic ANOVA and assuming an Ornstein-Uhlenbeck model (first P value) and a Brownian motion model (second P value)

Dependent (response) variables		Interaction Among independent variables
		Lifestyle
Skull table	GAtot	P = 0.0011
	GApit	P = untestable
	OArelat	P = 0.0009
Nasal	GAtot	P = 0.1075
	GApit	P = untestable
	OArelat	P = 0.0322

According to Wilberg's (2015) phylogenetic hypothesis, the transition from terrestrial to semi-aquatic lifestyle followed two distinct but parallel trends across the Triassic-Jurassic transition: marine adaptation in thalattosuchians and colonization of continental fresh waters by neosuchians (Fig. 5A). Based on this, our results argue that the last common ancestor of Thalattosuchia and Crocodyliformes acquired ornamentation, as earlier crocodylomorphs had no bone sculpture (Figs 2, 3) besides a few exceptions mentioned in published references (*Gracilisuchus stipanicicorum*, Butler *et al.*, 2014; *Carnufex carolensis*, Drymala, 2015; Drymala *et al.*, 2016; Zanno *et al.*, 2015). Indeed, *Carnufex carolensis* had a well-developed though much localized ornamentation on the jugal and *Gracilisuchus stipanicicorum* had a shallow-sculptured dermatocranium which does not show a clear network of consecutive pits and grooves separated by ridges. Thus, the sporadic presence of cranial ornamentation in early crocodylomorphs could have been a preliminary stage for its maintenance in later forms through natural selection. Subsequently, ornamentation increased in Neosuchia (GAtot), while remaining lower in *Protosuchus richardsoni*,

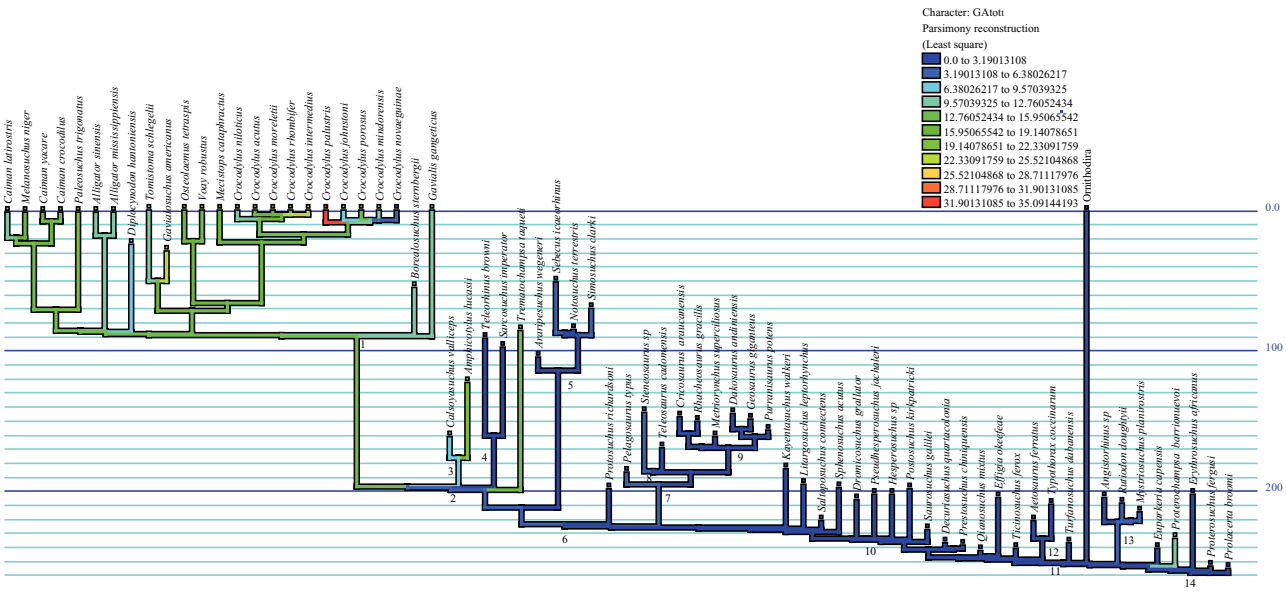

Figure 2. Optimization of the total gain in area due to bone ornamentation (GAtot) on the skull table using least squares (maximum of parsimony) on the pseudosuchians' phylogenetic tree. Branch lengths are scaled in million years. Node names: 1: Crocodylia; 2: Neosuchia; 3: Goniopholidae; 4: Pholidosauridae; 5: Notosuchia; 6: Crocodyliformes; 7: Thalattosuchia; 8: Teleosauridae; 9: Metriorhynchidae; 10: Crocodylomorpha; 11: Pseudosuchia; 12: Aetosauria; 13: Phytosauria; 14: Archosauriformes.

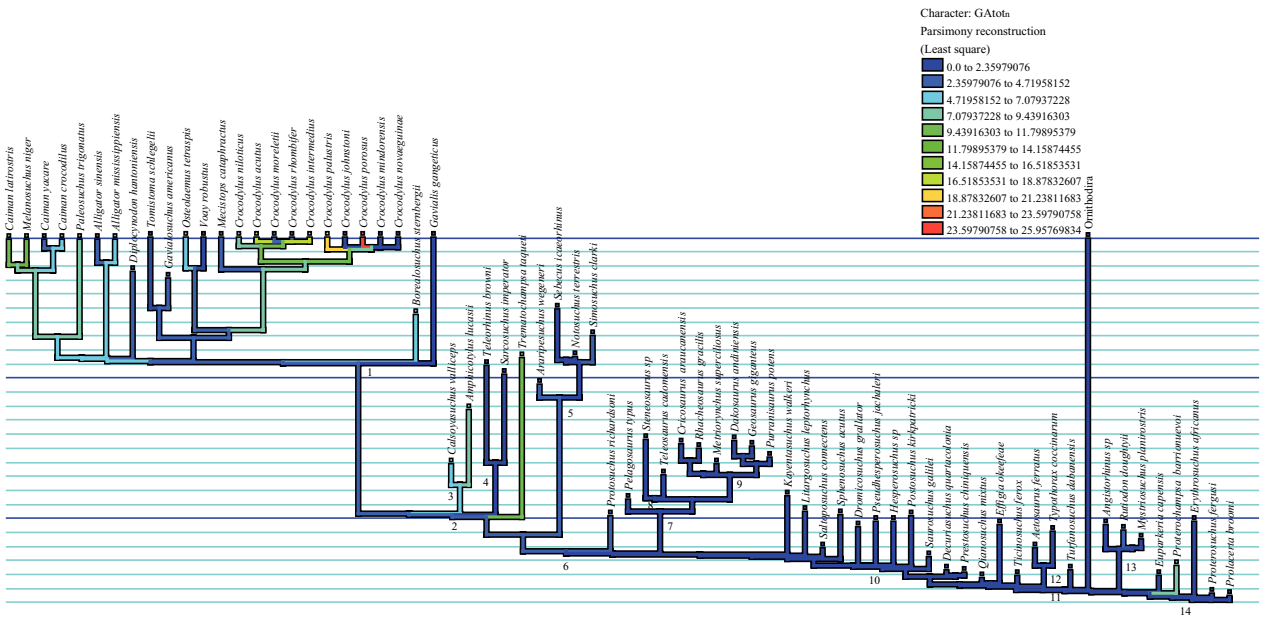

Figure 3. Optimization of the total gain in area due to bone ornamentation (GAtot) on the nasal using least squares (maximum of parsimony) on the pseudosuchians' phylogenetic tree. Branch lengths are scaled in million years. Node names: 1: Crocodylia; 2: Neosuchia; 3: Goniopholidae; 4: Pholidosauridae; 5: Notosuchia; 6: Crocodyliformes; 7: Thalattosuchia; 8: Teleosauridae; 9: Metriorhynchidae; 10: Crocodylomorpha; 11: Pseudosuchia; 12: Aetosauria; 13: Phytosauria; 14: Archosauriformes.

Notosuchia and Thalattosuchia. A slightly different result is obtained by using Bronzati's (2012) phylogeny as a reference: Thalattosuchia would then be included within Neosuchia, and Crocodyliformes would have experienced only one transition from land to water (Neosuchia), with a further expansion to sea for thalattosuchians, resulting in secondary reduction and loss of a previously well-developed ornamentation (Fig. 5B).

The ancestral lifestyle for Pseudosuchia remains controversial because the position of Phytosauria is unclear (Sereno & Arcucci, 1990; Nesbitt, 2011). If phytosaurs are basal pseudosuchians, the ancestral pseudosuchian could have been semi-aquatic and ornamented like the phytosaurs themselves and *Proterochampsa barrionuevoi* (Archosauriformes; Cerda *et al.*, 2015); conversely, if phytosaurs are outside crown-group Archosauria, the ancestral pseudosuchian might have been terrestrial and unornamented like the more basal Archosauriformes *Euparkeria* and *Erythrosuchus*. Nonetheless, whatever the position of the phytosaurs may be, the absence of ornamentation and a terrestrial lifestyle for ancestral archosaurs remains the most parsimonious scenario. Indeed, until now, there are no known ornithodiran with bone ornamentation made of pits and grooves resembling that of a pseudosuchian. Therefore, we may assume that the primitive condition for Archosauria and Pseudosuchia is the absence of bone ornamentation such as in the terrestrial early crocodylomorphs and in all dinosaurs.

Long bone histology suggests that non-archosauriform archosauromorphs had lower bone growth rates (and probably lower resting metabolic rates) than non-archosaurian archosauriforms (Ricqlès *et al.*, 2008; Werning & Irmis, 2011; Botha-Brink *et al.*, 2011; Werning *et al.*, 2011; Legendre, Segalen & Cubo, 2013). Phytosaurs may be an exception to this phylogenetic patterns because they are non-archosaurian archosaurifoms (Nesbitt, 2011) but show a reversion to low bone growth rates and probably low resting metabolic rates (Ricqlès, Padian & Horner, 2003; Cubo *et al.*, 2012). Within Archosauria, the terrestrial pseudosuchians such as *Terrestrisuchus* are characterized by high bone growth rates and probably high resting metabolic rates, whereas semi-aquatic neosuchians show moderate bone growth rate and low resting metabolic rates (Ricqlès *et al.*, 2003).

Functional adaptation

Our results confirm that the global gain in area due to bone ornamentation (GAtot) in Pseudosuchia is highly correlated with both pit depth and shape (expressed here by GApit) and pit extension on bone surface (OArelat), as previously shown in crown-group crocodylians (Clarac *et al.*, 2015). Our results also show a clear relationship between pseudosuchian lifestyles (pelagic, semi-aquatic, terrestrial), and degree of bone sculpture (GAtot, GApit, OArelat) in disregard of the phylogenetic relationships (Phylogenetic ANOVA;

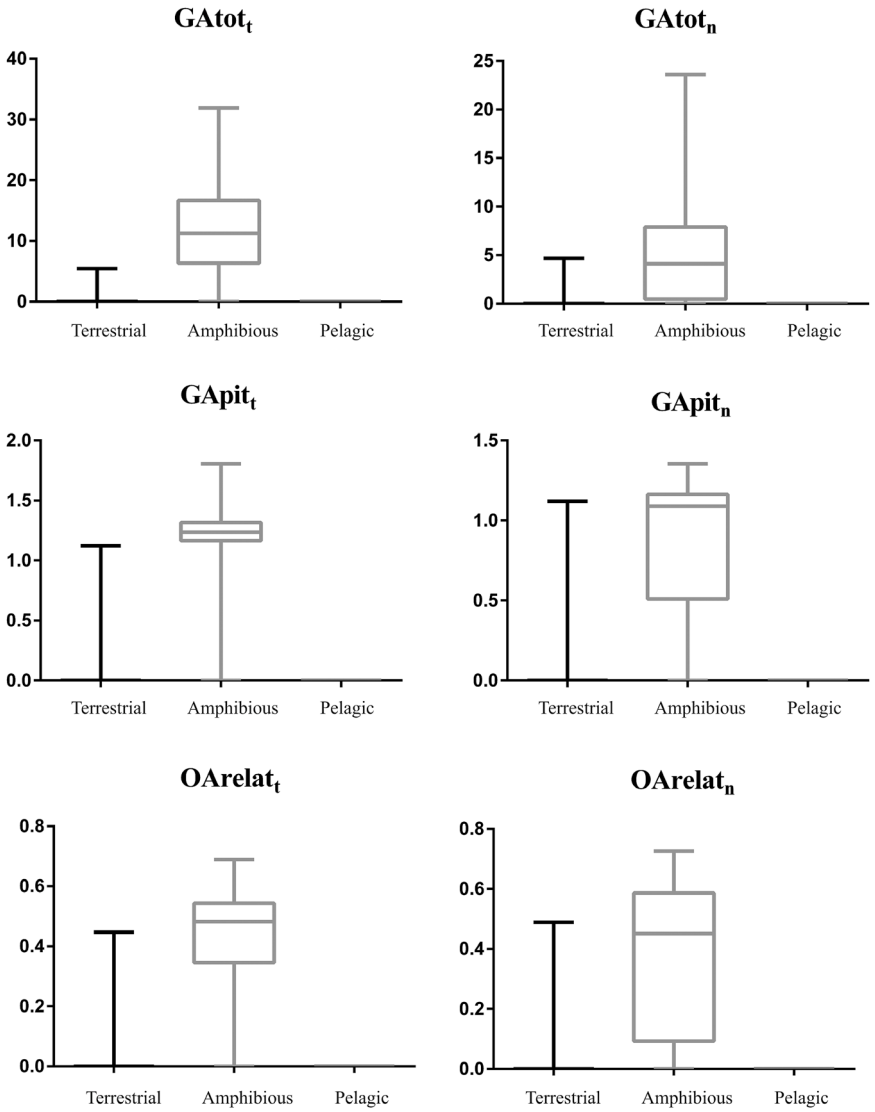

Figure 4. Boxplots of the variables defining ornamentation (GAtot, GApit, OArelat) in regard of the pseudosuchians' lifestyle.

Table 2). More precisely, ornamentation on both the skull table and nasal is particularly more developed in semi-aquatic pseudosuchians than in terrestrial or pelagic forms. Therefore, we conclude that the development of ornamentation was probably selected within the amphibious forms as it would confer an evolutionary advantage in this specific lifestyle. Indeed, in this context, a possible functional role for bone ornamentation would be to improve basking efficiency in organisms that, like modern crocodiles, have low mobility and produce little metabolic heat linked to muscle activity (Seebacher, Grigg & Beard, 1999). Even if the dermis, epidermis and keratin above the dermal bones do cover the ornamented surface regardless of the underlying ornamentation pattern, these tissues can drive the heat radiation to the ornamented bones which house a vascular network that may capture the heat and convey it to the general cardio-vascular system toward the dorsal veins (Grigg & Alchin, 1976; Seidel, 1979; Farlow, Hayashi & Tattersall, 2010). It would explain why most mobile terrestrial pseudosuchians such as the sphenosuchians, (Hoffstetter, 1955), protosuchians (Kälin, 1955), rauisuchians (Nesbitt, 2011) and sebecosuchians (Martin, 2014) could have both a dorsal shield and a skull roof residual ornamentation at best. In such forms, muscle activity collaterally would generate heat and contribute to homeothermic-like physiological conditions (Newman, 2011). In a different way, metriorhynchids that probably were ecto-poïkilothermic pelagic swimmers using

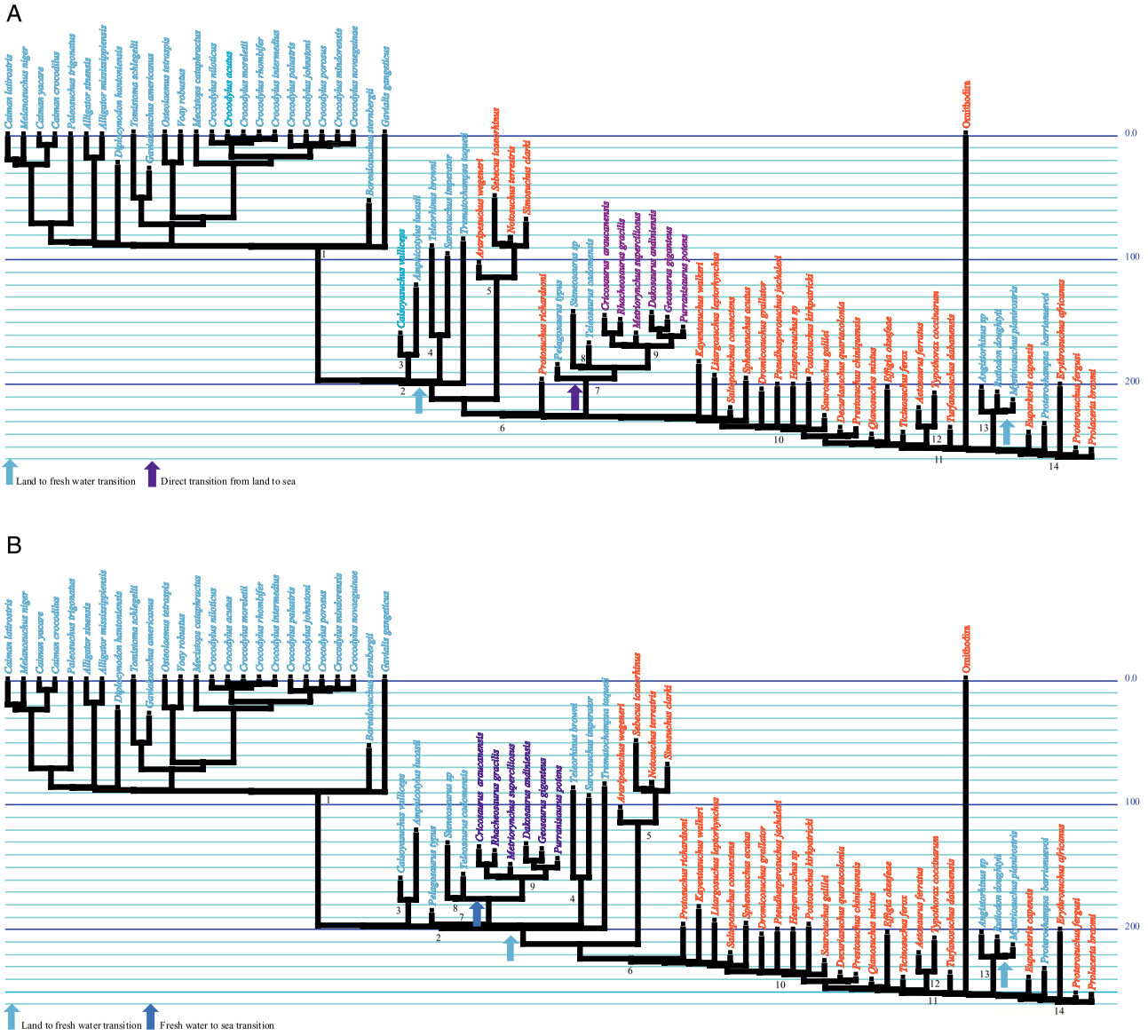

Figure 5. Phylogeny of the Pseudosuchia with both hypotheses on the origin of the Thalattosuchians: (A): Wilberg (2015), (B): Bronzati *et al.* (2012). The coloration of the name of the species stands for their lifestyle: Orange: terrestrial; Clear blue: semi-aquatic (amphibious); Purple: pelagic (off-shore). Branch lengths are scaled in million years. Node names: 1: Crocodylia; 2: Neosuchia; 3: Goniopholidae; 4: Pholidosauridae; 5: Notosuchia; 6: Crocodyliformes; 7: Thalattosuchia; 8: Teleosauridae; 9: Metriorhynchidae; 10: Crocodylomorpha; 11: Pseudosuchia; 12: Aetosauria; 13: Phytosauria; 14: Archosauriformes.

lift-based propulsion had lost their entire osteoderm shield and possessed a lightened skull with no ornamentation (Hua & Buffrénil, 1996; Young *et al.*, 2010). In this regard and in comparison with the amphibious forms, metriorhynchids were particularly skilled at climbing up and down into the water column by controlling their buoyancy. Moreover, since they were unable to gape (Spotila, Terpin & Dodson, 1977; Young *et al.*, 2010), metriorhynchids must have regulated their body temperature without basking on land. The loss of their dermal shield could be thus due to a required reduction of their skeleton in order to increase both their buoyancy (weight loss) and swimming speed by improving the skeleton flexibility along the antero-posterior axis (Buffetaut, 1982). The loss of the ornamentation on the skull could itself be due to morphological constraints (see below).

Morphological constraints

Among semi-aquatic forms, ornamentation is characteristically more pronounced on the skull table than on

the nasal (Fig. 4). This difference between these two anatomical regions is at least partly explained by different morphological constraints due to the shape variability between the snout and the skull table (Clarac *et al.*, 2016). Indeed, shape of the skull table remains stable from one species to the other in comparison with the snout, which shows a high variability from brevirostrines to longirostrines (Iordansky, 1973; Stubbs *et al.*, 2013; Blanco, Jones & Villamil, 2014; Piras *et al.*, 2014; Watanabe & Slice, 2014; Fernandez Blanco *et al.*, 2015; Foth, Bona & Desojo, 2015). In this regard, snout elongation tends to reduce expression of rostral ornamentation, whereas it remains well expressed on the skull table. The most plausible explanation for this pattern is that interference is likely to occur between the local growth rate and the resorption depth of the pits (Buffrénil *et al.*, 2015). Thus, as pelagic forms (metriorhynchids) are also characterized by relatively slender (Pierce, Angielczyk & Rayfield, 2009), fast-growing snouts, they are therefore under the same type of constraints as semi-aquatic longirostrines (e.g. *Gavialis*, *Tomistoma*, pholidosaurids, teleosaurids, phytosaurs). However, as bone ornamentation on the skull table of crocodylians is not influenced by skull morphology (Clarac *et al.*, 2016), the low to nil values of $GAtot_t$ in teleosaurids, phytosaurs and pholidosaurids (*Sarcosuchus imperator*, *Teleorhinus browni*) appear paradoxical. Nevertheless, the influence of the skull morphology on ornamentation has been, up to now, only studied in extant species in which the skull table shows a low morphological variability (as mentioned above). Indeed, contrary to the living species, the thalattosuchians (be they teleosaurids or metriorhynchids) and the pholidosaurids are characterized by an extreme size of supratemporal fenestrae in relation with the extension of jaws' adductor muscles (Steel, 1973; Buffetaut, 1982; Pierce *et al.*, 2009; Stubbs, 2013). This anatomical pattern necessarily reduces the surface of bones most liable to be ornamented (i.e. the frontal, the parietal, postorbitals and squamosals) and reduces the global ornamentation score of the cranial table.

Quantitative data from teleosaurids and the pholidosaurid *Sarcosuchus imperator* reveal that ornamentation can be quite pronounced on the dorsal osteoderms (GAtot values 20% and over 30%, respectively: Clarac *et al.*, 2015) and simultaneously absent on the nasal and cranial table (Figs 2, 3). These examples suggest that the poor global ornamentation score observed in slender-snouted skulls does not reflect a general loss of ornamentation in relation with a higher degree of adaptation to an aquatic environment in comparison with the mesorostrines and brevirostrines amphibious. Rather, it reflects local morphological constraints typical of longirostrine skulls (a slender snout and large upper temporal fenestra).

CONCLUSION

The skulls of amphibious pseudosuchians possess a dermal bone ornamentation significantly more developed than both the terrestrial and pelagic forms. Natural selection may be the main process leading to this evolutionary trend even if the functional significance of bone ornamentation is still unresolved. Indeed, after using phylogenetic analyses within a frame of 250 million years of evolution, it has been assessed that phylogeny does not entirely explain the variable degree of bone ornamentation in Pseudosuchia. In such an evolutionary context, the most plausible role would be for the ornamentation to improve basking efficiency for low-mobility (amphibious) ambush predators which secondarily returned to ecto-poïkilothermy. Nonetheless, it is also highly probable that morphological constraints due to snout elongation and the relative extension of the upper temporal fenestra tend to reduce the expression of bone ornamentation on the skull roof in the amphibious longirostrines and thus limit its possible function to the dermal shield.

ACKNOWLEDGEMENTS

We would like to thank Thibaud Souter for his expert advice in the use of the photogrammetry. Then, we would like to thank Raphaël Cornette and the UMR 7179 C.N.R.S/M.N.H.N (Département d'Ecologie et de Gestion de la Biodiversité) for giving us access to the Agisoft Photoscan software. In the same way, we will thank the UMS 2700 (MNHN/CNRS) for the access to the 3D scanner. We will also give thankful regards to all the collection managers whose participations were a key to the success in our sample acquisition: Salvador Bailon (MNHN), Carl Mehling (AMNH), Mark Norell (AMNH), Michael Brett-Surman (Smithsonian Institution), Jeremy F. Jacobs (Smithsonian Institution). With the same consideration, we also thank all the participants who have permitted us to download the scans of crocodylian skulls by the website Digimorph.org: Jessie Maisano, Timothy Rowe, Matthew Colbert (University of Texas), Dave W. Krause (Stony Brook University). Finally, we thank our South-African colleagues for giving us information about their specimens in collection which we could thus include in our sampling: Jennifer Botha-Brinck (University of Cape Town), Zaituna Erasmus, Roger M.H. Smith (Iziko Museum of South Africa). CAB was supported by US NSF DEB 0444133 (which generated some of the CT images) and DEB 1257786-125748.

REFERENCES

Alcober O. 2000. Redescription of the skull of *Saurosuchus galilei* (Archosauria: Rauisuchidae). *Journal of Vertebrate Paleontology* **20:** 302–316.

Behrensmeyer AK, Turner A. 2013. Taxonomic occurrences of Suidae recorded in the Paleobiology Database. Fossilworks. Available at: http://fossilworks.org.

Blanco RE, Jones WW, Villamil J. 2014. The 'death roll' of giant fossil crocodyliforms (Crocodylomorpha: Neosuchia): allometric and skull strength analysis. *Historical Biology* **27:** 1–11.

Blomberg SP, Garland T. 2002. Tempo and mode in evolution: phylogenetic inertia, adaptation and comparative methods. *Journal of Evolutionary Biology* **15:** 899–910.

Botha Brink J, Smith RMH. 2011. Osteology of the Triassic archosauromorphs *Prolacerta*, *Proterosuchus*, *Euparkeria*, and *Erythrosuchus* from the Karoo Basin of South Africa. *Journal of Vertebrate Paleontology* **31:** 1238–1254.

Brochu CA. 2003. Phylogenetic approaches toward crocodilian history. *Annual Review of Earth Planetary Science* **31:** 357–397.

Brochu CA. 2007. Morphology, relationships, and biogeographical significance of an extinct horned crocodile (Crocodylia, Crocodylidae) from the Quaternary of Madagascar. *Zoological Journal of the Linnean Society* **150:** 835–863.

Brochu C, Parris DC, Grandstaff BS, Denton RK Jr, Gallagher WB. 2012. A new species of *Borealosuchus* (Crocodyliformes, Eusuchia) from the late Cretaceous-early Paleogene of new Jersey A. *Journal of Vertebrate Paleontology* **32:** 105–116.

Bronzati M, Chinaglia-Montefeltro F, Langer MC. 2012. A species level supertree of the Crocodyliformes. *Historical Biology* **24:** 598–606.

Buffetaut E. 1982. Radiation évolutive, paléoécologie et biogéographie des crocodiliens mésosuchiens. *Mémoires de la Société Géologique de France, Nouvelle Série* **142:** 1–88.

Buffrénil V de, Clarac F, Fau M, Martin S, Martin B, Pelle E, Laurin M. 2015. Differentiation and growth of bone ornamentation in vertebrates: a comparative histological study among the Crocodylomorpha. *Journal of Morphology* **276:** 425–445.

Butler RJ, Sullivan C, Ezcurra MD, Liu J, Lecuona A, Sookias RB. 2014. New clade of enigmatic early archosaurs yields insights into early pseudosuchian phylogeny and the biogeography of the archosaur radiation. *BMC Evolutionary Biology* **14:** 128.

Bystrow AP. 1935. Morphologische untersuchungen der deckknochen des schädels der stegocephalen. 1. Mitteilung. Schädel der stegocephalen. *Acta Zoologica Stockholm* **16:** 65–141.

Cerda IA, Desojo JB, Trotteyn MJ, Scheyer TM. 2015. Osteoderm histology of Proterochampsia and Doswelliidae (Reptilia: Archosauriformes) and their evolutionary and paleobiological implications. *Journal of Morphology* **276:** 385–402.

Chatterjee S. 1985. *Postosuchus*, a new thecodontian reptile from the Triassic of Texas and the Origin of Tyrannosaurs. *Philosophical Transactions of the Royal Society of London B Biological Sciences* **309:** 395–460.

Clarac F, Souter T, Cornette R, Cubo J, de Buffrénil V. 2015. A quantitative assessment of bone area increase due to ornamentation in the Crocodylia. *Journal of Morphology* **276:** 1183–1192.

Clarac F, Souter T, Cubo J, de Buffrénil V, Brochu C, Cornette R. 2016. Does skull morphology constrain bone ornamentation? A morphometric analysis in the Crocodylia. *Journal of Anatomy* **229:** 292–301.

Clark MJ, Sues HD. 2002. Two new basal crocodylomorph archosaurs from the Lower Jurassic and the monophyly of the Sphenosuchia. *Zoological Journal of the Linnean Society* **13:** 77–95.

Cubo J, Le Roy N, Martinez-Maza C, Montes L. 2012. Paleohistological estimation of bone growth rate in extinct archosaurs. *Paleobiology* **38:** 335–349.

Desojo JB, Heckert AB, Martz JW, Parker WG, Schoch RR, Small BJ, Sulej T. 2013. Aetosauria: a clade of armoured pseudosuchians from the Upper Triassic continental beds. *Geological Society of London* **379:** 203–239.

Downs JP, Donoghue PC. 2009. Skeletal histology of Bothriolepis canadensis (Placodermi, Antiarchi) and evolution of the skeleton at the origin of jawed vertebrates. *Journal of Morphology* **270:** 1364–1380.

Drymala SM. 2015. *A new paracrocodylomorph (Archosauria, Suchia) from the Late Triassic of North Carolina*. MSc Thesis, North Carolina State University. Available at: http://www.lib.ncsu.edu/resolver/1840.16/10295

Drymala SM, Zanno LE. 2016. Osteology of Carnufex carolinensis (Archosauria: Psuedosuchia) from the Pekin formation of North Carolina and its implications for early Crocodylomorph evolution. *PLoS One* **11:** e0157528.

Ewer BYRF. 1965. The Anatomy of the thecodont reptile *Euparkeria capensis* Broom. *Philosophical Transactions of the Royal Society of London B Biological Sciences* **248:** 379–435.

Farlow J, Hayashi S, Tattersall GJ. 2010. Internal vascularity of the dermal plates of *Stegosaurus* (Ornithischia, Tyreophora). *Swiss Journal of Geosciences* **103:** 173–185.

Fernandez Blanco MV, Bona P, Olivares AI, Desojo JB. 2015. Ontogenetic variation in the skulls of *Caiman*: the case of *Caiman latirostris* and *Caiman yacare*. *Herpetological Journal* **25:** 65–73.

Foth C, Bona P, Desojo JB. 2015. Intraspecific variation in the skull morphology of the black caiman *Melanosuchus niger* (Alligatoridae, Caimaninae). *Acta Zoologica* **96:** 1–13.

França MA, Ferigolo J, Langer MC. 2011. Associated skeletons of a new middle Triassic 'Rauisuchia' from Brazil. *Die Naturwissenschaften* **98:** 389–395.

Garland T Jr, Dickerman AW, Janis CM, Jason AJ. 1993. Phylogenetic Analysis of Covariance by Computer Simulation. *Systematic Biology* **42:** 265–292.

Gow C. 1975. The morphology and relationships of '*Youngina capensis*' Broom and '*Prolacerta broomi*' Parrington. *Palaeontology of Africa* **131:** 89–131.

Grafen A. 1989. The phylogenetic regression. *Proceedings of the Royal Society of London B: Biological Sciences* **205:** 581–598.

Grigg GC, Alchin J. 1976. The Role of the cardiovascular system in thermoregulation of *Crocodylus johnstoni*. *Physiological Zoology* **49:** 24–36.

Herrera Y, Gasparini Z, Fernández MS. 2015. *Purranisaurus potens* Rusconi, an enigmatic metriorhynchid from the Late Jurassic–Early Cretaceous of the Neuquén Basin. *Journal of Vertebrate Paleontology* **35:** e904790.

Hill RV. 2010. Osteoderms of *Simosuchus clarki* (Crocodyliformes: Notosuchia) from the Late Cretaceous of Madagascar. *Journal Vertebrate Paleontoogy* **30:** 154–176.

Hoffstetter R. 1955. Thecodontia. In: Piveteau J, ed. *Traite de Paléontologie*, **Vol. 5**. Paris: Masson et Cie, 665–681.

Hua S, Buffrénil V de. 1996. Bone histology as a clue in the interpretation of functional adaptations in the Thalattosuchia (Reptilia, Crocodylia). *Journal of Vertebrate Paleontology* **16:** 703–717.

Iordansky NN. 1973. The skull of the Crocodilia. In: Gans C, ed. *Biology of the reptilia,* **Vol. 4**. London: Morphology D. Academic Press, 201–262.

Irmis RB, Nesbitt SJ, Sues HD. 2013. Early Crocodylomorpha. *Geological Society of London, Special Publications* **379:** 275–302.

Jouve S. 2014. The skull of *Teleosaurus cadomensis* (Crocodylomorpha; Thalattosuchia), and phylogenetic analysis of Thalattosuchia. *Journal of Vertebrate Paleontology* **29:** 88–102.

Kälin J. 1955. Crocodilia. In: Piveteau J, ed. *Traite de Paléontologie,* **Vol. 5**. Paris: Masson et Cie, 695–784.

Kley NJ, Sertich JJW, Turner AH, Krause DW, O'Connor PM, Georgi JA. 2010a. Craniofacial morphology of *Simosuchus clarki* (Crocodyliformes: Notosuchia) from the late Cretaceous of Madagascar. *Society of Vertebrate of Paleontology Memoirs (Journal of Vertebrate Paleontology)* **30**(Suppl. 6): 13–98.

Kley NJ, Sertich JJW, Turner AH, Krause DW, O'Connor PM, Georgi JA. 2010b. Appendicular skeleton of *Simosuchus clarki* (Crocodyliformes: Notosuchia) from the late Cretaceous of Madagascar. *Society of Vertebrate of Paleontology Memoirs (Journal of Vertebrate Paleontology)* **30**(Suppl. 6): 13–98.

Lautenschlager S, Desojo JB. 2011. Reassessment of the middle Triassic rauisuchian archosaurs *Ticinosuchus ferox and Stagonosuchus nyassicus*. *Palaontologische Zeitschrift* **85:** 357–381.

Legendre LJ, Segalen L, Cubo J. 2013. Evidence for high bone growth rate in Euparkeria obtained using a new paleohistological inference model for the humerus. *Journal of Vertebrate Paleontology* **33:** 1343–1350.

Li C, Wu XC, Cheng YN, Sato T, Wang L. 2006. An unusual archosaurian from the marine Triassic of China. *Die Naturwissenschaften* **93:** 200–206.

Liparini A, Schultz CL. 2013. A reconstruction of the thigh musculature of the extinct pseudosuchian *Prestosuchus chiniquensis* from the *Dinodontosaurus* Assemblage Zone (Middle Triassic Epoch), Santa Maria 1 Sequence, southern Brazil. In: Nesbitt SJ, Desojo JB, Irmis RB, eds. *Anatomy, phylogeny palaeobiology early archosaurs their kin*. London: Geological Society Special Publications **379**, 441–468.

Lucas SG, Heckert AB, Kahle R. 2002. Postcranial anatomy of Angistorhinus, a Late Triassic phytosaur from West Texas. *New Mexico Museum of Natural History and Science Bulletin* **21:** 157–164.

Lundberg JG, Aguilera O. 2003. The late Miocene *Phractocephalus* catfish (Siluriformes: Pimelodidae) from Urumaco, Venezuela: additional specimens and reinterpretation as a distinct species. *Neotropical Ichthyology* **1:** 97–109.

Maddison WP, Maddison DR. 2011. *Mesquite: a modular system for evolutionary analysis, Version 2.75*. Available at: http://mesquiteproject.org.

Martin JE. 2014. A sebecosuchian in a middle Eocene karst with comments on the dorsal shield in Crocodylomorpha. *Journal of Vertebrate Paleontology* **60:** 673–680.

Martin JE, Smith T, de Lapparent de Broin F, Escuillié F, Delfino M. 2014. Late Palaeocene eusuchian remains from Mont de Berru, France, and the origin of the alligatoroid *Diplocynodon*. *Zoological Journal of the Linnean Society* **172:** 867–891.

Munkemuller T, Lavergne S, Bzeznik B, Dray S, Jombart T, Schiffers K, Thuiller W. 2012. How to measure and test phylogenetic signal. *Methods in Ecology and Evolution* **3:** 743–756.

Nesbitt SJ. 2007. The anatomy of *Effigia okeeffeae* (Archosauria, Suchia), theropod-like convergence, and the distribution of related taxa. *Bulletin of American Museum of Natural History* **302:** 1–84.

Nesbitt SJ. 2011. The early evolution of archosaurs: relationships and the origin of major clades. *Bulletin of American Museum of Natural History* **352:** 1–292.

Newman SA. 2011. Thermogenesis, muscle hyperplasia, and the origin of birds. *Bioessays* **33:** 653–656.

Orme D, Freckleton R, Thomas G, Petzoldt T, Fritz S, Isaac N, Pearse W. 2012. *The caper package: comparative analysis of phylogenetics and evolution in R*. R package version 0.5.2, London. United Kingdom.

Ortega F, Gasparini Z, Buscalioni AD, Calvo JO. 2010. A new species of *Araripesuchus* (Crocodylomorpha, Mesoeucrocodylia) from the lower Cretaceous of Patagonia (Argentina). *Journal of Vertebrate Paleontology* **20:** 57–76.

Padian K, Li C, Pchelnikova J. 2010. The trackmaker of *Apatopus* (Late Triassic, north America): implications for the evolution of archosaurs stance and gait. *Palaeontology* **53:** 175–189.

Pagel M. 1999. Inferring the historical patterns of biological evolution. *Nature* **401:** 877–884.

Parrilla-Bel J, Young MT, Moreno-Azanza M, Canudo JI. 2013. The first metriorhynchid Crocodylomorph from the middle Jurassic of Spain, with implications for evolution of the subclade *Rhacheosaurini*. *PLoS One* **8**.

Parrish JM. 1986. The origin of Crocodilian Locomotion. *Paleobiology* **13:** 396–414.

Parrish JM. 1992. Phylogeny of the Erythrosuchidae (Reptilia: Archosauriformes). *Journal of Vertebrate Paleontology* **12:** 93–102.

Pierce SE, Benton MJ. 2006. *Pelagosaurus typus* (Mesoeucrocodylia: Thalattosuchia) from the Upper Lias (Toarcian, lower Jurassic) of Somerset, England. Journal of Vertebrate Paleontology 26: 621–635.

Pierce SE, Angielczyk KD, Rayfield EJ. 2009. Shape and mechanics in thalattosuchian (Crocodylomorpha) skulls: implications for feeding behaviour and niche partitioning. *Journal of Anatomy* **215:** 555–576.

Piras P, Buscalioni AD, Teresi L, Raia P, Sansalone G, Kotsakis T, Cubo J. 2014. Morphological integration and functional modularity in the crocodilian skull. *Integrative Zoology* **9:** 498–516.

Pol D. 2005. Postcranial remains of *Notosuchus terrestris* (Archosauria: Crocodyliformes) from the upper Cretaceous of Patagonia, Argentina. *Ameghiniana* **42:** 1–17.

Pol D, Gasparini Z. 2009. (Thalattosuchia: Crocodylomorpha) and the phylogenetic position of Thalattosuchia. *Journal of Systematic Palaeontology* **7:** 163–197.

Pol D, Leardib JM, Lecuonaa A, Krausea M. 2011. Postcranial anatomy of *Sebecus icaeorhinus* (Crocodyliformes, Sebecidae) from the Eocene of Patagoniae. *Journal of Vertebrate Paleontology* **32:** 328–354.

Pol D, Nascimento PM, Carvalho AB, Riccomini C, Pires-Domingues RA, Zaher H. 2014. A new notosuchian from the late Cretaceous of Brazil and the phylogeny of advanced notosuchians. *PLoS One* **9:** e93105.

R Development Core Team. 2012. *R: a language and environment for statistical computing*. Vienna. Austria. R Foundation for statistical Computing.

Ricqlès A de, Padian K, Horner JR. 2003. On the bone histology of some Triassic pseudosuchian archosaurs and related taxa. *Annales de Paleontologie* **89:** 67–101.

Ricqlès A de, Padian K, Knoll F, Horner JR. 2008. On the origin of high growth rates in archosaurs and their ancient relatives: complementary histological studies on Triassic archosauriforms and the problem of a 'phylogenetic signal' in bone histology. *Annales de Paleontologie* **94:** 57–76.

Rinehart LF, Lucas SG. 2013. The functional morphology of dermal bone ornamentation in temnospondyl amphibians. In: Tanner LH, Spielmann JA, Lucas SG, eds. *The Triassic system,* Vol. 61. Albuquerque: *New Mexico Museum of Natural History and Science*, 524–532.

Rowe T. 2002. *Digimorph: a national science foundation digital library at the 292 University of Texas at Austin*. Available at: http//:digimorph.org.

Scheyer TM, Martin Sander P, Joyce WG, Böhme W, Witzel U. 2007. A plywood structure in the shell of fossil and living soft-shelled turtles (Trionychidae) and its evolutionary implications. *Organisms Diversity and Evolution* **7:** 136–144.

Schoch R. 2007. Osteology of the small archosaur *Aetosaurus* from the Upper Triassic of Germany. *Neues Jahrbuch für Geologie und Paläontologie – Abhandlungen*. **246:** 1–35.

Seebacher F, Grigg GC, Beard LA. 1999. Crocodiles as dinosaurs: behavioural thermoregulation in very large ectotherms leads to high and stable body temperatures. *The Journal of Experimental Biology* **202:** 77–86.

Seidel MR. 1979. The osteoderms of the American alligator and their functional significance. *Herpetologica* **35:** 375–380.

Sereno PC, Arcucci AB. 1990. The monophyly of crurotarsal archosaurs and the origin of bird and crocodile ankle joints. *Neues Jahrbuch für Geologie und Paläontologie, Abhandlungen* **180:** 21–52.

Sereno PC, Larsson HC, Sidor CA, Gado B. 2001. The giant crocodyliform *Sarcosuchus* from the Cretaceous of Africa. *Science* **294:** 1516–1519.

Sereno PC, Larsson HCE. 2009. Cretaceous crocodyliforms from the Sahara. *Zookeys* **28:** 1–143.

Sertich J. 2010. Appendicular skeleton of *Simosuchus clarki* (Crocodyliformes: Notosuchia) from the late Cretaceous of Madagascar. *Journal of Vertebrate Paleontology* **30:** 122–153

Spotila JR, Terpin KM, Dodson P. 1977. Mouth gaping as an effective thermoregulatory device in alligators. *Nature* **265:** 235–236.

Steel R. 1973. Crocodylia. In: Kuhn O, ed. *Encyclopedia of Paleoherpetology*, part 16. Stuttgart, Germany: Gustav Fisher Verlag.

Stubbs TL, Pierce SE, Rayfield EJ, Anderson PSL. 2013. Morphological and biomechanical disparity of crocodile-line archosaurs following the end-Triassic extinction. *Proceedings of the Royal Society B Biological Sciences* **280:** 20131940.

Trotteyn MJ, Arcucci AB, Raugust T. 2013. Proterochampsia: an endemic archosauriform clade from South America. *Geological Society of London, Special Publications* **379:** 59–90.

Trutnau L, Sommerlad R. 2006. *Crocodilians their natural history & captive husbandry. Edition Chimaira*: Frankfurt am Main.

Tykoski RS, Rowe TB, Ketcham RA, Colbert MW. 2002. *Calsoyasuchus Valliceps*, a new Crocodyliform from the early Jurassic Kayenta formation of Arizona. *Journal of Vertebrate Paleontology* **22:** 593–611.

Walker AD. 1990. A revision of *Sphenosuchus acutus* Haughton, a crocodylomorph reptile from the Elliot formation (late Triassic or early Jurassic) of South Africa. Philos. *Proceedings of the Royal Society B Biological Sciences* **330:** 1–120.

Watanabe A, Slice DE. 2014. The utility of cranial ontogeny for phylogenetic inference: a case study in crocodylians using geometric morphometrics. *Journal of Evolutionary Biology* **27:** 1078–1092.

Werning S, Irmis RB. 2011. Reconstructing growth of the basal archosauromorph *Trilophosaurus*. *Integrative and Comparative Biology* **51:** E147.

Werning S, Irmis R, Smith N, Turner A, Padian K. 2011. Archosauromorph bone histology reveals early evolution of elevated growth and metabolic rates. *Journal of Vertebrate Paleontology* **31:** 213.

Wilberg EW. 2015. What's in an outgroup? The impact of outgroup choice on the phylogenetic position of Thalattosuchia (Crocodylomorpha) and the origin of Crocodyliformes. *Systematic Biology* **64:** 621–637.

Witzmann F. 2009. Comparative histology of sculptured dermal bones in basal tetrapods, and the implications for the soft tissue dermis. *Palaeodiversity* **2:** 233–270.

Witzmann F, Soler-Gijón R. 2010. The bone histology of osteoderms in temnospondyl amphibians and in the chroniosuchian *Bystrowiella*. *Acta Zoologica* **91:** 96–114.

Wu X, Russell A. 2001. Redescription of *Turfanosuchus dabanensis* (Archosauriformes) and new information on its phylogenetic relationships. *Journal of Vertebrate Paleontology* **21:** 40–50.

Young MT, Andrade MB de. 2009. What is Geosaurus? Redescription of *Geosaurus giganteus* (Thalattosuchia: Metriorhynchidae) from the upper Jurassic of Bayern, Germany. *Zoological Journal of the Linnean Society* **157:** 551–585.

Young MT, Brusatte SL, Ruta M, Andrade MB de. 2010. The evolution of Metriorhynchoidea (Mesoeucrocodylia, Thalattosuchia): an integrated approach using geometric morphometrics, analysis of disparity, and biomechanics. *Zoological Journal of the Linnean Society* **158:** 801–859.

Zanno LE, Drymala S, Nesbitt SJ, Schneider VP. 2015. Early crocodylomorph increases top tier predator diversity during rise of dinosaurs. *Scientific Reports* **5:** 9276.

SUPPORTING INFORMATION

Additional Supporting Information may be found in the online version of this article at the publisher's website:

Annex 1: Dataset of the variables defining ornamentation both on the skull table (t) and on the nasal (n) for each taxa with corresponding periods (in million years): GAtot (in percentage); GApit (no unity); OArelat (no unity).
Annex 2A: Sampled specimens with corresponding taxa references.
Annex 2B: Anatomical data with corresponding references used to infer the lifestyle of each sampled specimen.

Annex 1: Dataset of the variables defining ornamentation both on the skull table ($_t$) and on the nasal ($_n$) for each taxa with corresponding periods (in million years): GAtot (in percentage); GApit (no unity); OArelat (no unity).

TAXA	$GAtot_t$	$GApit_t$	$OArelat_t$	$GAtot_n$	$GApit_n$	$OArelat_n$	Lifestyle	Period
INCERTAE SEDIS								
Prolacerta broomi	0.00	0.00	0.00	0.00	0.00	0.00	terrestrial	252-251
Proterosuchus fergusi	0.00	0.00	0.00	0.00	0.00	0.00	terrestrial	252-251
Erythrosuchus africanus	0.00	0.00	0.00	0.00	0.00	0.00	terrestrial	247-201
Euparkeria capensis	0.00	0.00	0.00	0.00	0.00	0.00	terrestrial	247-242
PROTEROCHAMPSIA								235-222
Proterochampsa barrionuevoi	9.88	1.19	0.51	8.24	1.17	0.49	amphibious	235-228
PHYTOSAURIA								228-220
Mystriosuchus planirostris	6.15	1.15	0.41	2.20	1.07	0.31	amphibious	216-212
Rutiodon doughtyii	3.26	1.14	0.24	2.50	1.08	0.31	amphibious	221-206
Angistorhinus sp.	0.00	0.00	0.00	0.00	0.00	0.00	amphibious	221-206
PSEUDOSUCHIA								250-0
AETOSAURIA								230-220
Aetosaurus ferratus	0.00	0.00	0.00	0.00	0.00	0.00	terrestrial	215-212
Typothorax coccinarum	0.00	0.00	0.00	0.00	0.00	0.00	terrestrial	222-202
PARACROCODYLOMORPHA								247-0
Decuriasuchus quartacolonia	0.00	0.00	0.00	0.00	0.00	0.00	terrestrial	242-235
Qianosuchus mixtus	0.00	0.00	0.00	0.00	0.00	0.00	terrestrial	247-242
Ticinosuchus ferox	0.00	0.00	0.00	0.00	0.00	0.00	terrestrial	247-242
Saurosuchus galilei	0.00	0.00	0.00	0.00	0.00	0.00	terrestrial	235-222
Effigia okeefeae	0.00	0.00	0.00	0.00	0.00	0.00	terrestrial	206-202
Turfanosuchus dabanensis	0.00	0.00	0.00	0.00	0.00	0.00	terrestrial	247-235
Prestosuchus chiniquensis	0.00	0.00	0.00	0.00	0.00	0.00	terrestrial	242-235
RAUISUCHIA								242-202
Postosuchus kirkpatricki	0.00	0.00	0.00	0.00	0.00	0.00	terrestrial	222-206
CROCODYLOMORPHA								235-0
Kayentasuchus walkeri	0.00	0.00	0.00	0.00	0.00	0.00	terrestrial	197-183

Litargosuchus leptorhynchus	0.00	0.00	0.00	0.00	0.00	0.00	terrestrial	202-190
Hesperosuchus sp.	0.00	0.00	0.00	0.00	0.00	0.00	terrestrial	206-202
Pseudhesperosuchus jachaleri	0.00	0.00	0.00	0.00	0.00	0.00	terrestrial	221-205
Saltoposuchus connectens	0.00	0.00	0.00	0.00	0.00	0.00	terrestrial	216-212
Dromicosuchus grallator	0.00	0.00	0.00	0.00	0.00	0.00	terrestrial	235-206
Sphenosuchus acutus	0.00	0.00	0.00	0.00	0.00	0.00	terrestrial	202-190
THALATTOSUCHIA								200-133
Insertae sedis								
Pelagosaurus typus	4.52	1.08	0.58	0.00	0.00	0.00	amphibious	183-182
Teleosauridae								183-66
Teleosaurus cadomensis	2.71	1.18	0.50	0.00	0.00	0.00	amphibious	168-151
Steneosaurus sp.	3.60	1.39	0.09	0.00	0.00	0.00	amphibious	183-140
Metriorhynchidae								172-113
Metriorynchus superciliosus	0.00	0.00	0.00	0.00	0.00	0.00	pelagic	165-151
Dakosaurus andiniensis	0.00	0.00	0.00	0.00	0.00	0.00	pelagic	146-140
Geosaurus giganteus	0.00	0.00	0.00	0.00	0.00	0.00	pelagic	151-145
Cricosaurus araucanensis	0.00	0.00	0.00	0.00	0.00	0.00	pelagic	151-145
Rhacheosaurus gracilis	0.00	0.00	0.00	0.00	0.00	0.00	pelagic	151-146
Purranisaurus potens	0.00	0.00	0.00	0.00	0.00	0.00	pelagic	151-140
CROCODYLIFORMES								222-0
PROTOSUCHIA								222-113
Protosuchus richardsoni	2.07	1.07	0.32	4.67	1.12	0.39	terrestrial	202-197
NOTOSUCHIA								113-48
Sebecus icaeorhinus	4.05	1.11	0.37	1.84	1.08	0.24	terrestrial	56-48
Simosuchus clarki	5.46	1.12	0.45	4.30	1.09	0.49	terrestrial	71-66
Notosuchus terrestris	0.00	0.00	0.00	0.00	0.00	0.00	terrestrial	86-85
Araripesuchus wegeneri	2.92	1.11	0.27	4.31	1.09	0.49	terrestrial	122-100
INCERTAE SEDIS								
Trematochampsidae								130-66
Trematochampsa taqueti	15.16	1.07	0.61	10.91	1.21	0.53	amphibious	89-84
NEOSUCHIA								196-0
Goniopholidae								182-66

Amphicotylus lucasii	19.49	1.40	0.48	8.14	1.16	0.51	amphibious	156-145
Calsoyasuchus valliceps	7.81	1.18	0.43	5.21	1.16	0.33	amphibious	196-183
Pholidosauridae								163-94
Teleorhinus browni	0.00	0.00	0.00	0.00	0.00	0.00	amphibious	94-89
Sarcosuchus imperator	0.00	0.00	0.00	0.00	0.00	0.00	amphibious	100-94
Crocodylia								86-0
Alligator mississippiensis	10.21	1.10	0.50	6.67	1.14	0.55	amphibious	extant
Caiman crocodilus	14.08	1.22	0.60	5.93	1.09	0.54	amphibious	extant
Crocodylus acutus	16.88	1.27	0.59	17.98	1.27	0.68	amphibious	extant
Mecistops cataphractus	17.89	1.22	0.64	3.20	1.06	0.61	amphibious	extant
Crocodylus intermedius	25.46	1.50	0.50	17.67	1.29	0.67	amphibious	extant
Crocodylus niloticus	10.93	1.19	0.48	7.68	1.15	0.65	amphibious	extant
Crocodylus palustris	31.90	1.48	0.66	20.45	1.31	0.69	amphibious	extant
Crocodylus porosus	13.69	1.23	0.51	23.60	1.35	0.73	amphibious	extant
Crocodylus rhombifer	15.14	1.26	0.49	4.58	1.09	0.57	amphibious	extant
Gavialis gangeticus	10.21	1.11	0.46	0.00	0.00	0.00	amphibious	extant
Melanosuchus niger	16.88	1.25	0.49	12.26	1.22	0.61	amphibious	extant
Osteolaemus tetraspis	16.47	1.19	0.67	6.00	1.11	0.67	amphibious	extant
Paleosuchus trigonatus	20.33	1.24	0.69	7.28	1.02	0.62	amphibious	extant
Crocodylus moreletii	16.47	1.81	0.20	4.65	1.23	0.20	amphibious	extant
Crocodylus johnstoni	6.58	1.53	0.40	0.00	0.00	0.00	amphibious	extant
Tomistoma schlegelii	11.60	1.23	0.51	0.00	0.00	0.00	amphibious	extant
Caiman latirostris	10.68	1.26	0.40	10.59	1.26	0.40	amphibious	extant
Alligator sinensis	11.89	1.27	0.43	4.12	1.10	0.42	amphibious	extant
Caiman yacare	18.21	1.32	0.58	3.46	1.07	0.53	amphibious	extant
Crocodylus mindorensis	10.02	1.32	0.32	0.95	1.03	0.33	amphibious	extant
Crocodylus novaeguinae	5.66	1.28	0.20	1.64	1.09	0.19	amphibious	extant
Diplocynodon hantoniensis	9.21	1.28	0.33	3.32	1.07	0.51	amphibious	56-28
Gavialosuchus americanus	24.00	1.66	0.36	2.77	1.09	0.31	amphibious	29-23
Voay robustus	15.68	1.39	0.41	1.90	1.03	0.55	amphibious	0.012-0.002
Borealosuchus sternbergii	11.27	1.28	0.40	5.53	1.12	0.45	amphibious	66-63

Annex 2A: Sampled specimens with corresponding taxa references.

TAXA	Specimen reference	Taxa reference
INCERTAE SEDIS		
Prolacerta broomi	NMQR-3763	Parrington, 1935
Proterosuchus fergusi	NMQR-880	Broom, 1913
Erythrosuchus africanus	NMQR-3675	Broom, 1905
Euparkeria capensis	SAM-PK-005867	Broom, 1913
PROTEROCHAMPSIA		Kischlatt, 2000
Proterochampsa barrionuevoi	USNM-419692	Reig, 1959
PHYTOSAURIA		Jaeger, 1828
Mystriosuchus planirostris	AMNH-10644	Meyer, 1863
Rutiodon doughtyii	AMNH-4919	Emmons, 1856
Angistorhinus sp.	Lucas et al., 2002	Mehl, 1913
PSEUDOSUCHIA		Zittel, 1887
AETOSAURIA		Lyddeker, 1889
Aetosaurus ferratus	Schoch, 2007	Fraas, 1877
Typothorax coccinarum	Heckert et al., 2010	Cope, 1875
RAUISUCHIA		Von Huene, 1942
Postosuchus kirkpatricki	Chatterjee, 1985	Chatterjee, 1985
PARACROCODYLOMORPHA		Parrish, 1993
Decuriasuchus quartacolonia	Franca et al., 2011	Franca et al., 2011
Qianosuchus mixtus	Li et al., 2006	Li et al., 2006
Ticinosuchus ferox	Lautenshlager and Desojo, 2011	Krebs, 1965
Saurosuchus galilei	Alcober, 2000	Reig, 1959
Effigia okeefeae	Nesbitt, 2007	Nesbitt and Norell, 2006
Turfanosuchus dabanensis	Wu and Russel, 2001	Young, 1973
Prestosuchus chiniquensis	AMNH-3856	Huene, 1942
CROCODYLOMORPHA		Hay, 1930
Kayentasuchus walkeri	Clarck and Sues, 2002	Clark and Sues, 2002
Litargosuchus leptorhynchus	Clarck and Sues, 2002	Clarck and Sues,2002
Hesperosuchus sp.	Irmis et al., 2013	Colbert, 1952
Pseudhesperosuchus jachaleri	Irmis et al., 2013	Bonaparte, 1969

Saltoposuchus connectens	Irmis et al., 2013	Huene, 1921
Dromicosuchus grallator	Irmis et al., 2013	Sues et al., 2003
Sphenosuchus acutus	Walker, 1990	Haughton, 1915
Postosuchus kirkpatricki	Chatterjee, 1985	Chatterjee, 1985
THALATTOSUCHIA		Fraas, 1901
Insertae sedis		
Pelagosaurus typus	MNHN-1914-2	Bronn, 1841
Teleosauridae		Geoffroy, 1831
Teleosaurus cadomensis	MNHN.F RJN 464	Lamouroux, 1820
Steneosaurus sp.	AMNH-10646	Saint-Hilaire, 1825
Metriorhynchidae		Fitzinger, 2009
Metriorhynchus superciliosus	MNHN-1908-6	de Blainville, 1853
Dakosaurus andiniensis	Pol and Gasparini, 2009	Gasparini, 1996
Geosaurus giganteus	Young and Andrade, 2009	Sommerring, 1816
Cricosaurus araucanensis	Parrilla-Bel et al., 2013	Gasparini and Dellape, 1976
Rhacheosaurus gracilis	Parrilla-Bel et al., 2013	Meyer, 1831
Purranisaurus potens	Herrera et al., 2015	Rusconi, 1948
CROCODYLIFORMES		Hay, 1930
PROTOSUCHIA		Mook, 1934
Protosuchus richardsoni	AMNH-3024	Brown, 1933
NOTOSUCHIA		Gasparini, 1971
Sebecus icaeorhinus	UA 8679	Buckley et al., 2000
Simosuchus clarki	AMNH-3160	Simpson, 1937
Notosuchus terrestris	Kälin, 1955	Woodward, 1896
Araripesuchus wegeneri	MNN-GAD19	Buffetaut, 1981
INCERTAE SEDIS		
Trematochampsidae		Buffetaut, 1974
Trematochampsa taqueti	MNHN-IBC 235-087-1391-2075-2076-2077-2078	Buffetaut, 1974
NEOSUCHIA		Clarck, 1988
Goniopholidae		Cope, 1875
Amphicotylus lucasii	TMM 43631-1	Tykoski, 2002
Calsoyasuchus valliceps	AMNH-5782	Cope, 1878

Pholidosauridae		Von Zittel & Eastman, 1902
Teleorhinus browni	MNHN-GDF-662-100	Broin & Taquet, 1966
Sarcosuchus imperator	AMNH-5849	Osborn, 1904
Crocodylia		Owen, 1842
Crocodylus mindorensis	SMITH-228407	Schmidt, 1935
Crocodylus moreletii	TMM-M-4980	Duméril & Bibron, 1851
Crocodylus niloticus	MNHN-A5307	Laurenti, 1768
Crocodylus novaeguinae	SMITH 211290	Schmidt, 1928
Crocodylus palustris	MNHN-1944-229	Lesson, 1831
Crocodylus porosus	MNHN-A5316	Schneider, 1801
Crocodylus rhombifer	MNHN-1949-421	Cuvier, 1807
Crocodylus johnstoni	TMM-M-6807	Krefft, 1873
Gavialis gangeticus	MNHN-1944-249	Gmelin, 1789
Borealosuchus sternbergii	USNM-6533	Gilmore, 1910
Diplocynodon hantoniensis	AMNH-27632	Wood, 1846
Voay robustus	AMNH-3101	Grandidier & Vaillant, 1872
Osteolaemus tetraspis	MNHN-1931-45	Cope, 1861
Tomistoma schlegelii	TMM-M-6342	Müller, 1838
Gavialosuchus americanus	AMNH-5663	Sellards, 1915
Alligator mississippiensis	MNHN-1919-127	Daudin, 1802
Alligator sinensis	SMITH 292078	Fauvel, 1879
Caiman crocodilus	MNHN-1887-773	Linnaeus, 1758
Caiman yacare	SMITH 281286	Daudin, 1802
Caiman latirostris	MNHN-A5305	Daudin, 1802
Melanosuchus niger	MNHN-1900-112	Spix, 1825
Paleosuchus trigonatus	MNHN-ZA-AC-2014-1	Schneider, 1801
Crocodylus mindorensis	SMITH-228407	Schmidt, 1935
Crocodylus moreletii	TMM-M-4980	Duméril & Bibron, 1851
Crocodylus niloticus	MNHN-A5307	Laurenti, 1768

Annex 2B: Anatomical data with corresponding references used to infer the lifestyle of each sampled specimen.

	Lifestyle	Skull anatomy	Locomotion	Reference
INCERTAE SEDIS				
Prolacerta broomi	terrestrial	high skull lateral orbits and nostrils	bipedal	Gow, 1975
Proterosuchus fergusi	terrestrial	high skull lateral orbits and nostrils	bipedal	Gow, 1975
Erythrosuchus africanus	terrestrial	high skull lateral orbits and nostrils	erected quadrupedal	Hoffstetter, 1955 Parrish, 1992
Euparkeria capensis	terrestrial	high skull, lateral orbits and nostrils	erected quadrupedal, optional bipedal	Ewer, 1965
PROTEROCHAMPSIA				
Proterochampsa barrionuevoi	amphibious	flat skull, dorsal orbits and nostrils	no data	Trotteyn et al., 2013
PHYTOSAURIA				
Rutiodon doughty	amphibious	longirostrine skull, dorsal orbits and nostrils	semi-erected quadrupedal	Hoffstetter, 1955 Padian al., 2010
Mystriosuchus planirostris	amphibious	longirostrine skull, dorsal orbits and nostrils	semi-erected quadrupedal	Hoffstetter, 1955 Padian et al., 2010
Angisthorhinus sp.	amphibious	longirostrine skull, dorsal orbits and nostrils	semi-erected quadrupedal	Hoffstetter, 1955 Padian et al., 2010
PSEUDOSUCHIA				
AETOSAURIA				
Aetosaurus ferratus	terrestrial	high skull, lateral orbits and nostrils	erected quadrupedal	Desojo et al., 2013 Parrish, 1986

Typothorax coccinarum	terrestrial	high skull, lateral orbits and nostrils	erected quadrupedal	Desojo et al., 2013 Parrish, 1986
RAUISUCHIA				
Postosuchus kirkpatricki	terrestrial	high skull, lateral orbits and nostrils	erected quadrupedal	Parrish, 1986
PARACROCODYLOMORPHA				
Saurosuchus gallilei	terrestrial	high skull, lateral orbits and nostrils	erected quadrupedal	Desojo et al., 2013 Parrish, 1986
Decuriasuchus quartacolonia	terrestrial	high skull, lateral orbits and nostrils	erected quadrupedal	França et al., 2011 Parrish, 1986
Prestosuchus chiniquensis	terrestrial	high skull, lateral orbits and nostrils	semi-erected quadrupedal	Liparini and Schultz, 2013
Qianosuchus mixtus	terrestrial	high skull, lateral orbits and nostrils	erected quadrupedal	Li et al, 2006
Effigia okeefeae	terrestrial	high skull, lateral orbits and nostrils	bipedal	Nesbitt, 2007
Ticinosuchus ferox	terrestrial	high skull, lateral orbits and nostrils	erected quadrupedal	Lautenshlager and Desojo, 2011
Turfanosuchus dabanensis	terrestrial	high skull, lateral orbits and nostrils	erected quadrupedal	Wu and Russel, 2001
CROCODYLOMORPHA				
Kayentasuchus walkeri	terrestrial	high skull, lateral orbits and nostrils	fast-running erected quadrupedal	Clark and Sues, 2002 Irmis et al, 2013
Litargosuchus leptorhynchus	terrestrial	lateral orbits and nostrils	fast-running erected quadrupedal	Clark and Sues, 2002
Saltoposuchus connectens	terrestrial	high skull, lateral orbits and nostrils	fast-running erected quadrupedal	Irmis et al, 2013

Sphenosuchus acutus	terrestrial	high skull, lateral orbits and nostrils	fast-running erected quadrupedal	Irmis et al, 2013
Dromicosuchus grallator	terrestrial	high skull, lateral orbits and nostrils	fast-running erected quadrupedal	Irmis et al, 2013
Pseudhesperosuchus jachaleri	terrestrial	high skull, lateral orbits and nostrils	fast-running erected quadrupedal	Irmis et al, 2013
Hesperosuchus sp.	terrestrial	high skull, lateral orbits and nostrils	fast-running erected quadrupedal	Irmis et al, 2013
THALATTOSUCHIA				
Insertae sedis				
Pelagosaurus typus	amphibious	longirostrine skull, posterior position of the inner choanae dorsal nostrils	semi-erected quadrupedal	Pierce and Benton, 2006 Parrish, 1986
Teleosauridae				
Teleosaurus cadomensis	amphibious	longirostrine skull, posterior position of the inner choanae dorsal orbits and nostrils	semi-erected quadrupedal	Jouve, 2014 Parrish, 1986
Steneosaurus sp.	amphibious	longirostrine skull, posterior position of the inner choanae dorsal orbits and nostrils	semi-erected quadrupedal	Kälin, 1955 Parrish, 1986
Metriorhynchidae				
Metriorhynchus superciliosus	pelagic	loss of the mandibular fenestrae (impossible gape basking on land)	tail fluke paddle-like hindlimbs	Young et al., 2010 Kälin, 1955

Cricosaurus araucanensis	pelagic	loss of the mandibular fenestrae (impossible gape basking on land)	tail fluke paddle-like hindlimbs	Young et al., 2010 Kälin, 1955
Rhacheosaurus gracillis	pelagic	loss of the mandibular fenestrae (impossible gape basking on land)	tail fluke paddle-like hindlimbs	Young et al., 2010 Kälin, 1955
Dakosaurus andiniensis	pelagic	loss of the mandibular fenestrae (impossible gape basking on land)	tail fluke paddle-like hindlimbs	Young et al., 2010 Kälin, 1955
Geosaurus giganteus	pelagic	loss of the mandibular fenestrae (impossible gape basking on land)	tail fluke paddle-like hindlimbs	Young et al., 2010 Kälin, 1955
Purranisaurus potens	pelagic	loss of the mandibular fenestrae (impossible gape basking on land)	tail fluke paddle-like hindlimbs	Young et al., 2010 Kälin, 1955
CROCODYLIFORMES				
PROTOSUCHIA				
Protosuchus richardsoni	terrestrial	lateral orbits and nostrils	erected quadrupedal	Kälin, 1955 Parrish, 1986
NOTOSUCHIA				
Simosuchus clarki	terrestrial	skull pitched down along the longitudinal axis	heavy dermal shield (swimming is not possible)	Kley et al., 2010 Sertich and Groenke, 2010
Sebecus icaeorhinus	terrestrial	high skull, lateral orbits and nostrils	erected quadrupedal	Buffetaut, 1982 Pol et al., 2011
Notosuchus terrestris	terrestrial	lateral orbits and nostrils	erected quadrupedal	Kälin, 1955 Pol, 2005
Araripesuchus wegeneri	terrestrial	dorsolateral orbits, lateral nostrils	erected quadrupedal	Ortega et al, 2000 Sereno and Larsson, 2009
INCERTAE SEDIS				

Trematochampsidae				
Trematochampa taqueti	amphibious	flat large mandibular	semi-erected quadrupedal	Buffetaut, 1982
NEOSUCHIA				
Pholidosauridae				
Sarcosuchus imperator	amphibious	longirostrine dorsal orbits and nostrils	no data	Sereno et al., 2001
Teleorhinus browni	amphibious	longirostrine dorsal orbits and nostrils	semi-erected quadrupedal	Buffetaut, 1982
Goniopholidae				
Calsoyasuchus valliceps	amphibious	longirostrine dorsal orbits and nostrils	no data	Tykoski et al., 2002
Amphicotylus lucasii	amphibious	flat skull dorsal orbits and nostrils	semi-erected quadrupedal	Buffetaut, 1982
Crocodylia				
Borealosuchus sternbergii	amphibious	flat skull dorsal orbits and nostrils	semi-erected quadrupedal	Brochu et al., 2012 Parrish, 1986
Diplocynodon hantoniensis	amphibious	flat skull dorsal orbits and nostrils	semi-erected quadrupedal	Martin et al., 2014 Parrish, 1986
Voay robustus	amphibious	flat skull dorsal orbits and nostrils	semi-erected quadrupedal	Brochu, 2007 Parrish,1986
Gavialosuchus americanus	amphibious	longirostrine dorsal orbits and nostrils	semi-erected quadrupedal	Steel, 1973 Parrish, 1986

PARTIE 2: ETUDE DES IMPLICATIONS MORPHO-FONCTIONNELLES ET PHYSIOLOGIQUES DE L'ORNEMENTATION OSSEUSE DES PSEUDOSUCHIENS.

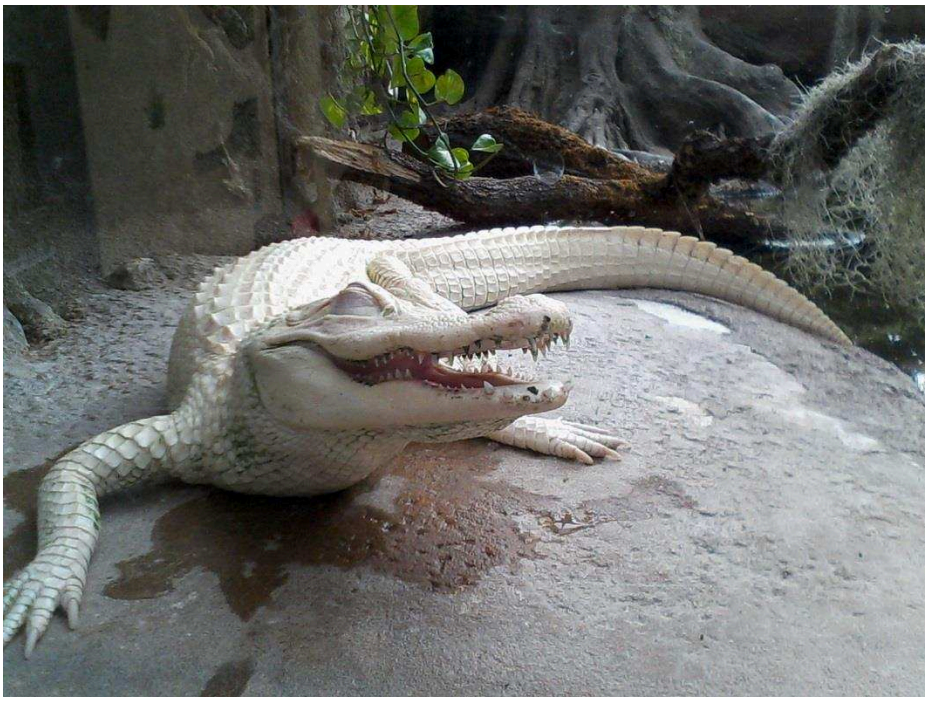

Alligator mississippiensis,

spécimen albinos (La Planète des Crocodiles, Civeaux 2016)

Plan rapproché sur les ostéodermes nuchaux

CHAPITRE 1: QUANTIFICATION DE LA CONDUCTION DE CHALEUR AU TRAVERS DU SQUELETTE DERMIQUE POST-CRANIEN CHEZ LES CROCODYLOMORPHES.

Crocodilus niloticus (La ferme aux Crocodiles, Pierrelatte 2015)

Journal of Thermal Biology 69 (2017) 39–53

Contents lists available at ScienceDirect

Journal of Thermal Biology

journal homepage: www.elsevier.com/locate/jtherbio

Do the ornamented osteoderms influence the heat conduction through the skin? A finite element analysis in Crocodylomorpha

F. Clarac[a,b,*], F. Goussard[b], L. Teresi[d], Vde. Buffrénil[b], V. Sansalone[c]

[a] Sorbonne Universités UPMC Univ Paris 6, CNRS, Institut des Sciences de la Terre de Paris (ISTeP), 4 place Jussieu – BC 19, 75005 Paris, France
[b] Département Histoire de la Terre, Museum National d'Histoire Naturelle, UMR 7207 (CR2P), Sorbonne Universités, MNHN/CNRS/UPMC, Bâtiment de Géologie, Paris Cedex 05 F-75231, France
[c] Université Paris-Est, Laboratoire Modélisation et Simulation Multi Echelle, MSME UMR 8208 CNRS, 61 avenue du Général de Gaulle, 94010 Créteil Cedex, France
[d] Università degli Studi Roma Tre Dept. of Mathematics & Physics, Via della Vasca Navale 84, 00146 Rome, Italy

ARTICLE INFO

Keywords:
Temperature
Heat transfer
Bone ornamentation
3D modeling
Simulation

ABSTRACT

In order to assess the implication of the crocodylomorph ornamented osteoderms on the skin conduction during basking, we have performed three dimensional modeling and finite element analyses on a sample which includes both extant dry bones and well-preserved fossils tracing back to the Early Jurassic. In purpose to reveal the possible implication of the superficial ornamentation on the osteoderm heat conduction, we repeated the simulation on an equivalent set of smoothed 3D-modeled osteoderms. The comparison of the results evidenced that the presence of the apical sculpture has no significant impact on the osteoderm global conduction. Furthermore, as we also aimed to assess the influence of the inner bone porosity on the osteoderm conduction, we modified the heat equation parameters so that the 3D-modeled osteoderms successively score the compact and the cancellous bone properties (*i.e.* mass density, heat capacity, thermal conductivity and thermal diffusivity). Finally, we repeated the analyses using the soft-dermis properties which lead to outline that neither the degree of porosity nor the presence of the osteoderms (in itself) significantly modifies the heat conduction through the crocodylomorph skin. Consequently, as hypothesized by previous authors, if the dermal shield happens to be involved into heat capture during basking for crocodylians, this process must mainly rely on a convective effect based on the osteoderm relative degree of vascularization. This last assumption could thus explain why the crocodylians which produce little metabolic heat would carry an entire vascularized osteoderm shield.

1. Introduction

Among vertebrates, the dermal ossification is a common process at the origin of both the dermatocranium and the osteoderms (Gilbert et al., 2001; Vickaryous and Sire, 2009). All these mineralized tissues can develop a superficial ornamentation (or sculpture) on their apical side which may show various morphological patterns (Zylberberg and Castanet, 1985; Märss, 2006; Downs and Donoghue, 2009; Young, 2009; Zylberberg et al., 2010; Lingham-Soliar, 2014). As mostly observed in ectothermic vertebrates, bone ornamentation usually consists of a network made of pits and grooves separated by ridges as in: the tryonichids (soft-shell turtles; Scheyer et al., 2007), the actinopterygians (Lundberg and Aguilera, 2003), the lissamphibians (Rage and Rocek, 2007; Evans et al., 2008; Skutchas, 2016), the temnospondyls (Bystrow, 1935, 1947; Schoch and Milner, 2000; Witzman, 2009; Witzmann et al., 2010; Rinehart and Lucas, 2013; Morkovin, 2015), the early archosauriforms and the crocodylomorphs (Buffrénil, 1982; Scheyer et al., 2014; Buffrénil et al., 2015; Cerda et al., 2013; Clarac et al., 2015). In most of these above mentioned taxa, the functional role of both the osteoderms (when present) and of the dermal bone apical sculpture is still uncertain. Nevertheless, in Crocodylomorpha, the development of both the dorsal shield and of the bone ornamentation correspond to a secondary acquisition which occurred in the early Jurassic. Indeed, like *Protosuchus richardsoni*, both the Triassic "rauisuchids" and "paracrocodylomorphs" presented a smooth or a scatter-sculpted skull and only two rows of shallow-ornamented osteoderms whereas the later forms show both a sculptured full body armor and a well-ornamented skull (Nesbitt, 2011; Scheyer and Desojo, 2011; Irmis et al., 2013; Drymala, 2015; Drymala and Zanno, 2016; Clarac et al., 2017). As the early archosauriforms had a high level of metabolism (Ricqlès et al., 2003, 2008; Seymour et al., 2004; Botha-Brink and Smith, 2011; Legendre et al., 2013, 2016), these modifications of the

* Corresponding author at: Institut des Sciences de la Terre de Paris (ISTeP), 4 place Jussieu – BC 19, 75005 Paris, France.
E-mail address: francois.clarac@mnhn.fr (F. Clarac).

http://dx.doi.org/10.1016/j.jtherbio.2017.06.003
Received 30 March 2017; Received in revised form 1 June 2017; Accepted 4 June 2017
Available online 10 June 2017

dermal skeleton would follow a transition to a low level of metabolism in Pseudosuchia (the crocodylomorph lineage). Consequently, this morphological development could hypothetically take part of a "cooling and warming" system combined with a behavioral thermoregulation which would have permitted to withstand such a change of metabolism (Seebacher et al., 1999). This morphological pattern would especially concern the semi-aquatic forms which are ambush predators characterized by long terrestrial and semi-emerged basking periods (Smith, 1979; Clarac et al., 2017). In this regard, it has been assumed by several authors that both the development of the osteoderm shield and of bone ornamentation in extant crocodylians may be involved in heat transfers (Seidel, 1979; Farlow et al., 2010). Indeed, the calcification of the dermis could both modify the heat conduction of the skin and convey this thermal energy to the general vascular circulation by the set-up of a vascular network (Seebacher and Franklin, 2004; Cerda et al., 2013; Buffrénil et al., 2015). Consequently, the development of the bone ornamentation could improve this heat exchange by blood convection through the vascular network. Furthermore, since it has been assessed that ornamentation provides a gain in the superficial bone area (Clarac et al., 2015) combined with a systematic loss of bone volume, it is possible that this feature also modifies the heat conduction through the dermal bones (as a corollary of the Allen, 1877). Aiming at testing this last assumption, we will use finite element analyses in order to quantify the gain in thermal energy that ornamented osteoderms provide during basking (warming). We will discuss this result with respect to both the corresponding modeled non-ornamented osteoderms and an equivalent shape of non-mineralized dermis. These comparisons will lead us to general conclusions concerning the influence of the dermal ossification on the heat conduction through the skin.

2. Materials and methods

2.1. Biological sample

The sample is composed of eight osteoderms of crocodylomorphs and of one osteoderm of "rauisuchid" (Crocodylomorpha out-group; Nesbitt, 2011; Table 1). They consist of either dry bones from extant species (*Osteolaemus tetraspis*, *Caiman crocodilus*) or well-preserved fossils that trace back to the Jurassic and later periods (*Machimosaurus hugii*, *Sarcosuchus imperator*, *Hyposaurus rogersii*, *Protosuchus richardsoni*, *Trematochampsa taqueti*). The full set of osteoderms represents eight taxa showing various degrees of bone ornamentation (Clarac et al., 2015). All the specimens were directly sampled in museum collection drawers: the MNHN (Muséum National d'Histoire Naturelle; Table 1), the Smithsonian Institution National Museum of Natural History and the AMNH collections (American Museum of Natural History; Table 1).

2.2. Three-dimensional model set-up

The six osteoderms from the MNHN and the Smithsonian collections were scanned with a Breuckmann StereoScan 3D - surface scanner, a device that reconstructs three-dimensional topography using phase contrast. The surface of the bones is virtually reconstructed as a meshwork of adjacent polygons, folded according to bone reliefs in a three-dimensional space. We used two scope ranges, depending on sample size, to obtain adequate mesh resolutions: small scope range (60 mm), resolution: 12 μm; medium scope range (250 mm), resolution: 18 μm. The five 3D-objects thus obtained were exported in PLY-format. Imperfections of the mesh (noise, artefacts, self-interactions, *etc.*), when present, were corrected using Geomagic Studio 2012 cleaning tools (Geomagic Worldwide).

Concerning the two osteoderms from the AMNH collections, we used a portable camera for taking a series of photographs of each osteoderm under various, repeatable angles in order to obtain a three dimensional photogrammetric reconstruction (see for details: Clarac et al., 2017). We used therefore a Canon 60D camera equipped with a Canon 60 mm/2 macro objective, and Canon Speedlite 320EX flash. Camera sensitivity was set to 100 ISO and objective aperture to 16. Moreover, exposure time was set automatically by the camera in order to get clear shots. The goal was to keep the camera fixed and let the object (target) rotate as if we used a Stereoscan 3D surface scanner. Each osteoderm was laid vertically on one edge on a rotating pad which was centered on an unmovable 360° graduated plastic sheet. Each specimen was then photographed every 10° while turning on itself along a 36 shot series. The distance between the camera and the object was set so that the osteoderm took the full size of the field for better definition. The 3D model was generated automatically for each specimen after uploading the 36 pictures in jpeg format into Agisoft Photoscan Professional Version: 1.1.4. This process involves four consecutive stages: aligning pictures, creating a dense cloud, meshworking, and building a surface texture.

As we aim at assessing the effect of ornamentation on the heat conduction through the osteoderms, we duplicated each three-dimensional-reconstructed osteoderm in order to create a copy that lacks ornamentation. This comparative model was set up by suppressing all the pits and replacing them with a smooth surface that would exist in absence of ornamentation (Fig. 1; using Geomagic studio 12) as the pits are known to be excavated by bone resorption (Buffrénil, 1982; Buffrénil et al., 2015). Moreover, in order to remove the effects of size differences between the specimens of the sample, we rescaled each one of them according to the following procedure. First, we measured the upper area of one ornamented osteoderm taken as a reference (*Caiman crocodilus* 1989-6489; Table 1) thanks to a dedicated tool in Geomagic studio 12: "compute selected area". Then, we computed a scale factor as the square root of the ratio between this reference area and the upper area of each ornamented osteoderm (the square root is needed since

Table 1
Sampled osteoderms with taxonomy references. The scaled dimensions are in millimeters and successively represent: the total longitudinal length (L), the total transversal length (l) and the vertical thickness (T). For the keeled osteoderms (*i.e. Osteolaemus tetraspis*, *Caiman crocodilus*, *Trematochampsa taqueti*, Rauisuchidae indet.), the vertical thickness is measured between the top of the keel and its vertical projection on the bottom surface. For the flat osteoderms (*i.e. Sarcosuchus imperator*, *Hyposaurus rogersii*, *Protosuchus richardsoni*, *Machimosaurus hugii*) the vertical thickness is measured between the two vertical projections of the centroid on the top and on the bottom surface.

Family	Gender	Species	Scaled Dimensions (L/l/T)	Collection number	Period
Crocodylidae	*Osteolaemus*	*tetraspis*	23.2/ 24.3/ 3.5	AC.1991.4488a	extant
Crocodylidae	*Osteolaemus*	*tetraspis*	26.2/ 24.8/ 3.6	AC.1991.4488b	extant
Alligatoridae	*Caiman*	*crocodilus*	27.8/ 18.2/ 4.6	1989-6489	extant
Pholidosauridae	*Sarcosuchus*	*imperator*	14.4/ 32.7/ 2.1	1966-15 Gad-4	Cretaceous
Dyrosauridae	*Hyposaurus*	*rogersii*	17.5/ 26.0/ 3.0	AMNH-2389	Cretaceous
Trematochampsidae	*Trematochampsa*	*taqueti*	28.5/ 18.1/ 9.0	IBC-501	Cretaceous
Protosuchidae	*Protosuchus*	*richardsoni*	26.8/ 23.1/ 2.6	AMNH-3024	Jurassic
Teleosauridae	*Machimosaurus*	*hugii*	23.5/ 24.0/ 3.9	SMNS 81608	Jurassic
Rauisuchidae	*Indet.*	*Indet.*	27.6/ 19.2/ 6.0	ZAR 33-1960	Triassic

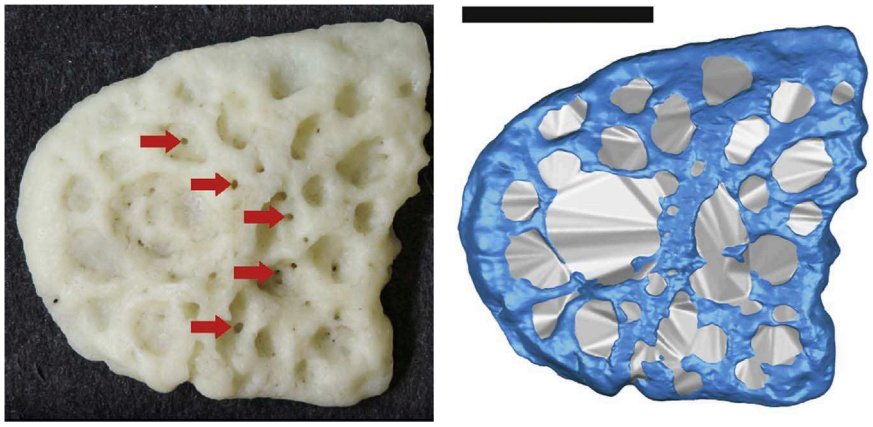

Fig. 1. Osteoderm of *Osteolaemus tetraspis* (AC.1991.4488a). On the left: picture taken from the dorsal view, the red arrows point the vascular canals connecting the outer apical surface with the inside of the osteoderm. On the right: three dimensional scan of the osteoderm with in grey the smoothed area overlying the pits on the non-ornamented version; Scale bar: 7 mm.

this scale factor is based on measures of area (mm^2)). Eventually, each specimen was rescaled using this scale factor (from the centroid of the osteoderm) by means of the function: "model change" (except of course for the reference osteoderm which has a scale factor equal to one: *Caiman crocodilus* 1989-6489; Table 1). This procedure led to a set of osteoderms which all have kept their original shape but which have been rescaled in order to score the same value of ornamented area. The same scale factors were then used on the corresponding smoothed osteoderms. Finally, we remeshed every 3D-model to reduce the number of polygons to between 20000 and 30000 (using Geomagic studio 12). This last step was required to reduce the computational time of the subsequent finite element analysis (FEA).

Table 2
Relevant material properties for the heat conduction problem in the dermis and osteoderm, taken from the ITIS foundation database (see text for complete reference).

Tissue	Mass density ρ [Kg/m^3]	Heat capacity C_p [J/kg °C]	Thermal conductivity k [W/m °C]	Thermal diffusivity α [m^2/s]
Dermis / Skin	1109	3391	0.37	8.84×10^{-8}
Osteoderm / Cortical bone	1908	1313	0.32	1.28×10^{-7}
Osteoderm / Cancellous bone	1178	2274	0.31	1.16×10^{-7}

2.3. Finite element analysis

Finite element analysis (FEA) was used to model heat transfer through the osteoderms in a situation corresponding to an animal basking at an outside temperature of 35 °C (Grigg and Alchin, 1976). The body temperature itself was set to a low value of 20 °C at the beginning of the simulation while the optimal temperature is known to be comprised between 31 °C and 33 °C (Grigg and Alchin, 1976; Johnson et al., 1976). For each osteoderm, we set up a FE model of the osteoderm and the surrounding dermis. Each osteoderm model was embedded into a box representing the surrounding dermis. Box cross section was adapted in order to tightly fit the osteoderm in the horizontal plane. Box height was set to the same value (80 mm) for all the osteoderms. Each osteoderm was placed at about the same distance (10 mm) from the top side of the box. Geometry of the FE model of a typical osteoderm (*Sarcosuchus imperator*) is depicted in Fig. 2A. Material properties of dermis and osteoderm (Table 2) were set equal to those of skin and cortical bone, respectively, by referring to the ITIS foundation database (Hasgall et al., 2015).

In general, crocodylomorph osteoderms are not entirely made up of compact bone but rather show a diploe structure (Scheyer and Desojo, 2011; Burns et al., 2013; Cerda et al., 2013; Buffrénil et al., 2015). However, the surface scanner used in this study cannot provide information about the inner structure of the osteoderm. Therefore, we

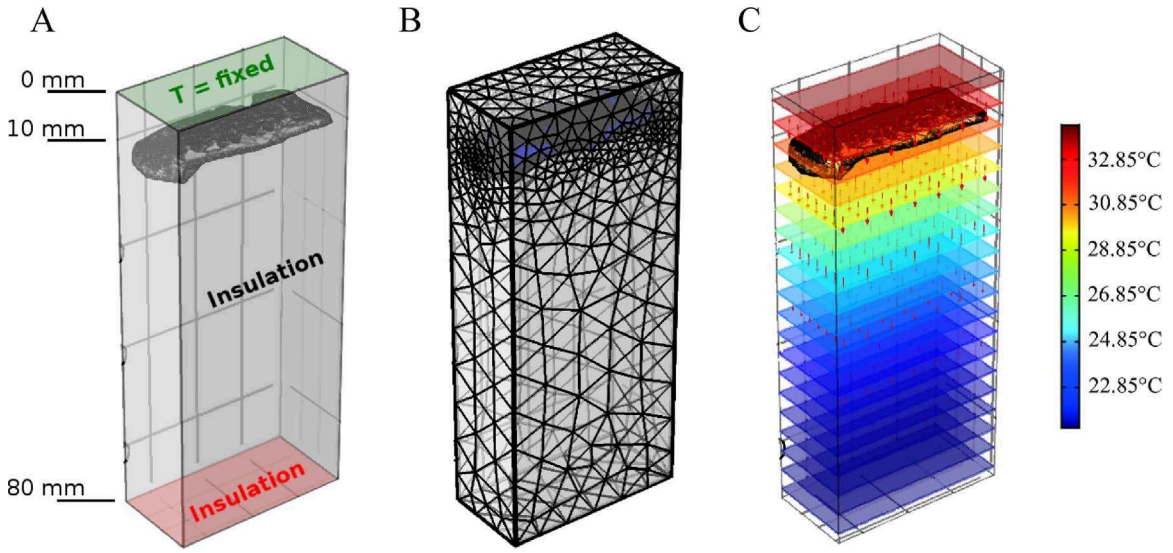

Fig. 2. Finite element model of *Sarcosuchus imperator*. A: Geometry and boundary conditions. B: Finite element mesh. C: Temperature field (isosurfaces) and heat flux field (arrows) after two hours of basking simulation. The temperature at the top of the box (dermis) is 35 °C, the temperature at its bottom is around 22 °C.

decided to model each osteoderm as a homogeneous system and used the material properties of compact bone for the whole sample. However, in order to assess the effects of this assumption, osteoderms of *Caiman crocodilus* (extant keeled osteoderm) and *Machimosaurus hugii* (fossilized flat osteoderm) were also modeled as entirely made up of cancellous bone, see Table 2. Considering an osteoderm as entirely made up of either cortical or cancellous bone provides two limit models of the actual osteoderm. Moreover, in purpose to assess the skin conduction without osteoderm, we performed a third computation on the full sample using the soft-dermis properties as a control simulation.

The heat equation and Fourier's law were used to describe the variation of temperature and the heat transfer in all the points **x** of the region **Ω** constituted by the osteoderm and the dermis during basking, reading respectively:

$$\rho\, C_\rho \frac{\partial T}{\partial t} + \nabla\cdot\mathbf{q} = 0, \tag{1}$$

$$\mathbf{q} = -k\ \nabla T, \tag{2}$$

where t is the time, T the temperature field, and **q** the heat flux (vector) field; moreover, ∇ and $\nabla\cdot$are the gradient and divergence operators, respectively, ρ is the mass density, C_ρ is the heat capacity and k is the thermal conductivity (Table 2). No bulk heat source nor convective heat transfer were considered in the heat equation. Combining Eqs. (Eqs. 1) and (2) leads to:

$$\frac{\partial T}{\partial t} - \alpha\ \nabla^2 T = 0, \tag{3}$$

where ∇^2 is the Laplace operator. Eq. (3) shows that the evolution of the temperature field is basically ruled by one material parameter, that is the thermal diffusivity $\alpha = k/(\rho C_\rho)$. Interestingly, cortical and cancellous bone have quite similar values of this parameter (Table 2). Eqs. (1)–(2), supplemented with suitable initial and boundary conditions (ICs and BCs), provide the time evolution of the temperature and heat flux in the dermis and osteoderm, *i.e.* the values $T(\mathbf{x},t)$ and $\mathbf{q}(\mathbf{x},t)$ of the temperature and of the heat flux, respectively, at all points **x** and all times *t*. Dependency of T and **q** on **x** and t was dropped in Eqs. (1)–(2) for sake of brevity. ICs and BCs were set up in order to simulate the basking conditions described before, that is:

$$ICs: \quad T(\mathbf{x},0) = T_0 \quad , \ \forall\, \mathbf{x} \in \mathbf{\Omega}$$

$$BCs: \begin{cases} T(\mathbf{x},\, t) = T_{ext}, & \forall\ \mathbf{x}\in\partial\mathbf{\Omega}_{top},\ t>0 \\ \mathbf{q}(\mathbf{x},\, t)\cdot\mathbf{n}(\mathbf{x}) = 0, & \forall\ \mathbf{x}\in\partial\mathbf{\Omega}_{btm}\bigcup\partial\mathbf{\Omega}_{lat},\ t>0 \end{cases} \tag{4}$$

where $\partial\mathbf{\Omega}_{top}$, $\partial\mathbf{\Omega}_{btm}$, and $\partial\mathbf{\Omega}_{lat}$ are the top, bottom, and lateral boundaries of **Ω**, respectively, and **n** is the outer unit normal. Eq. (4-a) sets the initial temperature of the whole region (dermis and osteoderm) to $T_0 = 20°C$. BCs in Eq. (4-b, c) set the values of either the temperature or the heat flux on the boundaries of the region for $t > 0$. On the top boundary, the temperature is suddenly increased from T_0 to the external temperature $T_{ext} = 35°C$. Insulation conditions (*i.e.*, no normal heat flux) were assumed on the lateral boundaries for symmetry reasons. BCs on the bottom boundary should account for heat exchange with the rest of the body of the animal. Temperature at the bottom boundary increases while heat flux is transmitted to the body. Therefore, neither fixed temperature nor insulation conditions would apply on $\partial\mathbf{\Omega}_{btm}$. However, these two types of BCs provide bounds for the actual BC which is likely to stay in between. Since no information is available in this respect, as a first approximation, no heat exchange was assumed on the bottom boundary leading to insulation conditions. This approximation is likely to lead to an underestimation of the time needed by the animal to reach an optimal temperature. BCs of a typical FE model are depicted in Fig. 2A. The difference between the initial temperature of the system and that of its top boundary induces a heat flux from the top of the box downward through the osteoderm. Basking time was assumed to last two hours as the average temperature on the bottom surface of the osteoderm ($t°_{bot}$) reaches the optimal physiological value by this period (between 31 °C and 32 °C; Johnson et al., 1976).

The FE model was implemented in Comsol software (COMSOL Multiphysics® v. 5.2. www.comsol.com. COMSOL AB, Stockholm, Sweden). Therefore, a tetrahedral mesh with local quadratic interpolation was used resulting in about 55000 elements per osteoderm and 140000 elements for the whole system. (FE models of *Protosuchus richardsoni* and *Trematochampsa taqueti* required 3 times less and 2 times more elements, respectively.) The FE mesh of *Sarcosuchus imperator* is depicted in Fig. 2B. A preliminary convergence study was performed on one model to set up the mesh parameters; then, mesh quality was systematically checked on each model to ensure reliability of the numerical solution. The heat conduction problem was solved by means of the default time-dependent Comsol solver (backward differentiation formula (BDF) with variable order from 1 to 2) and solution was recorded with a tiny time step (10 s). As a matter of example, the temperature field (isosurfaces) and heat flux field (arrows) in the FE model of *Sarcosuchus imperator* after two hours of basking simulation is depicted in Fig. 2C. Computation time was about fifteen minutes on a standard desktop computer for most of the models. At any time step, 3-D maps of temperature and heat flux within the osteoderm were computed as well as 2-D maps in three orthogonal cut planes passing through the centroid of the osteoderm. Moreover, average temperature and heat flux were computed within the osteoderm and on its upper and lower surfaces. Results were recorded every fifteen minutes.

FE simulations were performed for each model of ornamented osteoderm and then repeated for the corresponding non-ornamented model (except for the rauisuchid which naturally lacks ornamentation). Eventually, in order to assess the effects of the osteoderms on the heat transfer, FE simulations were also performed for baseline models without osteoderms. Baseline models were obtained by replacing the osteoderm with an equal volume of dermis.

2.4. Quantitative assessment of the bone ornamentation

Quantifying the gain in area due to ornamentation basically involves measuring the real area of the ornamented surface of bones with all its deep (pits) and protruding reliefs (ridges), and compare it to a theoretical smooth area, that would exist in the absence of ornamentation. Both these measurements were made with a dedicated tool in Geomagic studio 12, a software that was also used to obtain the smooth surface after converting the scans into PLY-format. The successive stages of this process have already been defined, tested and validated in a previous study (Clarac et al., 2015). Finally, this surface analysis lead to the acquisition of a continuous variable that defines the gain in area on the total surface of a bone (GAtot; in percentage).

Quantifying the loss in volume due to ornamentation requires first to measure the volume of both the ornamented osteoderm and of its smoothed copy. This process ends up with the acquisition of a new variable that defines the loss of bone volume of the osteoderm that is due to the pits excavated on the upper surface of the osteoderm (in percentage):

LV = $100(\frac{\text{SoV} - \text{RoV}}{\text{SoV}})$ SoV: Smoothed osteoderm volume; RoV: Real osteoderm volume.

3. Results

3.1. General description of the heat conduction through the osteoderms

During the warming simulation (basking), the heat energy comes abeam the apical side of the osteoderm driven by the temperature gradient established between the environment (top side of the box at 35 °C) and the body (20 °C). The energy crosses the osteoderm from the top to the bottom while creating a decreasing temperature gradient along the vertical axis during the 2 h basking simulation (Fig. 2). After

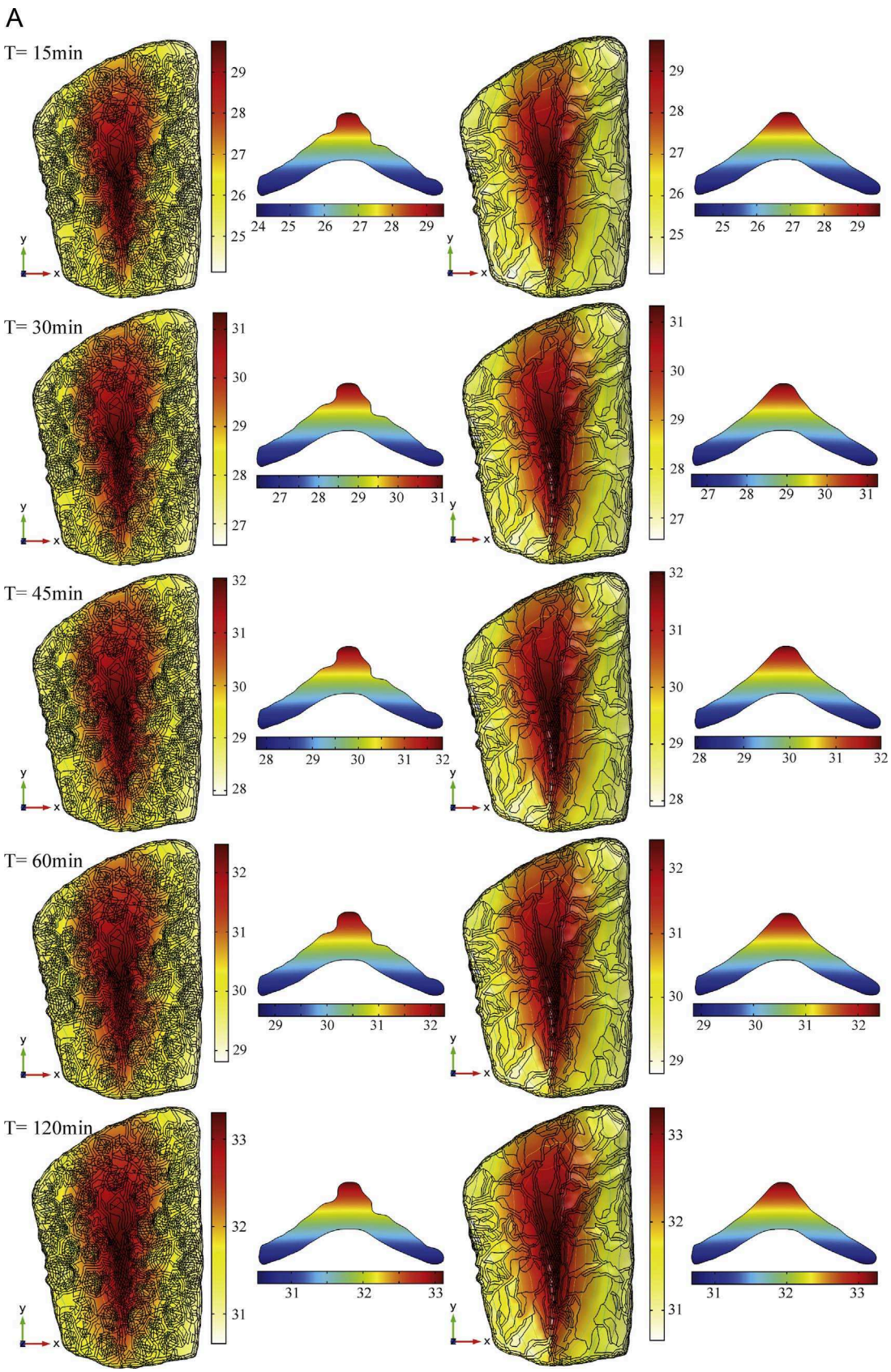

Fig. 3. A: Finite element analysis performed on *Caiman crocodilus* osteoderm: temperature evolution (time interval: 15 min) on the apical surface and in a vertical cross section of the osteoderm. Axes orientations: in green (Y): the longitudinal axis; in red (X): the transversal axis; in blue (Z): the vertical axis. Osteoderm dimensions (after rescaling; see Table 1): 27.8 mm (Y)/ 18.2 mm (X)/ 4.6 mm (Z). Fig. 3B: Finite element analysis performed on *Machimosaurus hugii* osteoderm: temperature evolution (time interval: 15 min) on the apical surface and in a vertical cross section of the osteoderm. Axes orientations: in red (Y): the longitudinal axis; in green (X): the transversal axis; in blue (Z): the vertical axis. Osteoderm dimensions (after rescaling): 23.5 mm (Y)/ 24.0 mm (X)/ 3.9 mm (Z). (For interpretation of the references to color in this figure legend, the reader is referred to the web version of this article.)

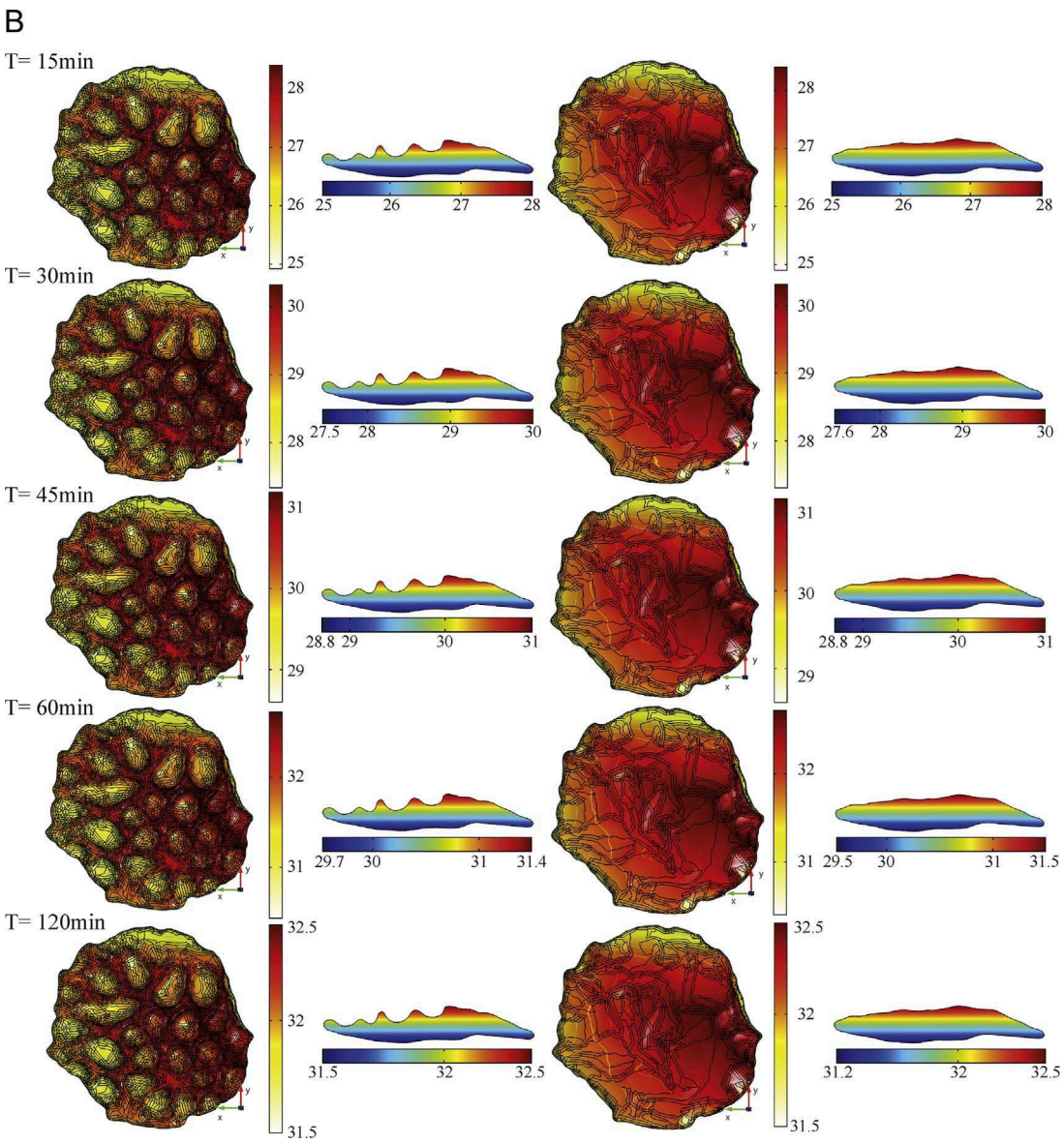

Fig. 3. (*continued*)

1 h basking, the heat conduction stops increasing and the temperature inside the osteoderm tends to be stable as the gradient of temperature between the top and the bottom decreases from 5 °C to 2 °C (Fig. 3). When the FEA is performed on a dorsal-keeled osteoderm (*i.e. Osteolaemus tetraspis, Caiman crocodilus, Trematochampsa taqueti,* Rauisuchidae indet.), the superficial temperature is about 5 °C higher on the keel than on the rest of the apical surface. This temperature difference decreases from 5 °C to 2 °C after two hour basking when the average temperature at the bottom surface of the osteoderm ($t°_{bot}$) reaches a value comprised between 31 °C and 32 °C which is the physiological temperature for extant crocodylians (Fig. 3A; Johnson et al., 1976). When performed on ornamented osteoderms, we observe a difference of temperature of 1 °C higher on the top of the crests than in the bottom of consecutive pits (Fig. 3) as the repartition of the temperature on the upper surface is heterogeneous.

3.2. Comparative assessments of the heat conduction through the osteoderms

At any moment of the basking simulation, the variation of the average temperature at the top surface ($t°_{top}$), at the bottom surface ($t°_{bot}$) or within the volume of the osteoderm ($t°_{ost}$) almost never exceeds 0.5 °C between the different three versions of each 3D-modeled osteoderm: ornamented, non-ornamented, non-mineralized (Table 3). However, except for *Trematochampsa taqueti* which shows by far the highest GAtot/LV ratio, the difference between $t°_{top}$ with either $t°_{ost}$ or $t°_{bot}$ is always slightly higher in absence of ornamentation ($\Delta t°1 < \Delta t°2$; $\Delta t°3 < \Delta t°4$; Fig. 4; Table 4). For *Protosuchus richardsoni*, which possesses the shallowest ornamentation (GAtot = 3.6%; LV = 0.99%), the temperature variations are equal between the ornamented osteoderm and its smoothed copy ($\Delta t°1 = \Delta t°2$ and $\Delta t°3 = \Delta t°4$). In order to assess if GAtot, LV, or GAtot/LV influence the heat conduction through the osteoderms, we ranked all the specimens by the time which the average temperature on their bottom surface takes to reach the half of its maximum value ($T_{1/2}$; $t°_{botmax}$; Table 5). We further performed a PCA (Fig. 5) and thus observed that GAtot/LV negatively covaries with $T_{1/2}$ even though there is no systematic relation between GAtot/LV and $T_{1/2}$ as some specimens show a higher ratio GAtot/LV than others although they score a higher $T_{1/2}$ (Table 5).

Table 3
Temperature evolution during the FEA basking simulation (recorded every fifteen minutes); $t°_{top}$: the average temperature on the top (apical) surface of the osteoderm; $t°_{ost}$: the average temperature within the osteoderm volume; $t°_{bot}$: the average temperature on the bottom (basal) surface of the osteoderm. Specimen references: * AC.1991.4488a; ** AC.1991.4488b.

*O.tetraspis**	Ornamented osteoderm			Non-ornamented osteoderm			Non-ossified dermis		
Time	Temperature (°C)			Temperature (°C)			Temperature (°C)		
(min)	t°top	t°ost	t°bot	t°top	t°ost	t°bot	t°top	t°ost	t°bot
0	20.00	20.00	20.00	20.00	20.00	20.00	20.00	20.00	20.00
15	26.59	26.11	25.28	26.69	26.18	25.26	26.41	25.98	25.23
30	28.80	28.39	27.67	28.88	28.45	27.65	28.68	28.31	27.66
45	29.87	29.52	28.88	29.94	29.56	28.86	29.79	29.47	28.90
60	30.56	30.24	29.68	30.62	30.28	29.66	30.50	30.21	29.71
75	31.04	30.75	30.24	31.09	30.78	30.22	30.99	30.74	30.28
90	31.38	31.12	30.65	31.43	31.15	30.63	31.35	31.11	30.69
105	31.66	31.41	30.98	31.70	31.44	30.96	31.63	31.41	31.02
120	31.89	31.66	31.25	31.93	31.68	31.23	31.87	31.66	31.29
*O.tetraspis***	Ornamented osteoderm			Non-ornamented osteoderm			Non-ossified dermis		
Time	Temperature (°C)			Temperature (°C)			Temperature (°C)		
(min)	t°top	t°ost	t°bot	t°top	t°ost	t°bot	t°top	t°ost	t°bot
0	20.00	20.00	20.00	20.00	20.00	20.00	20.00	20.00	20.00
15	26.47	26.06	25.26	26.63	26.12	25.23	26.42	25.96	25.17
30	28.71	28.35	27.64	28.84	28.39	27.61	28.69	28.30	27.60
45	29.79	29.48	28.86	29.90	29.51	28.83	29.80	29.46	28.85
60	30.48	30.21	29.66	30.58	30.23	29.63	30.50	30.20	29.66
75	30.97	30.72	30.22	31.05	30.74	30.19	31.00	30.73	30.23
90	31.32	31.09	30.63	31.39	31.11	30.60	31.35	31.10	30.65
105	31.60	31.38	30.96	31.67	31.40	30.94	31.64	31.40	30.98
120	31.83	31.63	31.23	31.90	31.65	31.21	31.87	31.65	31.26
C.crocodilus	Ornamented osteoderm			Non-ornamented osteoderm			Non-ossified dermis		
Time	Temperature (°C)			Temperature (°C)			Temperature (°C)		
(min)	t°top	t°ost	t°bot	t°top	t°ost	t°bot	t°top	t°ost	t°bot
0	20.00	20.00	20.00	20.00	20.00	20.00	20.00	20.00	20.00
15	26.27	26.05	25.14	26.37	26.06	25.12	26.11	25.92	25.09
30	28.51	28.32	27.53	28.60	28.33	27.50	28.40	28.24	27.51
45	29.62	29.45	28.76	29.69	29.46	28.74	29.53	29.40	28.76
60	30.33	30.18	29.57	30.39	30.18	29.54	30.27	30.15	29.58
75	30.82	30.69	30.14	30.88	30.70	30.11	30.78	30.68	30.16
90	31.19	31.07	30.56	31.24	31.07	30.54	31.16	31.06	30.59
105	31.49	31.38	30.90	31.53	31.38	30.88	31.47	31.38	30.94
120	31.73	31.63	31.18	31.77	31.63	31.16	31.71	31.63	31.22
S.imperator	Ornamented osteoderm			Non-ornamented osteoderm			Non-ossified dermis		
Time	Temperature (°C)			Temperature (°C)			Temperature (°C)		
(min)	t°top	t°ost	t°bot	t°top	t°ost	t°bot	t°top	t°ost	t°bot
0	20.00	20.00	20.00	20.00	20.00	20.00	20.00	20.00	20.00
15	27.44	27.03	26.48	27.52	27.06	26.47	27.30	26.93	26.45
30	29.51	29.17	28.72	29.57	29.19	28.71	29.42	29.12	28.72
45	30.48	30.19	29.81	30.53	30.21	29.79	30.42	30.17	29.82
60	31.10	30.84	30.50	31.14	30.86	30.49	31.05	30.83	30.53
75	31.52	31.29	30.99	31.56	31.31	30.98	31.49	31.29	31.02
90	31.83	31.62	31.34	31.86	31.63	31.33	31.81	31.62	31.37
105	32.08	31.88	31.62	32.11	31.89	31.61	32.06	31.89	31.66
120	32.28	32.10	31.85	32.31	32.11	31.84	32.26	32.10	31.89
M.hugii	Ornamented osteoderm			Non-ornamented osteoderm			Non-ossified dermis		
Time	Temperature (°C)			Temperature (°C)			Temperature (°C)		
(min)	t°top	t°ost	t°bot	t°top	t°ost	t°bot	t°top	t°ost	t°bot
0	20.00	20.00	20.00	20.00	20.00	20.00	20.00	20.00	20.00
15	26.73	26.08	25.19	26.91	26.21	25.17	26.52	25.92	25.13
30	28.92	28.36	27.58	29.07	28.46	27.55	28.78	28.26	27.56
45	29.98	29.48	28.80	30.09	29.57	28.78	29.87	29.43	28.81
60	30.65	30.21	29.60	30.75	30.28	29.58	30.57	30.18	29.63
75	31.11	30.72	30.17	31.20	30.78	30.14	31.06	30.70	30.21
90	31.45	31.09	30.58	31.53	31.14	30.55	31.41	31.08	30.62
105	31.72	31.38	30.91	31.80	31.44	30.89	31.69	31.38	30.96
120	31.95	31.63	31.19	32.02	31.68	31.16	31.92	31.63	31.24
H.rogersii	Ornamented osteoderm			Non-ornamented			Non-ossified dermis		
Time	Temperature (°C)			Temperature (°C)			Temperature (°C)		
(min)	t°top	t°ost	t°bot	t°top	t°ost	t°bot	t°top	t°ost	t°bot
0	20.00	20.00	20.00	20.00	20.00	20.00	20..00	20.00	20.00
15	27.35	26.77	26.07	26.89	26.32	25.54	27.18	26.64	26.02
30	29.44	28.95	28.36	29.06	28.57	27.90	29.32	28.88	28.36
45	30.42	30.00	29.49	30.10	29.67	29.09	30.34	29.96	29.51
60	31.04	30.67	30.22	30.76	30.38	29.86	30.98	30.65	30.25
75	31.47	31.14	30.74	31.21	30.87	30.41	31.43	31.13	30.77
90	31.78	31.47	31.11	31.54	31.23	30.80	31.75	31.47	31.14
105	32.03	31.75	31.40	31.81	31.52	31.12	32.00	31.75	31.44
120	32.23	31.97	31.65	32.03	31.75	31.38	32.21	31.98	31.69
T.taqueti	Ornamented osteoderm			Non-ornamented osteoderm			Non-ossified dermis		

(continued on next page)

Table 3 *(continued)*

*O.tetraspis** Time	Ornamented osteoderm Temperature (°C)			Non-ornamented osteoderm Temperature (°C)			Non-ossified dermis Temperature (°C)		
(min)	t°top	t°ost	t°bot	t°top	t°ost	t°bot	t°top	t°ost	t°bot
Time	Temperature (°C)			Temperature (°C)			Temperature (°C)		
(min)	t°top	t°ost	t°bot	t°top	t°ost	t°bot	t°top	t°ost	t°bot
0	20.00	20.00	20.00	20.00	20.00	20.00	20.00	20.00	20.00
15	27.37	26.20	24.76	27.24	26.26	24.74	27.04	25.93	24.64
30	29.43	28.42	27.14	29.31	28.46	27.12	29.20	28.25	27.09
45	30.39	29.51	28.39	30.28	29.55	28.37	30.23	29.41	28.39
60	31.00	30.22	29.22	30.90	30.25	29.20	30.88	30.16	29.25
75	31.42	30.71	29.80	31.34	30.74	29.79	31.34	30.68	29.85
90	31.73	31.08	30.24	31.65	31.10	30.22	31.66	31.06	30.30
105	31.97	31.37	30.59	31.90	31.39	30.57	31.92	31.36	30.65
120	32.18	31.61	30.88	32.11	31.63	30.86	32.14	31.62	30.95
P.richardsoni	Ornamented osteoderm			Non-ornamented osteoderm			Non-ossified dermis		
Time	Temperature (°C)			Temperature (°C)			Temperature (°C)		
(min)	t°top	t°ost	t°bot	t°top	t°ost	t°bot	t°top	t°ost	t°bot
0	20.00	20.00	20.00	20.00	20.00	20.00	20.00	20.00	20.00
15	26.76	26.14	25.46	26.92	26.29	25.65	26.57	26.00	25.41
30	28.96	28.42	27.83	29.09	28.55	28.00	28.83	28.34	27.82
45	30.01	29.54	29.03	30.12	29.66	29.18	29.92	29.50	29.05
60	30.68	30.27	29.81	30.78	30.37	29.94	30.61	30.24	29.84
75	31.15	30.77	30.36	31.24	30.86	30.48	31.10	30.76	30.40
90	31.49	31.15	30.77	31.57	31.22	30.87	31.45	31.14	30.81
105	31.77	31.45	31.10	31.83	31.51	31.18	31.73	31.45	31.14
120	32.00	31.69	31.37	32.05	31.75	31.44	31.96	31.70	31.41
Rauisuchidae	Ornamented osteoderm			Non-ornamented osteoderm			Non-ossified dermis		
Time	Temperature (°C)			Temperature (°C)			Temperature (°C)		
(min)	t°top	t°ost	t°bot	t°top	t°ost	t°bot	t°top	t°ost	t°bot
0	no data	no data	no data	20.00	20.00	20.00	20.00	20.00	20.00
15	no data	no data	no data	29.58	28.80	27.04	29.41	28.67	27.02
30	no data	no data	no data	31.02	30.41	29.04	30.92	30.35	29.06
45	no data	no data	no data	31.74	31.23	30.08	31.68	31.22	30.13
60	no data	no data	no data	32.17	31.73	30.72	32.13	31.73	30.78
75	no data	no data	no data	32.47	32.07	31.17	32.45	32.09	31.24
90	no data	no data	no data	32.70	32.34	31.51	32.69	32.36	31.58
105	no data	no data	no data	32.88	32.54	31.78	32.87	32.57	31.85
120	no data	no data	no data	33.02	32.71	32.00	33.02	32.74	32.07

3.3. Comparative assessments between compact and cancellous osteoderms

When we perform the analyses using the thermal properties of the cancellous bone for the osteoderms (Table 2) of both *Caiman crocodilus* (keeled osteoderm) and *Machimosaurus hugii* (flat osteoderm) specimens, we observe that all average temperature values ($t°_{top}$, $t°_{ost}$, $t°_{bot}$) remain equal as when using the compact bone properties. Indeed, the differences between the results obtained through the "compact-bone" and "cancellous-bone" models are lower than 0.05 °C at each moment of the simulation (Table 5; Appendix). This negligible variation is systematically in favor of the compact osteoderm rather than of its cancellous equivalent form whether the analysis is performed on the ornamented osteoderm or on its smoothed equivalent form.

4. Discussion

4.1. Limits of the model

The proposed modeling leads to assess the heat conduction through the crocodylomorph osteoderms during basking while considering these bones as a "closed system" (an object that allows energy transfer but no mass exchange). Nevertheless, in living organisms, osteoderms are actually "open system" since they are vascularized (Vickaryous and Hall, 2008; Vickaryous and Sire, 2009; Burns et al., 2013). Therefore, our calculations assess the heat conduction through osteoderms by disregarding the effects of vasculature on thermal exchanges. However, this new method leads to quantify the direct influence of the osteoderm morphology and degree of porosity on the heat conduction through the skin.

Another limit of the model is the lack of published references concerning the tissue-specific thermal properties (heat capacity; thermal conductivity) for the different vertebrate taxa. Indeed, we had to use global statistical data (ITIS; Hasgall et al., 2015) to perform our analyses. Measures on living crocodylians will increase the precision of the proposed model for this concerned taxa.

Even though our sample represents different crocodylomorph taxa which trace back to the Early Jurassic, it is however important to underline that the assessed variations between the sampled specimens are not only representative of the interspecific variability. Indeed, previous studies have shown that pseudosuchian osteoderms show an intraspecific morphological variability which is due to their position on the organism (Klein et al., 2009; Scheyer and Desojo, 2011; Burns et al., 2013). However, the interest of a large taxonomic sampling is to include a wide morphological diversity (keeled, flat, rectangle, square osteoderms) which extends the range of the obtained results.

4.2. Relative influence of the heat conduction through the osteoderm shield

Our results point out that the presence of the osteoderms does not affect noticeably the thermal response of the dermis as the temperature difference may only be shifted up to 0.3 °C ($\Delta t°4$ - $\Delta t°5$; Table 4; Fig. 3B) through a non-ornamented osteoderm in comparison with an equivalent volume of soft dermis during the first 30 min of a basking period. This assessment is of course relative to an osteoderm whose total surface is equivalent to the *Caiman crocodilus* specimen (27.8 mm longitudinal length, 18.2 mm transversal length, 4.6 mm thickness; Table 1). These differences are mainly due to the small variations of $t°_{top}$ whereas $t°_{bot}$ remains almost unchanged whether we consider an

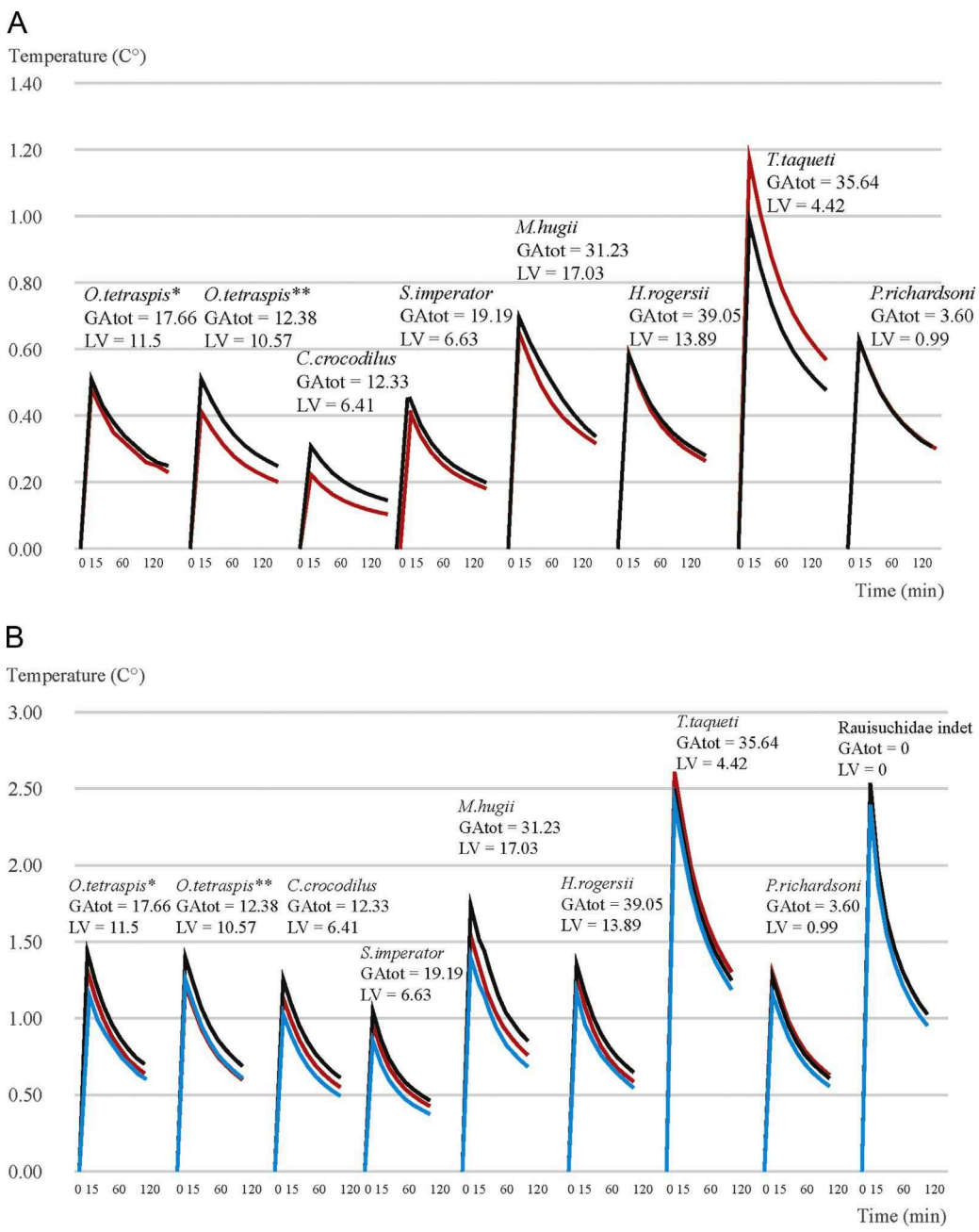

Fig. 4. A: Temperature evolution during the basking simulation: In abscissa: simulation time (min); In ordinates: difference between the average temperature on the apical surface ($t°_{top}$) of the osteoderm and the average temperature within the osteoderm volume ($t°_{ost}$; Celsius degrees); $\Delta t°1$ (red lines): ornamented osteoderms; $\Delta t°2$ (black lines): non-ornamented osteoderms (see Table 4). Quantification of bone ornamentation: GAtot (total gain in area) and LV (loss of volume) in percentage. Fig. 4B: Temperature evolution during the basking simulation on osteoderms: In abscissa: simulation time (minutes); In ordinates: difference between the average temperature on the apical surface ($t°_{top}$) of the osteoderm and the average temperature on the basal surface of the osteoderm ($t°_{bot}$) (Celsius degrees); $\Delta t°3$ (red lines): ornamented osteoderms; $\Delta t°4$: (black lines): non-ornamented osteoderms; $\Delta t°5$: non-ossified osteoderms (dermis; blue lines). Quantification of bone ornamentation: GAtot (total gain in area) and LV (loss of volume) in percentage. (For interpretation of the references to color in this figure legend, the reader is referred to the web version of this article.)

Table 4
Temperature evolution during the basking simulation. $\Delta t°1$: difference between the average temperature on the apical surface ($t°_{top}$) and the average temperature within the ornamented osteoderm volume ($t°_{ost}$); $\Delta t°2$: difference between the average temperature on the apical surface ($t°_{top}$) and the average temperature within the non-ornamented osteoderm volume ($t°_{ost}$); $\Delta t°3$: difference between the average temperature on the apical surface ($t°_{top}$) and the average temperature on the basal surface of the ornamented osteoderm ($t°_{bot}$); $\Delta t°4$: difference between the average temperature on the apical surface ($t°_{top}$) and the average temperature on the basal surface of the non-ornamented osteoderm ($t°_{bot}$); $\Delta t°5$: difference between the average temperature on the apical surface ($t°_{top}$) and the average temperature on the basal surface of the non-ossified osteoderm ($t°_{bot}$; dermis).

time (min)	$\Delta t°1$ (°C)	$\Delta t°2$ (°C)	$\Delta t°3$ (°C)	$\Delta t°4$ (°C)	$\Delta t°5$ (°C)
0	0.00	**0.00**	0.00	**0.00**	0.00
15	0.48	**0.51**	1.31	**1.43**	1.18
30	0.41	**0.43**	1.13	**1.23**	1.02
45	0.35	**0.38**	0.99	**1.08**	0.89
60	0.32	**0.34**	0.88	**0.96**	0.79
75	0.29	**0.31**	0.80	**0.87**	0.71
90	0.26	**0.28**	0.73	**0.80**	0.66
105	0.25	**0.26**	0.68	**0.74**	0.61
120	0.23	**0.25**	0.64	**0.70**	0.57
Osteolaemus tetraspis (AC.1991.4488a)					
time	$\Delta t°1$	$\Delta t°2$	$\Delta t°3$	$\Delta t°4$	$\Delta t°5$

(continued on next page)

Table 4 *(continued)*

time (min)	Δt°1 (°C)	Δt°2 (°C)	Δt°3 (°C)	Δt°4 (°C)	Δt°5 (°C)
(min)	(°C)	(°C)	(°C)	(°C)	(°C)
0	0.00	**0.00**	0.00	**0.00**	0.00
15	0.41	**0.51**	1.22	**1.40**	1.25
30	0.36	**0.44**	1.07	**1.22**	1.09
45	0.31	**0.39**	0.93	**1.06**	0.95
60	0.28	**0.34**	0.83	**0.95**	0.84
75	0.25	**0.31**	0.75	**0.86**	0.76
90	0.23	**0.29**	0.69	**0.79**	0.70
105	0.22	**0.27**	0.64	**0.73**	0.65
120	0.20	**0.25**	0.60	**0.69**	0.61
Osteolaemus tetraspis (AC.1991.4488b)					
time (min)	Δt°1 (°C)	Δt°2 (°C)	Δt°3 (°C)	Δt°4 (°C)	Δt°5 (°C)
0	0.00	**0.00**	0.00	**0.00**	0.00
15	0.22	**0.31**	1.13	**1.25**	1.02
30	0.19	**0.26**	0.98	**1.09**	0.89
45	0.16	**0.23**	0.86	**0.95**	0.77
60	0.14	**0.20**	0.76	**0.84**	0.68
75	0.13	**0.18**	0.69	**0.77**	0.62
90	0.12	**0.17**	0.63	**0.70**	0.57
105	0.11	**0.16**	0.59	**0.65**	0.53
120	0.10	**0.15**	0.55	**0.61**	0.49
Caiman crocodilus					
time (min)	Δt°1 (°C)	Δt°2 (°C)	Δt°3 (°C)	Δt°4 (°C)	Δt°5 (°C)
0	0.00	**0.00**	0.00	**0.00**	0.00
15	0.42	**0.46**	0.96	**1.05**	0.85
30	0.34	**0.37**	0.79	**0.86**	0.70
45	0.29	**0.32**	0.68	**0.65**	0.60
60	0.25	**0.28**	0.60	**0.58**	0.52
75	0.23	**0.25**	0.54	**0.53**	0.47
90	0.21	**0.23**	0.49	**0.86**	0.43
105	0.19	**0.21**	0.46	**0.50**	0.40
120	0.18	**0.20**	0.43	**0.46**	0.37
Sarcosuchus imperator					
time (min)	Δt°1 (°C)	Δt°2 (°C)	Δt°3 (°C)	Δt°4 (°C)	Δt°5 (°C)
0	0.00	**0.00**	0.00	**0.00**	0.00
15	0.59	**0.58**	1.29	**1.35**	1.16
30	0.49	**0.50**	1.07	**1.16**	0.97
45	0.42	**0.43**	0.92	**1.01**	0.83
60	0.37	**0.38**	0.81	**0.89**	0.73
75	0.33	**0.34**	0.73	**0.81**	0.66
90	0.31	**0.32**	0.67	**0.74**	0.60
105	0.28	**0.29**	0.63	**0.69**	0.56
120	0.26	**0.27**	0.58	**0.65**	0.52
Hyposaurus rogersii					
time (min)	Δt°1 (°C)	Δt°2 (°C)	Δt°3 (°C)	Δt°4 (°C)	Δt°5 (°C)
0	**0.00**	0.00	**0.00**	0.00	0.00
15	**1.17**	0.99	**2.61**	2.50	2.40
30	**1.01**	0.85	**2.29**	2.19	2.11
45	**0.88**	0.74	**2.00**	1.91	1.84
60	**0.78**	0.66	**1.78**	1.71	1.64
75	**0.71**	0.59	**1.62**	1.55	1.48
90	**0.65**	0.55	**1.49**	1.43	1.37
105	**0.61**	0.51	**1.39**	1.33	1.27
120	**0.57**	0.48	**1.30**	1.25	1.19
Trematochampsa taqueti					
time (min)	Δt°1 (°C)	Δt°2 (°C)	Δt°3 (°C)	Δt°4 (°C)	Δt°5 (°C)
0	0.00	0.00	0.00	0.00	0.00
15	0.62	0.63	1.30	1.27	1.16
30	0.54	0.54	1.13	1.09	1.00
45	0.47	0.47	0.98	0.95	0.87
60	0.42	0.41	0.87	0.84	0.77
75	0.38	0.37	0.79	0.76	0.70
90	0.35	0.35	0.72	0.70	0.64
105	0.32	0.32	0.67	0.65	0.60
120	0.30	0.30	0.63	0.61	0.56
Protosuchus richardsoni					
time (min)	Δt°1 (°C)	Δt°2 (°C)	Δt°3 (°C)	Δt°4 (°C)	Δt°5 (°C)
0	0.00	**0.00**	0.00	**0.00**	0.00

(continued on next page)

Table 4 *(continued)*

time (min)	Δt°1 (°C)	Δt°2 (°C)	Δt°3 (°C)	Δt°4 (°C)	Δt°5 (°C)
15	0.65	**0.70**	1.54	**1.74**	1.40
30	0.57	**0.60**	1.35	**1.51**	1.22
45	0.49	**0.52**	1.17	**1.32**	1.06
60	0.44	**0.47**	1.04	**1.17**	0.94
75	0.40	**0.42**	0.95	**1.06**	0.85
90	0.36	**0.39**	0.87	**0.98**	0.79
105	0.34	**0.36**	0.81	**0.91**	0.73
120	0.32	**0.34**	0.76	**0.85**	0.68
Machimosaurus hugii					
time (min)	Δt°1 (°C)	Δt°2 (°C)	Δt°3 (°C)	Δt°4 (°C)	Δt°5 (°C)
0	No data	**0.00**	No data	**0.00**	0.00
15	No data	**0.79**	No data	**2.54**	2.39
30	No data	**0.61**	No data	**1.98**	1.86
45	No data	**0.50**	No data	**1.65**	1.55
60	No data	**0.44**	No data	**1.45**	1.35
75	No data	**0.40**	No data	**1.30**	1.21
90	No data	**0.36**	No data	**1.19**	1.11
105	No data	**0.33**	No data	**1.10**	1.02
120	No data	**0.31**	No data	**1.03**	0.95

Rauisuchidae indet.

Table 5
The ornamented osteoderms' characteristics and properties. $T_{1/2}$ is the period for each osteoderm to reach the half of the final average temperature value on its bottom surface ($t°_{botmax}$). GAtot is the total gain in superficial area due to ornamentation; LV is the total loss of bony volume due to ornamentation. The lifestyle is referenced after Clarac et al. (2017).

$t°_{botmax}$(°C)	**30.88**	**31.85**	**31.65**	**31.37**	**31.25**	**31.23**	**31.19**	**31.18**
$T_{1/2}$(s)	**690**	**750**	**840**	**960**	**1000**	**1000**	**1010**	**1020**
GAtot(%)	35.64	19.19	39.05	3.6	17.66	12.38	31.23	12.33
LV(%)	4.42	6.63	13.89	0.99	11.55	10.5	17.03	6.41
GAtot/LV	**8.06**	2.89	2.81	3.63	1.53	1.18	1.83	1.92
Lifestyle	amphibious	amphibious	amphibious	terrestrial	amphibious	amphibious	amphibious	amphibious
Species	*T.taqueti*	*S.imperator*	*H.rogersii*	*P.richardsoni*	*O.tetraspis*	*O.tetraspis*	*M. hugii*	*C.crocodilus*

ornamented osteoderm, its non-ornamented corresponding form or its equivalent shape of non-mineralized soft dermis (Table 3). Since $t°_{bot}$ drives the heat conduction from the osteoderm to the body, we argue that the development of the dermal shield in itself does not noticeably either decrease or favor the heat conduction through the dermis of the crocodylomorphs during basking.

The difference in thermal behavior between *Trematochampsa taqueti* and the other specimens could be related to its very high ratio between its gain in superficial bony area (GAtot) and its global loss of bony volume (LV) which are due to ornamentation (GAtot/LV = 8.06; Table 5). Indeed, a high GAtot should rather increase the thermal exchange whereas a low LV does not significantly reduce the global thickness of the osteoderm whose thermal diffusivity is higher than the surrounding dermis' (Table 3). If we consider the sample as a whole, we do not notice any systematic relation between the osteoderm heat conduction with neither the global gain in superficial area (GAtot) nor the loss of bone volume (LV) due to ornamentation. However, the basking period required for each osteoderm to reach the half of its maximal temperature value at its bottom surface ($T_{1/2}$; Table 5) rather covaries with GAtot/LV (Allen's law, 1877; Fig. 5). Nonetheless, if there was a physical relation between GAtot/LV with $T_{1/2,}$ we would expect to observe a systematic relation. Therefore, we may conclude that there is no clear relation between the heat conduction through the osteoderms with neither the increase in superficial area nor the loss of bony volume due to the ornamentation which is set-up by pit resorption (Buffrénil, 1982; Buffrénil et al., 2015). As a matter of fact, most of the sampled well-ornamented osteoderms have a low GAtot/LV as they both score a high GAtot and a high LV; consequently a high value of GAtot/LV (as observed in the *Trematochampsa taqueti* specimen) shall not stand for a general pattern but rather for a particular case due to stochastic morphological variations.

Since our results suggest that the heat conduction through the osteoderms is not significantly different whether they are composed of compact or cancellous bone (*Caiman crocodilus*, *Machimosaurus hugii*, Tables 2, 6), we thus deduce that the variation of the porosity within the diploe has no influence on the global heat conduction. This is due to the fact that these two types of bone have quite similar values of thermal diffusivity α (see Eq. (3)) and therefore no significant difference occurs in the resulting thermal conduction. The main consequence

Table 6
The average temperature difference (Δt°) in the osteoderms between their compact and cancellous form: at the apical surface (top), within the osteoderm volume (ost), at the bottom surface (bot). The results were recorded every fifteen minutes during the basking simulation for *Caiman crocodilus* and *Machimosaurus hugii*.

	C.crocodilus			*M.hugii*		
Time (min)	Δt°top (°C)	Δt°ost (°C)	Δt°bot (°C)	Δt°top (°C)	Δt°ost (°C)	Δt°bot (°C°)
0	0.00	0.00	0.00	0.00	0.00	0.00
15	0.01	0.02	0.04	0.01	0.03	**0.04**
30	0.01	0.02	0.03	0.01	0.02	**0.04**
45	0.01	0.02	0.03	0.00	0.02	0.03
60	0.00	0.01	0.03	0.00	0.01	0.03
75	0.00	0.01	0.02	0.00	0.01	0.03
90	0.00	0.01	0.02	0.00	0.01	0.02
105	0.00	0.01	0.02	0.00	0.01	0.02
120	0.00	0.01	0.02	0.00	0.01	0.02

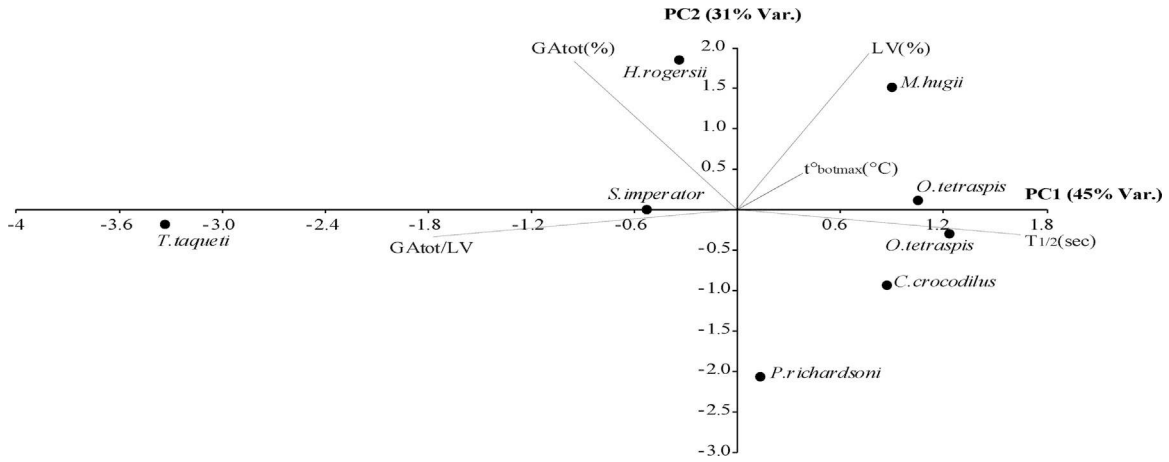

Fig. 5. Principal component analysis of the set of variables which define both the degree of ornamentation (GAtot, LV, GAtot/LV) and the heat conduction through the ornamented osteoderms ($T_{1/2}$; $t°_{botmax}$; performed on PAST version 2.17c, Hammer et al., 2001).

of this assessment is that either a compact or a diploë structure is likely to have no significant influence on the heat conduction through the osteoderms.

4.3. Functional implication of the osteoderms in the crocodylomorphs' natural history

Our study shows that neither the ossification of the dermal skeleton nor its ornamentation clearly influence the heat conduction through the dermis during basking. Nonetheless, we must consider that our model does not include the implication of the vascular system in heat transfer through the osteoderms (as mentioned above). Indeed, the ornamentation pits house a bunch of vascular canals which connect the overlying dermis to the inter trabecular spaces inside the osteoderms (Fig. 1). These erosion bays must contain blood vessels which are themselves connected with the general blood circulation through the bottom surface of the osteoderms (foramina; Seidel, 1979; Witzmann et al., 2010; Burns et al., 2013; Chen et al., 2014). Thus, the osteoderms could behave as thermal vectors during basking as the vascular network housed both inside the osteoderms and in the superficial pits could convey the external heat into the core of the animal through the dorsal median artery (Seidel, 1979). In this regard, previous telemetric measures on basking *Caiman latirostris* have shown that the temperature of the back overlying the osteoderms is always cooler than the part of the back which is free from osteoderms whether in a cold (16 °C) or in a warm (25 °C) atmosphere (Farlow et al., 2010). These data support the fact that osteoderms are permanently vascularized by a cool blood flow which would be warmed-up at the periphery of the organism within and straight above the dermal skeleton. The global body temperature is controlled by the cardiac beat which is increased during basking and further reduced when the body temperature is optimal (comprised between 31 °C and 33 °C; Johnson et al., 1976; Seebacher and Franklin, 2004).

If we consider the evolution of all crocodylomorphs, the presence of only two rows of non-ornamented osteoderms as in rauisuchids (Crocodylomorpha direct out-group) would be the primitive condition (Trutnau and Sommerlad, 2006; Nesbitt, 2011; Irmis et al., 2013; Fig. A1). At the Triassic-Jurassic transition, the number of rows increased and formed a dorsal shield (sometimes also ventral) in both crocodyliforms and teleosaurids while they shew a higher degree of bone ornamentation in parallel with their transition to a semi-aquatic ambush lifestyle (Clarac et al., 2015, 2017). A specificity of the amphibious forms is to be characterized by a low mobility which involves a little metabolic heat due to muscle activity (Seebacher et al., 1999). According to the last published references (Legendre et al., 2016), "rauisuchids" had a higher level of metabolism than the crocodyliforms and were thus possibly endothermic such as stem-archosaurs (Seymour et al., 2004). In this regard, both the development of the dorsal shield and of the ornamentation (whether cranial or post-cranial) could consist of hypothetical adaptations in a return to ectothermy within the evolution of the crocodylomorphs. Indeed, without modifying the skin global conduction, the ornamented osteoderms may thus supply a peripheral vascularization network which would be involved in the heat collection (as hypothesized by previous authors; Seidel, 1979; Farlow et al., 2010).

5. Conclusions

Our analyses lead to assess that the presence of an ornamented dermal shield made of osteoderms does not significantly affect the heat conduction through the crocodylians' skin. This assessment let us hypothesize that the possible implication of the osteoderms into heat transfer should be directly due to their relative degree of vascularization. Indeed, if the ornamented osteoderms house an extensive peripheral vascular network, they could therefore promote a convective exchange of the incoming heat with the cool blood circulating through their vasculature (within and straight above the bone apical surface). Under this condition, the ornamented osteoderms could consist of an adaptative feature in basking efficiency for large lethargic ectopoïkilothermic vertebrates such as the semi-aquatic crocodylomorphs.

Conflict of interest

The authors have no conflicts of interest.

Funding

This research did not receive any specific grant from funding agencies in the public, commercial, or not-for-profit sectors.

Acknowledgements

We would like to thank Salvador Bailon (MNHN), Ronan Allain (MNHN), Carl Mehling and Mark Norell (AMNH) for giving us access to the specimen collections. We also address our thankful regards to Allowen Evin (CNRS; Institut des Sciences de l'Evolution; Montpellier) for her advice concerning morphometrics.

Appendices

(See Fig. A1 and Table B1).

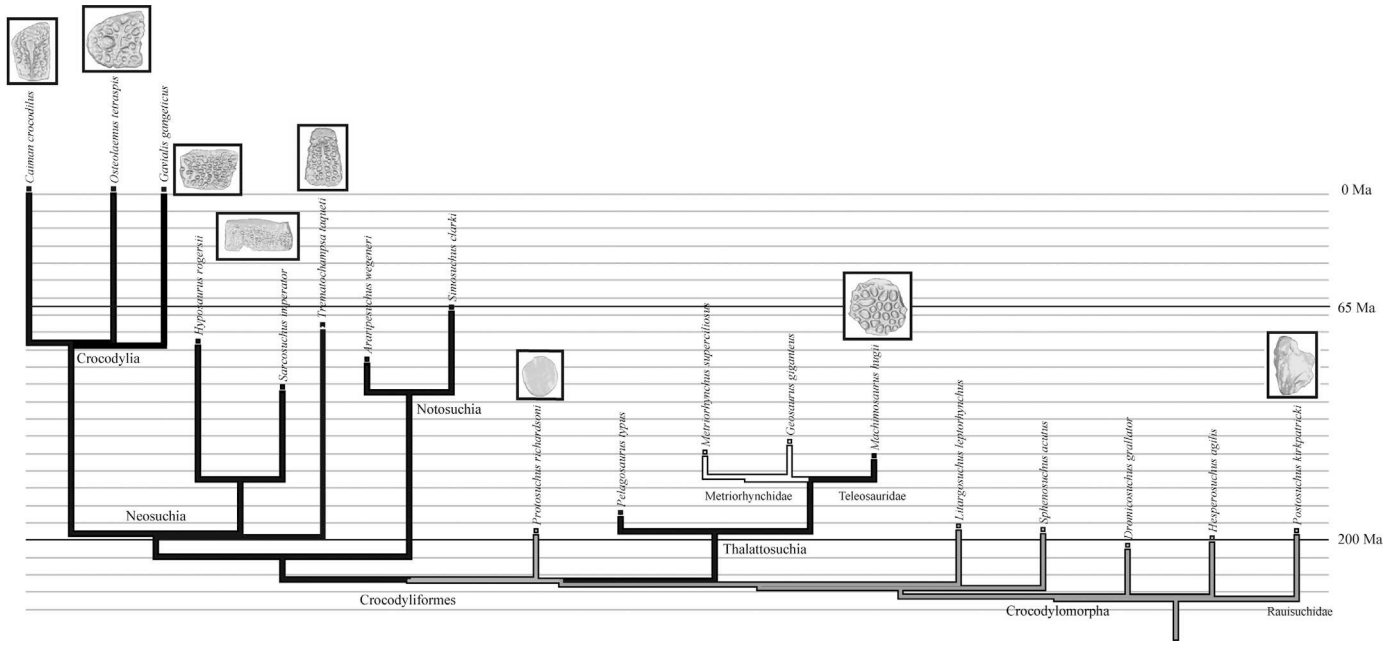

Fig. A1. Optimization of the number of osteoderm rows on the phylogeny of Crocodylomorpha using the maximum of parsimony (performed on Mesquite version 3.03 after Clarac et al., 2017; Maddison and Maddison, 2011). Branch color significations: Grey: presence of two sagittal osteoderm rows; Black: presence of more than two osteoderm rows; White: absence of osteoderms. Branch length are in million years.

Table B1
Temperature evolution during the FEA basking simulation for both *Caiman crocodilus* and *Machimosaurus hugii* using successively the compact bone properties and the cancellous bone properties (detailed in Table 2). $t°_{top}$: the average temperature on the top (apical) surface of the osteoderm. $t°_{ost}$: the average temperature within the osteoderm volume. $t°_{bot}$: the average temperature on the bottom (basal) surface of the osteoderm.

C.crocodilus	Ornamented osteoderm Temperature (°C)					
Time	Compact bone			Cancellous bone		
(min)	t°top	t°ost	t°bot	t°top	t°ost	t°bot
0	20.00	20.00	20.00	20.00	20.00	20.00
15	26.27	26.05	25.14	26.72	26.05	25.14
30	28.51	28.32	27.53	28.92	28.34	27.54
45	29.62	29.45	28.76	29.97	29.47	28.77
60	30.33	30.18	29.57	30.64	30.20	29.58
75	30.82	30.69	30.14	31.11	30.71	30.14
90	31.19	31.07	30.56	31.45	31.08	30.56
105	31.49	31.38	30.90	31.72	31.37	30.89
120	31.73	31.63	31.18	31.95	31.62	31.17
C.crocodilus	Non-ornamented osteoderm Temperature (°C)					
time	Compact bone			Cancellous bone		
(min)	t°top	t°ost	t°bot	t°top	t°ost	t°bot
0	20.00	20.00	20.00	20.00	20.00	20.00
15	26.37	26.06	25.12	26.36	26.04	25.08
30	28.60	28.33	27.50	28.59	28.31	27.47
45	29.69	29.46	28.74	29.68	29.44	28.71
60	30.39	30.18	29.54	30.38	30.17	29.52
75	30.88	30.70	30.11	30.87	30.68	30.09
90	31.24	31.07	30.54	31.24	31.06	30.51
105	31.53	31.38	30.88	31.53	31.37	30.86
120	31.77	31.63	31.16	31.77	31.62	31.14
M.hugii	Ornamented osteoderm Temperature (°C)					
Time	Compact bone			Cancellous bone		
(min)	t°top	t°ost	t°bot	t°top	t°ost	t°bot
0	20.00	20.00	20.00	20.00	20.00	20.00
15	26.73	26.08	25.19	26.72	26.05	25.14

(continued on next page)

Table B1 *(continued)*

C.crocodilus	Ornamented osteoderm Temperature (°C)					
Time	Compact bone			Cancellous bone		
(min)	t°top	t°ost	t°bot	t°top	t°ost	t°bot
30	28.92	28.36	27.58	28.92	28.34	27.54
45	29.98	29.48	28.80	29.97	29.47	28.77
60	30.65	30.21	29.60	30.64	30.20	29.58
75	31.11	30.72	30.17	31.11	30.71	30.14
90	31.45	31.09	30.58	31.45	31.08	30.56
105	31.72	31.38	30.91	31.72	31.37	30.89
120	31.95	31.63	31.19	31.95	31.62	31.17
M.hugii	Non-ornamented osteoderm Temperature (°C)					
Time	Compact bone			Cancellous bone		
(min)	t°top	t°ost	t°bot	t°top	t°ost	t°bot
0	20.00	20.00	20.00	20.00	20.00	20.00
15	26.91	26.21	25.17	26.90	26.18	25.12
30	29.07	28.46	27.55	29.06	28.44	27.51
45	30.09	29.57	28.78	30.09	29.55	28.74
60	30.75	30.28	29.58	30.74	30.27	29.54
75	31.20	30.78	30.14	31.20	30.77	30.11
90	31.53	31.14	30.55	31.53	31.13	30.53
105	31.80	31.44	30.89	31.79	31.42	30.86
120	32.02	31.68	31.16	32.01	31.67	31.14

References

Allen, J.A., 1877. The influence of physical conditions in the genesis of species. Radic. Rev. 1, 108–140.

Botha-Brink, J., Smith, R.M.H., 2011. Osteohistology of the Triassic archosauromorphs *Prolacerta*, *Proterosuchus*, *Euparkeria*, *Erythrosuchus* from the Karoo Basin of South Africa. J. Vertebr. Paleontol. 31, 1238–1254.

Buffrénil, Vde, 1982. Morphogenesis of bone ornamentation in extant and extinct crocodilians. Zoomorphology 99, 155–166.

Buffrénil, Vde, Clarac, F., Fau, M., Martin, S., Martin, B., Pellé, E., Laurin, M., 2015. Differentiation and growth of bone ornamentation in vertebrates: a comparative histological study among the Crocodylomorpha. J. Morphol. 21, 1–21.

Burns, M.E., Vickaryous, M.K., Currie, P.J., 2013. Histological variability in fossil and recent alligatoroid osteoderms: systematic and functional implications. J. Morphol. 274, 676–686.

Bystrow, A.P., 1935. Morphologische untersuchungen der deckknochen des schädels der stegocephalen. 1. Mitteilung.Schädel der stegocephalen. Acta Zool. Stock. 16, 65–141.

Bystrow, A.P., 1947. Hydrophilous and xerophilous Labyrinthodonts. Acta Zool. Stock. 28, 137–164.

Cerda, I.A., Desojo, J.B., Scheyer, T.M., Schultz, C.L., 2013. Osteoderm microstructure of ``rauisuchian'' archosaurs from South America. Geobios 46, 273–283.

Chen, I.H., Yang, W., Meyers, M.A., 2014. Alligator osteoderms: mechanical behavior and hierarchical structure. Mater. Sci. Eng. 35, 441–448.

Clarac, F., Souter, T., Cornette, R., Cubo, J., Buffrénil, Vde, 2015. A quantitative assessment of bone area increase due to ornamentation in the Crocodylia. J. Morphol. 276, 1183–1192.

Clarac, F., Buffrénil, Vde, Brochu, C.A., Cubo, J., 2017. The evolution of bone ornamentation in Pseudosuchia: morphological constraints versus ecological adaptation. Biol. J. Linn. Soc (doi: blw 034).

Downs, J.P., Donoghue, P.C.J., 2009. Skeletal histology of *Bothriolepis canadensis* (Placodermi, Antiarchi) and evolution of the skeleton at the origin of jawed vertebrates. J. Morphol. 270, 1364–1380.

Drymala, S.M., 2015. A new paracrocodylomorph (Archosauria, Suchia) from the Late Triassic of North Carolina. MSc Thesis, North Carolina State University. Available at: ⟨http://www.lib.ncsu.edu/resolver/1840.16/10295⟩.

Drymala, S.M., Zanno, L.E., 2016. Osteology of *Carnufex carolinensis* (Archosauria: pseudosuchia) from the Pekin formation of North Carolina and its implications for early crocodylomorph evolution. PLoS One 11, e0157528.

Evans, S.E., Jones, M.E.H., Krause, D.W., 2008. A giant frog with South American affinities from the Late Cretaceous of Madagascar. Proc. Natl. Acad. Sci. USA 105, 2951–2956.

Farlow, J.O., Hayashi, S., Tattersall, G.J., 2010. Internal vascularity of the dermal plates of *Stegosaurus* (Ornithischia, Thyreophora). Swiss J. Geosci. 103, 173–185.

Gilbert, S.F., Loredo, G.A., Brukman, A., Burke, A.C., 2001. Morphogenesis of the turtle shell: the development of a novel structure in tetrapod evolution. Evol. Dev. 3, 47–58.

Grigg, G.C., Alchin, J., 1976. The role of the cardiovascular system in thermoregulation of *Crocodylus johnstoni*. Physiol. Zool. 49, 24–36.

Hammer, Ø., Harper, D.A.T., Ryan, P.D., 2001. PAST: Paleontological statistics software package for education and data analysis. Palaeontol. Electron. 4 (1). ⟨http://palaeo-electronica.org/2001_1/past/issue1_01.htm⟩.

Hasgall, P.A., Di Gennaro, F., Baumgartner, C., Neufeld, E., Gosselin, M.C., Payne, D., Klingenböck, A., Kuster, N., 2015. ITIS Database for thermal and electromagnetic parameters of biological tissues, Version 3.0, September 01st, http://dx.doi.org/10.13099/VIP21000-03-0.

Irmis, R.B., Nesbitt, S.J., Sues, H.D., 2013. Early Crocodylomorpha. Geol. Soc. Lond. Spec. Publ. 379, 275–302.

Johnson, C.R., Webb, G.J.W., Tanner, C., 1976. Thermoregulation in crocodilians II. A telemetric study of body temperature in the Australian crocodiles, *Crocodylus johnstoni* and *Crocodylus porosus*. Comp. Physiol. 53A, 143–146.

Klein, N., Scheyer, T., Tütken, T., 2009. Skeletochronology and isotopic analysis of a captive individual of *Alligator mississippiensis* Daudin, 1802. Foss. Rec. 12 (2), 121–131.

Legendre, L., Segalen, L., Cubo, J., 2013. Evidence for high bone growth rate in *Euparkeria* obtained using a new paleohistological inference model for the humerus. J. Vertebr. Paleontol. 33, 1343–1350.

Legendre, L., Guénard, G., Botha-Brink, J., Cubo, J., 2016. Palaeohistological evidence for ancestral high metabolic rate in archosaurs. Syst. Biol. 0 (0), 1–8.

Lingham-Soliar, T., 2014. The Vertebrate Integument. Springer, Heidelberg.

Lundberg, J.G., Aguilera, O., 2003. The late Miocene *Phractocephalus* catfish (Siluriformes: Pimelodidae) from Urumaco, Venezuela: additional specimens and reinterpretation as a distinct species. Neotrop. Ichthyol. 1, 97–109.

Maddison ,W.P., Maddison, D.R., 2011. Mesquite: a modular system for evolutionary analysis. Version 2.75. ⟨http://mesquiteproject.org⟩.

Märss, T., 2006. Exoskeletal ultrasculpture of early vertebrates. J. Vertebr. Paleontol. 26, 235–252.

Morkovin, B.I., 2015. On the development of surface ornamentation of skull bones in the ontogeny of Early Triassic benthosuchids (Amphibia, Temnospondyli). Paleontol. J. 49, 57–69.

Nesbitt, S.J., 2011. The early evolution of archosaurs: relationships and the origin of major clades. Bull. Am. Mus. Nat. Hist. 352, 1–292.

Rage, J.C., Rocek, Z., 2007. A new species of *Thaumastosaurus* (Amphibia: anura) from the Eocene of Europe. J. Vertebr. Paleontol. 27 (2), 329–336.

Ricqlès, Ade, Padian, K., Horner, J.R., 2003. On the bone histology of some Triassic pseudosuchian archosaurs and related taxa. Ann. Paleontol. 89, 67–101.

Ricqlès, Ade, Padian, K., Knoll, F., Horner, J.R., 2008. On the origin of high growth rates in archosaurs and their ancient relatives: complementary histological studies on Triassic archosauriforms and the problem of a "phylogenetic signal" in bone histology. Ann. Paleontol. 94, 57–76.

Rinehart, L.F., Lucas, S.G., 2013. The functional morphology of dermal bone ornamentation in temnospondyl amphibians. In: Tanner, L.H., Spielmann, J.A., Lucas, S.G. (eds.), The Triassic System. Albuquerque: New. Mex. Mus. Nat. Hist. Sci. Bull. 61, 524–532.

Scheyer, T.M., Sander, M.P., Joyce, W.G., Böhme, W., Witzel, U., 2007. A plywood structure in the shell of fossil and living soft-shelled turtles (Trionychidae) and its evolutionary implications. Org. Diver. Evol. 7, 136–144.

Scheyer, T.M., Desojo, J.B., 2011. Palaeohistology and external microanatomy of rauisuchian osteoderms (Archosauria: Pseudosuchia). Palaeontology 54, 1289–1302.

Scheyer, T.M., Desojo, J.B., Cerda, I.A., 2014. Bone histology of phytosaur, aetosaur, and other archosauriform osteoderms (Eureptilia, Archosauromorpha). Anat. Rec. 297, 240–260.

Schoch, R.R., Milner, A.R., 2000. Handbuch der Paläoherpetologie. Verlag Dr. Friedrich Pfeil, München.

Seebacher, F., Grigg, G., Beard, L., 1999. Crocodiles as dinosaurs: behavioural thermoregulation in very large ectotherms leads to high and stable body temperatures. J. Exp. Biol. 202, 77–86.

Seebacher, F., Franklin, C.E., 2004. Integration of autonomic and local mechanisms in

regulating cardiovascular responses to heating and cooling in a reptile (*Crocodylus porosus*). J. Comp. Physiol. B 174, 577–585.
Seidel, M.R., 1979. The osteoderms of the American alligator and their functional significance. Herpetol. Leag. 35, 375–380.
Seymour, R.S., Bennett-Stamper, C.L., Johnston, S.D., Carrier, D.R., Grigg, G.C., 2004. Evidence for endothermic ancestors of crocodiles at the stem of archosaur evolution. Physiol. Biochem. Zool. 77, 1051–1067.
Skutchas, P.P., 2016. A new crown-group salamander from the middle Jurassic of Western Siberia, Russia. Paleobiodivers. Paleoenviron. 96 (1), 41–48.
Smith, E.N., 1979. Behavioral and physiological thermoregulation of crocodilians. Am. Zool. 19, 239–247.
Trutnau, L., Sommerlad, R., 2006. Evolution of crocodilians. In: Chimaira, B. (ed.), Crocodilians their Natural History and Captive Husbandry. Andreas S. Bram., Franckfurt am Main, pp. 21–31.
Vickaryous, M.K., Hall, B.K., 2008. Development of the dermal skeleton in *Alligator mississippiensis* (Archosauria, Crocodylia) with comments on the homology of osteoderms. J. Morphol. 269, 398–422.
Vickaryous, M.K., Sire, J.Y., 2009. The integumentary skeleton of tetrapods: origin, evolution, and development. J. Anat. 214, 441–464.
Witzman, F., 2009. Comparative histology of sculptured dermal bones in basal tetrapods, and the implications for the soft tissue dermis. Palaeodiversity 2, 233–270.
Witzmann, F., Scholz, H., Müller, J., Kardjilov, N., 2010. Sculpture and vascularization of dermal bones, and the implications for the physiology of basal tetrapods. Zool. J. Linn. Soc. 160, 302–340.
Young, G.C., 2009. An Ordovician vertebrate from western New South Wales, with comments on Cambro-Ordovician vertebrate distribution patterns. Alcheringa 33, 79–89.
Zylberberg, L., Castanet, J., 1985. New data on the structure and the growth of the osteoderms in the reptile *Anguis fragilis* (Anguidae, Squamata). J. Morphol. 186, 327–342.
Zylberberg, L., Meunier, F.J., Laurin, M., 2010. A microanatomical and histological study of the postcranial dermal skeleton in the Devonian sarcopterygian *Eusthenopteron foordi*. Acta Palaeont. Pol. 55, 459–470.

François Clarac: François Clarac is a PhD student at the Université Pierre et Marie Curie (Sorbonne Université) and the Muséum National d'Histoire Naturelle (Paris, France). His field of research are: evolutionary biology, paleobiology and functional morphology. His investigations mainly concern the study of the dermal skeleton and the evolution of the crocodylian lineage.

Florent Goussard: Holder of a PhD in paleontology of the Museum National d'Histoire Naturelle (MNHN) of Paris since 2009, my researches mainly concerned the functional morphology of the hand of sauropodomorph dinosaurs with inferences based on anatomical reinterpretations and redescriptions, finite element analysis and comparisons with paleoichnological record. I was recruited as a Scientific imaging Engineer just after my thesis in order to develop and manage the 3D facilities of the paleontology laboratory (CR2P CNRS) of the MNHN. Today we perform multiple approaches, from virtual dissection and fossil preparation to 3D reconstruction and animation of both extant and extinct species.

Luciano Teresi: Luciano Teresi is associate professor in Mechanics at the Dept. of Mathematics and Physics, Roma TRE University (Italy) and is the coordinator of the Modeling and Simulation Lab. He received his M.S. in Aerospace Engineering from the Sapienza, Università di Roma (Italy) and his Ph.D. in Applied and Theoretical Mechanics from the same university. His scientific interests pertain to soft matter, living tissues, and foundational aspects of continuum physics.

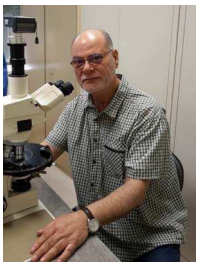

Vivian de Buffrénil: Vivian de Buffrénil is a histologist and paleobiologist at the Muséum National d'Histoire Naturelle in Paris (associate professor). His investigations especially concern growth dynamics and adaptation of the tetrapod skeleton to a secondarily aquatic lifestyle. He is also specialized in life history and population dynamics of exploited or threatened reptile taxa (crocodylians and monitor lizards).

Vittorio Sansalone: Vittorio Sansalone is associate professor in mechanics at the Université Paris-Est Créteil (France). He is member of the Biomechanics team of the Multiscale modeling and simulation CNRS laboratory (MSME UMR 8208 CNRS, France). Vittorio received his M.S. in Civil engineering from the Università della Calabria (Italy) and his Ph.D. in mechanics from the Università "Roma Tre" (Italy). His primary research interests include image-based finite-element modeling and simulation of biological structures.

CHAPITRE 2: LA VASCULARISATION DES OSTEODERMES:

IMPLICATIONS PHYSIOLOGIQUES DE L'ORNEMENTATION.

Crocodilus niloticus (La ferme aux crocodiles, Pierrelatte 2015)

Vascularization in ornamented osteoderms: Physiological implications in ectothermy and amphibious lifestyle in the crocodylomorphs?

F. Clarac[1, 2], V. de Buffrénil[2], J. Cubo[1], A. Quilhac[1]

[1]Sorbonne Universités, UPMC Univ Paris 06, CNRS, Institut des Sciences de la Terre Paris (ISTeP), 4 place Jussieu, BC 19, F-75005, Paris, France
[2]*Département Histoire de la Terre, Museum National d'Histoire Naturelle, UMR 7207 (CR2P), Sorbonne* Universités, MNHN/CNRS/UPMC, Bâtiment de Géologie Paris Cedex 05, F-75231, France

Corresponding author: francois.clarac@mnhn.fr; Phone: +33144273124

Running title: Vascularization in ornamented osteoderms.

Keywords: Crocodylians; dermal bones; bone sculpture; blood vessels; heat transfer; acidosis buffering.

Abstract

Vascularization in the core of crocodylian osteoderms, and in their superficial pits has been hypothesized to be a key feature involved in physiological thermoregulation and/or acidosis buffering during anoxia (apnea). However, up to now, there have been no quantitative data showing that the inner, or superficial, blood supply of the osteoderms is greater than that occurring in neighboring dermal tissues. We provide such data: our results clearly indicate that the vascular networks in both the osteoderms and the pits forming their superficial ornamentation are denser than in the overlying dermis. These results support previous physiological assumptions and indicate that vascularization in pseudosuchian (crocodylians and close relatives) ornamented osteoderms could be part of a broad eco-physiological adaptation towards ectothermy and aquatic ambush predation acquired by the crocodylomorphs during their Post-Triassic evolution. Moreover, regressions demonstrate that the number of enclosed vessels is correlated with the sectional area of the cavities housing them (superficial pits and inner cavities). These regressions can be used to infer the degree of vascularization on dry and fossilized osteoderms and thus document the evolution of the putative function of the osteoderms in the Pseudosuchia.

Introduction

Extant crocodylians possess a post-cranial dermal skeleton composed of both isolated and articulated osteoderms displaying a pronounced ornamentation (Trutnau and Sommerlad, 2006; Burns et al., 2013; Buffrénil et al., 2015). These bones are formed inside the dermis (Gilbert et al., 2001; Vickaryous and Hall, 2008; Vickaryous and Sire, 2009) and have a diploe structure which is supposed to be well-vascularized both within the inner spongiosa and on the sculptured apical surface of the osteoderm (Scheyer and Sander, 2009; Witzmann, 2009; Witzmann et al., 2010). This is why important physiological functions were attributed to them: increasing the efficiency of heat transfers (Seidel, 1979; Farlow et al., 2010) and/ or contributing to acidosis buffering during anoxia (Jackson et al., 2003; Janis et al., 2012). A similar a role in thermoregulation had also been considered for the dermal plates of the stegosaurians (Ornithischia), based on the observations that the plates housed dense vascular networks circulating in hollow "pipes" visible within the plates (Buffrénil et al., 1986; Farlow et al., 2010). However, up to now, blood vessels have not been formally identified within the core of osteoderms nor in the dermis in immediate contact with the osteoderm ornamented surface. As a consequence, in the absence of this basic anatomical clue, the actual functional role of the osteoderms and their ornamentation remain conjectural. In this study, we provide for three extant crocodylian species, a description and a quantification of the vascular networks associated with osteoderms, and compared to the vessels occurring in neighboring dermal tissues. These quantitative data will be used to build an inference model for further paleohistological studies aimed at assessing the blood supply that once existed in dermal bones of extinct taxa.

Material and methods

Biological sample

The specimens used for this study were nine farmed crocodylians: four Crocodylus niloticus from la Ferme aux Crocodiles (395, allée de Beauplan 26700 Pierrelatte, France), three Caiman crocodilus and two Alligator mississippiensis from La Planète des Crocodiles (Route de fond d'Orveau 86320 Civaux, France; Table 1). These animals are acknowledged by Samuel Martin (La Ferme aux Crocodiles) and Fabrice Thète (La Planète des Crocodiles) for the keeping of exotic reptiles, and comply with the directives of the European parliament and the council of 22 September 2010 on the protection of animals used for scientific purposes (Directive 2010/63/EU).

Specimens	Reference number	Breeding farm	Stage	SVL (cm)	Sex	Sampled osteoderms (×2)
Crocodylus niloticus (1)	IAX119*	LFC	Juvenile	36	N/A	Post-Occipital
Crocodylus niloticus (2)	IAX119*	LFC	Juvenile	40	N/A	Post-Occipital
Crocodylus niloticus (3)	IAX119*	LFC	Juvenile	29.5	N/A	Post-Occipital
Alligator mississippiensis (1)	250 22 96 000 53 465 **	LPC	Sub-adult	67	Male	Nuchal
Alligator mississippiensis (2)	250 22 96 000 52 013 **	LPC	Sub-adult	69	Male	Nuchal
Caiman crocodilus (1)	250 22 96 000 36 907***	LPC	Adult	61	N/A	Nuchal
Caiman crocodilus (2)	250 22 96 000 36 557***	LPC	Adult	73	Female	Nuchal
Caiman crocodilus (3)	250 22 96 000 35 742***	LPC	Adult	71	Female	Nuchal

Table 1: Biological sample. LFC: La Ferme aux Crocodiles. LPC: La Planète des Crocodiles. * CITES number of the specimen's parents (reproductive couple). ** Microchip number of the specimen's parents (reproductive couple born in captivity). *** Microchip number of the specimens born in captivity.

Sampling method

After capture and local disinfection and anesthesia (2 ml of 5 % tricaine methane sulfonate [MS222] in subcutaneous injection), two post-occipital or nuchal osteoderms with a thin layer of underlying dermis were carefully sampled from each animal (Fig. 1A, B). We thus had a total sample of 18 osteoderms. The area of anatomical sampling was then disinfected with Aluspray (vetoquinol) and the animals were simply released in their vivarium. No local infection or other pathological evolution (including behavioral disturbance) was noticed in any of the animal sampled. For light microscopy, the samples were immediately fixed in Bouin's mixture for one week, and were subsequently demineralized for three weeks in several baths, changed every three days, of 5% thrichloracetic acid in a solution with 10% formaldehyde in distilled water. All samples were finally dehydrated in butanol for 3 days, impregnated in two baths of paraffin for two days and embedded in paraffin. They were sectioned transversally (cross-sections perpendicular to osteoderm keel) at 50 microns with a microtome and stained with a one-step trichrome or with orcein following Gabe's instructions (Gabe, 1968).

Quantification of the blood vessels

In order to assess quantitatively the development of the vascular networks in the osteoderms, including in their superficial pits and in the overlying dermis, we first considered a convex contour of each osteoderm, thus distinguishing the area located within the pits from the dermal territories located outside the convex contour. The convex contour corresponds to an envelope of the osteoderm, tangent to the top of the ridges on the ornamented surface, as shown on figure 1E. We then performed a series of morphometric measures on a set of nineteen sections: six from Caiman crocodilus, eight from Alligator mississippiensis and five from Crocodylus niloticus. To this purpose, we took close-up pictures of each cross section through a photonic microscope (Axiover 35) and analyzed these photographs with image J (Rasband, W.S., ImageJ, U. S. National Institutes of Health, Bethesda, Maryland, USA, http://imagej.nih.gov/ij/, 1997-2016). In this software, we used the "polygon selection" tool in order to surround and measure the cross-sectional area of each superficial pit which was present on the different cross sections (N = 57; Fig. 1F). Using the same selection tool, we measured all the cross-sectional areas of the vessels which were present within each pit section. We then took the same measurements for five randomly selected intertrabecular spaces and their inner blood vessels within the osteoderm spongiosa (N = 100; Fig. 1G). Finally, we repeated these measurements in portions of the overlying dermis which were defined using the "rectangular selection" tool by tracing surfaces which included its entire depth between the epidermis and the external surface of the osteoderm (Fig. 1H). We randomly sampled these dermis portions in an equal amount to the number of pits which were present on each cross section (N = 57). Finally, for each histological region (overlying dermis, ornamentation pits, intertrabecular spaces), we calculated the relative area of the vessels, called here Vascular Proliferation (VP) as a ratio of the total area of the vessels to the total area of the selected zone (overlying dermis, $VP_{derm.}$; ornamentation pits, $VP_{pit.}$; intertrabecular spaces, VP_{sp}; no unity).

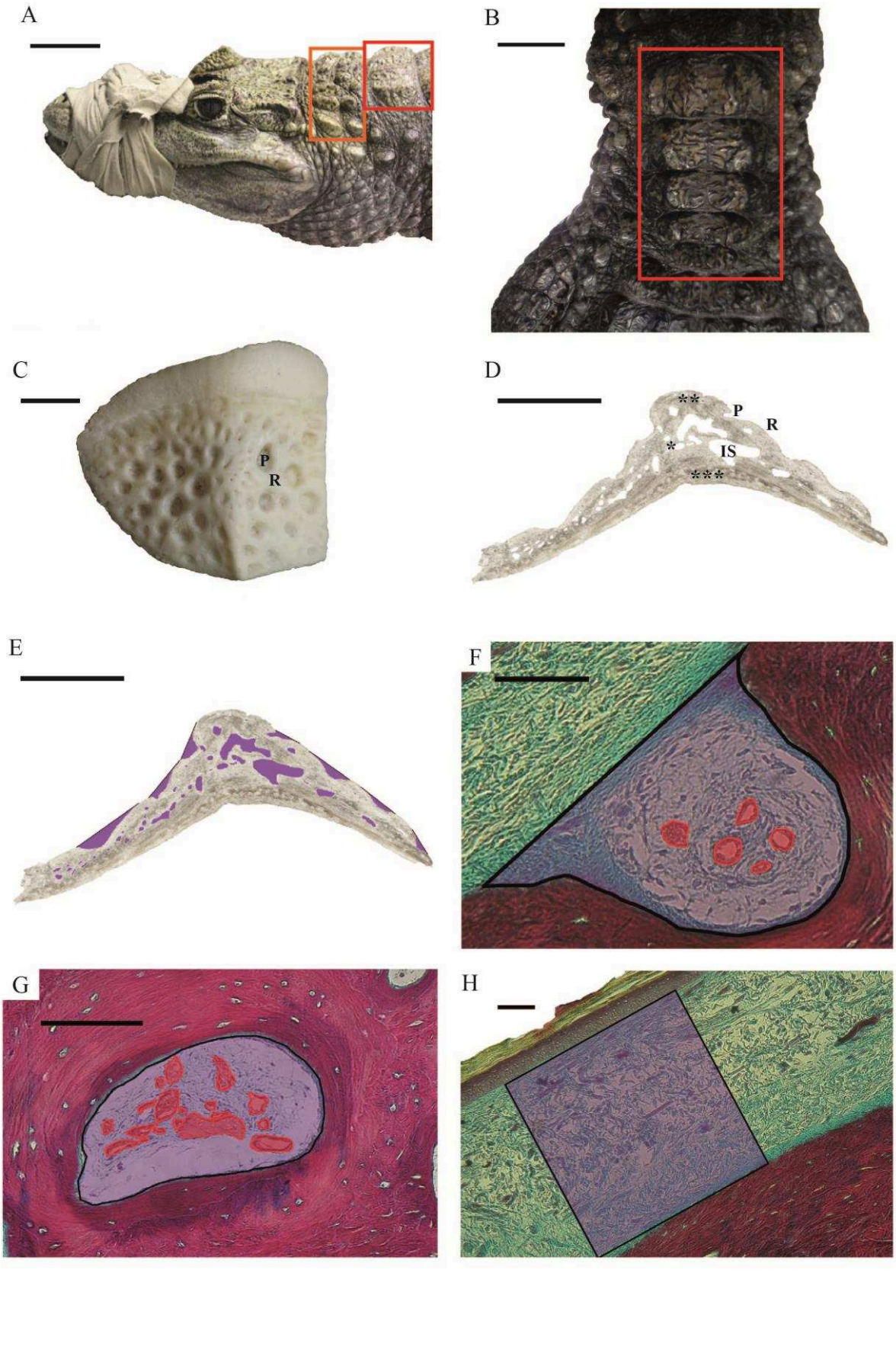
A
B
C
P
R
D
**
P
R
*
IS
***
E
F
G
H

Figure 1: Experimental protocol leading to the assessment of the osteoderm vascularization. A: a sampled specimen (Caiman crocodilus; scale bar: 5cm), the post-occipital osteoderm rows are framed within an orange rectangle, the first nuchal osteoderm row is framed within a red rectangle. B: Close-up on the nuchal region, the nuchal osteoderm rows are framed within a red rectangle; scale bar: 3cm. C: Dorsal view on a Caiman crocodilus dry nuchal osteoderm (collection number: 1988.6489, MNHN); P: pit; R: ridge; scale bar: 5mm. D: Cross-section of a Caiman crocodilus dry nuchal osteoderm; P: pit; R: ridge; IS: intertrabecular space; single asterisk: cancellous bone; double asterisk: paralleled-fiber bone; triple asterisk: lamellar bone; scale bar: 5mm. E: Cross-section of a Caiman crocodilus dry nuchal osteoderm; the whole cross-sectional area of both the pits and intertrabecular spaces are colored in pale purple; scale bar: 5mm. F: Quantification of a pit cross-sectional area and of its included vessels; the pit cross-sectional area is in pale purple; the vessels are circled with a red ellipse and their cross-sectional area is in pale red; scale bar: 100µm. G: Quantification of an intertrabecular space cross-sectional area and of its included vessels; the intertrabecular space sectional area is in pale purple; the vessels are circled with a red ellipse and their cross-sectional area is in pale red; scale bar: 100µm. H: Quantification of the vessels included in the overlying dermis; in pale purple: a rectangular surface which includes the entire dermis' depth between the epidermis and the osteoderm apical surface. No vessel is identified in this portion; scale bar: 100µm.

$$VP = \frac{\text{Total cross-sectional area of the vessels}}{\text{Total cross-sectional area of the selected anatomical zone}}$$

In addition, individual blood vessels visible in osteoderm cavities (be they inner cavities or superficial pits) were counted and used to create an index of Vascular Density (VD; in mm^{-2}):

$$\text{VD} = \frac{\text{Total number of the vessels}}{\text{Total cross-sectional area of the selected anatomical zone}}$$

with distinction of $VD_{derm.}$, $VD_{pit.}$, $VD_{sp.}$.

Statistical analyses

In order to compare the degree of vascularization between the three histological regions of interest, we first performed ANOVAs (two-tailed and one-tailed) and t-tests (two-paired and unpaired) for the indices VP and VD in disregard of the specimen's taxonomic position. We used Past software (PAST version 2.17c, Hammer et al., 2001) for such analyses. Furthermore, to test the correlation between the size of the pits and of the intertrabecular spaces with their own degree of vascularization (total cross-sectional area of the vessels; number of the vessels), we performed a bivariate phylogenetic generalized least square (PGLS, Grafen, 1989), using the « caper » package (Orme et al., 2012) with reference to a morphology-based phylogeny of Crocodylia (Brochu; 2003). We performed the PGLS analyses on R (R Development Core Team, 2012). In this regard, we defined the cross-sectional area of the pits and intertrabecular spaces as independent variables (X). We defined the number of vessels and the total cross-sectional area of the vessels per region (overlying dermis, superficial pits, intertrabecular spaces) as dependent variables (Y).

Results

Qualitative description

On the external part of each cross-section, we observe a layer of keratin that fully covers the epidermis. Deep to the epidermis, we notice a poorly vascularized dermis which covers the underlying osteoderm (Fig. 2A&B). The dermis adjacent to the basolateral corners of each osteoderm is composed of densely-packed collagen bundles whereas collagen bundles tends to be more loosely arranged superficial to the external surface of the osteoderm. The osteoderms are usually made of a cancellous bone matrix in the core (spongiosa), which is surrounded by two more compact layers (Fig. 1D; Fig. 2A, C, E). The external compact layer is excavated by pits and grooves (ornamentation) that house one or more blood vessels communicating with the core spongiosa (Fig. 2C, D, G). Within this spongiosa, there are erosion bays (intertrabecular spaces; Fig. 2H) that are also well vascularized with both transverse and longitudinally-oriented vessels similarly as in the pits. However, the blood vessels, whether located within the core spongiosa or in the ornamental pits, occupies a small part of available cross-sectional area and are seldom in direct contact with the walls of the cavities housing them (Fig. 2D, G, H). At the basal side of the osteoderms, blood vessels connect deeper arteries and veins deep to the osteoderms (Fig. 2E&F).

Quantitative data and statistical analyses

The vascular proliferation in the dermis $VP_{derm.}$ remains under 8 % whereas it reaches 27% in the pits ($VP_{pit.}$) and scores values which are ranged between 2% to 44% in the intertrabecular cavities ($VP_{sp.}$; Fig. 3). As suspected by the qualitative observations, there is a significant difference between these values according to the ANOVA ($P_{value} < 0.0001$; whether two-tailed or one-tailed; Table 2). The t-tests (unpaired) reveal that the vascularization is, significantly higher in the inter trabecular spaces (spongiosa) than in the pits (ornamentation) and significantly higher in the pits than in the overlying dermis ($VP_{sp.} > VP_{pit.} > VP_{derm.}$; Pvalue < 0.0001; Table 2).

The vascular density in the dermis $VD_{derm.}$ ranges between 0 and 47 vessels per mm², whereas this values ranges up to 434 vessels per mm² ($VD_{pit.}$) in the pits and up to 1566 per mm² in the intertrabecular cavities ($VD_{sp.}$; Fig. 3). When repeating the statistical tests which we performed for VP (ANOVA, t-tests), we obtain the same significant differences (Table 2): $VD_{sp.} > VD_{pit.} > VD_{derm.}$.

The PGLS analyses indicate that, in the osteoderm series, there is a significant correlation between the cross-sectional area of the pits and of the inter trabecular spaces in terms of the total cross-sectional area and number of vessels they house (Fig. 4; Table 2).

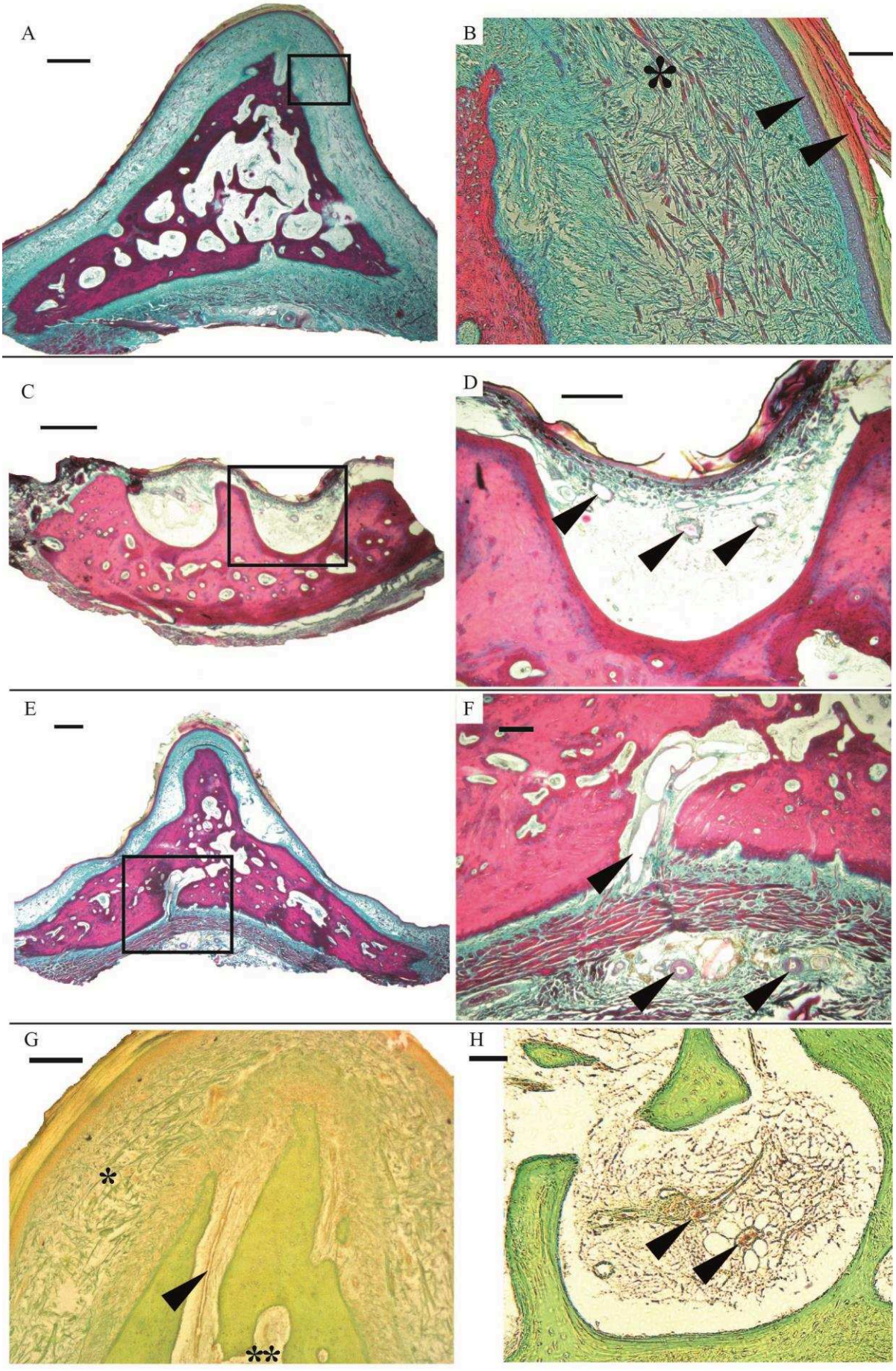
A
B
C
D
E
F
G
H

Figure 2: A: osteoderm of Crocodylus niloticus; scale bar: 1mm. B: close-up on the avascular dermis (asterisk) which is covered by the epidermis and a keratin layer (arrows); scale bar: 333µm. C: Osteoderm of Caiman crocodilus; scale bar: 1mm. D: close-up on an ornamentation pit which encloses several vessels (arrows); scale bar: 333µm. E: Osteoderm of Alligator mississippiensis; scale bar: 1mm. F: close-up on a basal foramen which encloses vessels and opens into the deeper stratum compactum which is vascularized by arterioles (arrows); scale bar: 333µm. G: osteoderm of Crocodylus niloticus with orcein coloration, close-up on a pit containing a transverse vessel (arrow) that connects the overlying dermis (single asterisk) with the spongiosa (double asterisk). H: osteoderm of Crocodylus niloticus with orcein coloration, close-up on an intertrabecular space containing blood vessels (arrow) scale bar: 100 µm.

	O.Dermis $N_{OD} = 57$	Pits $N_{Pit} = 57$	I.T.Spaces $N_{ITS} = 100$
Anova (two-tailed)	Pvalue < 0.0001		
Anova (one-tailed)	Pvalue < 0.0001		
t-test (paired)	Pvalue < 0.0001		
t-test (unpaired)	Pvalue < 0.0001		
t-test (paired)		Pvalue < 0.0001	
t-test (unpaired)		Pvalue < 0.0001	

VD	O.Dermis $N_{OD} = 57$	Pits $N_{Pit} = 57$	I.T.Spaces $N_{ITS} = 100$
Anova (two-tailed)	Pvalue < 0.0001		
Anova (one-tailed)	Pvalue < 0.0001		
t-test (paired)	Pvalue < 0.0001		
t-test (unpaired)	Pvalue < 0.0001		
t-test (paired)		Pvalue < 0.0001	
t-test (unpaired)		Pvalue < 0.0001	

Table 2: VP (vascular proliferation) and VD (vascular density): statistical variations between the osteoderms histological regions (overlying dermis, superficial pits, intertrabecular space). "N" is the number of sampled cavities (pits or inter trabecular spaces) or random portions of overlying dermis in the whole specimens.

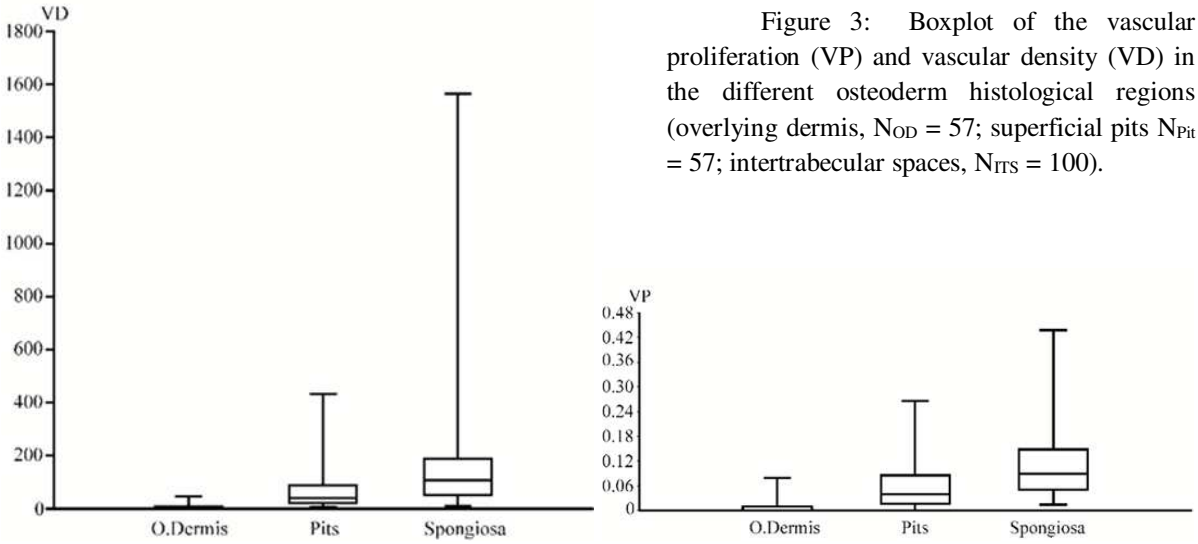

Figure 3: Boxplot of the vascular proliferation (VP) and vascular density (VD) in the different osteoderm histological regions (overlying dermis, $N_{OD} = 57$; superficial pits $N_{Pit} = 57$; intertrabecular spaces, $N_{ITS} = 100$).

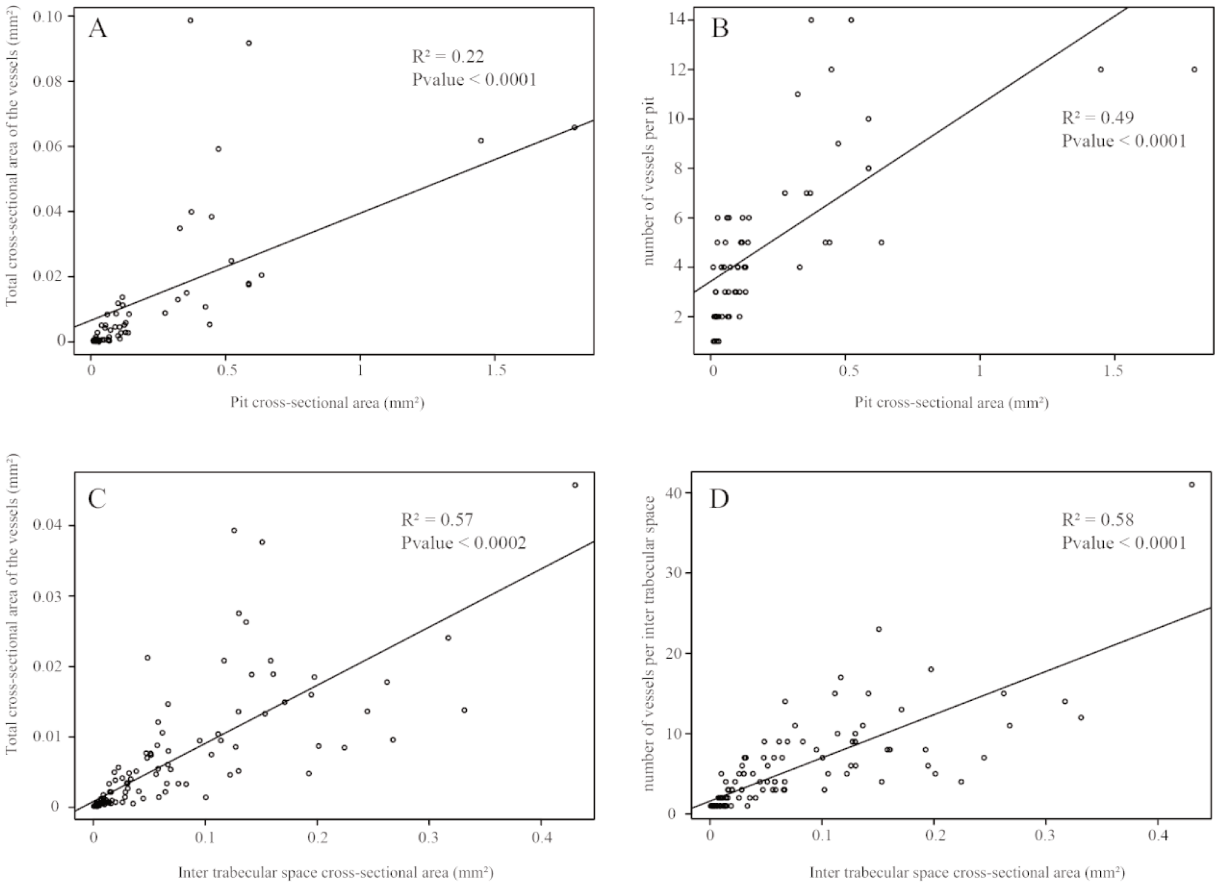

Figure 4: A: Regression line (obtained by PGLS) showing the significant correlations between the cross-sectional area of the ornamentation pits and the total cross-sectional area of the enclosed vessels. B: Regression line (obtained by PGLS) showing the significant relation between the cross-sectional area of the ornamentation pits and the number of enclosed vessels. C: Regression line (obtained by PGLS) showing the significant relation between the cross-sectional area of the intertrabecular spaces and the total cross-sectional area of the enclosed vessels. D: Regression line (obtained by PGLS) showing the significant relation between the cross-sectional area of the intertrabecular spaces and the number of enclosed vessels.

Discussion

The osteoderms functional implications

Although the functional role of the osteoderms is often assumed to be general mechanical protection by some authors (Coldiron, 1974; Sun and Chen, 2013; Yang et al., 2013; Chen et al., 2014), both the bone matrix and the superficial pits could as well provide more targeted a protection for the peripheral blood vessels by offering a mineralized shield. Besides, beyond any protective role, the crocodylians' ornamented osteoderms may have at least one physiological function as supported by our results. Indeed, we point out that the degree of vascularization is clearly higher in the osteoderms than in the overlying dermis. The presence of osteoderms thus create a repetitive pattern of dense vascular clusters, extensively distributed on the dorsal and, to a lesser extent, ventral sides of the crocodylian body, close (some millimeters at most) to its outer limit. The prerequisite for a possible involvement of osteoderms in thermoregulation (Seidel, 1979) and / or acidosis buffering is thus supported.

Concerning the acidosis buffering hypothesis, a previous study in Caiman latirostris has shown that lactate is accumulated in the osteoderms (Jackson et al., 2003) during prolonged apnea as in aquatic turtle shells (Jackson and Heisler, 1982; Jackson, 2000; Jackson et al., 1999, 2000a, 2000b, 2012). This process could first rely on an extensive supply of the lactate-rich plasma the osteoderms due to high vascular density. Subsequently, inner and superficial remodeling of the osteoderms (Buffrénil, 1982; Buffrénil et al., 2015), would release enough carbonates (including calcium, magnesium and potassium) to buffer the lactate and reduce blood acidity (Jackson et al., 2003). This theoretical interpretation could explain why osteoderm remodeling is more active in semi-aquatic crocodyliforms (e.g. Buffrénil et al., 2015; Scheyer and Desojo, 2011; Scheyer et al., 2014), and why these forms tend to have a more deeply excavated ornamentation than the earliest terrestrial pseudosuchians (Triassic taxa), which were unlikely to regularly endure apnea (Ricqlès et al., 2003; Clarac et al., 2017). However, this physiological interpretation faces a problem of timing: bone resorption by osteoclasts is a relatively slow process, as compared to immediate (and vital) needs for acidosis buffering. Moreover, this assumption is likely paradoxical with the loss of both the skull ornamentation and the entire osteoderm shield in pelagic crocodyliforms (metriorhynchids; Buffetaut, 1982) during the Jurassic. Indeed, these off-shore marine forms must have undergone periods of apnea at least as long as those experienced by the semi-aquatic crocodyliforms (teleosaurids and neosuchians). Notwithstanding, the metriorhynchids' adaptation to the pelagic lifestyle implied drastic morphological modifications (i.e. skull elongation, weight loss, flexibility along the antero-posterior axis, etc. Buffetaut, 1982; Clarac et al., 2016; Young et al., 2010), which may have constrained the development of the dorsal shield in disregard of its physiological implication(s).

Testing the thermoregulation hypothesis (Seidel, 1979), relies on the measurement of osteoderm temperature, which is always lower than in the surrounding skin that is free from dermal ossification, whether the environmental temperature is high or low (Farlow et al., 2010). Indeed, this assessment indirectly demonstrates that the organism's cool blood is permanently driven, under a controlled flow, from the core to the periphery of the body in order exchange the heat with the surrounding environment (ecto-poïkilothermy; Huey, 1982). Thus, the rich vascular network, which is housed both inside the osteoderms and in the superficial pits must capture and convey the incoming heat into the dorsal arteries through the basal foramina of the osteoderms (Fig. 2E&F). When crocodiles bask, exposing their back to solar radiations, their osteoderms are heated and the heart rate is accelerated (Seebacher and Franklin, 2004). As a consequence, the local blood flow is increased and the heat exchange from the environment towards superficial capillaries is accelerated (Grigg and Alchin, 1976; Seebacher and Franklin, 2007). When optimal body temperature is reached (31°C - 33°C; Johnson et al., 1976), heart rate decreases, and the specimen may entirely submerge into the water to reduce its temperature and avoid overheating (Smith, 1979). This whole process is likely made more efficient by a significant proliferation of the blood vessels within the osteoderms. This condition is likely to constitute an evolutionary advantage for large ecto-poïkilothermic vertebrates, which are characterized by a low mobility and thus a low production of endogenous (mainly muscular) heat (Bartholomew, 1982).

Of course, all crocodylian bones have an inner and, to a lesser extent, outer (periosteal) vascular supply, as is the case for example for the endochondral bones forming the appendicular skeleton. However, such « ordinary » blood vessels in bone differ by several features from the peculiar vascular clusters created by osteoderm vascularity. 1) Osteoderm blood supply is not influenced by individual age or growth stage, whereas vascular networks progressively rarify to finally disappear in newly formed superficial bone layers of adults (see e.g. section pictures in Buffrénil, 1982). 2) The vessels housed within osteoderms extend outside the bony elements proper to ramify as vascular balls in the ornamental pits. This situation is unknown in other, non-ornamented bones. 3) Both the vessels inside the osteoderms and their extensions in the pits are located very close to skin outer surface. Conversely, deep (endochondral) bones are separated from the outer surface of the body by the whole thickness of the dermis and underlying fat, and by the strong muscles attached to these skeletal elements (Gasc, 1981). This complex assemblage of tissues is obviously an obstacle to the diffusion of heat towards the inner blood vessels that could be housed in bone cortices. Finally, the general anatomical « device » created by the osteoderms and their vascularization, i.e. regularly spaced vascular clusters located within the dermis just under epidermal surface, and is the only one to meet the basic requirements of an efficient heat exchanger system. Moreover, it is encountered in no other region of the crocodylian body than osteoderm shields, with exception for other dermal (superficial) bones, such as the skull roof or the lateral sides of the mandible, which themselves exhibit well-pronounced ornamentation (Iordansky, 1973; Clarac et al., 2016).

Perspectives in evolutionary biology

According to our results, a rough estimation of both the total cross-sectional area and the number of the vessels is feasible in dry or well-preserved fossilized osteoderms with phylogenetic-informed regressions. The development of further analyses to provide a confidence interval for each inferred value (Phylogenetic Eigenvector Maps; Guénard et al., 2013) is nevertheless needed in the perspective of evolutionary reconstructions.

Early terrestrial pseudosuchians (but also later forms such as notosuchians) had shallow ornamentation and only two rows of compact and poorly vascularized, (Scheyer and Desojo, 2011; Irmis et al., 2013; Scheyer et al., 2014). These forms are hypothesized to have had a higher basal/resting metabolic rate than the modern forms (Ricqlès et al., 2003, 2008; Legendre et al., 2013, 2016). At the Triassic-Jurassic transition, the development of a well-vascularized dermal shield could have accompanied the adaptation of the crocodyliforms to the role of semi-aquatic ambush predators (Buffetaut, 1982). Quantifying the progressive increase in osteoderm blood supply provides a key insight into the history of thermal physiology in tetrapods.

Conclusion

Our analyses assess that crocodylians' ornamented osteoderms are particularly well-vascularized with regard to the surrounding dermis. Ecto-poïkilothermic thermoregulation and acidosis buffering remain the two principal hypotheses because both of these functions represent important aspects in the evolution of crocodylomorphs. Indeed, these vertebrates secondarily evolved from terrestrial forms with high basal metabolic rates into ectothermic semi-aquatic ambush predators. The contribution of osteoderm vascularization to thermoregulation would concern the superficial heat exchange when basking (fully emerged or semi-emerged). During apnea (submerged), the osteoderm vascular network would convey the lactate into the bone matrix and may supply with osteoclasts which would release both the bone calcium combining with the blood lactate and the bone carbonates themselves directly increasing the plasma pH.

Acknowledgements

We would like to thank and to salute the memory of Fabrice Thete, who friendlily welcomed us to la Planète des Crocodiles and gave us access to the largest and most dangerous specimens composing our sample (Alligator mississippiensis, Caiman crocodilus). We also thank his employees (Geoffrey Fomel and Cédric Goetgheluck) for giving us technical assistance in catching these specimens in their vivarium. We send our thankful and friendly regards to Samuel Martin and his employees for welcoming us to la Ferme aux Crocodiles and giving us access to their nursery, in which we sampled the Crocodylus niloticus specimens. Finally, we acknowledge Hayat Lamrous for her huge technical investment in the preparation of the histological sections.

Literature cited

Bartholomew GA. 1982. Physiological control of body temperature. In: Gans C, Pough FH editors. Biology of the Reptilia volume 12C: Physiological ecology. Ithaca, NY, USA: Academic Press. p 168-211.

Buffetaut E. 1982. Radiation évolutive, paléoécologie et biogéographie des crocodiliens mésosuchiens. Mémoires de la Société Géologique de France N S 142: 1–88.

Buffrénil Vde. 1982. Morphogenesis of bone ornamentation in extant and extinct crocodilians. Zoomorphology 99: 155–166.

Buffrénil Vde, Farlow JO, Ricqlès Ade. 1986. Growth and function of Stegosaurus plates: evidence from bone histology. Paleobiology 12(4): 459-473.

Buffrénil Vde, Clarac F, Fau M, Martin S, Martin B, Pellé E, Laurin M. 2015. Differentiation and growth of bone ornamentation in vertebrates: A comparative histological study among the Crocodylomorpha. J Morphol 21: 1–21.

Brochu CA. 2003. Phylogenetic approaches toward crocodilian history. Annu Rev Earth Planet Sci 31: 357–397.

Burns ME, Vickaryous MK, Currie PJ. 2013. Histological variability in fossil and recent alligatoroid osteoderms: systematic and functional implications. J Morphol 274: 676-686.

Chen IH, Yang W, Meyers MA. 2014. Alligator osteoderms: Mechanical behavior and hierarchical structure. Mater Sci Eng C 35: 441–448.

Clarac F, Souter T, Cubo J, Buffrénil Vde, Brochu CA, Cornette R. 2016. Does skull morphology constrain bone ornamentation? A morphometric analysis in the Crocodylia. J Anat 229: 292–301.

Clarac F, Buffrénil Vde, Brochu CA, Cubo J. 2017. The evolution of bone ornamentation in Pseudosuchia: Morphological constraints versus ecological adaptation. Biol J Linn Soc: blw034.

Coldiron RW. 1974. Possible functions of ornament in the labyrinthodont amphibians. Occ Pap Mus Nat Hist Kansas 33: 1-19.

Farlow JO, Hayashi S, Tattersall GJ. 2010. Internal vascularity of the dermal plates of Stegosaurus (Ornithischia, Thyreophora). Swiss J Geosci 103: 173–185.

Gabe M. 1968. Techniques histologiques. Paris: Masson.

Gans C. 1973. Axial musculature B. Crocodilia. In: Gans C, Parson TS editors. Biology of the Reptilia volume 11F: Morphology. London: Academic Press. p. 372–375.

Gilbert SF, Loredo GA, Brukman A, Burke AC. 2001. Morphogenesis of the turtle shell : the development of a novel structure in tetrapod evolution. Evol Dev 3: 47–58.

Grafen A. 1989. The phylogenetic regression. Proc R Soc London Ser B 205: 581–598.

Grigg GC, Alchin J. 1976. The role of the cardiovascular system in thermoregulation of

Crocodylus johnstoni. Physiol Zool 49: 24–36.

Guénard G, Legendre P, Peres-Neto P. 2013. Phylogenetic eigenvector maps: a framework to model and predict species traits. Methods Ecol Evol 4: 1120–1131.

Hammer Ø, Harper DAT, Ryan PD. 2001. PAST: Paleontological statistics software

package for education and data analysis. Palaeontol. Electron. 4 (1). ⟨http://palaeoelectronica.

org/2001_1/past/issue1_01.htm⟩.

Huey RB. 1982. Temperature, physiology and the ecology of the reptiles. In: Gans C, Pough FH editors. Biology of the Reptilia volume 12C: Physiological ecology. Ithaca, NY, USA: Academic Press. p 168-211.

Iordansky NN. 1973. The skull of the Crocodilia. In: Gans C, Parson TS editors. Biology of the Reptilia volume 4D: Morphology. London: Academic Press. p. 201–262.

Irmis RB, Nesbitt SJ, Sues HD. 2013. Early Crocodylomorpha. Geol Soc London Spec Publ 379: 275–302.

Jackson DC, Heisler N. 1982. Plasma ion balance in submerged anoxic turtles at 3°c: the role of calcium lactate formation. Res Physiol 49: 159-174.

Jackson DC, Goldberger Z, Visuri S, Armstrong RN. 1999. Ionic exchanges of turtle shell in vitro and their relevance to shell function in the anoxic turtle. J Exp Biol 202: 503-520.

Jackson DC. 2000. Living without oxygen: lessons from the freshwater turtle. Comp Biochem Physiol A 125: 299-315.

Jackson DC, Crocker CE, Ultsch GR. 2000a. Bone and shell contribution to lactic acid buffering of submerged turtles Chrysemys picta bellii at 3°C. Am J Physiol-Reg 278: R1964-1571.

Jackson DC, Ramsey AL, Paulson JM, Crocker CE, Ultsch GR. 2000b. Lactic acid buffering by bone and shell in anoxic softshell and painted turtles. Phys Chem Zool 73(3): 290-297.

Jackson DC, Andrade D, Abe AS. 2003. Lactate sequestration by osteoderms of the broad-nose caiman, Caiman latirostris, following capture and forced submergence. J Exp Biol 206: 3601-3606.

Janis CM, Devlin K, Warren DE, Witzmann F. 2012. Dermal bone in early tetrapods: a palaeophysiological hypothesis of adaptation for terrestrial acidosis. P Roy Soc B 279: 3035-3040.

Johnson CR, Webb GJW, Tanner C. 1976. Thermoregulation in crocodilians II. A

telemetric study of body temperature in the Australian crocodiles, Crocodylus johnstoni and Crocodylus porosus. Comp Physiol 53A: 143–146.

Legendre L, Segalen L, Cubo J. 2013. Evidence for high bone growth rate in Euparkeria obtained using a new paleohistological inference model for the humerus. J Vertebr Paleontol 33: 1343–1350.

Legendre L, Guénard G, Botha-Brink J, Cubo J. 2016. Palaeohistological evidence for ancestral high metabolic rate in archosaurs. Syst Biol 65(6): 989-996.

Orme D, Freckleton R, Thomas G, Petzoldt T, Fritz S, Isaac N, Pearse W. 2012. The caper package: Comparative analysis of phylogenetics and evolution in R. R package version 0.5.2.

Rasband WS. ImageJ, U. S. National Institutes of Health, Bethesda, Maryland, USA, http://imagej.nih.gov/ij/, 1997-2016.

Ricqlès Ad, Padian K, Horner JR. 2003. On the bone histology of some Triassic pseudosuchian archosaurs and related taxa. Annls Paléont 89: 67–101.

Ricqlès Ad, Padian K, Knoll F, Horner JR. 2008. On the origin of high growth rates in archosaurs and their ancient relatives: Complementary histological studies on Triassic archosauriforms and the problem of a “phylogenetic signal” in bone histology. Annls Paléont 94: 57–76.

Scheyer TM, Sander PM. 2009. Bone microstructures and mode of skeletogenesis in osteoderms of three pareiasaur taxa from the Permian of South Africa. J Evol Biol 22: 1153–1162.

Scheyer TM, Desojo JB. 2011. Palaeohistology and external microanatomy of rauisuchian osteoderms (Archosauria: Pseudosuchia). Palaeontology 54: 1289–1302.

Scheyer TM, Desojo JB, Cerda IA. 2014. Bone histology of phytosaur, aetosaur, and other archosauriform osteoderms (Eureptilia, Archosauromorpha). Anat Rec 297: 240–260.

Seebacher F, Franklin CE. 2004. Integration of autonomic and local mechanisms in regulating cardiovascular responses to heating and cooling in a reptile (Crocodylus porosus). J Comp Physiol B 174: 577–585.

Seebacher F, Franklin CE. 2007. Redistribution of blood within the body is important for thermoregulation in an ectothermic vertebrate (Crocodylus porosus). J Comp Physiol B 177: 841–848.

Seidel MR. 1979. The osteoderms of the American Alligator and their functional significance. Herpetol Leag 35: 375–380.

Smith EN. 1979. Behavioral and physiological thermoregulation of crocodilians. Am Zool 19: 239–247.

Sun CY, Chen PY. 2013. Structural design and mechanical behavior of alligator (Alligator mississippiensis) osteoderms. Acta Biomater 9: 9049–9064.

Trutnau L, Sommerlad R. 2006. Morphological characteristics. In: Chimaira B editor. Crocodilians their Natural History and Captive Husbandry. Franckfurt am Main: Andreas S. Bram. p 75–78.

Vickaryous MK, Hall BK. 2008. Development of the dermal skeleton in Alligator mississippiensis (Archosauria, Crocodylia) with comments on the homology of osteoderms. J Morphol 269: 398-422.

Vickaryous MK, Sire JY. 2009. The integumentary skeleton of tetrapods: origin, evolution and development. J Anat 214: 441–464.

Witzmann F. 2009. Comparative histology of sculptured dermal bones in basal tetrapods, and the implications for the soft tissue dermis. Palaeodiversity 2: 233–270.

Witzmann F, Scholz H, Müller J, Kardjilov N. 2010. Sculpture and vascularization of dermal bones, and the implications for the physiology of basal tetrapods. Zool J Linn Soc 160: 302–340.

Yang W, Chen IH, Gludovatz B, Zimmermann EA, Ritchie RO, Meyers MA. 2013. Natural Flexible Dermal Armor. Adv Mater 25: 31–48

Young MT, Brusatte SL, Ruta M, Andrade MBde. 2010. The evolution of Metriorhynchoidea (Mesoeucrocodylia,Thalattosuchia): an integrated approach using geometric morphometrics, analysis of disparity, and biomechanics. Zool J Linn Soc 158: 801–859.

Appendix: Dataset of the measurements and calculated variables for each sampled area on the different cross sections (A: in the overlying dermis; B: in the ornamentation pits; C: in the spongiosa). N: sampled area number (OD: overlying dermis; Pit: ornamentation pits; ITS intertrabecular spaces).VD: vascular density; VP: vascular proliferation.

A	Overlying Dermis					
Species	Cross section Label	N_{OD}	VD (mm^{-2})	VP (no unity)	Number of vessels	Total cross-sectional area of the vessels (µm²)
C.niloticus	cro3A4	1	9.1	0	3	1001.62
C.niloticus	cro3A4	2	2.46	0.01	1	3583.92
C.niloticus	cro3A14	3	0	0	0	0
C.niloticus	cro3A14	4	2.93	0	1	171.99
C.niloticus	cro3A14	5	0	0	0	0
C.niloticus	cro3A14	6	0	0	0	0
C.niloticus	cro3A14	7	0	0	0	0
C.niloticus	cro3A14	8	7.71	0.01	4	4376.1
C.niloticus	cro3A21	9	0	0	0	0
C.niloticus	cro3A21	10	3.82	0	2	214.12
C.niloticus	cro3A21	11	5.73	0	2	1550.36
C.niloticus	cro3A22O	12	0	0	0	0
C.niloticus	cro3A22O	13	9.28	0	3	776.91
C.niloticus	cro3A22O	14	10.42	0.01	5	3871.47
C.niloticus	cro3b3	15	0	0	0	0
C.niloticus	cro3b3	16	0	0	0	0
C.niloticus	cro3b3	17	0	0	0	0
C.niloticus	cro3b3	18	31.04	0.01	5	1789.13
A.mississippiensis	C4BBT9	19	0	0	0	0
A.mississippiensis	C4BBT9	20	0	0	0	0
A.mississippiensis	C4BT3	21	0	0	0	0
A.mississippiensis	C4BT3	22	14.73	0.01	3	2170.8
A.mississippiensis	C4BT5	23	0	0	0	0
A.mississippiensis	C4BT5	24	0	0	0	0
A.mississippiensis	C4BT5	25	9.74	0.01	2	1303.22
A.mississippiensis	C4BT17	26	12.41	0.01	4	4110.97
A.mississippiensis	C4BT23	27	13.72	0.01	9	8951.05
A.mississippiensis	C5BT14	28	0	0	0	0
A.mississippiensis	C5BT14	29	23.2	0.01	2	564.85
A.mississippiensis	C5BT14	30	0	0	0	0
A.mississippiensis	C5BT14	31	21.37	0.02	2	2062.12
A.mississippiensis	C5BT14	32	0	0	0	0
A.mississippiensis	C5BT14	33	0	0	0	0
A.mississippiensis	C5BT15	34	7.22	0	1	72.22
A.mississippiensis	C5BT15	35	31.45	0.02	4	2264.83
A.mississippiensis	C5BT15	36	0	0	0	0
A.mississippiensis	C5BT28	37	0	0	0	0
A.mississippiensis	C5BT28	38	0	0	0	0
A.mississippiensis	C5BT28	39	46.09	0.01	4	654.29
A.mississippiensis	C5BT28	40	46.1	0.01	5	1295.97
A.mississippiensis	C5BT28	41	34.13	0.01	6	1512.26
C.crocodilus	C1AT11	42	0	0	0	0
C.crocodilus	C1AT11	43	0	0	0	0
C.crocodilus	C1BO6bis	44	0	0	0	0
C.crocodilus	C1BO6bis	45	7.83	0.02	1	2722.18
C.crocodilus	C1BO10	46	0	0	0	0

C.crocodilus	C1BO10	47	4.13	0.02	1	4838.49
C.crocodilus	C1BO10	48	0	0	0	0
C.crocodilus	C1BT7	49	0	0	0	0
C.crocodilus	C1BT7	50	36.87	0.08	1	2184.19
C.crocodilus	C1BT9	51	0	0	0	0
C.crocodilus	C1BT9	52	0	0	0	0
C.crocodilus	C1BT9	53	0	0	0	0
C.crocodilus	C1BT9	54	0	0	0	0
C.crocodilus	C1BT11	55	0	0	0	0
C.crocodilus	C1BT11	56	0	0	0	0
C.crocodilus	C1BT11	57	0	0	0	0

B	Pits						
Species	Cross section Label	N_{pit}	VD (mm^{-2})	VP (no unity)	Pit cross-sectional area (µm²)	Number of vessels	Total cross-sectional area of the vessels (µm²)
C.niloticus	cro3A4	1	98.86	0.14	60692.29	6	8404.04
C.niloticus	cro3A4	2	86.86	0.02	23026.03	2	353.34
C.niloticus	cro3A14	3	55.05	0.05	72660.54	4	3622.11
C.niloticus	cro3A14	4	36.09	0.02	138539.59	5	2777.2
C.niloticus	cro3A14	5	47.47	0.02	42130.08	2	646.07
C.niloticus	cro3A14	6	29.23	0	68420.94	2	341.51
C.niloticus	cro3A14	7	44.72	0.02	111805.46	5	2744.67
C.niloticus	cro3A14	8	91.95	0.09	54375.28	5	5086.48
C.niloticus	cro3A21	9	88.8	0.02	67568.64	6	1488.27
C.niloticus	cro3A21	10	33.57	0	29791.74	1	44.11
C.niloticus	cro3A21	11	30.87	0.02	129557.99	4	2905.82
C.niloticus	cro3A22O	12	39.78	0.02	100551.78	4	1848.51
C.niloticus	cro3A22O	13	27.83	0.01	107813.25	3	986.59
C.niloticus	cro3A22O	14	45.44	0.01	66028.13	3	673.66
C.niloticus	cro3b3	15	33.35	0.05	89954.52	3	4587.02
C.niloticus	cro3b3	16	65.89	0.03	15177.63	1	399.91
C.niloticus	cro3b3	17	66.85	0.02	29918.64	2	555.88
C.niloticus	cro3b3	18	50.69	0.1	118361.72	6	11299.26
A.mississippiensis	C4BBT9	19	23.12	0.05	129730.23	3	5855.01
A.mississippiensis	C4BBT9	20	32.1	0.04	124606.05	4	5199.09
A.mississippiensis	C4BT3	21	25.39	0.03	275741.72	7	8839.92
A.mississippiensis	C4BT3	22	42.75	0.12	116969.8	5	13734.45
A.mississippiensis	C4BT5	23	155.7	0.06	12845.44	2	765.08
A.mississippiensis	C4BT5	24	34.05	0.04	323092.81	11	12977.75
A.mississippiensis	C4BT5	25	56.86	0.08	52761.59	3	4250.68
A.mississippiensis	C4BT17	26	74.55	0.09	93900.15	7	8621.61
A.mississippiensis	C4BT23	27	31.25	0.01	64005.66	2	521.39
A.mississippiensis	C5BT14	28	204.22	0.12	24482.84	5	2854.65
A.mississippiensis	C5BT14	29	80.87	0.01	49465.03	4	646.8
A.mississippiensis	C5BT14	30	101.42	0.01	19719.16	2	220.64
A.mississippiensis	C5BT14	31	39.71	0.12	100737.36	4	11851.82
A.mississippiensis	C5BT14	32	44.81	0.01	22317.25	1	248.87
A.mississippiensis	C5BT14	33	110.33	0.05	18128.08	2	831.07
A.mississippiensis	C5BT15	34	49.39	0.06	141729.8	7	8511.33
A.mississippiensis	C5BT15	35	18.64	0.04	107268.06	2	4546.12
A.mississippiensis	C5BT15	36	161.72	0.08	18550.53	3	1517.89
A.mississippiensis	C5BT28	37	235	0.02	25532.05	6	630.41

A.mississippiensis	C5BT28	38	159.38	0.01	18822.39	3	123.7
A.mississippiensis	C5BT28	39	96.45	0.01	20735.97	2	303.94
A.mississippiensis	C5BT28	40	433.49	0.04	9227.47	4	382.69
A.mississippiensis	C5BT28	41	97.28	0.02	10280.08	1	171.59
C.crocodilus	C1AT11	42	8.28	0.04	1448730	12	61768
C.crocodilus	C1AT11	43	6.68	0.04	1796158	12	65796
C.crocodilus	C1BO6bis	44	12.1	0.11	330527.83	4	34857.16
C.crocodilus	C1BO6bis	45	13.64	0.16	586597.04	8	91687.79
C.crocodilus	C1BO10	46	11.33	0.01	441169.07	5	5321.32
C.crocodilus	C1BO10	47	7.89	0.03	633780.39	5	20490.19
C.crocodilus	C1BO10	48	18.99	0.12	473838.64	9	59202.36
C.crocodilus	C1BT7	49	19.68	0.04	355702.92	7	15032.25
C.crocodilus	C1BT7	50	18.93	0.27	369771.2	7	98634.11
C.crocodilus	C1BT9	51	11.74	0.03	425817.77	5	10752.96
C.crocodilus	C1BT9	52	101.43	0.13	39435.99	4	5099
C.crocodilus	C1BT9	53	26.84	0.05	521678.78	14	24876.4
C.crocodilus	C1BT9	54	26.77	0.09	448190.06	12	38402.45
C.crocodilus	C1BT11	55	13.65	0.03	585966.56	8	17936.02
C.crocodilus	C1BT11	56	17.07	0.03	585941.95	10	17508.35
C.crocodilus	C1BT11	57	37.5	0.11	373350.43	14	39895.91

C	Spongiosa						
Species	Cross section Label	N_{ITS}	VD (mm^{-2})	VP (no unity)	Intertrabecular space cross-sectional area (µm²)	Number of vessels	Total cross-sectional area of the vessels (µm²)
C.crocodilus	C1AT11	1	78.13	0.15	51193.49	4	7654.24
C.crocodilus	C1AT11	2	293.41	0.04	3408.23	1	137.99
C.crocodilus	C1AT11	3	212.83	0.24	14095.68	3	3335.05
C.crocodilus	C1AT11	4	257.97	0.14	3876.4	1	552.93
C.crocodilus	C1AT11	5	218.97	0.15	31967.97	7	4855.35
C.crocodilus	C1bO6bis	6	122.44	0.15	57171.21	7	8809.37
C.crocodilus	C1bO6bis	7	438.79	0.18	2278.97	1	411
C.crocodilus	C1bO6bis	8	86.62	0.09	11545.17	1	1030.95
C.crocodilus	C1bO6bis	9	59.88	0.22	66800.11	4	14664.87
C.crocodilus	C1bO6bis	10	1565.14	0.26	638.92	1	164.6
C.crocodilus	C1bO10	11	26.08	0.09	153363.39	4	13296.35
C.crocodilus	C1bO10	12	342.22	0.16	2922.08	1	470.38
C.crocodilus	C1bO10	13	38.41	0.03	26036.57	1	726.64
C.crocodilus	C1bO10	14	354.82	0.07	2818.35	1	198.35
C.crocodilus	C1bO10	15	232.87	0.12	30059.58	7	3458.5
C.crocodilus	C1BT7	16	145.68	0.15	48050.39	7	7013.84
C.crocodilus	C1BT7	17	109.95	0.09	9094.95	1	861.67
C.crocodilus	C1BT7	18	111.52	0.14	8967.31	1	1291.89
C.crocodilus	C1BT7	19	69.02	0.21	57957.48	4	12101.55
C.crocodilus	C1BT7	20	252.75	0.12	3956.48	1	467.92
C.crocodilus	C1BT9	21	47.39	0.07	105506.19	5	7481.51
C.crocodilus	C1BT9	22	45	0.09	66666.07	3	6067.16
C.crocodilus	C1BT9	23	208.85	0.07	28728.27	6	2150.6
C.crocodilus	C1BT9	24	308.44	0.06	3242.16	1	186.53
C.crocodilus	C1BT9	25	367.91	0.17	2718.06	1	465.7

C.crocodilus	C1BT11	26	113	0.07	8849.53	1	606.15
C.crocodilus	C1BT11	27	141.98	0.05	14086.81	2	746.11
C.crocodilus	C1BT11	28	227.36	0.09	30788.19	7	2680.86
C.crocodilus	C1BT11	29	130.36	0.13	38354.96	5	5129.11
C.crocodilus	C1BT11	30	24.85	0.04	201246.22	5	8708.1
A.mississippiensis	C4BBT9	31	222.48	0.2	8989.67	2	1762.16
A.mississippiensis	C4BBT9	32	177.64	0.07	11258.48	2	776.39
A.mississippiensis	C4BBT9	33	44.17	0.13	158485.07	7	20828.55
A.mississippiensis	C4BBT9	34	178.7	0.25	22384.03	4	5658.34
A.mississippiensis	C4BBT9	35	178.58	0.05	5599.69	1	272.88
A.mississippiensis	C4BT5	36	87.73	0.08	113980.61	10	9490.24
A.mississippiensis	C4BT5	37	49.79	0.12	160673.07	8	18906.52
A.mississippiensis	C4BT5	38	69.41	0.1	129667.59	9	13580.81
A.mississippiensis	C4BT5	39	116.32	0.14	51580.55	6	7424.72
A.mississippiensis	C4BT5	40	53.48	0.08	56099.14	3	4695.75
A.mississippiensis	C4BT15	41	46.15	0.21	130024.35	6	27538.67
A.mississippiensis	C4BT15	42	130.14	0.08	69156.65	9	5380.85
A.mississippiensis	C4BT15	43	145.79	0.17	61731.87	9	10592.91
A.mississippiensis	C4BT15	44	188.43	0.14	15920.93	3	2168.54
A.mississippiensis	C4BT15	45	312.26	0.09	3202.45	1	299.78
A.mississippiensis	C4BT17	46	86.11	0.09	197414.62	17	18502.77
A.mississippiensis	C4BT17	47	115.68	0.16	25934.15	3	4147.1
A.mississippiensis	C4BT17	48	152.51	0.2	19670.75	3	3845.47
A.mississippiensis	C4BT17	49	76.32	0.06	13102.65	1	736.38
A.mississippiensis	C4BT17	50	47.68	0.31	125851.76	6	39310.96
A.mississippiensis	C4BT23	51	80.6	0.19	136471.18	11	26300.7
A.mississippiensis	C4BT23	52	96.48	0.04	82921.28	8	3282.93
A.mississippiensis	C4BT23	53	29.9	0.12	33446.13	1	4013.03
A.mississippiensis	C4BT23	54	157.3	0.1	6357.13	1	622.09
A.mississippiensis	C4BT23	55	9.95	0.01	100540.34	1	1420.64
A.mississippiensis	C5BT14	56	152.45	0.25	150867.37	23	37659.83
A.mississippiensis	C5BT14	57	494.74	0.44	48510.19	24	21237.18
A.mississippiensis	C5BT14	58	106	0.13	141504.29	15	18852.8
A.mississippiensis	C5BT14	59	164.79	0.11	30342.54	5	3327.81
A.mississippiensis	C5BT15	60	30.81	0.08	194718.95	6	16000.65
A.mississippiensis	C5BT15	61	63.43	0.16	47298.03	3	7704.01
A.mississippiensis	C5BT15	62	145.51	0.18	116834.04	17	20831.24
A.mississippiensis	C5BT15	63	108.71	0.03	64388.93	7	2196.64
A.mississippiensis	C5BT15	64	495.57	0.07	10089.34	5	702.57
A.mississippiensis	C5BT28	65	208.58	0.12	67120.97	14	7998.08
A.mississippiensis	C5BT28	66	180.37	0.06	16632.15	3	972.96
A.mississippiensis	C5BT28	67	199.41	0.04	10029.47	2	419.83
A.mississippiensis	C5BT28	68	144.81	0.04	75962.81	11	3351.63
A.mississippiensis	C5BT28	69	134.47	0.09	111548.34	15	10405.38
C.niloticus	Cro3A2	70	84.14	0.1	95080.91	8	9470.46
C.niloticus	Cro3A2	71	51.19	0.02	58609.95	3	1445.89
C.niloticus	Cro3A2	72	36.21	0.04	331411.6	12	13794.83
C.niloticus	Cro3A2	73	69.16	0.09	57840.93	4	5474.32
C.niloticus	Cro3A2	74	268.73	0.15	7442.33	2	1084.17
C.niloticus	Cro3A3O	75	127.08	0.04	15737.7	2	562.78
C.niloticus	Cro3A3O	76	57.18	0.07	262333.99	15	17774.47
C.niloticus	Cro3A3O	77	56.27	0.02	35545.48	2	537.16
C.niloticus	Cro3A3O	78	95.28	0.11	430327.76	41	45743.81
C.niloticus	Cro3A3O	79	306.36	0.08	3264.09	1	259.46

C.niloticus	Cro3A4	80	28.6	0.06	244718.46	7	13620.62
C.niloticus	Cro3A4	81	67.88	0.15	14732.88	1	2189.28
C.niloticus	Cro3A4	82	105.84	0.05	28343.88	3	1453.03
C.niloticus	Cro3A4	83	480	0.09	2083.33	1	186.03
C.niloticus	Cro3A4	84	151.97	0.18	6580.17	1	1190.62
C.niloticus	Cro3A220	85	76.01	0.09	171026.48	13	14927.04
C.niloticus	Cro3A220	86	53.2	0.27	18798.02	1	4984.72
C.niloticus	Cro3A220	87	49.16	0.06	40683.21	2	2275.52
C.niloticus	Cro3A220	88	17.83	0.04	224314.88	4	8483.13
C.niloticus	Cro3A220	89	44.16	0.08	317036.74	14	24051.56
C.niloticus	Cro3A220	90	221.69	0.05	4510.88	1	219.79
C.niloticus	Cro3A221	91	70.76	0.07	127185.14	9	8586.87
C.niloticus	Cro3A221	92	45.64	0.05	65733.43	3	3374.48
C.niloticus	Cro3A221	93	41.1	0.04	267645.93	11	9589.48
C.niloticus	Cro3A221	94	41.55	0.02	192535.17	8	4803.86
C.niloticus	Cro3A221	95	73.42	0.05	13621.11	1	649.27
C.niloticus	Croco3b3	96	40.91	0.04	122224.82	5	4617.08
C.niloticus	Croco3b3	97	89.62	0.03	44634.02	4	1253.2
C.niloticus	Croco3b3	98	77.08	0.04	129731.21	10	5171.49
C.niloticus	Croco3b3	99	150.91	0.04	19879.48	3	732.31
C.niloticus	Croco3b3	100	29.36	0.04	102196.02	3	3693.81

CHAPITRE 3: INFLUENCE DE L'ORNEMENTATION OSSEUSE SUR LA RESISTANCE MECANIQUE DES OSTEODERMES DES PSEUDOSUCHIENS.

Crocodylus niloticus (La Ferme aux Crocodiles, Pierrelatte 2015)

The influence of bone ornamentation on the osteoderm mechanical resistance: A finite element analysis in Pseudosuchia.

Clarac F[1,2] Goussard F[2], Buffrénil Vde[2], Sansalone V[3]

[1]Sorbonne Universités UPMC Univ Paris 6, CNRS, Institut des Sciences de la Terre de Paris (ISTeP), 4 place Jussieu – BC 19 - 75005 Paris, France
[2]*Département Histoire de la Terre, Museum National d'Histoire Naturelle, UMR 7207 (CR2P), Sorbonne* Universités, MNHN/CNRS/UPMC, Bâtiment de Géologie Paris Cedex 05, F-75231, France
[3]Laboratoire de Modélisation et Simulation Multi Echelle Equipe Biomécanique Université Paris-Est Créteil Val de Marne Faculté des Sciences et Technologie 61 avenue du Général de Gaulle 94010 Créteil Cedex

Key words: 3D Modeling – Simulation **-** Von Mises stress – Dermal shield – Bone resorption - Crocodylians.

Abstract

In order to assess the influence of bone ornamentation on the pseudosuchian osteoderm mechanical resistance, we have performed three dimensional modeling and finite element analyses on a sample which includes both extant dry bones and well-preserved fossils tracing back to the Late Triassic (215 million years old). We simulated an external attack under variable angles on the apical surface of each osteoderm and further repeated the simulation on an equivalent set of smoothed 3D-modeled osteoderms. The comparative results evidenced that the presence of an apical sculpture has no significant influence on the Von Mises stress repartition in the osteoderm volume although it involves a slight increase in its numerical score. Moreover, performing parametric analyses, we evidenced that the Young's modulus in the osteoderm which may vary depending on the bone porosity, the collagen fiber orientation or the calcification density has no impact on the Von Mises stress repartition inside the osteoderm volume. As the crocodylian bone ornamentation is continuously remodeled by pit resorption and secondary bone deposit, we assume that the apical sculpture may be the outcome of a "trade-off" between the bone mechanical resistance and a recurrent mineral release which could be recycled in different physiological and biochemical pathways (adenosine triphosphate synthesis, muscle activity, egg shelling…). Moreover, as proved by previous studies, the crocodylian bone ornamentation also provides a superficially excavated three dimensional support for the extension of a bone vascular peripheral network which is possibly involved in physiological exchanges such as heat transfers during basking and acidosis buffering during apnea (lactate sequestration). On a general morphological aspect, the osteoderm geometrical variability within our sample lead us to assess that the global osteoderm geometry (whether square or rectangular) does not influence the Von Mises stress whereas the presence of a dorsal keel would rather reduce the stress along the vertical axis.

Introduction

Among the different bones which compose the vertebrate skeleton, the osteoderms (when present) are set up through an integumentary ossification of the dermis (Gilbert et al., 2001; Vickaryous and Hall, 2008; Vickaryous and Sire, 2009). As the osteoderms occupy an outer position along the post-cranial region, the functional role of these bony elements is often claimed to be involved in body protection (Sun and Chen, 2013; Chen et al., 2014). Even though this implication seems obvious when the osteoderms form a continuous shield as in the turtles (Acrai & Wagner, 2013; Chen et al., 2015), the xenarthres (Vickaryous et al., 2006; Chen et al., 2011; Wolf et al., 2012), the ankylosaurs (Scheyer and Sander, 2004), the aetosaurs (Cerda & Desojo, 2011), the squamates (Anguidae; Zylberberg & Castanet, 1985; Anjan et al., 2008; Bochaton et al., 2013), the "armored fishes" (Yang et al., 2013a&b) and the crocodylians (Trutnau and Sommerlad, 2006), it is however more controversial in some other taxa in which the osteoderms consist of a few antero-posterior raws: the chondrosteans (Burdak, 1986), the early pseudosuchians (Nesbitt, 2011; Irmis et al., 2013) and thyreophoran dinosaurs (Main et al., 2005). In this regard, as the osteoderms provide a vascular proliferation in the dermis (Clarac et al., 2017b), it has been assumed that these bones may also be involved in different physiological functions such as the acidosis buffering during apnea in semi-aquatic taxa (turtles and crocodylians; Jackson and Heisler, 1982; Jackson, 2000; Jackson et al., 1999, 2000a, 2000b, 2003, 2012) and heat exchanges in both large ectothermic vertebrates (crocodylians) and ornitischian dinosaurs (Seidel 1979, Farlow et al., 2010). Nonetheless, since the dermal bones (both the dermatocranium and the osteoderms) usually show a pronounced superficial ornamentation within most taxa which present a well-developed integumentary shield (mentioned above), it has been proposed that this feature may play a role in the dermal bone global mechanical strengthening (Coldiron, 1974). Therefore, as the crocodylian osteoderms show a well-developed ornamentation (made of resorbed pits and grooves; Buffrénil 1982, Buffrénil et al., 2015), they consist of a good model to test if the presence of bone ornamentation modifies the dermal bone strengthening. To this purpose, we first performed a finite element analysis to assess Von Mises stress on a set of 3D-modeled ornamented osteoderms. Further, we repeated this calculation on a second set composed of the smoothed equivalent osteoderms (modeled without ornamentation) in order to draw a comparison.

Material and Methods

Biological sampling

The sample includes six pseudosuchian osteoderms (Table 1). They consist of either dry bones from extant species (Osteolaemus tetraspis, Caiman crocodilus) or well-preserved fossils which trace back to the Triassic or later periods (Aetosaurus sp., Sarcosuchus imperator, Hyposaurus rogersii). The full set of osteoderms represents five different taxa showing a well-developed bone ornamentation and were all directly sampled in museum collection drawers: the MNHN (Muséum National d'Histoire Naturelle), the Smithsonian Institution National Museum of Natural History and the AMNH collections (American Museum of Natural History; Table 1).

Family	Gender	Species	Collection number	Author	Year	Period
Crocodylidae	Osteolaemus	tetraspis	MNHN-AC.1991.4488a	Cope	1861	extant
Crocodylidae	Osteolaemus	tetraspis	MNHN-AC.1991.4488b	Cope	1861	extant
Alligatoridae	Caiman	crocodilus	MNHN-1989-6489	Linnaeus	1758	extant
Pholidosauridae	Sarcosuchus	imperator	MNHN-1966-15 Gad-4	Broin & Taquet	1966	Cretaceous
Dyrosauridae	Hyposaurus	rogersii	AMNH-2389	Owen	1849	Cretaceous
Aetosauridae	Aetosaurus.	sp.	AMNH-19331	Fraas	1887	Triassic

Table 1: Sampled specimens with taxonomy references

Three-dimensional modeling

The four osteoderms from the MNHN were scanned with a Breuckmann StereoScan 3D- surface scanner, a device that reconstructs three-dimensional objects using phase contrast. The surface of the bones is virtually reconstructed as a mesh of adjacent polygons, folded according to bone reliefs inside a three-dimensional space. We used two scope ranges, depending on sample size, to obtain adequate mesh resolutions: small scope range (60 mm), resolution: 12µm; medium scope range (250 mm), resolution: 18µm. The four 3D-objects thus obtained were exported in PLY-format. Imperfections of the mesh (noise, artefacts, self-interactions, etc.), when present, were corrected using Geomagic Studio 2012 cleaning tools (Geomagic Worldwide Headquarters 430 Davis drive, Marisville, NC 27560 USA).

The two osteoderms from the AMNH paleontology collection were reconstructed in three dimensions thanks to a photogrammetric technic. Therefore, we used a portable camera for taking a series of photographs of each osteoderm under various, repeatable angles. To this purpose, we used a Canon 60D camera equipped with a Canon 60mm/2 macro objective, and Canon Speedlite 320EX flash). Camera sensitivity was set to 100 ISO, objective aperture set to 16, and exposure time set automatically by the camera in order to get clear shots. The aim was to let fix the camera in a position aimed at the object (target), which would rotate as if we used a Stereoscan 3D surface scanner. Each osteoderm was laid on one edge on a rotating pad which was centered on an unmovable 360° graduated plastic sheet. Each specimen was then shot every 10° while turning on itself along a 36 shot series. The distance between the camera and the object was set so that the osteoderm took the full size of the field for better definition. The 3D-model was generated automatically for each specimen after uploading the 36 pictures in jpeg format into (Agisoft Photoscan Professional Version: 1.1.4). This process involves four consecutive stages: aligning pictures, creating a dense cloud, meshworking and building a surface texture. Pictures partially blurred by short field depth, were manually deleted as all pictures were previously checked one by one before the automatic alignment.

As we aim to test the effect of ornamentation on the bone strengthening through the osteoderms, we duplicated each three-dimensional-reconstructed osteoderm in order to create a copy that lacks ornamentation. This comparative model was set up by suppressing all the pits before replacing them by a smooth bone surface that would exist in absence of ornamentation

as the pits are known to be excavated by bone resorption (de Buffrénil, 1982; de Buffrénil et al., 2015; using Geomagic studio 12). Moreover, in order to test the influence of ornamentation on bone strengthening in disregard of the size difference between the sampled specimens, we rescaled each one of them so that they share an equal size. To this purpose, we first measured the upper area of one sampled ornamented osteoderm (thanks to a dedicated tool in Geomagic studio 12: "compute selected area") that we chose to be the scale reference (Caiman crocodilus MNHN-1989-6489). We then calculated the square root of the ratio between this value and the upper area of each ornamented osteoderm (it is necessary to calculate a square root since the calculation of this scale factor is based on a measure of area (mm^2)). This calculated scale factor was next used to rescale each specimen (with respect to its centroid) by means of the function: "model change" (except of course for the osteoderm of reference which has a scale factor value equal to 1: Caiman crocodilus 1989-6489; Table 2). The result of this operation was the acquisition of a set of six osteoderms which all have kept their original shape but which have been rescaled in order to score the same value of ornamented area. The same calculated scale factor values were then used on the corresponding smoothed osteoderms. Finally, we remeshed every 3D-model so that the number of polygons composing each one of them turned out to be comprised between 20k and 30k (using Geomagic studio 12). This last step was required to reduce the computational time of the subsequent finite element analysis (FEA).

Species	**Shape**	**Scaled Dimensions (Ly/Lx/Lz) mm**	**Linear scale factor**	**Scaled volume (ornamented) mm^3**	**Scaled volume (smoothed) mm^3**	**ΔVolume mm^3**	**ΔMass mg**	**LV %**
Osteolaemus tetraspis	Keeled square	23.2/ 24.3/ 3.5	1.74	878	992	114	228	11.5
Osteolaemus tetraspis	Keeled square	26.2/ 24.8/ 3.6	1.83	939	1050	111	222	10.6
Caiman crocodilus	Keeled rectangular	27.8/ 18.2/ 4.6	1	800	855	55	110	6.5
Sarcosuchus imperator	Flat rectangular	14.4/ 32.7/ 2.1	0.13	602	643	41	82	6.4
Hyposaurus rogersii	Flat rectangular	17.5/ 26.0/ 3.0	0.5*	654	754	100	200	13.3
Aetosaurus. sp.	Spiked reactangular	13.2/ 40.2/ 4.4	0.2*	595	659	64	128	9.7

Table 2: Sampled osteoderms with morphometric data. The ΔMass is calculated assuming a bone density of $2g/cm^3$. Footnote: * The presented linear factor is an estimated value based on the osteoderm real size and not the value which we used for scaling after the 3D-model specimens which were reconstructed using photogrammetrics (Hyposaurus rogersii, Aetosaurus sp.). Indeed, in this case, the value we used for scaling calculation is not based on the real osteoderm size but on an arbitrary assigned data by Geomagic studio 12 when first opening the STL file because the photogrammetry acquisition does not include a scaling process unlike the surface scanner.

Finite element analysis

The 3D models of osteoderms were uploaded into Comsol software (COMSOL Multiphysics® v. 5.2. www.comsol.com. COMSOL AB, Stockholm, Sweden) to perform a finite element analysis (FEA) simulating an external attack from another predator. In particular, a comparative analysis was performed on ornamented and smoothed models of osteoderms looking at the distribution of the Von Mises stress. Moreover, a sensitivity analysis was also performed with respect to several modeling parameters.

The osteoderm was assumed to be made of a homogeneous, isotropic, linearly elastic material characterized by a Young's modulus Eo and a Poisson ratio νo. The value of Eo was arbitrarily set to 10 GPa which roughly corresponds to the Young's modulus of cortical bone. Indeed, this value can vary under different parameters such as the bone porosity and the collagen fiber orientation (Sun and Chen, 2013). As outlined by previous authors (Scheyer and Desojo, 2011; Cerda et al., 2013; Burns et al., 2013; Buffrénil et al., 2015), the crocodylomorph osteoderms show a variable porosity and are not only composed by compact bone but rather show a diploe structure (at least in the modern forms). Moreover, microcrack orientation can introduce some anisotropy in the elastic moduli of the osteoderm (Chen et al., 2014). Therefore, we performed a parametric analysis in Caiman crocodilus in order to estimate the effects of the variation of the Young's modulus of the osteoderm. No experimental measures exist for the value of the Poisson ratio of the osteoderms. Then, we set νo = 0.18 which is typical of compact bovine femoral bone (Pithioux, 2002).

The attack of a predator was modeled by applying a force F = 1000 N abeam the apical surface of each specimen (above the centroid). This value is an approximation of a Caiman crocodilus molariform bite force (Ftot; resumed after Erickson et al., 2012) which simulates an external attack in an intraspecific fight or in a predator ambush such as a jaguar claw (Panthera onca; Da Silveira et al., 2010; Azevedo et al., 2012). The orientation of the force was initially set in the vertical direction (z axis), then the force direction was tilted at an angle $\alpha = \pm 45°$ towards either the transversal axis x ($\lambda = 0°$) or the longitudinal axis y ($\lambda = 90°$) as an attack (whether a bite or a claw) may come under different orientations (see Fig. 1A). Thus, components of the force read: $Fx = F \sin(\alpha) \cos(\lambda)$, $Fy = F \sin(\alpha) \sin(\lambda)$, and $Fz = F \cos(\alpha)$.

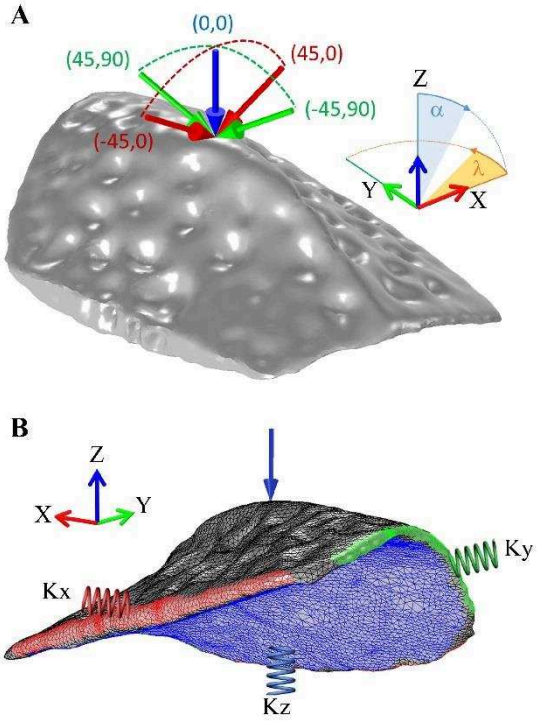

Figure 1: A: Geometry and forces applied on a typical osteoderm (Caiman crocodilus) to simulate a bite coming from different directions. The force direction is parameterized by the pair of angles (α, λ). Numerical values are expressed in degrees. B: Finite element mesh and boundary conditions on a typical osteoderm (Caiman crocodilus). Elastic springs are applied on the lateral (red and green) and basal (blue) sides of the osteoderm.

The FE mesh and the other boundary conditions (BCs) are shown in Fig. 1B. The geometry was meshed using the built-in tools of Comsol software, resulting in about 10e5 tetrahedral elements. Quadratic polynomial shape functions were used in each element to locally interpolate the displacement field. Besides the bite force, we applied BCs on the osteoderm simulating its actual configuration in vivo. Since each osteoderm is connected to its neighbors along its four lateral edges within the dorsal shield (Sun and Chen, 2013), we applied distributed springs on its lateral boundaries. Spring stiffness was

estimated as Kx = Eo / (Nx. Lx) for the springs acting along the transversal axis (x direction, red springs in Fig. 1B), where Nx is the numbers of neighboring osteoderms and Lx is the typical dimension of the osteoderm in the x direction. Kx has physical dimensions of [N/L².L] and represents the force per unit area needed to produce a unit displacement. Similarly, the stiffness of the springs acting along the longitudinal axis (y direction, green springs in Fig. 1B) was estimated as Ky = Eo /(Ny. Ly). The values of Lx and Ly of all the osteoderms can be found in Table 2. Nx and Ny are free parameters of the model. Numerical results of all the osteoderms were computed by setting Nx = Ny = 1. However, we performed a parametric study in Caiman crocodilus by considering up to 5 neighboring osteoderms in each direction. Since the dorsal shield is carried by the axial musculature (Gasc, 1981), we applied distributed elastic springs on the basal side of the osteoderm whose stiffness was estimated as Ky = Eb/ Lz, where Eb and Lz are the Young's modulus and thickness of the basal soft tissue, respectively. These two parameters are quite hard to identify. We arbitrarily set Eb =100 MPa (slightly smaller than the Young modulus of muscles measured in tensile conditions (McKee 2011) and Lz =1 cm (typical distance between the osteoderm and the underlying skeletal structure) in our simulations. As the value of Eb can span several orders of magnitude according to the loading conditions (Akhtar 2011, McKee 2011, Kot 2012), we performed a parametric study in Caiman crocodilus by letting Eb vary from 0.1 to 1000 MPa.

Quantitative assessment of the bone ornamentation

In this study, we aim at investigating the mechanical effects of the loss of bony mass due to the ornamentation of the osteoderms. On the one side, from a mechanical point of view, comparison between ornamented and smoothed osteoderms is made in both qualitative and quantitative terms with respect to the Von Mises stress. Qualitative comparison is made looking at the distribution of Von Mises stress in the osteoderm. Quantitative comparison is made by means of suitable stress-related indexes, namely: (i) the average Von Mises stress in the osteoderm:

$$\bar{\sigma}_{VM} = \frac{1}{\mathrm{Vo}} \int_{Vo} \sigma_{VM}\, dV$$

where σ_{VM} is the Von Mises stress and Vo the volume of the osteoderm; and (ii) the volume of the osteoderm where the Von Mises stress is higher than a fixed threshold σ_i:

$$V_i = \int_{Vo} 1_{\sigma_{VM} > \sigma_i}\, dV$$

where $1_{\sigma_{VM} > \sigma_i}$ is the corresponding characteristic function. Two thresholds were fixed in this study, namely σ_1=100 MPa (which roughly corresponds to the strength of compact bone) and $\sigma_2=\sigma_1/2$.

On the other side, from a morphological point of view, comparison between ornamented and smoothed osteoderms is made looking at the mass loss due to ornamentation which is excavated by pit resorption in the apical cortex of the osteoderms. This mass quantification is resumed by the loss of volume as the bone density in the peripheral cortex (compact bone) may be considered as constant (2g/cm3; after Blanton & Biggs, 1968). Herein, quantifying the loss

of volume due to ornamentation requires first to measure the volume within the ornamented osteoderm before repeating the operation on a smoothed copy. This process ends up in the acquisition of a variable that defines the loss of bone volume of the full osteoderm that is due to the excavation of the pits into the upper surface of the bone (in percentage; Clarac et al., 2017a):

$$LV = 100(\frac{SoV-RoV}{SoV})$$

SoV: "Smoothed osteoderm volume" and RoV: "Real osteoderm volume". Table 2 resumes all the relevant morphometric data of ornamented and smoothed osteoderms.

Results

Parametric analysis in Caiman crocodilus

Fig. 2A shows the Von Mises stress in the Caiman crocodilus osteoderm (on the left) and the high-stress regions where the Von Mises stress exceeds the stress thresholds σ_1 and σ_2 (on the right, in blue and in purple, respectively) as a function of the Young's modulus of the osteoderm (Eo). The same results are shown in Fig. 2B as a function of the Young's modulus of the basal tissue (Eb). Qualitatively, the stress distribution in the osteoderm is not affected noticeably by the value of Eo. By contrast, Eb does affect the stress distribution in the osteoderm, smaller values of Eb being associated to higher stress.

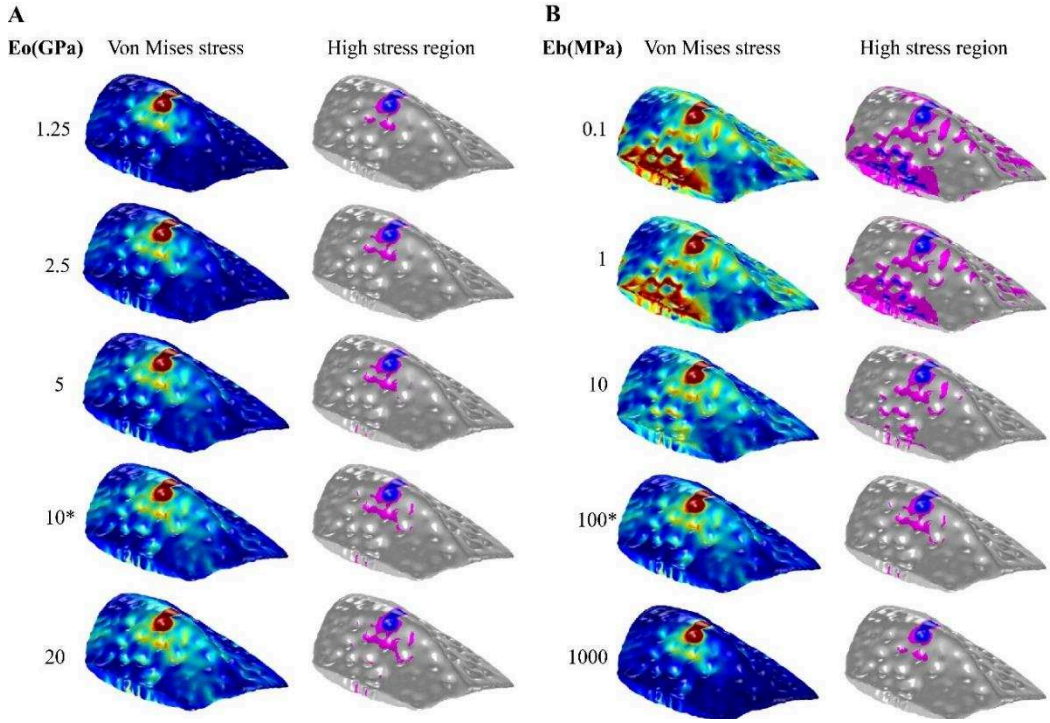

Figure 2: A: Parametric analysis with respect to the Young's modulus of the osteoderm (Eo). On the left: Von Mises stress; Color scale: 0 (blue) to 100 MPa (red). On the right: high-stress regions. Relevant reference parameters are: Eb = 0.1 GPa (Young's modulus of the basal tissue); N = 1 (Number of lateral osteoderms); λ= 0° & α= 0° (Force orientation). A star (*) denotes the reference value of Eo. B: Parametric analysis with respect to the Young's modulus of the basal tissue (Eb). On the left: Von Mises stress; Color scale: 0 (blue) to 100 MPa (red). On the right: high-stress regions. Relevant reference parameters are: Eo = 10 GPa (Young's modulus of the osteoderm); N = 1 (Number of lateral osteoderms); λ = 0° & α = 0° (Force orientation). A star (*) denotes the reference value of Eb.

The parametric analysis shows that both the average Von Mises stress ($\bar{\sigma}_{VM}$) and the high-stress volumes (V_1 and V_2) increase as the Young's modulus of the osteoderm increases (Eo, Fig. 3A&B). Conversely, both the average Von Mises stress and the high-stress volumes of the osteoderm decrease as the Young's modulus Eb of the basal tissue increases (Fig. 3C&D). Nevertheless, both Eb and Eo have very little effect on the volume V_1 where the Von Mises stress reaches very high values (orange lines in Fig. 3B&D).

The parametric analysis with respect to the number of lateral osteoderms (N = Nx = Ny) has shown that this parameter does not affect sensibly either the average Von Mises stress (which increases of about 2% as N increases from 1 to 5) or the high-stress volumes (V_1 is almost unaffected whereas V_2 increases from 5% to 6% of Vo as N increases from 1 to 5).

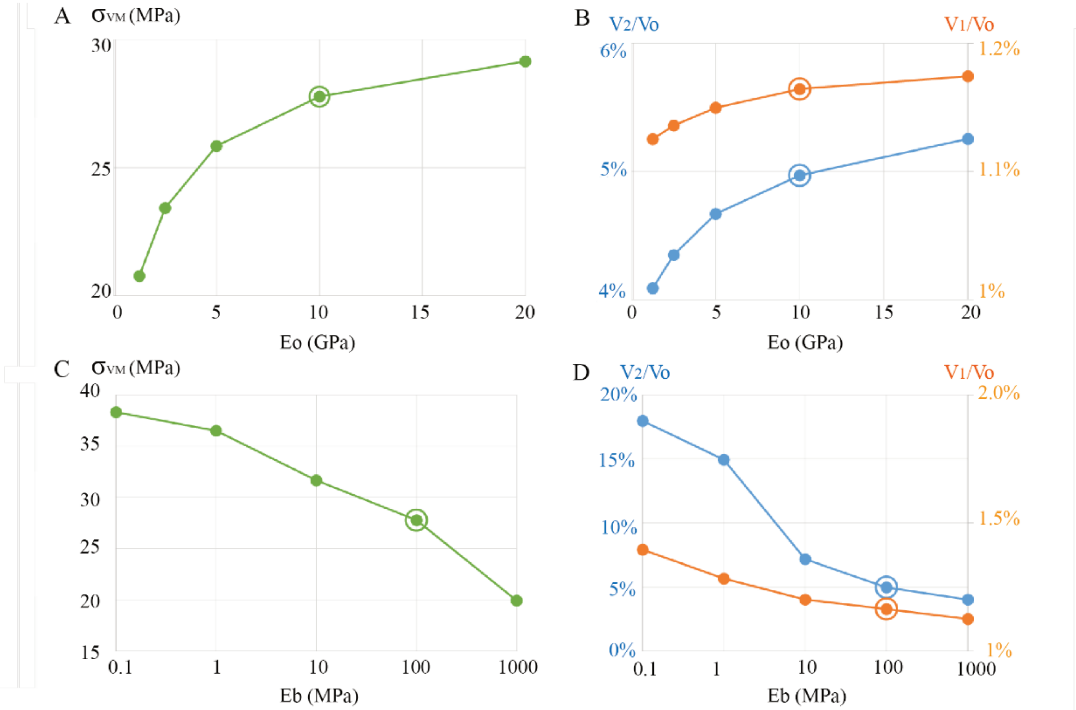

Figure 3: Parametric analysis in Caiman crocodilus with respect to the Young's modulus of the osteoderm (A, B) and of its basal tissue (C, D). A: Average Von Mises stress in the osteoderm as a function of the Young's modulus of the osteoderm (Eo). B: high-stress volume fractions as a function of the Young's modulus of the osteoderm (Eo). C: Average Von Mises stress in the osteoderm as a function of the Young's modulus of the basal tissue (Eb); D: high-stress volume fractions as a function of the Young's modulus of the basal tissue (Eb). Relevant reference parameters are: Eo = 10 GPa (Young's modulus of the osteoderm); Eb = 0.1 GPa (Young's modulus of the basal tissue); N = 1 (Number of lateral osteoderms); $\lambda = 0°$ & $\alpha = 0°$ (Force orientation).

The influence of the osteoderm global morphology on the mechanical resistance

We performed a principal component analysis (PCA, Fig. 4) using the $\bar{\sigma}_{VM}$, V1 and V2 scores on the full set of the ornamented osteoderms (Table 3). The main component (PC1) explains 91.7% of the variance and is closely correlated with $\bar{\sigma}_{VM}$ (when α and λ are nil). The keeled osteoderms score negative PC1 values whereas both the spiked and flat osteoderms show rather nil or positive values. Nevertheless, we do not observe any clear pattern distinguishing the square with the rectangular osteoderms either along PC1 or PC2 (explaining 5.4% of the variance).

Aetosaurus sp.		Ornamented			Smoothed		
λ	α	$\bar{\sigma}_{VM}$ (MPa)	V_1 (mm^3)	V_2 (mm^3)	$\bar{\sigma}_{VM}$ (MPa)	V_1 (mm^3)	V_2 (mm^3)
0	-45	47.00	177	48.2	40.06	164.95	35.85
0	0	52.51	205	72.7	45.53	199.45	59.25
0	45	46.11	167	46.9	40.54	158.40	40.21
90	-45	44.11	172	47	38.64	165.83	41.34
90	0	52.51	205	72.7	45.53	199.45	59.25
90	45	41.72	150	46.2	36.02	135.33	39.80
Caiman crocodilus		Ornamented			Smoothed		
λ	α	$\bar{\sigma}_{VM}$ (MPa)	V_1 (mm^3)	V_2 (mm^3)	$\bar{\sigma}_{VM}$ (MPa)	V_1 (mm^3)	V_2 (mm^3)
0	-45	32.89	109.98	21.73	29.48	85.05	15.83
0	0	27.77	39.75	9.31	25.18	34.09	8.29
0	45	30.24	101.10	18.25	27.12	81.73	16.03
90	-45	25.96	55.50	11.48	23.05	55.59	10.23
90	0	27.77	39.75	9.31	25.18	34.09	8.29
90	45	27.31	57.07	11.57	25.61	46.68	10.43
Hyposaurus rogersii		Ornamented			Smoothed		
λ	α	$\bar{\sigma}_{VM}$ (MPa)	V_1 (mm^3)	V_2 (mm^3)	$\bar{\sigma}_{VM}$ (MPa)	V_1 (mm^3)	V_2 (mm^3)
0	-45	32.32	99.49	20.04	25.81	71.35	11.65
0	0	37.10	131.53	35.82	29.37	112.02	20.96
0	45	31.95	93.89	22.10	26.04	72.70	12.28
90	-45	34.00	107.05	23.60	27.98	90.93	13.31
90	0	37.10	131.53	35.82	29.37	112.02	20.96
90	45	32.32	92.84	20.03	26.24	71.28	11.15
Osteolaemus tetraspis		Ornamented			Smoothed		
λ	α	$\bar{\sigma}_{VM}$ (MPa)	V_1 (mm^3)	V_2 (mm^3)	$\bar{\sigma}_{VM}$ (MPa)	V_1 (mm^3)	V_2 (mm^3)
0	-45	24.44	75.19	13.69	21.22	52.23	10.01
0	0	30.02	122.73	22.64	24.69	76.34	10.29
0	45	29.65	117.19	28.52	22.69	56.77	10.90
90	-45	27.14	87.16	14.51	22.38	52.76	9.83
90	0	30.02	122.73	22.64	24.69	76.34	10.29
90	45	26.87	84.21	16.89	21.82	47.60	10.44
Osteolaemus tetraspis		Ornamented			Smoothed		
λ	α	$\bar{\sigma}_{VM}$ (MPa)	V_1 (mm^3)	V_2 (mm^3)	$\bar{\sigma}_{VM}$ (MPa)	V_1 (mm^3)	V_2 (mm^3)
0	-45	26.13	91.41	18.10	23.00	70.24	12.57
0	0	28.01	99.49	14.64	25.50	85.21	10.79
0	45	26.11	82.60	17.74	23.27	68.33	11.98
90	-45	26.06	72.24	17.55	22.92	62.13	11.54
90	0	28.01	99.49	14.64	25.50	85.21	10.79
90	45	24.18	60.71	12.49	21.87	49.90	10.53

Sarcosuchus imperator		Ornamented			Smoothed		
λ	α	$\bar{\sigma}_{VM}$ (MPa)	V_1 (mm^3)	V_2 (mm^3)	$\bar{\sigma}_{VM}$ (MPa)	V_1 (mm^3)	V_2 (mm^3)
0	-45	46.07	153.91	41.60	42.30	149.83	38.73
0	0	43.40	151.84	53.20	39.50	147.56	50.31
0	45	39.32	158.86	33.23	35.22	139.97	30.64
90	-45	36.40	121.44	36.99	32.89	113.25	32.36
90	0	43.40	151.84	53.20	39.50	147.56	50.31
90	45	39.02	131.62	38.66	36.06	129.84	35.39

Table 3: Quantification of the Von Mises stress in the sampled specimens. $\bar{\sigma}_{VM}$: Average Von Mises stress in the osteoderm. V_1 and V_2: Volumes of regions where the Von Mises stress exceeds the stress thresholds σ_1 and σ_2, respectively. See text for more details.

The influence of bone ornamentation on the osteoderm mechanical resistance

The pattern of the Von Mises stress is globally similar in each osteoderm whether in presence or in absence of ornamentation (Fig. 5, 6). We notice that both the average Von Mises stress ($\bar{\sigma}_{VM}$) and the high-stress volumes (V_1 & V_2) are slightly higher in presence of ornamentation (Fig. 5, 6). The differences of these three mechanical indexes between smoothed and ornamented ornaments are presented in Table 3 with the corresponding differences in Table 4. The orientation of the attack (-45°, 0°, 45°) modifies the stress pattern but to a little extent the values of the average Von Mises stress (Table 3&4 and Fig. 7).

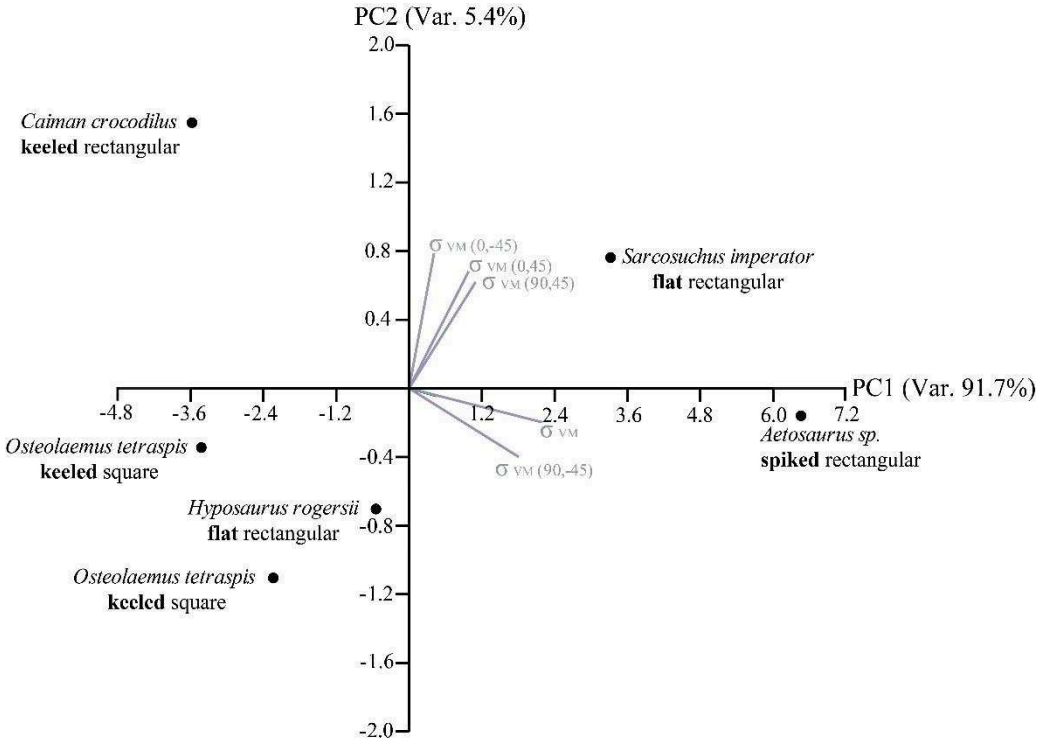

Figure 4: Principal component analysis of the sampled osteoderm stress variables: $\bar{\sigma}_{VM}$, V_1, V2 with variation of α (0, 45, -45) and λ (0, 90, -90). Performed on PAST version 2.17c, Hammer et al., 2001.

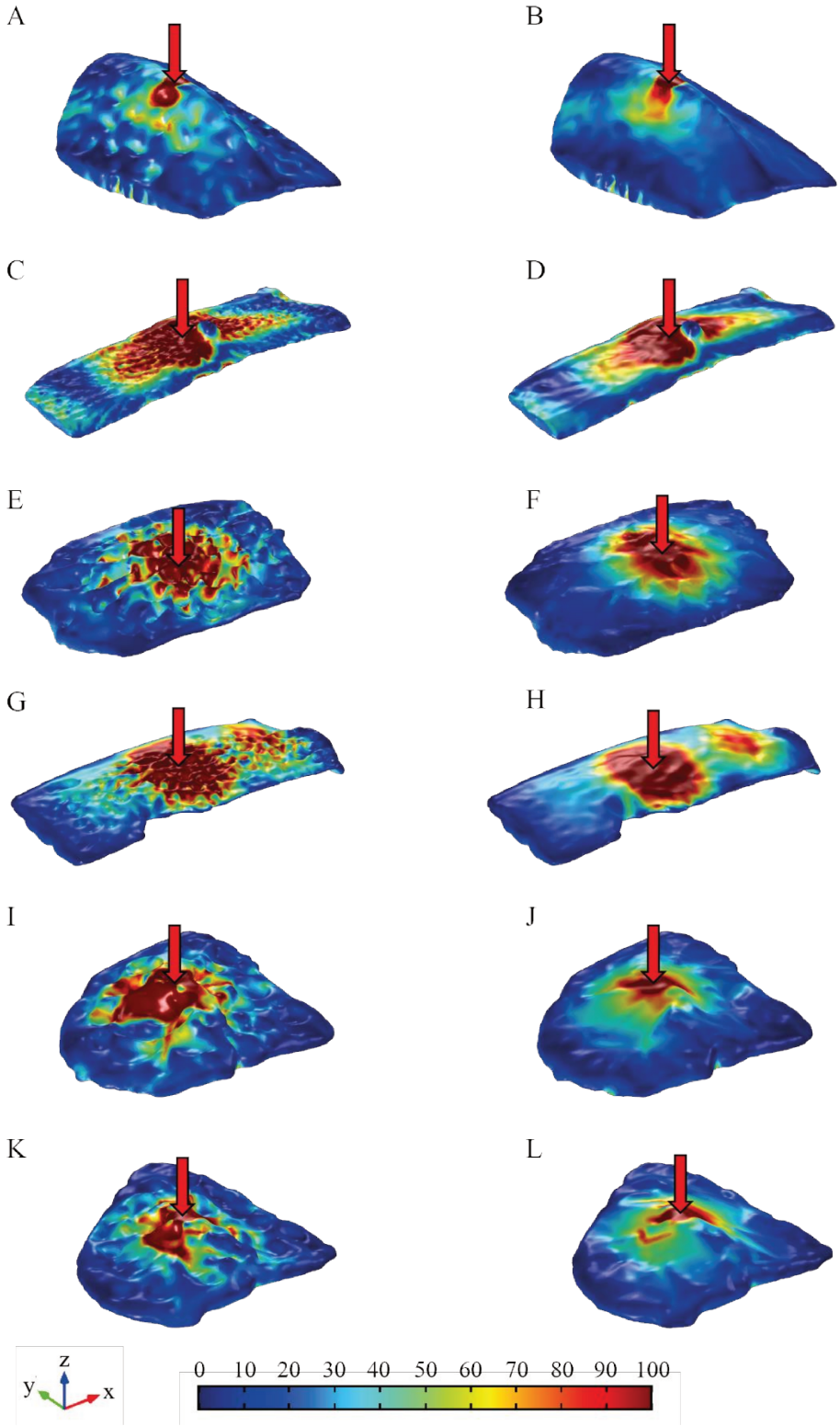

Figure 5: Von Mises stress in the 3D-modeled osteoderms (in MPa). A: Ornamented osteoderm of Caiman crocodilus. B: Smoothed osteoderm of Caiman crocodilus. C: Ornamented osteoderm of Aetosaurus sp. D: Smoothed osteoderm of Aetosaurus sp. E: Ornamented osteoderm of Hyposaurus rogersii. F: Smoothed osteoderm of Hyposaurus rogersii. G: Ornamented osteoderm of Sarcosuchus imperator. H: Smoothed osteoderm of Sarcosuchus imperator. I: Ornamented osteoderm of Osteolaemus tetraspis (AC.1991.4488a). J: Smoothed osteoderm of Osteolaemus tetraspis (MNHN-AC.1991.4488a). K: Ornamented osteoderm of Osteolaemus tetraspis (MNHN-AC.1991.4488b). L: Smoothed osteoderm of Osteolaemus tetraspis (AC.1991.4488b). X: the transversal axis; Y: the longitudinal axis. Z: the vertical axis. All plots refer to $(\lambda,\alpha) = (0°,0°)$.

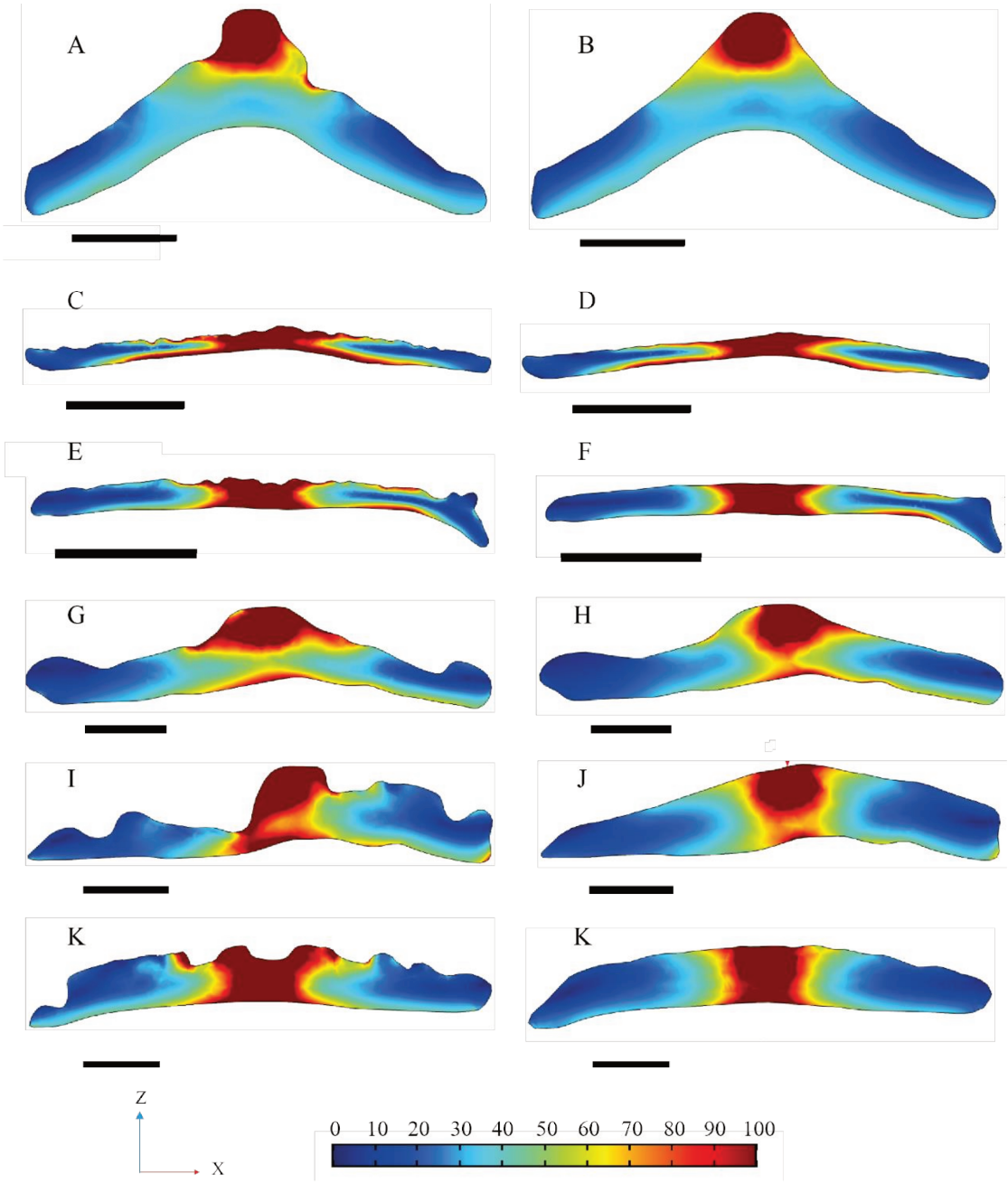

Figure 6: Von Mises stress in the 3D-modeled osteoderms in transversal cross section (in MPa). A: Ornamented osteoderm of Caiman crocodilus; Scale bar: 4 mm. B: Smoothed osteoderm of Caiman crocodilus; Scale bar: 4 mm. C: Ornamented osteoderm of Aetosaurus sp.; Scale bar: 10 mm. D: Smoothed osteoderm of Aetosaurus sp. Scale bar: 10 mm. E: Ornamented osteoderm of Sarcosuchus imperator; Scale bar: 10 mm. F: Smoothed osteoderm of Sarcosuchus imperator; Scale bar: 10 mm. G: Ornamented osteoderm of Osteolaemus tetraspis (MNHN-AC.1991.4488a); Scale bar: 4 mm. H: Smoothed osteoderm of Osteolaemus tetraspis (MNHN-AC.1991.4488b). Scale bar: 4 mm. I: Ornamented osteoderm of Hyposaurus rogersii; Scale bar: 4 mm. J: Smoothed osteoderm of Hyposaurus rogersii; Scale bar: 4 mm. All plots refer to (λ,α) = (0°,0°).

Aetosaurus sp.				
λ	α	$\Delta\bar{\sigma}_{VM}$ (MPa)	ΔV_1 (mm^3)	ΔV_2 (mm^3)
0	-45	-6.94	-12.05	-12.35
0	0	-6.98	-5.55	-13.45
0	45	-5.57	-8.60	-6.69
90	-45	-5.47	-6.17	-5.66
90	0	-6.98	-5.55	-13.45
90	45	-5.70	-14.67	-6.40
Caiman crocodilus				
λ	α	$\Delta\bar{\sigma}_{VM}$ (MPa)	ΔV_1 (mm^3)	ΔV_2 (mm^3)
0	-45	-3.41	-24.94	-5.89
0	0	-2.59	-5.67	-1.02
0	45	-3.12	-19.37	-2.21
90	-45	-2.92	0.09	-1.25
90	0	-2.59	-5.67	-1.02
90	45	-1.70	-10.39	-1.14
Hyposaurus rogersii				
λ	α	$\Delta\bar{\sigma}_{VM}$ (MPa)	ΔV_1 (mm^3)	ΔV_2 (mm^3)
0	-45	-6.51	-28.14	-8.39
0	0	-7.72	-19.51	-14.86
0	45	-5.91	-21.19	-9.83
90	-45	-6.02	-16.12	-10.29
90	0	-7.72	-19.51	-14.86
90	45	-6.09	-21.56	-8.88

Osteolaemus tetraspis (MNHN-AC.1991.4488a)				
λ	α	$\Delta\bar{\sigma}_{VM}$ (MPa)	ΔV_1 (mm^3)	ΔV_2 (mm^3)
0	-45	-3.22	-22.96	-3.68
0	0	-5.33	-46.39	-12.36
0	45	-6.97	-60.42	-17.63
90	-45	-4.75	-34.40	-4.68
90	0	-5.33	-46.39	-12.36
90	45	-5.06	-36.60	-6.45
Osteolaemus tetraspis (MNHN-AC.1991.4488b)				
λ	α	$\Delta\bar{\sigma}_{VM}$ (MPa)	ΔV_1 (mm^3)	ΔV_2 (mm^3)
0	-45	-3.14	-21.17	-5.54
0	0	-2.51	-14.28	-3.84
0	45	-2.84	-14.27	-5.76
90	-45	-3.14	-10.12	-6.01
90	0	-2.51	-14.28	-3.84
90	45	-2.31	-10.81	-1.96
Sarcosuchus imperator				
λ	α	$\Delta\bar{\sigma}_{VM}$ (MPa)	ΔV_1 (mm^3)	ΔV_2 (mm^3)
0	-45	-3.77	-4.08	-2.87
0	0	-3.89	-4.28	-2.89
0	45	-4.10	-18.89	-2.59
90	-45	-3.50	-8.19	-4.64
90	0	-3.89	-4.28	-2.89
90	45	-2.96	-1.77	-3.27

Table 4: Comparative values between the smoothed form of the sampled osteoderms and their original ornamented form; the combination between λ & α represensts the angle of attack inside the 3D environment; X is the transversal axis, Y is the longitudinal axis.

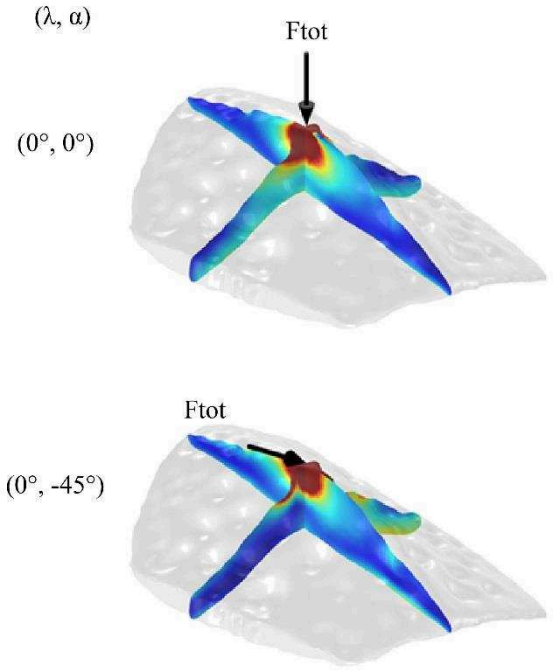

In general, the average Von Mises stress as well as the high-stress volumes are higher when the force is applied vertically (λ = 0° & α = 0°) in both ornamented and smoothed osteoderms. However, the opposite trend is observed in a few cases (e.g., in Caiman crocodilus). The loss of volume due to ornamentation is comprised between 5 and 15% which corresponds to a weight loss which scales between 82 and 228 mg per osteoderm (Table 2) assuming a density of $2g/cm^3$ (compact bone; After Blanton & Biggs, 1968). This weight loss directly depends on the degree of ornamentation and is relative to an osteoderm whose size is equivalent to the Caiman crocodilus

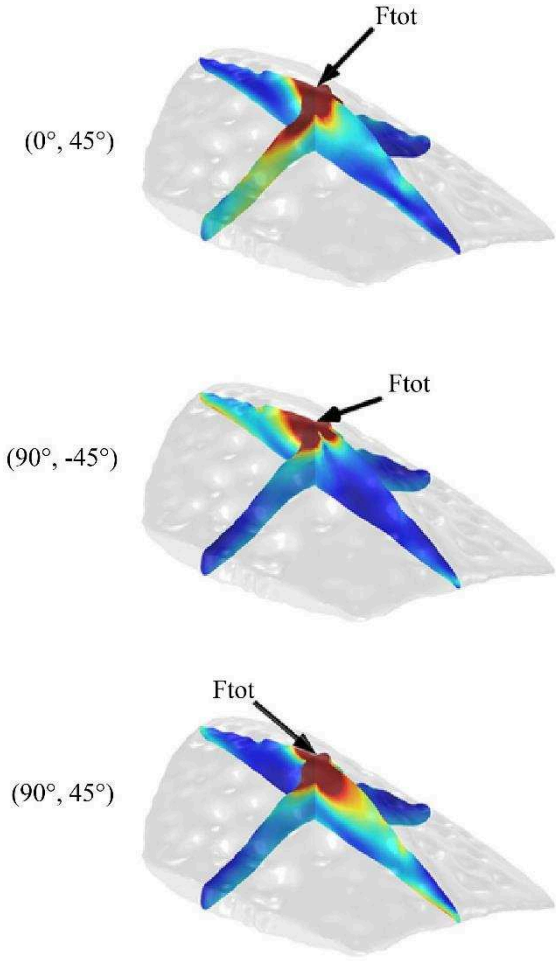

specimen (scale reference; 27.8 mm(Y)/ 18.2 mm (X)/ 4.6 mm (Z); Alligatoridae; Table 2). As an Alligator mississippiensis adult specimen (Alligatoridae) carries about seventy osteoderms on its dorsal shield (after Sun and Chen, 2013), the corresponding estimated total weight loss due to bone ornamentation should be comprised between 6g and 16g for any crocodylian presenting a similar dorsal shield and a global size equal to the *Caiman crocodilus'* (between 2 and 2.5m; after Groombridge, 1987)

Figure 7: Von Mises stress in Caiman crocodilus osteoderm presented in both longitudinal and transversal cross sections for different loading conditions parameterized by the pair of angles (λ,α).

Discussion

Limits of the model

Crocodylian osteoderms are complex mechanical structures; firstly, their degree of mineralization is heterogeneous and is noticeably higher in the central keel (when present; Sun and Chen, 2013). Moreover, ornamented osteoderms may be composed of different types of bone with both a variable porosity and different collagen fiber orientations (i.e. woven bone, parallel-fibered and lamellar; Burns et al., 2013). In this regard, it has been assessed that the Young's modulus vary within the osteoderm volume and furthermore that osteoderms may not be considered as isotropic (Sun and Chen, 2013). Nevertheless, our parametric analysis has proved that the variation of the Young's Modulus in the osteoderm volume has no significant influence on the volume of the osteoderm in which the Von Mises stress may be critical with respect to its mechanical resistance (Fig. 2A; Fig. 3B). Consequently, we can assume that the comparative assessment which we propose between the ornamented osteoderms and their hypothetical smoothed equivalent form is suitable in order to assess the influence of bone ornamentation on the osteoderm mechanical resistance in disregard of the osteoderm internal variation (woven or parallel-fibered, porosity…).

Since the smoothed osteoderms are modeled by considering a quasi-convex fictive envelope joining the top of the ridges (SoV > RoV), this proposed model is not suitable to assess the influence of bone ornamentation when this latter is not set-up by resorption but by a differential

apposition such as in temnospondyls, lepospondyls and placoderms (Witzmann, 2009; Buffrénil et al., 2016). In this case, smoothed 3D models could be built by creating a smooth apical bone surface which would average the position of the mesh between the bottom of the pits and the top of the crests if we consider that the differential apposition consists of consecutive local growth variations resulting in a field of pits and crests.

The influence of the osteoderm global morphology on the Von Mises stress

The performed PCA (Fig. 4) reveals that the keeled osteoderms score lower Von Mises stress than both the flat and spiked osteoderms whether sharing a square or a rectangular global shape. These results rather confirm that the presence of a central keel improves the osteoderm strengthening (Sun and Chen, 2013). In this regard, on the contrary of all other sampled osteoderms, the specimen which shows the more pronounced central keel (Caiman crocodilus, Fig. 6) does not score a higher Von Mises stress when the attack is vertical ($\alpha \neq 0°$; Table 3). Eventually, as evidenced by the parametric analyses, the number of neighboring osteoderms has a negligible influence on the Von Mises stress in the impacted osteoderm, therefore we assume that the relative location of each osteoderm on the body should not have a significant influence on its mechanical resistance.

The function(s) of the osteoderm ornamentation in the pseudosuchians

According to previous studies (Sun and Chen, 2013; Chen et al., 2014), the presence of inter trabecular spaces excavated by osteoclast resorption in the core of the osteoderms tends to enhance the bending stiffness and energy absorption ability with reduced weight. Concerning the superficial resorption which excavates the ornamentation pits in the crocodylian osteoderm external surface, our results argue that this osteoclast activity tends to slightly increase the local stress values when enduring an external attack but without serious consequence on the global stress pattern (Table 4). Consequently, we can now assess that the presence of ornamentation on the crocodylian osteoderms does not strongly modify their mechanical resistance (contra Coldiron, 1974) but could rather optimize a "trade-off" between the bone resistance and the mineral component release by superficial bone resorption. The direct physical consequence of this mass release either on buoyancy or on any swimming and locomotion performance is of course negligible as the estimated resulting weight loss is about no more than tens of grams for a whole organism which weights tens of kilograms (Caiman crocodilus; Staton & Dixon, 1975). Notwithstanding, this mineral release (with a high proportion of calcium and phosphor) may be used in many different physiological pathways such as muscle activity (Ca^{2+}), egg shelling (Ca^{2+}; Dacke et al., 2015), ATP synthesis (PO_4^{2-}; Mg^{2+}). Indeed, the pit resorption followed by secondary bone deposit on the pit bottoms is a recurrent process along the crocodylian lifetime (Buffrénil, 1982, Buffrénil et al., 2015) and may therefore be involved in the phosphor-calcic homeostasis like any type of bone remodeling. Even if some early pseudosuchian like aetosaurs probably experienced the predation of giant terrestrial predators such as rauisuchians during the Triassic (Nesbitt et al., 2013), it is questionable that the main function of ornamented osteoderm in extant large crocodylians is still about body protection. Indeed, even if the small species such as Caiman crocodilus still endure predation once adult (Panthera onca; Da Silveira et al., 2010; Azevedo et al., 2012), all the larger species are apex predators once reaching the adult size (Trutnau and Sommerlad, 2006). Therefore, we may assume that the maintain of the

ornamented dermal shield in the evolution of the crocodylians may be firstly due to its implications in physiological functions based on the osteoderm relative degree of vascularization rather than to biomechanical considerations: 1) buffering lactate acidosis during apnea (Jackson et al., 2003); 2) heat transfers between the organism and the environment during basking (Seidel, 1979, Farlow et al., 2010). In this regard, the superficial excavation of the bone ornamentation would thus extend the superficial area for the vessel proliferation with no significant consequence on the osteoderm mechanical resistance.

The function(s) of bone ornamentation in extinct lineages

Although the osteoclast resorption is involved in the set-up of bone ornamentation in crocodylomorphs, this cellular activity seems to be absent in the genesis of bone ornamentation in some extinct lineages such as temnospondyls, lepospondyls and placoderms (Buffrénil et al., 2016). In these taxa, the differential apposition in the superficial cortex may be the only histological process leading to the formation of a superficial network made of pits and grooves separated by ridges. This set-up of bone ornamentation should have a different incidence on the dermal bone mechanical behavior than when involving bone resorption because it does not imply a retraction of mineralized tissue. Moreover, any of the mentioned above physiological implications of bone ornamentation relying on the recycle of mineral elements (homeostasis) is beyond consideration in this case. Notwithstanding, despite the differences in the bone ornamentation genesis within the evolution of vertebrates, both the crocodylian and the early vertebrate ornamented dermal bones seem to share a convergent characteristics: supporting a vascular proliferation within the pits (Witzmann et al., 2010). These blood vessels are probably involved in key physiological aspects such as heat transfers (Seidel, 1979) and acidosis buffering in prolonged apnea in semi-aquatic taxa as mentioned above (Jackson et al., 1999; Jackson, 2000; Jackson et al., 2000a&b; Jackson et al., 2003; Janis et al., 2012). In this regard, the general protective role of bone ornamentation may be rather to shelter the blood vessels within the superficial pits and grooves than to modify the dermal bone mechanical resistance. Although these physiological hypotheses relying on the set-up of a dermal bone superficial vessel proliferation are plausible for either amphibious or terrestrial vertebrates they are nevertheless not suitable for fully aquatic forms (i.e. placoderms, Early Paleozoic "stem-fishes"; Smith & Hall, 1990; Smith et al., 1995) in which both the physiological and mechanical possible role(s) of bone ornamentation are therefore to be entirely explored.

Acknowledgments

We would like to thank the paleontology and comparative anatomy collection managers for giving us access to the specimens: Salvador Bailon, Ronan Allain, Noureddine Jalil (MNHN), Carl Mehling and Mark Norell (AMNH). We also send our respectful regards to the UMS 2700 (MNHN/CNRS) for the access to the 3D scanner. We finally address our acknowledgments regards to Allowen Evin (CNRS; Institut des Sciences de l'Evolution; Montpellier) for her advice concerning morphometrics.

References

Acrai, B. Wagner, HD., 2013. Micro-structure and mechanical properties of the turtle carapace as a biological composite shield. Acta Biomaterialia 9, 5890–5902.

Akhtar, R. Sherratt, MJ. Kennedy Cruickshank, J. Derby B., 2011. Characterizing the elastic properties of tissues. Materialstoday 14(3), 96-105.

Anjan, B. Bhullar, S., 2008. Osteoderms of the California legless lizard Anniella (Squamata: Anguidae) and their relevance for considerations of miniaturization. Copeia 4, 785-793.

Azevedo, FCC. Verdade, LM., 2011. Predator–prey interactions: jaguar predation on caiman in a floodplain forest. Journal of Zoology 286, 200–207.

Blanton, PL. Biggs, NL., 1968. Density of fresh and embalmed human compact and cancellous bone. American Journal of Physiological Anthropology 29, 39-44.

Bochaton, C. Buffrenil, Vde. Lemoine, M. Bailon, S. Ineich Y., 2013. Body location and tail regeneration effects on osteoderms morphology—are they useful tools for systematic, paleontology, and skeletochronology in diploglossine lizards (Squamata, Anguidae)? Journal of Morphology 276, 1333-1344.

Buffrénil, Vde., 1982. Morphogenesis of bone ornamentation in extant and extinct crocodilians. Zoomorphology 99, 155–166.

Buffrénil, Vde. Clarac, F. Fau, M. Martin, S. Martin, B. Pellé, E. Laurin, M., 2015. Differentiation and growth of bone ornamentation in vertebrates: A comparative histological study among the Crocodylomorpha. Journal of Morphology 21, 1–21.

Buffrénil, Vde. Clarac, F. Canoville, A. Laurin, M., 2016. Comparative data on the differentiation and growth of bone ornamentation in gnathostomes (Chordata: Vertebrata). Journal of Morphology 277, 634–670.

Burdak, VD., 1986. Fonction de protection et fonction de dissimulation du squelette externe. In : Meunier, FJ., Sire, JY. (Eds.), Morphologie fonctionnelle du tégument écailleux des poissons. Société Française d'Ichtyologie, Paris, 10(3), 31-88.

Burns, ME. Vickaryous, MK. Currie, PJ., 2013. Histological variability in fossil and recent alligatoroid osteoderms: systematic and functional implications. Journal of Morphology 274, 676-686.

Cerda, IA. Desojo, JB., 2011. Dermal armour histology of aetosaurs (Archosauria: Pseudosuchia), from the Upper Triassic of Argentina and Brazil. Lethaia 44, 417–428.

Cerda, IA. Desojo, JB. Scheyer, TM. Schultz, CL., 2013. Osteoderm microstructure of ``rauisuchian'' archosaurs from South America. Geobios. 46, 273–283.

Chen, IH. Kiang, JH. Correa, V. Lopeza, MI. Chen, PY. McKittrick, J. Meyers, MA., 2011. Armadillo armor: Mechanical testing and micro-structural evaluation. Journal of the mechanical behavior of biomedical materials 4(5), 713-722.

Chen, IH. Yang, W. Meyers, MA., 2014. Alligator osteoderms: Mechanical behavior and hierarchical structure. Material Science Engineering C 35, 441-448.

Chen, IH. Yang, W. Meyers, MA., 2015. Leatherback sea turtle shell: A tough and flexible biological design. Acta Biomaterialia 28, 2-12.

Clarac, F. Goussard, F. Teresi, L. Buffrénil, Vde. Sansalone, V., 2017. Do the ornamented osteoderms influence the heat conduction through the skin? A finite element analysis in Crocodylomorpha. Journal of Thermal Biology 69, 39–53.

Clarac, F. Buffrénil, Vde. Cubo, J. Quilhac A., 2017. Vascularization in ornamented osteoderms: Physiological implications in ectothermy and amphibious lifestyle in the crocodylomorphs? The Anatomical Record. Revised version submitted (20/07/2017).

Coldiron, RW., 1974. Possible functions of ornament in the labyrinthodont amphibians. Occasional Papers of the of Museum National History of Kansas 33, 1-19.

Da Silveira, R. Ramalho, EE. Thorbjarnarson, JB. Magnusson WE., 2010. Depredation by jaguars on caimans and importance of reptiles in the diet of jaguar. Journal of Herpetology 44(3), 418-424.

Dacke, CG. Elsey, RM. Trosclair, PL. Sugiyama, T. Nevarez, JG. Schweitzer MH., 2015 Alligator osteoderms as a source of labile calcium for eggshell formation. Journal of Zoology 297(4), 255-264

Downs, JP. Donoghue, PCJ., 2009. Skeletal histology of Bothriolepis canadensis (Placodermi, Antiarchi) and evolution of the skeleton at the origin of jawed vertebrates. Journal of Morphology 270, 1364–1380.

Erickson, GM. Gignac, PM. Steppan, SJ. Lappin, AK. Vliet, KA. Brueggen, JD. Inouye, BD. Kledzik, D. Webb, GJW., 2012. Insights into the ecology and evolutionary success of crocodilians revealed through bite-force and tooth-pressure experimentation. PLoS ONE 7(3), e31781. doi:10.1371/journal.pone.0031781.

Farlow, JO. Hayashi, S. Tattersall, GJ., 2010. Internal vascularity of the dermal plates of Stegosaurus (Ornithischia, Thyreophora). Swiss Journal of Geosciences 103, 173–185.

Gasc, JP., 1981. Axial musculature B. Crocodilia. In: Gans, C., Parsons, TS. (Eds.), Biology of the Reptilia Volume 11. Academic press Inc, London, pp. 372-376.

Gilbert, SF. Loredo, GA. Brukman, A., Burke, AC., 2001. Morphogenesis of the turtle shell : the development of a novel structure in tetrapod evolution. Evolution and Development 3, 47–58.

Groombridge, B.,1987. The distribution and status of world crocodilians. In: Webb, GJW., Manolis, SC., Xhitehead, PJ., (Eds.), Wildlife management – Crocodiles and alligators. Surrey Beatty and Sons, Chipping Norton, NSW, Australia, pp. 9-21.

Hammer, Ø. Harper, DAT. Ryan, PD., 2001. PAST: Paleontological statistics software package for education and data analysis. Palaeontologia Electronica 4(1): 9pp. http://palaeo-electronica.org/2001_1/past/issue1_01.htm.

Irmis, RB. Nesbitt, SJ. Sues, HD., 2013. Early Crocodylomorpha. Geological Society of London Special Publications 379, 275–302.

Jackson, DC. Heisler, N., 1982. Plasma ion balance in submerged anoxic turtles at 3°c: the role of calcium lactate formation. Respiration Physiology 49, 159-174.

Jackson, DC. Goldberger, Z. Visuri, S. Armstrong, RN., 1999. Ionic exchanges of turtle shell in vitro and their relevance to shell function in the anoxic turtle. Journal of Experimental Biology 202, 503-520.

Jackson, DC. 2000. Living without oxygen: lessons from the freshwater turtle. Comparative Biochemistry and Physiology Part A 125, 299-315.

Jackson, DC. Crocker, CE. Ultsch, GR., 2000a. Bone and shell contribution to lactic acid buffering of submerged turtles Chrysemys picta bellii at 3°C. American Journal of Physiology. Regulatory, Integrative and Comparative Physiology 278, R1964-1571.

Jackson, DC. Ramsey, AL. Paulson, JM. Crocker, CE. Ultsch, GR., 2000b. Lactic acid buffering by bone and shell in anoxic softshell and painted turtles. Physiological and Biochemical Zoology 73(3), 290-297.

Jackson, DC. Andrade, D. Abe, AS., 2003. Lactate sequestration by osteoderms of the broad-nose caiman, Caiman latirostris, following capture and forced submergence. Journal of Experimental Biology 206, 3601-3606.

Janis, CM. Devlin, K. Warren, DE. Witzmann, F., 2012. Dermal bone in early tetrapods: a palaeophysiological hypothesis of adaptation for terrestrial acidosis. Proceedings of the Royal Society of London B 279, 3035-3040.

Kot, BCW. Zhang, ZJ. Lee, AWC. Leung, VYF. Fu, SN., 2012. Elastic modulus of muscle and tendon with shear wave ultrasound elastography: variations with different technical settings. PLoS ONE 7(8), e44348. doi:10.1371/journal.pone.0044348.

Main, RP. Ricqlès, Ade. Horner, JR. Padian, K., 2005. The evolution and function of thyreophoran dinosaur scutes: implications for plate function in stegosaurs. Paleobiology, 31(2), 291-314.

McKee, CT. Last, JA. Russell, P. Murphy, CJ., 2011. Indentation versus tensile measurements of Young's Modulus for soft biological tissues. Tissue Engineering Part B 17(3), 155-164.

Nesbitt, SJ., 2011. The early evolution of archosaurs: relationships and the origin of major clades. Bulletin of American Museum of Natural History 352, 1–292.

Nesbitt, SJ. Desojo, JB. Irmis, RB., 2013. Anatomy, phylogeny and palaeobiology of early archosaurs and their kin. Geological Society, London, Special Publications 379, 1-7.

Pithioux, M. Lasaygues, P. Chabrand, P., 2002. An alternative ultrasonic method for measuring the elastic properties of cortical bone. Journal of Biomechanics 35, 961–968.

Scheyer, TM. Sander, PM., 2004. Histology of ankylosaur osteoderms: implications for systematics and function. Journal of Vertebrate Paleontology 24(4), 874-893.

Scheyer, TM. Desojo, JB., 2011. Palaeohistology and external microanatomy of rauisuchian osteoderms (Archosauria: Pseudosuchia). Palaeontology 54, 1289–1302.

Seidel, MR., 1979. The osteoderms of the American alligator and their functional significance. Herpetologica 35, 375–380.

Smith, MM. Hall, BK., 1990. Development and evolutionary origins of vertebrate skeletogenic and odontogenic tissues. Biological Reviews 65, 277-373.

Smith, MM. Sansom, IJ. Smith, P., 1995. Diversity of the dermal skeleton in Ordovician to Silurian vertebrate taxa from North America: histology, skeletogenesis and relationships. Geobios 19, 65-70.

Staton, MA. Dixon, JR., 1975. Studies on dry season biology of Caiman crocodilus crocodilus from the Venezuela Llanos. Memoria de la Sociedad de Ciencias Naturales La Salle 101, 237-265.

Sun, CY. Chen, PY., 2013. Structural design and mechanical behavior of alligator (Alligator mississippiensis) osteoderms. Acta Biomaterialia 9, 9049–9064.

Trutnau, L. Sommerlad, R., 2006. Evolution of crocodilians. In: Chimaira, B. (Ed.), Crocodilians their natural history and captive husbandry. Andreas S. Bram., Franckfurt am Main, pp. 21–31.

Vickaryous, MK. Hall, BK., 2006. Osteoderm morphology and development in the nine-banded armadillo, Dasypus novemcinctus (Mammalia, Xenarthra, Cingulata). Journal of Morphology 267, 1273–1283.

Vickaryous, MK. Hall, BK., 2008. Development of the dermal skeleton in Alligator mississippiensis (Archosauria, Crocodylia) with comments on the homology of osteoderms. Journal of Morphology 269, 398-422.

Vickaryous, MK. Sire, JY. 2009. The integumentary skeleton of tetrapods: origin, evolution and development. Journal of Anatomy 214, 441–464.

Witzmann, F., 2009. Comparative histology of sculptured dermal bones in basal tetrapods, and the implications for the soft tissue dermis. Palaeodiversity 2, 233–270.

Witzmann, F. Scholz, H. Müller, J. Kardjilov, N., 2010. Sculpture and vascularization of dermal bones, and the implications for the physiology of basal tetrapods. Zoological Journal of the Linnean Society 160, 302–340.

Wolf, D. Kalthof, DC. Sander, PM., 2012. Osteoderm histology of the Pampatheriidae (Cingulata, Xenarthra, Mammalia): Implications for systematics, osteoderm growth, and biomechanical adaptation. Journal of Morphology 273, 388–404.

Yang, W. Chen, IH. Gludovatz, B. Zimmermann, EA. Ritchie, RO. Meyers MA., 2013. Natural flexible dermal armor. Advanced Material 25, 31–48.

Yang, W. Gludovatz, B. Zimmermann, EA. Bale, HA. Ritchie, RO. Meyers, MA., 2013. Structure and fracture resistance of alligator gar (Atractosteus spatula) armored fish scales. Acta Biomaterialia 9, 5876–5889.

Zylberberg, L. Castanet, J., 1985. New data on the structure and the growth of the osteoderms in the reptile Anguis fragilis (Anguidae, Squamata). Journal of Morphology 186, 327–342.

CONCLUSION ET PERSPECTIVES

I. Synthèse des résultats obtenus

Patrons d'expression de l'ornementation au cours de l'évolution des pseudosuchiens

L'ensemble des résultats montre que l'ornementation à la surface os dermiques des pseudosuchiens suit des patrons d'expression en lien avec la morphologie globale du crâne, la position phylogénétique et l'écologie des différents taxons. En effet, l'expression de l'ornementation semble montrer un fort signal phylogénétique chez les pseudosuchiens à l'image des « formes modernes » (Neosuchia), clade au sein duquel l'ornementation s'est développée et maintenue au travers des différentes radiations évolutives depuis le jurassique inférieur. L'utilisation d'ANOVA phylogénétiques (Garland et al., 1993) a permis de mettre en avant un signal écologique dans l'expression du degré d'ornementation en soustrayant l'influence des relations phylogénétiques lors des analyses de corrélation testant les relations entre le degré d'expression de l' ornementation osseuse et le mode de vie adopté par les pseudosuchiens au cours de l'évolution (terrestre, amphibie, pélagique). Nous avons ainsi pu montrer que c'est au sein des espèces semi-aquatiques que l'on retrouve le plus haut degré d'expression de l'ornementation au niveau crânien et post-crânien tant parmi les « formes modernes » (néosuchiens) que parmi les thalattosuchiens (téléosauridés) qui se sont éteints au Crétacé inférieur (Fanti et al., 2016). Toutefois, les analyses en morphométrie 3D au sein de ces groupes montrent que les espèces longirostres présentent une réduction de l'ornementation crânienne liée aux contraintes morphologiques qu'exercent l'allongement du rostre et l'élargissement des fosses temporales supérieures. En revanche, l'ornementation des ostéodermes ne semble être influencée ni par leur taille, ni par leur forme, ni par leur mode d'articulation. L'étroite corrélation entre le retour à la vie aquatique chez les pseudosuchiens à la transition Trias-Jurassique et le développement de l'ornementation osseuse suggère que celle-ci pourrait avoir deux implications fonctionnelles majeures et complémentaires: 1) tamponner l'acidité sanguine pendant les phases d'apnée prolongée (pour empêcher l'acidose respiratoire); 2) faciliter les échanges de chaleur entre l'organisme et l'environnement pendant les phases émergées et semi-émergées.

Le rôle de l'ornementation osseuse dans les transferts de chaleurs

L'acquisition de l'ectothermie est considérée comme un caractère dérivé chez les crocodiliens car les analyses histologiques amenant à estimer le niveau métabolique chez les archosauriformes et pseudosuchiens du Trias conduisent à inférer que l'ancêtre des archosaures était endotherme (Ricqlès et al., 2003, 2008; Legendre et al., 2016). Sur le plan de l'anatomie cardiaque, il existe chez les crocodiliens des caractères évoquant également un retour secondaire vers l'ectothermie: le foramen de Panizza et la « valve dentée ». Cette valve permet, à partir d'un cœur cloisonné en quatre cavités comme chez les mammifères et oiseaux (endothermes), d'établir le passage d'une circulation sanguine fermée vers une circulation sanguine ouverte qui mélange sang artériel et veineux. Cette transition a pour conséquence direct de réduire la pression artérielle vers de basse valeurs qui caractérisent la physiologie ectotherme (Francklin & Axelsson, 2000; Seymour et al., 2004) à l'image des squamates et des lissamphibiens qui disposent d'un cœur non-cloisonné de par leur héritage ancestral (Jensen et al, 2013). Concernant les transferts de chaleur entre l'organisme et le milieu ambiant au travers du squelette dermique, les analyses en éléments finis ont montré que l'expression de l'ornementation, tout comme le développement du squelette dermique post-crânien, n'ont pas d'incidence significative sur la conduction de chaleur à travers la peau pendant les phases d'exposition. Toutefois, d'après les analyses histologiques, les ostéodermes ornementés sont très vascularisés et leur ornementation augmente le degré de vascularisation de la peau en abritant des vaisseaux au sein des cupules. Les bouquets vasculaires superficiels ainsi crées peuvent faciliter les échanges de chaleur entre l'organisme et le milieu extérieur. Les crocodiliens, ainsi que les autres vertébrés ectothermes, sont connus pour augmenter leur rythme cardiaque en phase d'exposition (Seebacher et al., 1999; Seebacher and Franklin, 2004), processus qui, en liaison avec le dense réseau sanguin périphérique portés par les ostéodermes ornementés, est de nature à accélérer les échanges thermiques. Les travaux de Seidel (1979) et de Farlow et al. (2010) ont montré que, quelle que soit la température de l'environnement, les régions de la peau occupées par des ostéodermes sont toujours plus froides que celles qui en sont dépourvues. Ce résultat suggère que les ostéodermes ornementés sont irrigués par le sang relativement froid provenant des régions profondes de l'organisme et donc qu'ils joueraient un rôle d'échangeur thermique via un système de convection forcé et contrôlé par l'activité cardiaque.

Le rôle de l'ornementation osseuse dans le tampon de l'acidose respiratoire

Le réseau vasculaire possiblement impliqué dans les échanges de chaleur en phase émergée et semi-émergée pourrait également avoir un autre intérêt physiologique pendant les phases d'apnée prolongées. En régime anaérobie, les cellules utilisent la fermentation homolactique pour synthétiser de l'énergie (ATP) car la voie mitochondriale (cycle de Krebbs et pompes à protons) n'est pas fonctionnelle en absence d'oxygène. Or, la synthèse du lactate et l'accumulation du dioxyde de carbone entrainent une augmentation de l'acidité du plasma sanguin qui doit être corrigée afin d'empêcher divers disfonctionnements physiologiques. Il a ainsi été montré que le lactate était acheminé et stocké dans les os, particulièrement dans le squelette dermique, chez les vertébrés amphibies au cours des phases d'apnée (crocodiliens, Jackson et al., 2003; chéloniens, Jackson and Heisler, 1982; Jackson, 2000; Jackson et al., 1999, 2000a, 2000b). Deux mécanismes seraient alors impliqués pour remplir cette fonction: 1) le stockage direct du lactate dans la matrice osseuse, processus qui serait facilité par un réseau vasculaire propice aux échanges; 2) la libération d'éléments minéraux (calcium, carbonates) se liant au lactate sanguin pour inhiber son effet acidifiant. Or, concernant ce second mécanisme, nous avons montré que l'ornementation était formée, chez les pseudosuchiens, par une activité de résorption superficielle dont la conséquence immédiate est la libération de minéraux dans le plasma (Buffrénil et al., 2015). De ce fait, l'activité ostéoclastique à l'origine de la formation des cupules pourrait avoir pour effet de tamponner l'acidité sanguine. Toutefois, la cinétique de ce processus demeure mal connue et il n'est pas certain que le recrutement des ostéoclastes et leur activité de résorption soit suffisamment rapides pour répondre à des besoins physiologiques immédiats lors des phases de plongée.

Le rôle de l'ornementation osseuse dans l'équilibre de l'homéostasie phospho-calcique

Il n'est pas exclu que la résorption à l'origine de la formation des cupules chez les pseudosuchiens (voir l'introduction) puisse intervenir dans des mécanismes physiologiques à moyen terme qui impliqueraient notamment par libération du calcium. En effet, il a été montré que la libération de calcium à partir des ostéodermes pendant la période précédant la ponte était accrue chez les femelles d'Alligator mississippiensis (Dacke et al., 2015); la calcification de la coquille des œufs est ainsi facilitée. De façon plus générale, les crocodiliens sont parfois soumis à des phases de jeun prolongé (jusqu'à un an; Trutnau and Sommerlad, 2006). Sachant que nos observations de l'histologie osseuse de l'ornementation montrent que du dépôt osseux secondaire a lieu a posteriori au fond des cupules

précédemment résorbées (Buffrénil et al., 2015), la formation et l'évolution de l'ornementation au cours de l'ontogénie pourrait notamment être le résultat de phases cycliques de jeun ou de dépenses métaboliques succédées par des phases de stockage de minéraux d'origine alimentaire. La libération de calcium et de phosphore contribuerait alors (comme tout processus de remaniement) au maintien de l'homéostasie phospho-calcique.

Le rôle de l'ornementation dans la résistance mécanique osseuse

Les analyses en éléments finis montrent que la présence d'ornementation ne modifie pas de façon significative la répartition des contraintes mécaniques (Von Mises) dans les ostéodermes lors d'une attaque externe par des objets pointus (griffes ou dents). Ce caractère ne présente donc pas d'intérêt mécanique, du moins face à ce type d'agression. En revanche, il pourrait correspondre à la géométrie optimale permettant l'augmentation la vascularisation des ostéodermes et le recyclage des éléments minéraux sans dégradation de la résistance mécanique des os. On notera, par ailleurs, qu'un éventuel rôle de protection mécanique est d'autant plus improbable chez les crocodiliens que, d'une part, les adultes ne subissent pas de prédation significative et que, d'autre part, les prédateurs qui s'attaquent aux juvéniles ingèrent les os des proies de petite taille (oiseaux, varans, serpents, fauves; Trutnau and Sommerlad, 2006). Toutefois, au sein de certains groupes de pseudosuchiens disparus comme les aetosaures, qui ont vécu au Trias (230-200Ma) dans un contexte écologique très différent, il n'est pas exclu que le bouclier dermique ait pu servir de protection face à certains prédateurs de grande taille tels que d'autres pseudosuchiens carnivores (rauisuchiens; Nesbitt et al., 2013).

II. Perspectives

A — Inférer et analyser les patrons d'*évolution de la vascularisation des ostéodermes des* pseudosuchiens depuis le Trias à partir *d'un modèle actualiste*

Les résultats obtenus à partir de l'identification et de la quantification de la vascularisation des os dermiques des crocodiliens actuels a permis d'établir une relation physique entre, d'une part, la taille des cupules et des cavités internes des ostéodermes et, d'autre part, la surface relative des vaisseaux qu'elles contiennent. Cette relation mathématique va permettre, via une projection actualiste, d'estimer la densité vasculaire à la fois présente au niveau de l'ornementation et au niveau des cavités intra-osseuse des ostéodermes au sein de l'ensemble du registre fossile des pseudosuchiens. Toutefois, les crocodiliens actuels constituant un reliquat de la diversité passée, on ne peut donc pas envisager une reconstitution de la densité vasculaire par « Extant Phylogenetic Bracket » (Witmer, 1995) car la majorité des pseudosuchiens dont les fossiles sont datés à plus de 85 Ma se placent en groupe externe du clade Crocodylia (formes actuelles). Toutefois, en s'appuyant sur le principe selon lequel les la présence d'ostéodermes est homologue chez les pseudosuchiens, on peut supposer que la composition des tissus mous qu'ils contiennent demeure semblable de part un héritage phylogénétique depuis l'ancêtre des archosaures (Nesbitt, 2011). Nous pourrions alors, en guise d'étape préliminaire, tester cette homologie sur la phylogénie des archosauriformes en utilisant le principe de reconstruction des états aux nœuds internes par parcimonie (logiciel Mesquite; Maddison and Maddison, 2011). Si l'hypothèse d'homologie est validée, alors nous projetterons nos mesures de quantification de la densité vasculaire des ostéodermes de crocodiliens actuels sur l'ensemble du registre fossile des pseudosuchiens (moyennant une augmentation de l'échantillonnage parmi les spécimens vivants). Ces nouvelles données constitueront alors un indice permettant de tester les différentes hypothèses d'ordre physiologique se basant sur l'existence et le développement d'un réseau vasculaire au sein des ostéodermes des différents taxons (Neosuchia, Notosuchia, Protosuchia, Thalattosuchia). Par exemple, l'implication de ce réseau vasculaire dans le tampon du lactate augmentant la tolérance à l'apnée prolongée pourra être testée en confrontant ces données aux différents modes de vie adoptés par les pseudosuchiens au cours de leur évolution (terrestre, amphibie, pélagique). De plus, ces données pourront être confrontées à des quantifications histologiques sur les os longs des pseudosuchiens tel que cela a déjà été fait chez certains taxons. En effet, certaines données quantitatives mesurées à partir des os longs (exemple: densité vasculaire et densité des ostéocytes; Legendre et al., 2016) permettent d'estimer le taux métabolique et

secondairement d'en déduire le régime thermique (endotherme, ectotherme). Il serait en effet intéressant de tester si une augmentation du développement vasculaire des ostéodermes pourrait être corrélé à la chute du métabolisme des pseudosuchiens et donc à leur retour vers un régime ectotherme. L'existence d'une telle corrélation pourrait corroborer l'implication des ostéodermes dans les échanges thermiques. Si de telles analyses statistiques (analyses phylogénétiques comparées) donnent des résultats significatifs, nous pourrons alors construire un modèle 3D simulant les échanges thermiques au sein d'un ostéoderme actuel grâce à des analyses en éléments finis qui seraient paramétrées à partir des mesures quantitatives de la vascularisation déjà établies et des valeurs de température mesurées in vivo par caméra infrarouge. Des données sur les flux de chaleur calculés (W/m^2) pourront alors être inférées sur les ostéodermes fossiles à partir de la quantification estimée de leur réseau vasculaire (mesure de la porosité intra osseuse et du degré d'ornementation) afin de produire des données inédites concernant la physiologie de taxons disparus.

B — Étude de *l'implication* fonctionnelle des os dermiques ornementés dans la « sortie des eaux » chez les tétrapodes.

A l'inverse des crocodiliens, les premiers tétrapodes (« stégocéphales ») ont quitté le milieu aquatique pour coloniser le milieu terrestre. Toutefois, la période à laquelle cette transition s'est produite tout comme les processus morphologiques et physiologiques ayant permis une telle transition restent encore débattus (Alberg and Milner, 1994; Clack, 2002a ; Niedźwiedzki et al, 2010). A l'instar des néosuchiens, les « stégocéphales » possédaient un dermocrâne très ornementé qui a pu jouer un rôle dans le tampon de l'acidose respiratoire lors de la « sortie des eaux » (Janis et al., 2012) puis dans les échanges de chaleur lors des phases émergées dans le cadre d'une transition vers la vie terrestre chez des organismes initialement ectothermes (Witzmann & Brainerd, 2017). Toutefois, au sein des faunes actuelles, aucun groupe de tétrapode n'a gardé ce morphotype présentant une tête en forme de plaque ornementée car les derniers représentants de ces formes se sont éteints au Crétacé (temnospondyles; Warren et al., 1997). Par conséquent, contrairement aux pseudosuchiens, il n'est pas possible d'effectuer des inférences à partir de prélèvements provenant de formes actuelles en combinant directement le principe de l'homologie et l'actualisme. Toutefois, la récurrence homoplasique de l'ornementation osseuse chez les vertébrés à l'image de certains anoures (Ceratophrys) ou actinoptérygiens (Chondrostei, Siluriformes, Lepidostei; Buffrénil et al., 2016) font de ces derniers de potentiels modèles actuels pour inférer l'organisation et la vascularisation des tissus encrés sur le squelette dermique ornementé des « stégocéphales ». Ainsi, nous avons effectué

une première analyse exploratoire basée sur des prélèvements puis des analyses histologiques après coloration d'os dermiques crâniens provenant d'anoures (Ceratophrys ornata, Ceratophrys aurita, Ceratophrys cranwelli) et de chondrostéens (Acipenser baerii). Les premières observations ont mis en évidence que l'ornementation héberge une prolifération vasculaire (bouquet) uniquement lorsqu'elle se forme par résorption. Dans le cas où l'ornementation se forme par apposition préférentielle, les cupules n'hébergent pas de bouquet vasculaire et la vascularisation péri-osseuse se limite au débouché direct du canal centro-cupulaire. Sachant que l'ornementation des os dermiques se forme presque exclusivement par apposition préférentielle chez les « stégocéphales », nos premiers résultats nous amèneraient à penser que l'ornementation des os dermiques était peu vascularisée chez ces formes d' « amphibiens » en comparaison avec les crocodiliens. Par conséquent, ces observations préliminaires tendraient à contredire une possible implication de l'ornementation crânienne dans les échanges de chaleur et le tampon de l'hypercapnie chez les « stégocéphales ». A contrario, ces résultats viendraient plutôt conforter l'hypothèse selon laquelle ces formes étaient aquatiques comme peut le suggérer l'existence d'une ligne latérale chez certains taxons (formes du Dévonien et temnospondyles, Witzmann, 2006, 2010). Cependant, notre échantillonnage de départ doit être élargi notamment en incluant notamment des téléostéens (Phractocephalus hemioliopterus) puis nous effectuerons des analyses quantitatives comme cela a été fait sur les crocodiliens dans le cadre de cette thèse (voir Partie 2, chapitre 2: La vascularisation des ostéodermes: Implications physiologiques de l'ornementation). En parallèle, grâce à la technologie synchroton, nous pourrons quantifier la présence et la densité de canaux vasculaires traversant les cupules qui composent l'ornementation crânienne chez les « stégocéphales » en incluant à la fois des représentants des premiers tétrapodes (Dévonien) et des formes plus récentes (temnospondyles, lépospondyles, reptiliomorphes). Ainsi nous pourrons établir un indice de vascularisation de la surface des os dermiques ornementés en combinant la quantification du réseau vasculaire péri-osseux au sein des modèles actuels avec une quantification du nombre de canaux traversant les cupules chez les formes fossiles en s'appuyant sur un socle commun entre taxons fossiles et actuels: le mode de mise en place de l'ornementation (apposition différentielle ou résorption). Fort de cette estimation quantitative de la densité vasculaire présente en surface des os dermiques ornementés des « stégocéphales », nous pourrons tracer l'évolution de ce caractère sur la phylogénie des tétrapodes. En fonction des patrons d'expression obtenus, nous serons amenés à discuter des possibles rôles physiologiques pour les différents taxons concernés (premiers tétrapodes, temnospondyles, lépospondyles, reptiliomorphes): le tampon de l'hypercapnie en milieu terrestre (Janis et al.,

2012) et les échanges de chaleur en phase émergée et semi-émergée chez des vertébrés initialement aquatiques et ectothermes (Seidel, 1979, Farlow et al., 2010). A l'appui de ces résultats, nous discuterons alors de la possible implication des os dermiques ornementés dans la première « sortie des eaux » des tétrapodes qui reste encore souvent évoquée comme une phase majeure de l'évolution des vertébrés (Clack, 2002b; Ahlberg & Clack, 2006).

Références

Ahlberg PE, Milner AR. 1994. The origin and early diversification of tetrapods. Nature 368: 507-514.

Ahlberg PE, Clack JA. 1996. A firm step from water to land. Nature 440: 747-749.

Buffrénil Vd, Clarac F, Fau M, Martin S, Martin B, Pellé E, Laurin M. 2014. Differentiation and growth of bone ornamentation in vertebrates: A comparative histological study among the Crocodylomorpha. J Morphol 276:425–445.

Buffrénil Vde, Clarac F, Canoville A, Laurin M. 2016. Comparative data on the differentiation and growth of bone ornamentation in Gnathostomes (Chordata: Vertebrata). J Morphol 277: 634-670.

Bystrow AP. 1947. Hydrophilous and xerophilous labyrinthodonts. Acta Zool Stock 28:137–164.

Cerda IA, Desojo JB. 2011. Dermal armour histology of aetosaurs (Archosauria: Pseudosuchia), from the Upper Triassic of Argentina and Brazil. Lethaia 44: 417–428.

Clack JA. 2002a. An early tetrapod from 'Romer's Gap'. Letters to Nature 418: 72-76.

Clack JA. 2002b. Patterns and processes in the early evolution of the tetrapod ear. Developmental neurobiology 53(2): 251-264.

Dacke CG, Elsey RM, Trosclair PL, Sugiyama T, Nevarez JG, Schweitzer MH. 2015. Alligator osteoderms as a source of labile calcium for eggshell formation. J Zool 297(4): 255-264.

Fanti F, Miyashita T, Cantelli L, Mnasri F, Dridi J, Contessi M, Cau A. 2016. The largest thalattosuchian (Crocodylomorpha) supports teleosaurid survival across the Jurassic-Cretaceous boundary. Cretaceous Res 61: 263-274.

Farlow JO, Hayashi S, Tattersall GJ. 2010. Internal vascularity of the dermal plates of Stegosaurus (ornithischia, tyreophora). Swiss J Geosci 103:173–185.

Francklin CE, Axelsson M. 2000. Physiology: An actively controlled heart valve. Nature 406: 847-848.

Garland T Jr, Dickerman AW, Janis CM, Jason AJ. 1993. Phylogenetic Analysis of Covariance by Computer Simulation. Sys Biol 42: 265–292.

Jackson DC, Heisler N. 1982. Plasma ion balance in submerged anoxic turtles at 3°c: the role of calcium lactate formation. Res Physiol 49: 159-174.

Jackson DC, Goldberger Z, Visuri S, Armstrong RN. 1999. Ionic exchanges of turtle shell in vitro and their relevance to shell function in the anoxic turtle. J Exp Biol 202: 503-520.

Jackson DC. 2000. Living without oxygen: lessons from the freshwater turtle. Comp Biochem Physiol A 125: 299-315.

Jackson DC, Crocker CE, Ultsch GR. 2000a. Bone and shell contribution to lactic acid buffering of submerged turtles Chrysemys picta bellii at 3°C. Am J Physiol-Reg 278: R1964-1571.

Jackson DC, Ramsey AL, Paulson JM, Crocker CE, Ultsch GR. 2000b. Lactic acid buffering by bone and shell in anoxic softshell and painted turtles. Phys Chem Zool 73(3): 290-297.

Jackson DC, Andrade D, Abe AS. 2003. Lactate sequestration by osteoderms of the broad-nose caiman, Caiman latirostris, following capture and forced submergence. J Exp Biol 206: 3601-3606.

Janis CM, Devlin K, Warren DE, Witzmann F. 2012. Dermal bone in early tetrapods: A palaeophysiological hypothesis of adaptation for terrestrial acidosis. Proc Biol Sci 279: 3035–3040.

Jensen B, Wang T, Christoffels VM, Moorman AFM. 2013. Evolution and development of the building plan of the vertebrate heart. Biochim Biophys Acta 1833: 783–794.

Legendre L, Guénard G, Botha-Brink J, Cubo J. 2016. Palaeohistological evidence for ancestral high metabolic rate in archosaurs. Syst Biol 65(6): 986-996.

Maddison WP, Maddison DR. 2011. Mesquite: A modular system for evolutionary analysis. Version 2.75. Available at: http://mesquiteproject.org.

Nesbitt SJ. 2011. The early evolution of archosaurs: relationships and the origin of major clades. Bull Am Mus Nat Hist 352: 1–292.

Nesbitt SJ, Desojo JB, Irmis RB. 2013. Anatomy, phylogeny and palaeobiology of early archosaurs and their kin. Geol Soc London Spe Pub 379: 1-7.

Niedzwiedzki G, Szrek P, Narkiewicz K, Narkiewicz M, Ahlberg PE. 2010. Tetrapod trackways from the early Middle Devonian period of Poland 463: 43-48.

Ricqlès Ade, Padian K, Horner JR. 2003. On the bone histology of some Triassic pseudosuchian archosaurs and related taxa. Annls Paléont 89: 67–101.

Ricqlès Ade, Padian K, Knoll F, Horner JR. 2008. On the origin of high growth rates in archosaurs and their ancient relatives: complementary histological studies on Triassic archosauriforms and the problem of a ‘phylogenetic signal’ in bone histology. Annls Paléont 94: 57–76.

Seebacher F, Grigg G, Beard L. 1999. Crocodiles as dinosaurs: behavioural thermoregulationin very large ectotherms leads to high and stable body temperatures. J Exp Biol 202: 77–86.

Seebacher F, Franklin CE. 2004. Integration of autonomic and local mechanisms in regulating cardiovascular responses to heating and cooling in a reptile (Crocodylus porosus). J Comp Physiol B 174: 577–585.

Seidel MR. 1979. The osteoderms of the American alligator and their functional significance. Herpetologica 35:375–380.

Seymour RS, Bennett-Stamper CL, Johnston SD, Carrier DR, Grigg GC. 2004. Evidence for endothermic ancestors of crocodiles at the stem of archosaur evolution. Physiol Biochem Zool 77: 1051–1067.

Trutnau L, Sommerlad R. 2006. Behavior of crocodilians. In: Crocodilians their Natural History and Captive Husbandry. (ed.Chimaira B), pp. 143–261. Andreas S. Bram: Franckfurt am Main.

Warren AA, Rich PV, Rich TH. 1997. "The last, last labyrinthodonts?". Palaeontographica Abt. A 247: 1–24.

Wilmer LM. 1995. The Extant Phylogenetic Bracket and the importance of reconstructing soft tissues in fossils. In: Functional morphology in vertebrate paleontology. (ed Thomason JJ), pp. 19-33. Cambridge University Press.

Witzmann F. 2006. Cranial morphology and ontogeny of the Permo-Carboniferous temnospondyl Archegosaurus decheni Goldfuss, 1847 from the Saar–Nahe Basin, Germany. Trans R Soc Edinburgh Earth Sci 96: 131–162.

Witzmann F. 2010. A skull fragment of a Devonian tetrapod with a unique lateral line morphology in the collection of the Museum für Naturkunde Berlin. Foss Rec 13(2): 297–302.

Witzmann F, Brainerd E. 2017. Modeling the physiology of the aquatic temnospondyl Archegosaurus decheni from the early Permian of Germany. Foss Rec: 20, 105–127.

ANNEXES

JOURNAL OF MORPHOLOGY 276:425–445 (2015)

Differentiation and Growth of Bone Ornamentation in Vertebrates: A Comparative Histological Study Among the Crocodylomorpha

V. de Buffrénil,[1] F. Clarac,[1] M. Fau,[1] S. Martin,[2] B. Martin,[2] E. Pellé,[3] and M. Laurin[1]*

[1]*Département Histoire de la Terre, Muséum National d'Histoire Naturelle, UMR 7207 (CR2P), Sorbonne Universités, MNHN/CNRS/UPMC, Bâtiment de Géologie Paris Cedex 05, F-75231, France*
[2]*Ferme à Crocodiles de Pierrelatte, Pierrelatte, F-26700, France*
[3]*Direction des Collections, Muséum National d'Histoire Naturelle, Paris Cedex 05, F-75231, France*

ABSTRACT Bone ornamentation, that is, hollow (pits and grooves) or protruding (ridges) repetitive reliefs on the surface of dermal bones, is a frequent, though poorly studied and understood, feature in vertebrates. One of the most typical examples of this characteristic is given by the Crurotarsi, a taxon formed by the crocodilians and their closest allies, which generally display deep ornamentation on skull roof and osteoderms. However, the ontogenetic process responsible for the differentiation and development of this character remains controversial. This study was conducted to settle the question on histological and microanatomical evidence in several crurotarsan taxa. Observational and experimental data in extant and extinct crocodyliforms show that bone ornamentation is initially created, and later maintained during somatic growth (that is indefinite in crocodilians), by a complex process of bone remodeling comprising local resorption of superficial bone cortices, followed by partial reconstruction. The superficial reliefs of crocodilian dermal bones are thus permanently modified through pit enlargement, drift, stretching, shrinking, or complete filling. Ridges are also remodeled in corresponding ways. These processes allow accommodation of unitary ornamental motifs to the overall dimensions of the bones during growth. A parsimony optimization based on the results of this study, but integrating also published data on bone histology in non-crocodyliform crurotarsans and some non-crurotarsan taxa, suggests that the peculiar mechanism described above for creating and maintaining bone ornamentation is a general feature of the Crurotarsi and is quite distinct from that attributed by previous authors to other vertebrates. J. Morphol. 276:425–445, 2015.

KEY WORDS: Crurotarsi; bone sculpturing; paleohistology; development; remodeling

INTRODUCTION

Bone ornamentation (or "sculpture") is a common and recurrent feature in vertebrates, including the most ancient ones, such as the Ordovician arandaspids (Young, 2009), Silurian and Devonian heterostracans and osteostracans (Märss, 2006), and Devonian placoderms (Giles et al., 2013), where ornamentation is often composed of dentine and enamel (Lingham-Soliar, 2014), though ornamentation composed of dermal bone proper appears also in Devonian taxa, such as the finned stem-tetrapods *Eusthenopteron* (Zylberberg et al., 2010), *Panderichthys* (Vorobyeva and Schultze, 1991), *Elpistostege* (Schultze and Arsenault, 1985), and *Tiktaalik* (Daeschler et al., 2006). Bone ornamentation refers to a broad variety of morphological patterns that share two basic characteristics: a) they only occur on the outer surface of dermal bones (skull roof, lateral side of mandibles, some elements of the shoulder girdle, and osteoderms); b) they consist of positive or negative, repetitive reliefs distinct from the vascular imprints displayed by most bone cortices. Three major categories of bone ornamentation have been described hitherto. Granular ornamentation (called "tubercular" or "pustular" by some authors) consists in globular or ogival protuberances, as displayed by, for example, the skull roof and osteoderms of some temnospondyls (Witzmann and Soler-Gijón, 2010); Witzmann et al., 2010) or squamates (Hoffstetter, 1955; Buffrénil et al., 2011). Vermicular ornamentation is represented by shallow, sinuous, and interconnected grooves, as displayed by the osteoderms of some squamates (e.g., *Anguis fragilis*: cf. Zylberberg and Castanet, 1985). Pit and ridge ornamentation consists of rounded pits separated by a network of crests displaying variable sharpness, as displayed by, for example, the Devonian limbed stem-tetrapod

*Correspondence to: M. Laurin, Département Histoire de la Terre, Muséum National d'Histoire Naturelle, CNRS-UMR 7207 (CR2P), Bâtiment de Géologie Paris Cedex 05, F-75231, France.
E-mail: laurin@mnhn.fr

Received 16 September 2014; Revised 27 October 2014;
Accepted 8 November 2014.

Published online 8 December 2014 in
Wiley Online Library (wileyonlinelibrary.com).
DOI 10.1002/jmor.20351

Acanthostega (Clack 2002) or several temnospondyls (Piveteau and Deschaseaux, 1955a, b; Laurin and Soler-Gijón, 2006), among many other vertebrates. On a same bone, the pits are often associated with variably elongated, straight furrows, especially in the peripheral regions of the bones. The latter type is by far the most frequent, and occurs, with great morphological consistency, in all major clades of vertebrates, from heterostracans (Novitskaya, 1971) to actinopterygians (Grande and Bemis, 1998: Fig. 16), finned sarcopterygians (Janvier and Martin, 1979), and tetrapods (Bystrow, 1935; Kälin 1955; Witzmann et al., 2010), except birds and mammals.

The taxonomic distribution of this kind of ornamentation in vertebrates raises a series of developmental, evolutionary, and functional questions, the most fundamental ones being relative, on the one hand, to the osteogenic processes responsible for the differentiation and growth of pits, grooves, and ridges during ontogeny and, on the other hand, the evolutionary history of this characteristic in the taxa that display it. These questions received little attention so far; they are called an "unresolved enigma" by Witzmann et al. (2010). The corollary problem of the relationships that may exist at a geometrical level, between the growth of pits and grooves and that of the bones bearing them, remains nearly undocumented. An early study dealing exclusively with five eusuchian crocodile species concluded that pits were mainly created by local bone resorption, with complex processes of erosion/reconstruction (remodeling) resulting in an adaptation of the depth and diameter of the pits to the overall size of the bones (or osteoderms) during growth (Buffrénil, 1982). According to this interpretation, grooves result from an asymmetric remodeling of pits. Such a growth pattern was rejected by Vickaryous and Hall (2008) because the occurrence of osteoclasts, the cells responsible for bone erosion, on the ornamented surface of dermal bones had not been evidenced. Consequently, bone ornamentation in crocodilians was considered to result exclusively from preferential apposition on the crests, a process that is otherwise acknowledged as an explanation for the development of bone ornamentation in temnospondyls (Witzmann and Soler-Gijón, 2010). Although obvious signs of superficial remodeling on ornamented bones were recently mentioned in a taxon closely related to the Crocodyliformes, the aetosaurs (Scheyer et al., 2014), the question remains open for crocodilians. Contradictions in reported data and interpretations tend to create some confusion and suggest that, beyond strikingly similar morphological patterns, pit and ridge ornamentation may be caused by different processes in distinct taxa. Thus, the issue in question is whether this type of ornamentation is homologous among the many taxa that display it, or is only a homoplasy. This study is aimed at further documenting this problem.

MATERIAL AND METHODS

Three methodological approaches were used. 1) Basic histological observations were conducted in a comparative sample of extant and extinct taxa. 2) An experimental study based on in vivo labelling of bone growth was conducted in two extant species. 3) All comparative data, including data available in literature, were analyzed in a phylogenetic context through parsimony in Mesquite (Maddison and Maddison, 2014) to reveal evolutionary patterns within the Crurotarsi, a taxon also known as Pseudosuchia (e.g., Scheyer and Desojo, 2011).

Biological Sample

The biological sample used for histology consists of entire or fragmentary skull bones: frontal, parietal, jugal or angular, and osteoderms (irrespective of their position on the body) from 32 extant or extinct crocodyliform taxa (five are not identified down to the species level), generally classified into 13 families (one, a phytosaur is determined only at a higher nomenclatural level) and 20 identified genera (from a total of 25 genera: Table 1). The taxonomic identification for most of the material is not problematic. However, two samples from the MNHN require comments. One osteoderm is from an undetermined Dyrosauridae from the Paleocene of Bolivia (C. de Muizon, personal communication from May 19, 2014). This is probably the taxon that was briefly described, but not named, in Buffetaut (1991). Another osteoderm from the same site belongs to a sebecid (C. de Muizon, personal communication from May 19, 2014). This is probably *Sebecus querejazus* (Buffetaut and Marshall,

TABLE 1. General composition of the biological sample used for simple naked-eye observations (indicated in italics), and for photonic or electronic microscopy (plain text)

Family	Genus	Species	Geol. Age	Bone	Reference
Crocodyliformes					
Alligatoridae	*Alligator*	*mississippiensis*	Extant	Front., par., osteod., *skull*	MNHN. AC no ref.; MNHN. H-1986.945, pers. coll. cf. FCP
	Alligator	*sinensis*	Extant	Osteod.	Pers. Coll./FCP
	Allognathosuchus	*wartheni*	Late Paleocene (Wasatchian)	Osteod.	UCMP 113731
	Brachychampsa	*montana*	Late Cretaceous (Maastrichtian)	Osteod.	UCMP 133901
	Caiman	*crocodilus*	Extant	Front., par., osteod., *skull*	MNHN.H-1986.454, 1988.6489, MNHN.

TABLE 1. (continued)

Family	Genus	Species	Geol. Age	Bone	Reference
					AC-1987.773, Pers. coll./FCP
	Diplocynodon	*ratelii*	Lower Miocene	Front., par., osteod.	MNHN.F-SG 673, 685
	Diplocynodon	*remensis*[a]	Late Paleocene (Thanetian)	Osteod.	MNHN. F. No number
	Paleosuchus	*palpebrosus*	Extant	Osteod., *skull*	MNHN.AC-1909.204, MNHN.H- 1991.4480
	Paleosuchus	*trigonatus*	Extant	Osteod., *skull*	MCL 420003939, MNHN AC–2014-1
	Undescr. stem alligatoridae	indet.[b]	Late Cretac. (Maastrichtian)	Osteod.	UCMP 131693
Crocodylidae	*Crocodylus*	*acutus*	Extant	Osteod., *skulls*	MNHN.AC-1909.275, 1944.266, 1870.500
	Crocodylus	*niloticus*	Extant	Front., osteod.	MNHN.AC- 1920.90, PC
	Mecistops [Crocodylus]	*cataphractus*	Extant	Osteod., *skull*	MNHN.AC-1962.267, MNHN.H-1991.4490
	Osteolaemus	*tetraspis*	Extant	Osteod., *skull*	MNHN.AC-1991.4488, MNHN.H-1991.4480
Other Crocodylia	*Crocodylus [Asiatosuchus]*	*depressifrons*.	Lower Eocene	Osteod.	MNHN. F. No number
	'Crocodylus'	*affinis*	Lower Eocene (Bridgerian)	Front., par., osteod.	YPM 511, UCMP 131762
	Indet.	*Indet*.	Cretaceous of Madagascar	Osteod.	MNHN.F. No number
Crocodylia inserta sedis	*Borealosuchus*	*wilsoni*	Late Paleocene (Wasatchian)	Osteod.	UCMP 131696
	Borealosuchus	*sternbergii*	Late Cretac. /Eoc. (Puercan)	Osteod.	UCMP 138375, 133903
Bernissartiidae	*Bernissartia*	*fagesii*	Early Cretac. (Wealdian)	Osteod.	IRSNB Vert-5144-03
Goniopholidae	*Goniopholis*	*simus*	Early Cretac. (Wealdian)	Osteod.	IRSNB Vert-5144-04
Dyrosauridae	*Indet*.	*indet*.	Lower Paleoc.	Osteod.	MNHN.F. Bolivia. No number
Pholidosauridae	*Sarcosuchus*	*imperator*	Upper Cretac.	Osteod.	MNHN.F.GDF 380
	Indet.	*indet*.	Lower Cretac. (Berriasian)	Osteod.	MNHN. F. No number
Teleosauridae	*Machimosaurus*	*hugii*	Late Juras.	Osteod.	SMNS 81608
	Platysuchus	*multiscrobilatus*	Lower Juras.	Osteod.	SMNS 15919
	Teleosaurus	*cadomensis*	Middle Juras.	Osteod.	MNHN. F. No number
Mahajangasuchidae	*Mahajangasuchus*	*insignis*	Late Cretac.	Osteod.	UA 9962, 9963, 9964
Trematochampsidae	*Trematochampsa*	*taqueti*	Upper Cretac.	Front., par., osteod.	MNHN.F.Ibc 2, 12, 34, 2031, 3032
Chimaerasuchidae	*Simosuchus*	*clarki*	Late Cretac.	Osteod.	UA 9965
Sebecidae	*Sebecus*	*querejazus*.	Lower Paleoc.	Osteod.	MNHN.F. Bolivia. No Number
Uruguaysuchidae	*Araripesuchus*	*tsangatsangana*	Late Cretac.	Osteod.	UA 9966
Phytosaurs					
Indet.	Indet.	Indet.	Upper Triassic	Osteoderm	MNHN. F. No number

The numbers of specimens available for each species are not detailed. They vary from 1 (single partial or entire bone) to the totality of dermal bones in one or several specimens (case of, e.g., *Alligator mississippiensis* or *Caiman crocodilus*). Additional precisions on specific samples are given in the main text (cf. Material and Methods).

Meaning of abbreviations (in order of succession in the table)—MNHN: Muséum national d'Histoire Naturelle (Paris, France), collection of fossils (F), collection of comparative anatomy (AC) or herpetological collection (H). Pers. coll./FCP: Personal collection of samples from the Crocodile Farm of Pierrelatte (FCP). UCMP: University of California, Museum of Paleontology (Berkeley, CA). SMNS: Staatliches Museum für Naturkunde Stuttgart (Germany). MCL: Musée des Confluences (Lyon, France). IRSNB: Institut Royal des Sciences Naturelles (Bruxelles, Belgium). UA: Université d'Antananarivo, Madagascar. Specimens communicated to the authors by Stony Brook University, Department of Anatomical sciences (New York). YPM: Yale Peabody Museum (Yale).

[a]Species recently described (Martin et al., 2014).

[b]A fossil informally called "*Protocaiman*" (in the sense of a stem-caiman, though its age suggests it might be a stem-alligatorid) in the paleontological collections of the University of California (Berkeley).

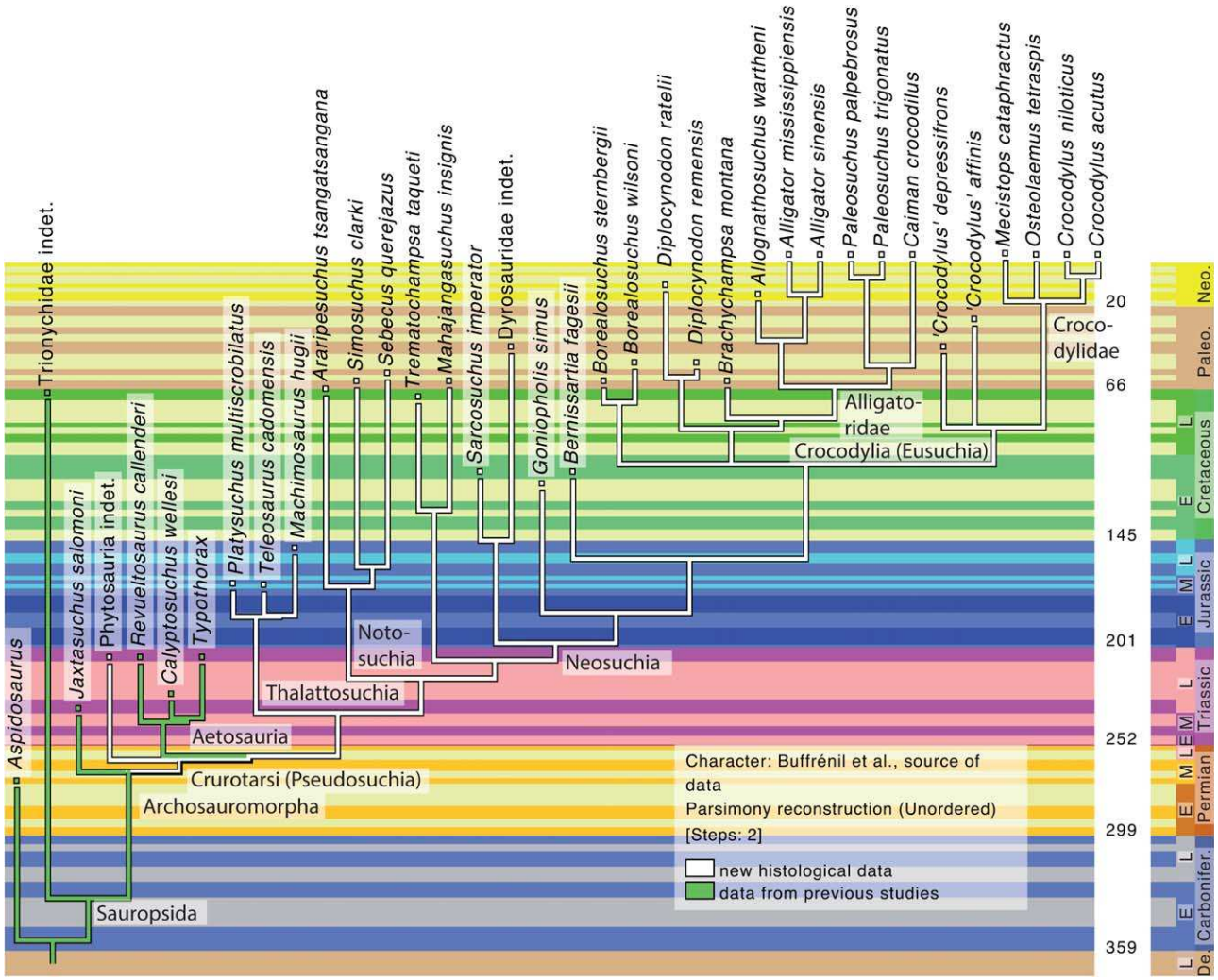

Fig. 1. Phylogenetic relationships among sampled taxa. A few taxa outside Archosauromorpha are included to better constrain the primitive condition for stegocephalians (limbed vertebrates) through parsimony optimization**.** These include the temnospondyl *Aspidosaurus* and an undetermined Cretaceous trionychid turtle. Histological information about these taxa is, respectively, from Witzmann and Soler-Gijón (2010), and from Scheyer et al. (2014). Geological timescale from Gradstein et al. (2012). Individual stages are shown, but not their names, for lack of space. E, early; M, middle; indet., indeterminate; L, late. Figure based on an edited screen capture of Mesquite (Maddison and Maddison, 2014) with the Stratigraphic Tools (Josse et al., 2006).

1991). In addition, one non-crocodyliform crurotarsan specimen, an undetermined phytosaur, was added to the sample to better polarize the characters. Phytosaurs, a Triassic clade (known from the Carnian to the Rhetian), are here considered to be the sister-group of all other crurotarsans (Brusatte et al., 2010), even though they have also been proposed to occupy a more basal position in archosauromorphs (Nesbitt, 2011). Our taxonomic sample should be representative of the major crocodyliform clades. However, two important gaps remain in the sample: the taxa located closest to the base of Crocodylomorpha, formerly called "protosuchians," from the Late Triassic to Early Jurassic, and the Metriorhynchidae, a clade of Jurassic and Early Cretaceous Neosuchia highly adapted to pelagic life. In both cases, bone ornamentation is poorly differentiated or absent, apparently because it was either incipient (Protosuchia) or regressed and lost (Metriorhynchidae). All other taxa display a typical, well differentiated, pit and ridge ornamentation on both skull roof (at least on the cranial table) and osteoderms. Figure 1 shows a time-calibrated phylogenetic tree of the sample. The nomenclature used for crocodilian taxa, as well as the preferred phylogenetic relationships, vary between authors. We adopt here the most recent and inclusive trees: Wilberg (2012) for Crocodylomorpha, Bronzati et al. (2012) for the whole clade of the Crocodyliformes, Buscalioni et al. (2011) for the Neosuchia, which contains all extant crocodilians, and Brochu (2000) for *Crocodylus* and extinct taxa that have been attributed to this genus. We completed the phylogeny using, on the one hand, more inclusive studies on phylogenetic relationships among the archosaurs (e.g., Brusatte et al., 2010; Nesbitt, 2011) and, on the other hand, detailed studies of relevant taxa, such as Delfino and Smith (2009) to determine the affinities of "*Crocodylus*" *depressifrons* (sometimes called *Asiatosuchus depressifrons*) and Brochu et al. (2012) for *Borealosuchus*.

In addition to the sample used for histology, nine frontal bones of *Trematochampsa taqueti* forming a growth series, and 12 entire skulls from seven extant species (Table 1) were examined for gross, qualitative morphological observations about the topographic features of bone ornamentation. In the species for which juvenile, subadult and adult growth stages were represented (*T. taqueti*, *Caiman crocodilus*, and *Crocodylus acutus*),

the frontal bone was further considered for morphometric information on the ontogenetic development of pit size.

As proposed by Witzmann et al. (2010), the deep, nonornamented side of bones or osteoderms will be called deep surface, or deep cortex, and the ornamented side superficial cortex, superficial face, or ornamented surface.

Basic Morphometry and Observations in Scanning Electronic Microscopy

In the species (including *T. taqueti*) for which juvenile and adult individuals were available, each frontal bone was photographed in dorsal view with precise scale indication for pit size measurements. The latter were restricted to the frontal, a bone that offered the most variable set of pit sizes. The two largest perpendicular diameters (D_1, D_2) of each pit on each frontal bone were measured directly on the computer screen using the image analyzer software Image J (National Institute of the Health). The photographs were enlarged (50×–100×), and the resulting accuracy of measurements was about $D \pm 10$ μm to $D \pm 20$ μm, depending on the original size of the frontal. Basic measurements were then transformed into a mean unitary pit diameter, D_u, for each pit ($D_u = [D_1+D_2]/2$), and a mean pit diameter, D, for each bone ($D = \sum_{1-n} D_u/n$). Usual statistical comparisons and tests were made with the software Prism (GraphPad Software, San Diego), considering a significance threshold of 0.05.

For detailed observations about the earliest differentiation stages of bone ornamentation, a set of 12 osteoderms from the neck and back region of a very young *Alligator mississippiensis* (unnumbered specimen in MNHN-AC collections; total skull length from snout to occipital condyle about 97 mm; mean dimensions of 10 dorsal osteoderms: 9.91 × 10.30 mm), and six osteoderms from a juvenile *Mecistops cataphractus* was observed in both classical microscopy and scanning electronic microscopy, using a Geol JMC-6000 Operated at 10 kV. Only moderate enlargement (200× at most) was necessary.

Histological Observations

All bones were embedded under vacuum in a polyester resin (bones from extant species were dehydrated and defatted in ethanol and acetone before embedding) and each was processed into three thin sections 100, 80, and 60 μm in thickness, following the classical procedures for this kind of preparations (e.g., Padian and Lamm, 2013). The sections were observed microscopically at low (25×) and medium (400×) power magnification, in ordinary or polarized transmitted light. The terminology used to describe bone microanatomy and histology follows Francillon-Vieillot et al. (1990). Soft tissue histology was not used in this study because our aim was to conduct a broad comparative survey including extant and extinct taxa. Moreover, with respect to the general subject of this study, we considered that the structural details displayed by bone matrix as interpreted in reference to the most classical and broadly acknowledge data on bone histology and growth (e.g., Hancox, 1972a; Francillon-Vieillot et al., 1990; Ricqlès et al., 1991; Hall, 2005) are relevant clues for deciphering bone growth patterns.

Experimental Study

In vivo labelling of bone growth was performed in two specimens of *Caiman crocodilus* and two of *Crocodylus niloticus*, originating from, and housed in, the Crocodile Farm of Pierrelatte, France, an institution habilitated under habilitation number DDPP A 26-101-1 (Direction Départementale des la Protection des Populations, Drôme, France) to handle, keep, breed protected reptile species, and conduct simple surgical operations and laboratory tests. These individuals represent the second (F2) generation born in captivity at the farm; the crocodiles being of source "C" (for captive), and the caimans of source "R" (custom seizure), according to CITES regulations (Convention on the International trade in Endangered Species of Fauna and Flora). Since they remained inside the French territory, these specimens or their products were not concerned by CITES or European (CIC) circulation permits. At the beginning of the experiment, they were aged about 1 year, and had snout-vent lengths of 333 and 368 mm, respectively, for the two caiman specimens, and 271 and 327 mm for the two crocodiles. Growing bones were labelled with two dyes, DCAF, the acronym for 2.7bis-[di(carboxymethyl) aminomethyl]-fluoresceïn, commonly called *Calceïn* (Merck, Germany), and alizarin sulfonate (Rhone Poulenc, Manchester, UK). According to classical procedures for reptiles (cf. Castanet and Naulleau, 1974; Castanet, 1982), these dyes were used in 1% solutions at a dose of 40 mg/kg for DCAF and 80 mg/kg for Alizarin. Injections were made in the abdominal cavity, and perfectly tolerated by the crocodiles. The first injection was DCAF. After a period of 194 days, one specimen of each species received Alizarin, and the other a second DCAF dose. One hundred thirty nine days after this injection, all specimens again received DCAF. At the time of each injection, the specimens were weighed, measured, and radiographed. One dorsal osteoderm was sampled under local anesthesia at the moment of the second and third injections and, at last, 83 days after the third injection. The total experiment thus lasted 416 days. Osteoderm sampling is a common method, used in crocodile population surveys for permanent individual labelling (e.g., Ross et al., 1994). Bleeding is very limited and healing occurs quickly. For the whole duration of this experiment, the crocodiles were housed under veterinarian control (by Dr. Samuel Martin, Doctor in veterinarian medicine, executive manager of Pierrelatte Crocodile Farm) in Pierrelatte Crocodile Farm in a pond 4 × 4 m (half area in water), with the same thermal and feeding conditions as for similar-sized animals in the farm. The 12 sampled osteoderms were cleaned with saline and enzyme solution (papain: 1g/L) raised to a temperature of 40° for 24 h and then immersed in warm soapy water for 1 h before rinsing and drying at room temperature, to remove flesh and skin residues. They were then dehydrated, defatted and subsequently treated as all other bone samples for making thin sections. The latter were observed in ultraviolet light (Zeiss Axioscop inverted microscope) and standard transmitted light, in addition to the other, classical modes of observation mentioned above. Only the biggest *Caiman crocodilus* was sacrificed at the end of the experiment for several studies in progress, including the sampling of ornamented skull bones.

Evolutionary Analyses

The timetree was compiled using Mesquite, with a geological timescale inserted using the Stratigraphic Tools (Josse et al., 2006). The characters were optimized onto the tree using parsimony to assess the primitive condition for Crurotarsi in terms of amount of dermal ornamentation and developmental mechanisms involved in the creation and growth of pits and ridges. Some comparative data published in previous studies (Witzmann and Soler-Gijón, 2010; Scheyer et al., 2012) and representing non-archosaurian taxa (one temnospondyl and one chelonian species) were also used for this optimization.

RESULTS

Anatomical Remarks

The external observation of entire skulls, isolated bones, and osteoderms reveals four basic characteristics of crocodilian ornamentation that are relevant for this work.

1. In subadult and adult specimens, ornamentation is continuous over the skull roof. It forms a consistent pattern that is not influenced by the limits of individual bones (Fig. 2A,B). This situation clearly differs from that displayed by

Fig. 2. Gross anatomical observations. (**A**) Dorsal view of the calvarium of *Paleosuchus trigonatus* (MNHN-AC 2014-1). The geometric features of bone ornamentation are homogeneous over the skull roof and are not influenced by the limits of the bones. (**B**) Anterior part of the skull table in an adult *Crocodylus acutus* (MNHN-AC 1944. 266). At least two large pits extend across the sutures between frontal (Fr.), parietal (Par.), and postorbitals (P-orb.). The thick arrow points to the anterior (cranial) direction. (**C**) Difference in pit size on the frontal bone between a juvenile (MNHN-F Ibc 25) and an adult (MNHN-F Ibc 11) *Trematochampsa taqueti*. Scale bars: 1 cm.

ornamented actinopterygian or several Permo-Carboniferous stegocephalian skulls in which each bone has its own ornamental pattern (Bystrow, 1935; Lehman, 1955; Piveteau and Deschaseaux, 1955a, b). In juvenile crocodilians, there is a faint influence of individual bone contours on the local design of bone ornamentation, but it soon disappears with growth.

2. As a consequence of Point 1, it is frequent to observe individual pits crossing sutures and extending on two (or more) adjacent bones (Fig. 2B).
3. In a given species, the absolute dimensions of pits increase during growth with the size of the bones that bear them. For example, in a growth series of nine entire frontal bones of *Trematochampsa taqueti* (Fig. 2C), mean pit diameter is 3.29 mm in the largest specimen (maximal width of frontal at the suture with postorbitals = 43.8 mm), and 2.01 mm in the smallest (maximal width of frontal 26.10 mm). This difference is highly significant (*t* test: $P < 0.0001$), whereas there is no significant difference for variance (*F* test: $P = 0.0764$).
4. The osteoderms of the very young *Alligator* and *Mecistops* specimens, observed with both light microscopy and scanning electron microscopy, show the early stages of bone ornamentation, at least on elements other than nuchal osteoderms (ornamentation is more precocious on neck than on back, flank, or belly osteoderms). The superficial, convex face of these osteoderms (the deep surface is concave) is smooth and devoid of sharp or protruding ridges (except for the longitudinal keel, when present); however, it displays numerous small pits 100–250 μm in diameter (Fig. 3A–C), corresponding to the superficial openings of inner neurovascular canals. Some of these small pits are strongly enlarged and deepened to form much broader circular depressions

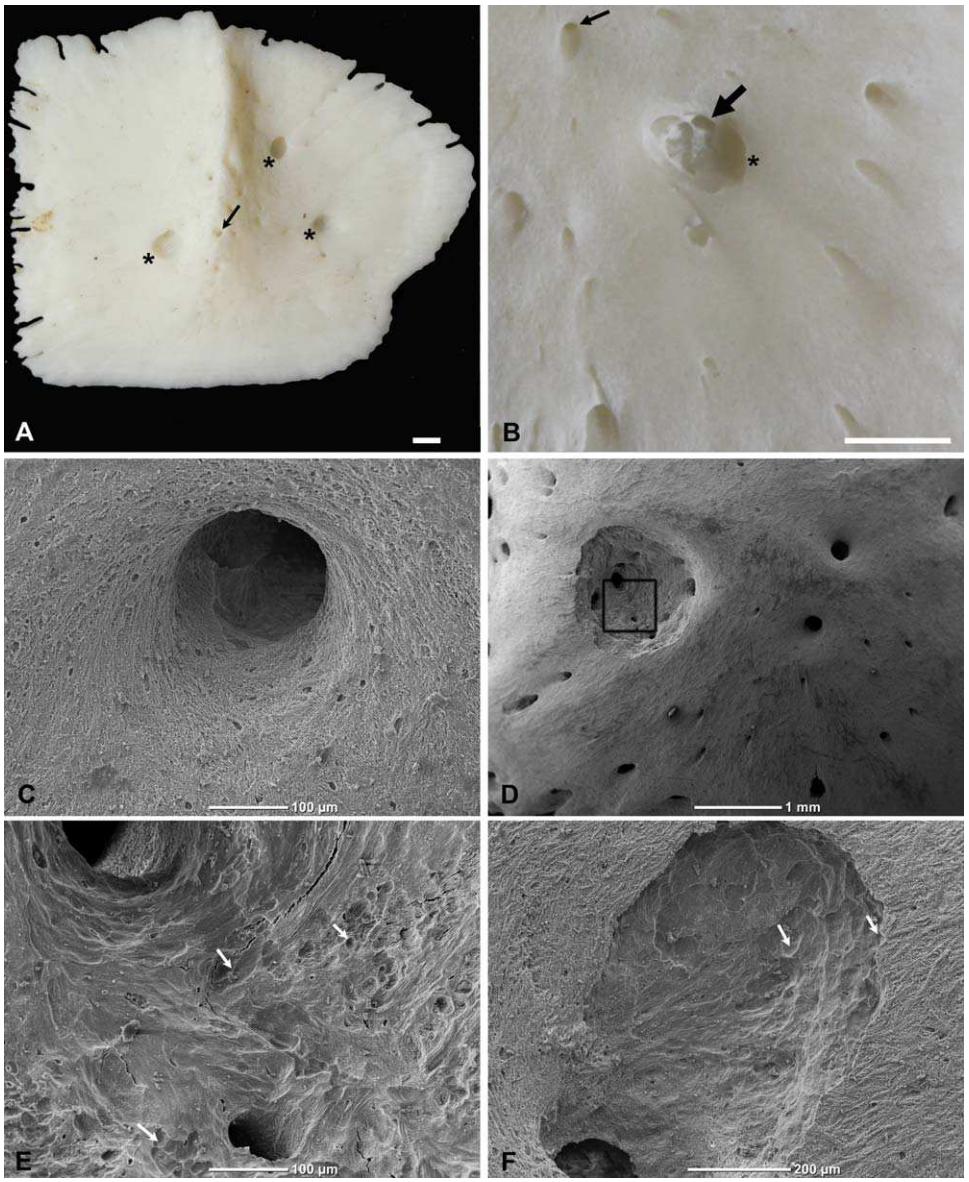

Fig. 3. Early formation of pits of the ornamentation on the osteoderms of young specimens of *A. mississippiensis* and *M. cataphractus*. (**A**) General view of the superficial cortex of a dorsal osteoderm in *M. cataphractus*. The cortical surface is basically smooth and flat with vascular pits (arrow) and few early ornamental pits (asterisks); however, no ridge is differentiated, except for the longitudinal (nonornamental) keel. (**B**) Detail of the superficial (convex) face of a young alligator osteoderm showing the early formation of a pit of the ornamentation (asterisk) around a vascular canal. The thin arrow points to an "ordinary" vascular pit, and the thick arrow points to the original vascular canal, whose superficial opening has been enlarged to form the ornamental pit. (**C**) Detail of an "ordinary" vascular pit with smooth edges devoid of any trace of resorption. (**D**) Initial pit of the ornamentation forming around vascular pits. Notice the crenellated edges of the ornamental pit. The rectangle shows the field illustrated in part E. (**E**) Detail of the wall of the pit of the ornamentation in an early developmental stage shown in Fig. D. The wall is entirely covered with Howship's lacunae (arrows) created by bone resorption. (**F**) Close view of the wall of a forming pit of the ornamentation on another osteoderm. Howship's lacunae are also present. Scale bars: A, B: 1 mm.

800 to 1200 µm in diameter (Fig. 3B,D–F). These large pits are apparently distributed at random on the bone surface. Moreover, they are generally not centered on the axis of the initial vascular pits, and their contours are irregular and crenellated (Fig. 3D–F), an aspect that results from the presence of typical Howship's lacunae. These enlarged pits are interpreted as the early differentiation stage of ornamental pits. As shown in Figure 3, they precede the formation of ridges; therefore, bone ornamentation, at least on osteoderms, would initially depend on the formation of hollow, rather than protruding, reliefs. In the three *Simosuchus clarki* osteoderms included in the sample, bone ornamentation is at an incipient differentiation

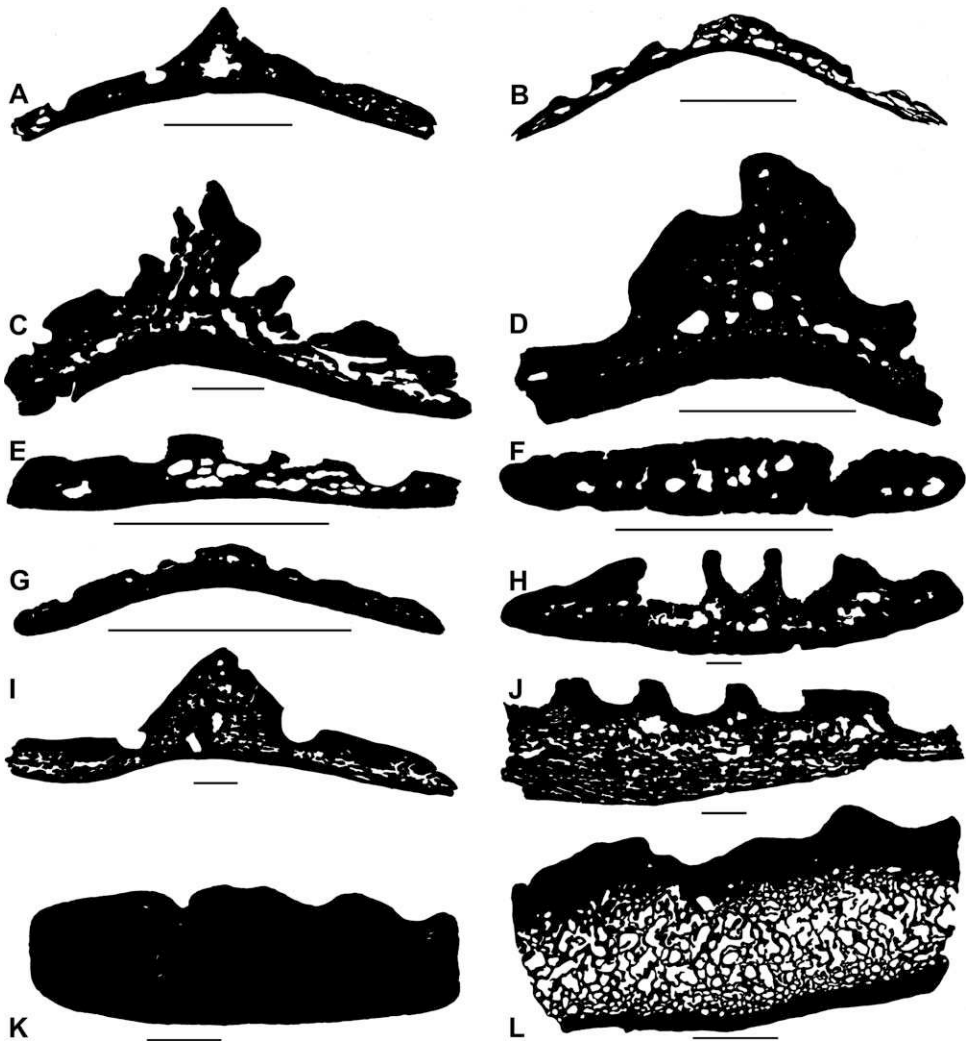

Fig. 4. Inner architecture of ornamented osteoderms viewed in cross section. (**A**) Nuchal osteoderm of a juvenile *A. mississippiensis*. (**B**) Nuchal osteoderm of a juvenile *Caiman crocodilus*. (**C**) Nuchal osteoderm of an adult *Diplocynodon remensis*. (**D**) Nuchal osteoderm of an adult *Allognathosuchus warteni*. (**E**) Dorsal osteoderm of a juvenile *Caiman crocodilus*. (**F**) Dorsal osteoderm of a juvenile *Mecistops* [*Crocodylus*] *cataphractus*. (**G**) Dorsal osteoderm of an adult *Araripesuchus tsangatsangana*. (**H**) Dorsal osteoderm of an adult *Sarcosuchus imperator*. (**I**) Dorsal osteoderm of an adult *Crocodylus niloticus*. (**J**) Dorsal osteoderm of an adult *Machimosaurus hugii*. (**K**) Osteoderm of a Dyrosaur from the Paleocene of Bolivia. (**L**) Osteoderm of an undetermined phytosaur showing a typical diploe architecture. Scale bars = 5 mm.

stage similar to that visible on the osteoderms of the young alligator specimen. This is also the case for all known *Simosuchus clarki* osteoderms, including the holotype (Hill, 2010), a specimen (UA 8679—University of Antananarivo) that undoubtedly represents an adult (Georgi and Krause, 2010). Ornamentation is also poorly characterized on skull bones (especially the maxilla, premaxilla, and dentary) in this taxon, as is also the case for several other small notosuchians (Kley et al., 2010).

These first three characteristics suggest that bone ornamentation in crocodiles is a dynamic feature, influenced by body size, and controlled by local osteogenic processes that are extrinsic to the bones considered individually and, at least, partly independent from their anatomical limits.

Microanatomical Observations

The inner architecture of ornamented bones, be they skull bones or osteoderms, as also their global compactness (Figs. 4 and 5), are variable, and the same skeletal elements can greatly differ in this respect within a single species. In general, inner cavities are concentrated in the core region of skull bones and osteoderms, but they seldom suffice to lower local compactness under the threshold of 50% considered to define cancellous tissue (Currey, 2002). In the frontal, for example, this situation was observed only in a juvenile alligator

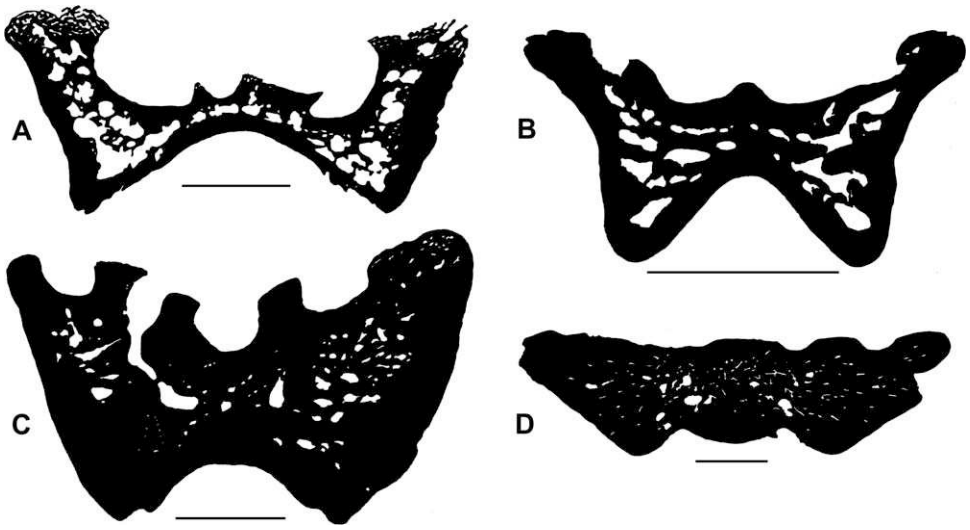

Fig. 5. Inner architecture of ornamented frontals viewed in cross section. (**A**) Frontal of a juvenile *A. mississippiensis*. (**B**) Frontal of a juvenile *Caiman crocodilus*. (**C**) Frontal of an adult *Diplocynodon ratelli*. (**D**) Frontal of an adult *Trematochampsa taqueti*. Scale bars: 5 mm.

(compactness of core region: 49.7%; cf. Fig. 5A), whereas the core region of the frontal in adult *Diplocynodon* (Fig. 5C) and *Trematochampsa* (Fig. 5D) is, respectively, 88.9 and 93.6%. The dyrosaur osteoderms (Fig. 4K) are remarkably compact with very few cavities more than 100 μm in diameter (mean core compactness ca. 99%), but numerous, regularly spaced, openings of narrow vascular canals some 50 μm, or less, in diameter (they actually correspond to the lumen of primary and secondary osteons). The deep and superficial cortices of ornamented bones are always highly compact (compactness >94%). In general, the global bone structure thus created by a relatively cancellous core associated with highly compact cortices is roughly reminiscent of a diploe, but this architecture is far from occurring in all individuals and all bones, and is clearly realized only in early juveniles and in the osteoderm of the phytosaur (Fig. 4L).

Histological Observations

The primary bone tissue occupying the core of all ornamented bones, be they osteoderms or skull bones, is monorefringent in polarized light (Fig. 6A), often strongly remodeled, and tends to persist in adults as remnants only, bordered by secondary plate-like deposits (Fig. 6A,B). It contains globular or multipolar osteocyte lacunae displaying a variable number of canaliculi, and distributed at random within the bone matrix (Fig. 6C). This set of histological features defines woven-fibered bone tissue. However, this tissue looks atypical, especially in osteoderms, because the monorefringence that it displays is irregular, due to the occurrence of thick, variably oriented, birefringent fiber bundles (Fig. 6D). In osteoderms, the bundles often cross orthogonally in a single plane, thus realizing a pattern reminiscent of a very regular basket weaving. When extensive resorption erodes the surface of the basal cortex in osteoderms, a fibrillar meshwork with this type of geometrical organization becomes apparent (Fig. 6E).

In skull bones and osteoderms, the inner cavities localized in the core region result from imbalanced remodeling of originally compact tissue, a process during which eroded bone tissue is not entirely compensated by reconstructive (or secondary) deposits (Fig. 6F). Local bone trabeculae display signs of intense remodeling, with a core made of preexisting primary tissue (that can be woven-fibered or parallel-fibered tissue), covered by platings of endosteal secondary deposits of lamellar bone (Fig. 6F,G). In the osteoderms and skull bones of some large specimens, intense, repeated remodeling of the core region results in nearly compact formations of dense Haversian tissue (Fig. 6H). No significant disparity was observed in the basic histological features of the core region of ornamented bones among the various taxa examined in this study, including the phytosaur.

Basal and superficial cortices in all ornamented bones are made of parallel-fibered bone tissue, typically characterized by a strong mass birefringence in polarized light (Fig. 7A,B), and the occurrence of flat or spindle-like osteocyte lacunae, all oriented parallel to the peripheral contour of the bones or to inner cortical layers, when the latter are underlined by cyclic growth marks (Fig. 7C). This tissue often turns into true lamellar bone, with all intermediate stages between these two

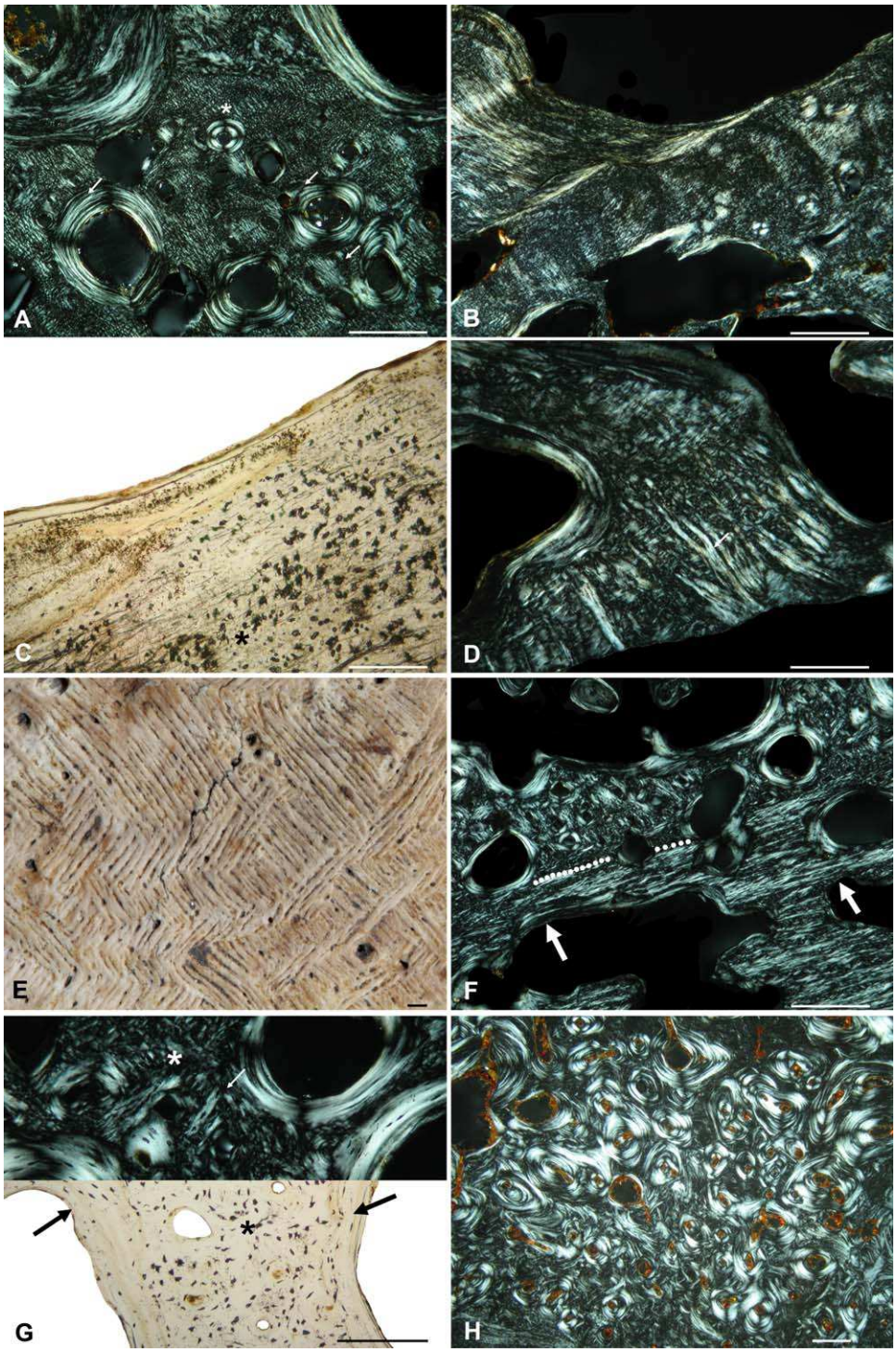

Fig. 6. Histology of the core region in ornamented bones (frontal and osteoderms). (**A**) *Borealosuchus sternbergii* osteoderm viewed in polarized light. The core of the osteoderm is occupied by an atypical woven-fibered tissue (asterisk) colonized by secondary osteons (arrows). (**B**) Frontal of *Diplocynondon ratelli* (cross section) in polarized light. (**C**) Woven-fibered bone (asterisk) in the frontal of *D. ratelii*. Ordinary transmitted light. (**D**) Woven-fibered tissue with thick, birefringent fiber bundles (arrow) in an osteoderm of *M.* [*Crocodylus*] *cataphractus*. Cross section in polarized light. (**E**) Superficial aspect of the basal cortex in an undetermined (most probably *Caiman*) specimen from the Pleistocene of Brazilian Amazonia. Bone resorption provoked the outcrop of a fiber meshwork similar in geometry to a basket weaving. (**F**) Transition between the core region and the deep part of the cortex in a *Teleosaurus cadomensis* osteoderm. The dotted lines indicate the limit between these two regions. The deep cortex is made cancellous by scattered resorption (thick arrows). Cross section in polarized light. (**G**) Remodeled bone trabecula in the core of *T. cadomensis* osteoderm. Upper half: polarized light; lower half: ordinary transmitted light. The core of the trabecula still retains the primary woven-fibered tissue (asterisks), while its periphery is covered by secondary layers of endosteal lamellar (arrows) tissue. (**H**) Dense Haversian tissue due to intense remodeling in the core of an osteoderm of *Trematochampsa taqueti*. Cross section in polarized light. Scale bars: 0.5 mm, except for part G (0.2 mm).

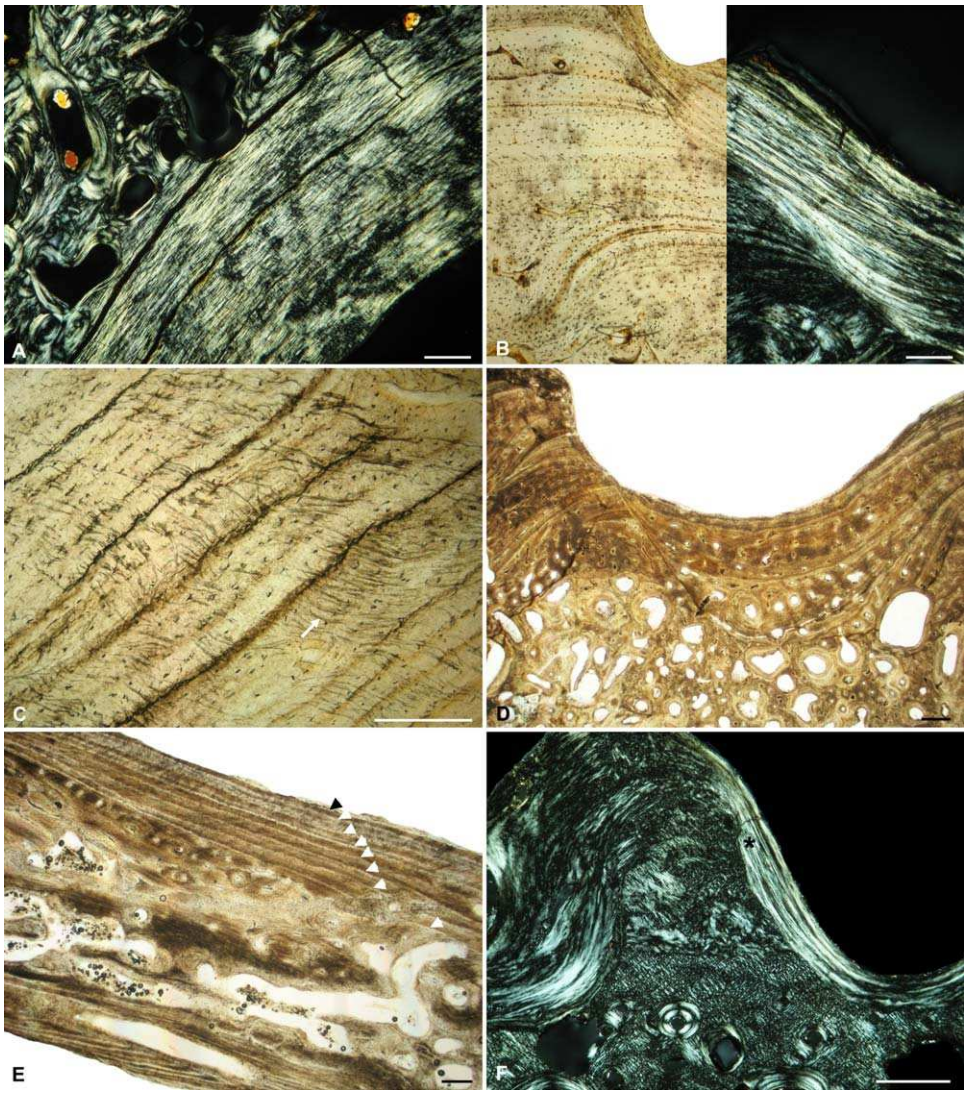

Fig. 7. General histology of the basal and superficial cortices in ornamented bones. (**A**) Cancellous, remodeled core region (upper left corner) and compact, non-remodeled basal cortex (lower right corner) made of birefringent parallel-fibered bone tissue, in a *Diplocynodon remensis* osteoderm. Cross section in polarized light. (**B**) Lamellar tissue forming the superficial cortex in the osteoderm shown on figure A. Left half: ordinary transmitted light; right half: polarized light. (**C**) Bundles of Sharpey's fibers (arrow) in the basal cortex of the *D. remensis* osteoderm. (**D**) Densely vascularized superficial cortex in an osteoderm from an undetermined crocodilian from the Cretaceous of Madagascar. (**E**) Cyclic growth marks in the superficial and basal cortices of a *Crocodylus niloticus* osteoderm. At least 8 growth marks are visible in the superficial cortex (arrow heads). The surface of the basal cortex had been submitted to erosion that was not followed by reconstruction. (**F**) Continuity of the superficial bone layer deposited on the walls of a pit (asterisk) and the layer capping the top of a ridge. Notice the modification of the histological characteristics of this layer from pit wall (the bone is highly birefringent) to ridge top (the bone is much less birefringent). Cross section in polarized light. Scale bars: 0.5 mm.

histological types. The only disparity observed among taxa for this tissue concerns the abundance of vascular canals, a feature that seems to be closely dependent on the size of the skeletal elements considered (Fig. 7D): cortical vascularization is dense in the largest taxa (e.g., *Sarcosuchus* or *Machimosaurus*), but absent in the smallest ones (e.g., *Osteolaemus*, *Paleosuchus*, *Bernissartia*, etc.). Cyclical growth marks, in the form of annuli or lines of arrested growth (Fig. 7C,E), are very frequent in the cortices of crurotarsan skull bones and osteoderms, although the sharpness of such marks is highly uneven among taxa. In all bones, superficial and basal cortices display short, but abundant Sharpey's fibers (Fig. 7C). Histologically, the transition between the woven-fibered tissue occupying the core of ornamented bones, and the parallel-fibered bone composing the cortices is often gradual (when it is not marked by a reversion line), and the deepest cortical layers display characteristics intermediate between these two kinds of osseous tissues (Fig. 7F).

In all the taxa examined in this study, basal and lateral cortices never show any sign of outer remodeling in the typical form of resorption and reconstruction cycles, although the surface of the basal cortex of some osteoderms (e.g., adult *Crocodylus niloticus* shown in Fig. 7E) displays evidence of extensive resorption not followed by reconstruction. Conversely, the superficial cortex of ornamented bones is always remodeled in direct topographical relationships with pits, grooves, and ridges (Fig. 8). This situation involves all the taxa composing the biological sample, including the phytosaur, with the exception of the osteoderms of *Simosuchus clarki* that do not display well-

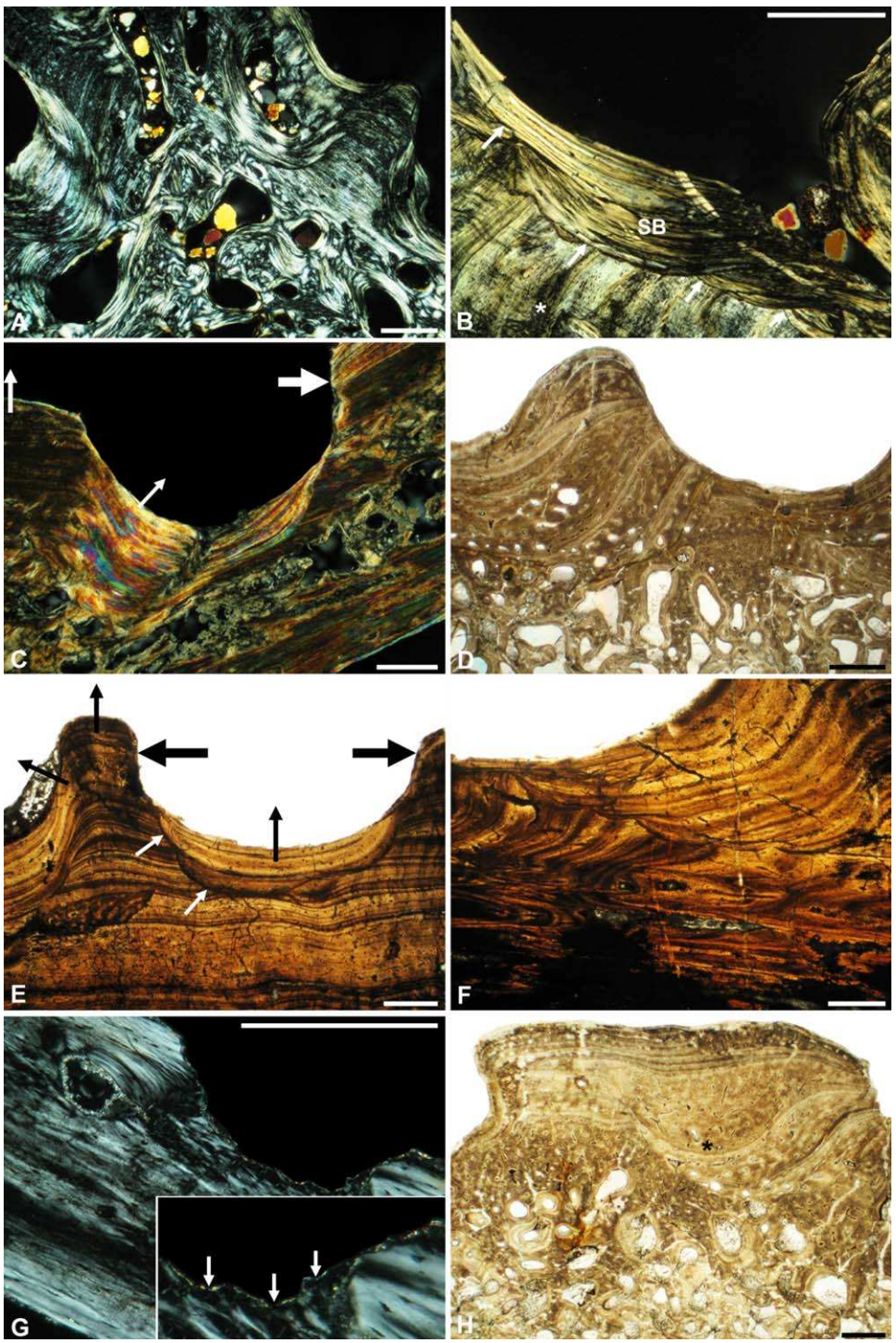

Fig. 8.

differentiated ornamentation; it should consequently be considered as a general characteristic of the crurotarsan taxa that were examined. A birefringent layer of parallel-fibered or lamellar tissues of variable thickness covers the bottom and walls of most ornamental pits (Fig. 8A–C). This layer is separated from subjacent bone tissues by a reversion line (also called cementing line; cf. Francillon-Vieillot et al., 1990), and can be distinguished from subjacent tissues by both a different histological structure and a discordant orientation (Fig. 8B,C,E,F). These features are obvious evidence that the lamellar (or parallel-fibered) layer is a secondary, reconstructive bone deposit, set in place after the end of a local resorption episode. The parts of pit bottom or walls that are not covered by this layer display Howship's lacunae (Fig. 8C,G), typically created by a resorption process that was still active by the time the animals died. In addition, the layers of primary bone tissue at this level are sharply eroded by the resorption process (Fig. 8C,D,G).

The location of secondary deposits, reversion lines, and traces of active bone resorption on the bottom and walls of pits can exhibit four main patterns briefly described below. Beyond minor differences mainly related to specific size, all Crurotarsi share similar characteristics on this aspect, at least for the skeletal elements examined in this study. Therefore, the following descriptions involve the sample as a whole.

1. Reversion lines, as also the secondary deposits located above them, can be centered relative to the axis of a pit (Fig. 8E). In this case, several reversion lines frequently occur (especially in large bones) under a single pit, one line marking the deepest (and most ancient) limit of the secondary bone deposit, and the others subdividing this deposit into several thinner strata set in place at different periods. In this case, the lines and the secondary bone deposits gradually increase in width from depth to surface, following the slope of pit walls. This situation obviously reflects the local occurrence of successive resorption—reconstruction cycles that, on the one hand, provided a progressive widening of pit diameter (resorption phase) and, on the other hand, maintained a similar proportion between pit depth and ridge height during growth (reconstruction deposits). This type of pit remodeling mainly occurs in the central part of bones or osteoderms.
2. In more lateral parts, secondary deposits can be off-centered. In this case, they always occur on the medial wall of the pits; the lateral wall then displays traces of surface resorption (Figs. 8C and 9D). Such a situation can also be traced in the depth of the bone cortex, and reveals a sequential migration of pit position that reflects bone growth (Fig. 8F), and that can be accompanied or not by a progressive deformation of the pits by stretching. Such an off-centered (or asymmetric) secondary reconstruction represents the most frequent remodeling pattern in pits. In this situation, secondary deposits are not limited to the bottom or walls of a pit; they also extend to the neighboring ridge (Fig. 8C,E). Therefore, during pit drift, the lateral wall of a ridge is reconstructed, while its medial wall undergoes resorption due to the drift of the preceding (medially situated) pit (Fig. 8C). As a consequence, ridges also migrate in pace with pits. Secondary, reconstructive bone deposits on pit bottom and walls are in continuity with local primary deposits on top of the neighboring ridges (situated in medial position) where no reversion line exist (Fig. 7F). The same bone deposit can, therefore, be considered secondary if present on the previously eroded bottom or walls of a pit, and primary if extending onto the neighboring ridge. The primary or secondary nature of this bone layer is thus dictated by topographic factors.

Fig. 8. Remodeling process of the superficial cortex. (**A**) Partial view (cross section in polarized light) of a *Diplocynodon remensis* osteoderm showing the complex processes of resorption and reconstruction that occur on the superficial cortex of crocodilian ornamented bones. (**B**) Typical aspect of bone remodeling on the superficial cortex in an osteoderm of *Crocodylus depressifrons* (cross section in polarized light): primary deposits (asterisk) are resorbed to form a pit whose walls are then covered with secondary lamellar or parallel-fibered bone (SB) bordered by one or several reversion (or cementing) lines (arrows). (**C**) Asymmetric (or off-centered) remodeling of the superficial cortex in an osteoderm of *Crocodylus niloticus* (cross section in polarized light). On this picture, the lateral (here, on the right) side of the pit was submitted to active resorption (thick arrow) when the animal died, while reconstruction (thin arrow) was proceeding on the medial (left) side and bottom of the pit. This is the general pattern in the ornamented bones of crocodilians. (**D**) Sharp resorption of the superficial cortex in an osteoderm of an unidentified Cretaceous crocodilian from Madagascar. (**E**) A case of centered pit remodeling in the frontal of *Crocodylus affinis*. At least two resorption/reconstruction cycles (which created two reversion lines: arrows) are visible and a third one, here at the erosion stage (thick arrows), was developing. The width of the pit was thus progressively increased from one cycle to another, while the bottom of the pit was sequentially elevated by secondary deposits compensating for the elevation of the ridges. The ridge on the left was rising, in continuity with the medial wall of the left pit (thin arrows). (**F**) Off-centered remodeling and progressive drift of a pit as traced in the depth of the superficial cortex in *C. affinis* frontal. (**G**) Recently excavated pit in an osteoderm of *Araripesuchus tsangatsangana* (cross section in polarized light). Pit bottom and walls are devoid of secondary deposits, but display Howhip's lacunae. Insert: enlargement (2 x compared with the rest of part G) of pit wall with arrows for Howship's lacunae. (**H**) Entire filling, and consecutive disappearance of a pit in an osteoderm of unknown Cretaceous crocodilian from Madagascar. The surface of the bone once bore a pit (asterisk) that was later eliminated by filling. A similar process is visible on part A, right upper part of the bone. Scale bars: 1 mm, except for G (0.5 mm).

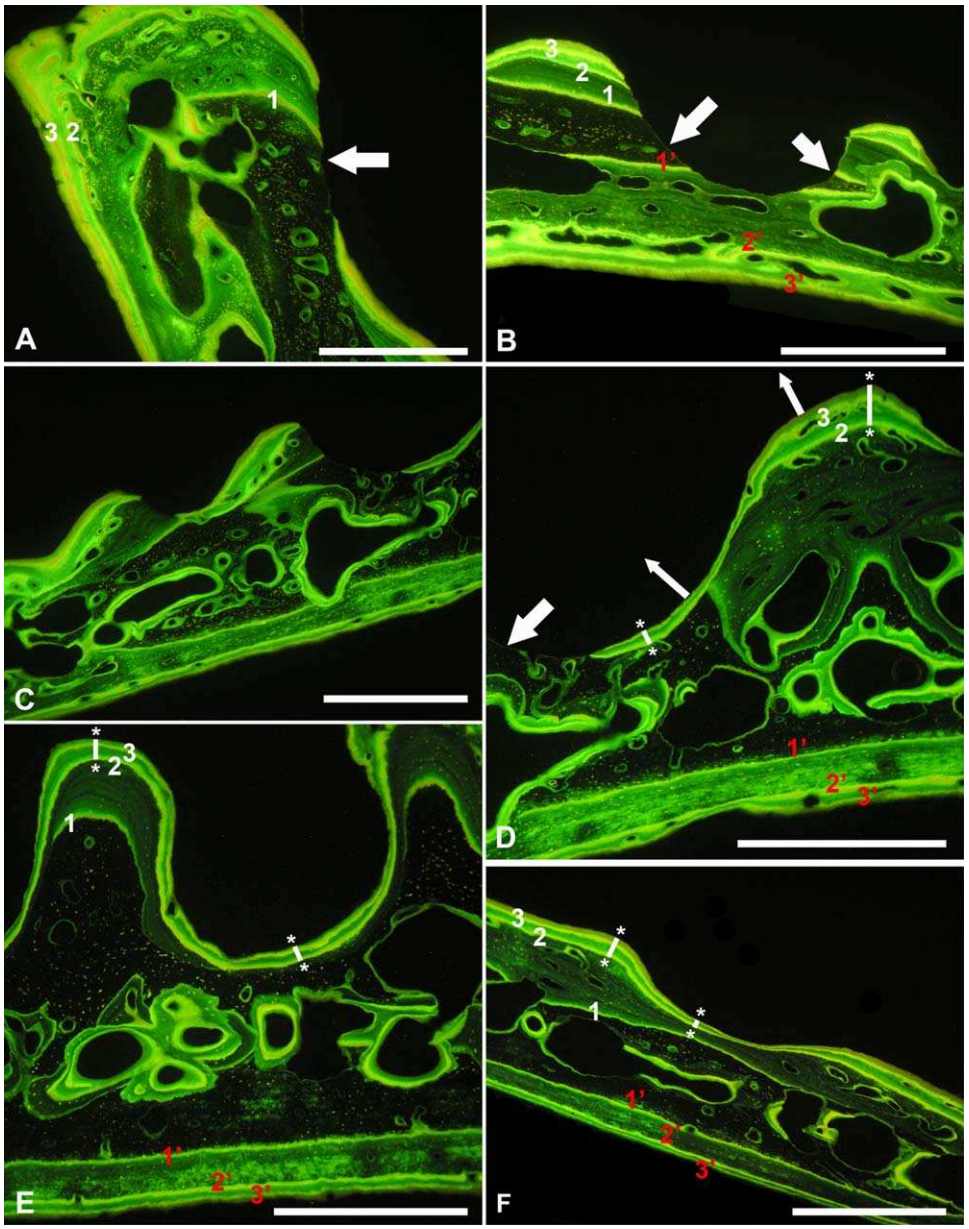

Fig. 9. In vivo labelling of bone growth in *Caiman crocodilus* (specimen FCP n° 8561). (**A**) Lateral side of the frontal. The three fluorescent labels (1, 2 and 3, following the chronological order of injections) are visible, as also an extended, active resorption front (thick arrow) that was sharply eroding the bone surface by the time the animal was sacrificed. (**B**) Dorsal osteoderm of the same specimen. A deep pit is created by resorption of the superficial cortex (thick arrows). Bone growth occurred on both the superficial cortex, as shown by the fluorescent labels 1, 2 and 3, and on the basal surface, with the corresponding labels 1′, 2′, and 3′. (**C**) Active remodeling of both the superficial, ornamented cortex, and the core of a dorsal osteoderm. The basal cortex remains untouched by inner or outer remodeling. Notice the asymmetric resorption and reconstruction process in the pits of the superficial cortex. (**D**) Closer view of the remodeling pattern that prevails on the superficial cortex. The left (lateral) side of the pit is under resorption (thick arrow), while primary (ridge) or secondary (pit wall) accretion is occurring on its medial side and on the neighboring ridge (thin arrows). The segments between asterisks indicate the places where the growth rate was measured. Notice that the first fluorescent label in the superficial cortex was erased by previous, extensive resorption. (**E**) Continuity of the primary bone deposits occurs on ridges with the secondary deposits covering the walls and bottom of the pits. Segments between asterisks have the same meaning as in part D. (**F**) Faint difference in the accretion rate of primary and secondary bone tissues between a crest and the neighboring pit in a dorsal osteoderm. Scale bars: 1 cm.

3. The bottom and walls of a given pit can be devoid of secondary deposits, and only display the traces of a recent resorption activity in the form of Howship's lacunae (Fig. 8G). This process creates new pits, especially (but not exclusively) in the peripheral regions of growing bones or osteoderms.
4. In some cases, the distribution of osseous layers in the depth of bone cortices shows that pits can

be entirely filled during growth, and thus cease to be visible on the cortical surface (Fig. 8A,H).

The spacing of growth marks and the histological nature of bone tissue can be used to infer and compare, at least qualitatively, local growth rates on bone cortices. In some specimens, or in some parts of a single bone, growth mark spacing indicates that the accretion rate is higher on the ridges than on the bottom or walls of the pits (e.g., Fig. 7F); however, this difference is relatively faint. In other specimens, there is no obvious difference in bone accretion rates between the ridges and the other parts of the cortices (Fig. 8E).

Results of In Vivo Bone Labelling

In vivo labelling of growing bones in *Caiman crocodilus* and *Crocodylus niloticus* confirm the observations mentioned above: pits are mainly created by a superficial resorption process that deeply notches the surface of dermal bones (Fig. 9A,B). This process can involve the entire surface of pit walls and bottom (Fig. 9B) or be limited to the lateral part of them, the medial part being in reconstruction (Fig. 9C,D). In the meantime, the core of the bones is submitted to intense remodeling biased toward resorption, through which compact formations (of woven-fibered tissue, mostly) are made cancellous (Fig. 9B–F). The result of these combined remodeling processes (outer and inner) is a complex structure, with several intermixed "waves" of resorption and reconstruction, accompanied by a general displacement (or drift) of bone reliefs and cavities. In the sections examined, accretion rate of primary bone deposits on top of the ridges is generally faster than the reconstructive part of the same deposits that occur on the walls and bottom of the pits. However, this difference is variable and rarely exceeds a 3-fold discrepancy: in Figure 9D, accretion rate between the date of the second injection and that of osteoderm sampling is 0.270 μm/day in the bottom of the pit, and 0.811 μm/day on top of the neighboring crest. These rates are, respectively, 0.248 and 0.676 μm/day on Figure 9E, and 0.171 and 0.563 μm/day on Figure 9F. The higher accretion rate generally observed on top of the ridges does not necessarily mean that local, instantaneous bone growth is accelerated at this level; it may merely reflect more continuous, uninterrupted growth (without resorption), which results in a globally average faster growth than in pits, where secondary, reconstructive deposits of lamellar or parallel-fibered bone occur after resorption episodes. These observations suggest that the contribution of the ridges in the differentiation of the superficial reliefs on ornamented bones is both variable and relatively minor in importance; the most important contribution is obviously the digging of pits through cortical resorption. Bone labelling also reveals that in osteoderms, the superficial cortex considered as a whole (as visible in its parts spared by resorption), can either grow faster (Fig. 9E,F) or more slowly (Fig. 9B) than the basal cortex.

DISCUSSION

Remarks on the Formation of Ornamented Bones

The formation of cranial ornamented bones, as described in detail by Vickaryous and Hall (2008) in *A. mississippiensis*, results from typical dermal osteogenesis, a process that basically relies on the activity of osteoblasts (derived from condensations of fibroblast-like cells). The formation of osteoderms involves a different process: they result from a direct mineralization of dermal connective tissue (metaplasia), at least in juveniles less than 200 mm SVL (Vickaryous and Hall, 2008). Reference to this peculiar osteogenic process has been made about the osteoderms of various taxa, including temnospondyls and chroniosuchians (Witzmann and Soler-Gijón, 2010; Buchwitz et al. 2012), squamates (Zylberberg and Castanet, 1985; Levrat-Calviac, 1986; Levrat-Calviac et al., 1986), dinosaurs (Ricqlès et al., 2001; Cerda and Powell, 2010), xenarthran mammals (Hill, 2006), and possibly some non-crocodilian crurotarsi (Scheyer and Desojo, 2011).

The results of this study suggest a complement to Vickaryous and Hall's (2008) interpretation of osteoderm morphogenesis. In crocodilian specimens less than 200 mm SVL, whatever their species, the development of osteoderms is at an incipient stage. If the existence of a metaplastic process at this stage is strongly evidenced by Vickaryous and Hall's histological observations, further osteoderm growth in subadult and adult specimens seems to involve a different osteogenic process. The general occurrence of a continuous, consistent layer of lamellar or parallel-fibered bone around the osteoderms, and especially in both their basal and superficial cortices, in all the specimens that we studied (ranging from juveniles to adults), suggests that osteoderms at these developmental stages are not composed mostly of metaplastic bone. This was expected because the fibrillar structure of the dermis varies with depth, as mentioned by Vickaryous and Hall (2008) in *Alligator*, or Levrat-Calviac and Zylberberg (1986) in squamates (see also Landmann, 1986). However, such differences in the geometric organization and density of collagen fibers are not reflected in osteoderm histology. This organization rather suggests that a population of active osteoblasts is involved in osteoderm growth at late ontogenetic stages. This conclusion is supported by the abundant secondary, endosteal deposits of lamellar bone tissue lining the inner cavities of the osteoderms (inner remodeling). Endosteal osteoblasts indeed

originate from the outer periphery of the bones and penetrate in their inner cavities via the walls of the vascular canals that open outside (Krstic, 1988; Karaplis, 2008). The observations made in this study suggest that crocodilian osteoderms may have a basic growth pattern similar to some extent to that attributed to the osteoderms of the Glytosaurinae, a group of extinct anguid squamates (Buffrénil et al., 2011): the formation of an initial nucleus of possible metaplasic origin, followed by the accretion of lamellar or parallel-fibered bone of osteoblastic origin (glyptosaur osteoderms also include a superficial hypermineralized tissue that does not exist in crocodilians). Though relatively frequent in tetrapods (see, e.g., Haines and Mohuiddin, 1968), metaplasia is not the unique or mandatory process involved in the development of osteoderms; it does not occur in the armadillo *Dasypus novemcinctus* (Vickaryous and Hall 2006), and possibly also in several extinct taxa: some temnospondyls such as *Gerrothorax* (Witzmann and Soler-Gijón 2010), pareiasaurs, a clade of parareptiles (Scheyer and Sander, 2009), the heavily armored aetosaurs, the Triassic archosauriforms, *Jaxtasuchus* and *Revueltosaurus* (Scheyer et al., 2014), and in most rauisuchians (Scheyer and Desojo, 2011).

Interpretation of Observations

The origin of bone ornamentation in *Alligator* was attributed by Vickaryous and Hall (2008) to a basic difference between the deep (nonornamented) and the superficial surfaces of ornamented skeletal elements: the former being smooth, while the latter displays rod-like protuberances or "spicules" which later develop into ridges through local (accelerated?) growth. However, the results of this study necessarily prompt a different interpretation.

Anatomical and histological observations converge to show that, in skull dermal bones, as well as in osteoderms, bone ornamentation is related to dynamic remodeling processes occurring during most of the course of postnatal skeletal growth. The latter is, at least potentially, indefinite in crocodilians (Andrews, 1982); therefore, the dynamic transformation of superficial bone reliefs would also be continuous. This basic result, evidenced by extensive histological and microanatomical observations and some experimental data, is beyond reasonable doubt. In all the taxa examined in this study, the simplest (or even the only possible) explanation for the histological observations presented above is that the development of bone ornamentation during ontogeny in crocodilians corresponds to the model developed below:

Whatever the process involved in the formation of the bones (membrane ossification vs metaplasia), the ornamentation is absent or indistinct in very young individuals, whose bones are initially smooth and only display minute openings of vascular canals and shallow depressions linked to them. Our observations in the young *Alligator* and *Mecistops* specimens suggest that, at the level of these depressions, bone resorption occurs and the superficial outcrops of vascular canals turn into much wider pits. Though osteoclasts have not been formally evidenced (this was not the aim of this study, and this was not possible with the methods used), the action of such cells, brought in situ by the blood vessels housed in the canals, can be indirectly inferred from the occurrence of Howship's lacunae on the walls of these initial pits. According to this interpretation, the earliest differentiation stage of bone ornamentation would thus be the creation of hollow reliefs by superficial cortical resorption. Of course, this hypothesis remains to be ascertained from further histological and cytological arguments. However, the occurrence of Howship's lacunae is classically considered as clear, uncontroversial evidence of recent bone resorption, even if the lacunae are not immediately associated with osteoclasts (see discussion of this point in, e.g., Hancox 1956, 1972b). Moreover, the obvious signs of bone resorption observed in the following growth stages reinforce the likelihood of this interpretation.

Histological observation and experimental bone labelling indeed show that, in later growth stages, the initial pits are permanently widened and deepened by a remodeling process involving repeated cycles of bone resorption and reconstruction. The resorption process is abundantly evidenced in all specimens by unquestionable histological clues, such as Howship's lacunae and reversion lines separating discordant bone deposits (see, e.g., syntheses in Enlow, 1963; Francillon-Vieillot et al., 1990). After resorption, the bottom and the walls of the pits are reconstructed, presumably though the activity of the osteoblast population surrounding the bone or osteoderm. Histological observations suggest that the formation of ridges does not prominently result from a local acceleration of bone growth, as compared to nonornamented cortical regions or to the reconstructed bottom and walls of the pits. Instead, to a large extent, the differentiation of ridges may rather represent a consequence of the resorption occurring in pits. In parallel with the combined resorption and reconstruction processes occurring over the ornamented surface of the bones, their core is submitted to a similar process, presumably involving the same cell populations: blood-born osteoclast precursors and endosteal osteoblasts deriving from osteoblasts situated outside the limits of calcified bone tissue (as mentioned above).

The observations presented in this study strongly suggest that pit and ridge remodeling actually results in an adaptation of pit size and

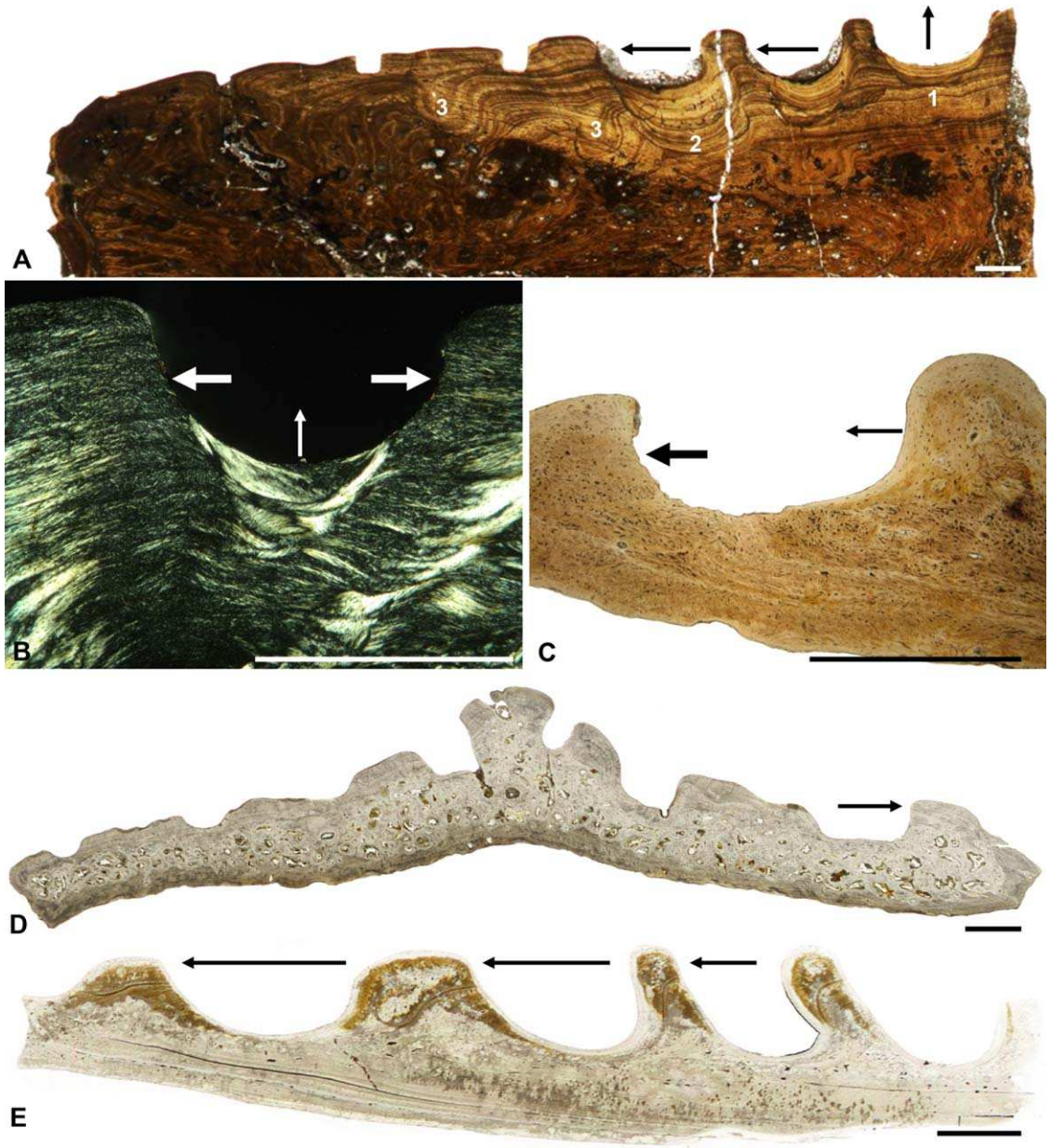

Fig. 10. Synthesis of the dynamic patterns in the remodeling of crocodilian ornamented cortices. (**A**) Three aspects of pit remodeling in a single cross section of the frontal of *Crocodylus affinis*. Pits can be simply enlarged and symmetrically reconstructed around their own axis (1); they can be submitted to asymmetric remodeling with lateral drift but no shape change (2); and they can also be filled and disappear (3). Ridges are also submitted to the same processes. (**B**) Other view of symmetrical pit enlargement: osteoderm of *Diplocynodon ratelii* in transmitted polarized light. (**C**) Asymmetric remodeling with change in pit shape. Fast resorption occurs on the lateral wall (thick arrow), and slower reconstruction on the medial wall (thin arrow). *Allognathosuchus wartheni* osteoderm. (**D**) Cross section in an osteoderm of *Diplocynodon ratelii*. The arrow indicates the stretching of a lateral pit. (**E**) Lateral drift of pits and ridges with progressive change in pit shape (*Borealosuchus sternbergii* osteoderm). Resorption (lateral walls of pits, on the left) is faster than reconstruction (medial wall), and pit shape is consequently stretched. Crests are also remodeled asymmetrically, with resorption on their medial side and reconstruction on their lateral side. Scale bars: 2 mm, except for part C (1 mm).

depth to the overall dimensions of the bones during growth. Starting from the initial formation of pits, this process remains active as long as growth proceeds, and can display five main aspects, summarized as follows and synthetically illustrated on Figure 10 (see also Figs. 8 and 9): 1) simple pit digging by local resorption of the superficial cortex (Figs. 8G and 9B). This process creates new pits, and consequently new ridges, mostly in the peripheral regions of growing bones or osteoderms. 2) Local, symmetric pit enlargement by resorption and reconstruction (Figs. 8E and 10A,B). This

process occurs in the central, that is, most ancient, region of bones and tends to extend toward bone periphery with decreasing growth rate. Pits remodeled this way do not migrate on the cortical surface. 3) Off-centered remodeling with maintenance of pit shape (Figs. 8C,F and 10A). In this situation, resorption rate on the lateral wall of pits, and reconstruction rate on their medial wall are balanced. Pits and ridges thus retain the same shape, but they tend to migrate toward the peripheral margins of the bones. 4) Off centered remodeling with modification of pit shape (Fig. 10C–E). Imbalance between fast resorption and slower reconstruction creates stretching of the pits that turn into grooves. This process is characteristic of the most peripheral regions of the bones. In later growth stages, peripheral regions are relocated more centrally, where growth rate in diameter (or width) drops to zero. In this situation, resorption on the lateral walls of pits ceases while reconstruction still proceeds on their medial walls. As a consequence, grooves become shorter, and finally recover the characteristic rounded shape of pits. The latter are themselves submitted to successive (mainly symmetric) episodes of resorption and reconstruction. 5) The combination of remodeling and drift processes can result in the total filling and superficial disappearance of pits. The latter nevertheless remain visible in cortical depth (through histological observation) if inner remodeling is locally mild (Figs. 8A,H and 10A).

This synthetic interpretation of our histological data on the structure of ornamented cortices shows that, beyond apparent geometric stability, bone ornamentation in Crocodilians is in permanent transformation through continuous remodeling processes. At all growth stages (especially in young, fast growing individuals), pits and ridges are created, stretched, displaced, enlarged, and finally filled, to be eventually dug up again by local resorption. This complex remodeling process must be considered in three dimensions because it occurs synchronously with, and thus integrates the constraints of, both the "horizontal" growth of the bones (i.e., expansion of peripheral limits parallel to the ornamented surface) and their "vertical" growth (growth in thickness perpendicular to that surface).

Our observations thus confirm the interpretation proposed by Buffrénil (1982). Of course, for the earliest differentiation stage of bone ornamentation, this interpretation differs from Vickaryous and Hall's (2008) alternative conclusion, according to which ornamentation is initiated by the development of ridges, as a result of preferential bone formation on preexisting spicules in very early developmental stages, around Ferguson's (1985, 1987) Stage 19. We cannot comment on the fate of these spicules; however, given that the osteoderms of the youngest specimens that we examined (well after Ferguson's last stage, 28) are smooth (with exception for minute vascular pits), these early spicules or incipient ornamentation apparently have no direct link with the ornamentation observed in subadult or adult crocodylomorphs.

Comparative and Phylogenetic Considerations

Very few studies were hitherto specifically conducted to tackle the morphogenetic processes involved in the formation and development of bone ornamentation in vertebrates, and still fewer in the crurotarsans or pseudosuchians. Among non-crocodyliform crurotarsans, the descriptions and illustrations by Scheyer et al. (2014) show that, in the aetosaurs *Calyptosuchus*, *Desmatosuchus*, *Tecovasuchus*, *Typothorax*, as also in other basal archosauriforms, such as *Revueltosuchus* and *Jaxtasuchus*, ornamented cortices show remodeling traces identical to those described here in the Crocodyliformes. Using the whole set of data available on this topic (Fig. 11), the parsimony character optimization reveals that the morphogenetic process that appears to occur in the crocodyliformes, that is, ornamentation developing through remodeling processes emphasizing resorption in pits, is likely to characterize all crurotarsans, and apparently first appeared in stem-archosaurs, as suggested by its presence in *Jaxtasuchus*. Thus, our data document a single appeareance of resorption-based bone ornamentation in reptiles. More distant relatives of archosaurs, araeoscelidians (Reisz, 1981; deBraga and Reisz, 1995) and most early synapsids (Laurin, 1993, 1994) generally lack bone ornamentation, other than vascular pitting. Ornamentation is less common in Avemetatarsalia, which includes dinosaurs (e.g., Sereno, 1991) and pterosaurs (Padian, 1984; Wellnhofer, 1987), but whenever it is present, our results suggest that its development must emphasize resorption in developing pits.

Conversely, histological data on other vertebrate groups, such as turtles (Scheyer et al., 2012), temnospondyls (Witzmann and Soler-Gijón, 2010), and placoderms (Giles et al., 2013) that bear ornamentation superficially similar to the crocodiles', suggest that the morphogenetic interpretation developed above is not applicable to most other vertebrates: in these taxa, ornamentation develops chiefly through deposition on the ridges, whereas pits represent a passive consequence of this process, and this appears to be the primitive condition for stegocephalians (Fig. 11). When the osteogenic mechanisms controlling the development of bone ornamentation are taken into account, the striking phenotypic similarity in ornamentation between crurotarsans and other vertebrates should be considered as a mere convergence. This intriguing question calls for a broader investigation in all

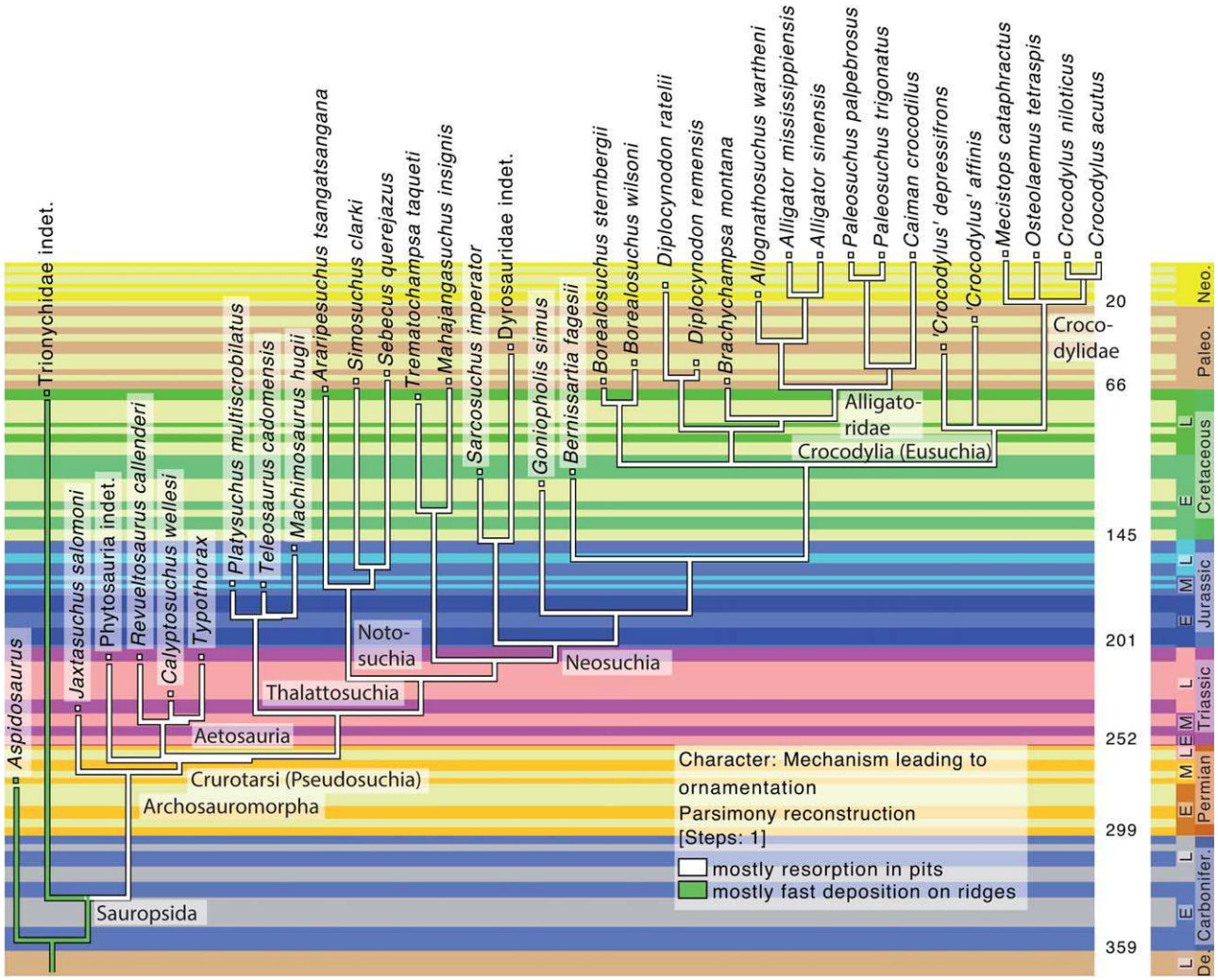

Fig. 11. Parsimony optimization showing the evolution of the morphogenetic process responsible for the development of ornamentation in stegocephalians (limbed vertebrates). For more explanations, see Figure 1.

vertebrate groups displaying the pit and crest (honeycomb) type of ornamentation.

ACKNOWLEDGMENTS

The authors are extremely grateful to all the colleagues who generously accepted to give or facilitate access to extant or fossil bone samples for this study: France de Lapparent de Broin (MNHN, Paris, France), Annelise Folie (IRSNB, Bruxelles, Belgium), Kevin Padian (UC, Berkeley, USA), David Krause (Stony Brook University, New York, USA), Rainer Schoch (SMNS, Stuttgart, Germany), Jean-François Tournepiche (Angoulème Museum, France), Christian de Muizon (MNHN, Paris), and Salvador Bailon (MNHN, Paris). The authors also thank Hayat Lamrous (UPMC, Paris) and Vincent Rommevaux (MNHN, Paris) for their technical collaboration. The manuscript of this study has been greatly improved by the remarks and suggestions of Chris Brochu and two anonymous referees.

LITERATURE CITED

Andrews RM. 1982. Patterns of growth in Reptiles. In: Gans C, Bellairs A. d'A and Parsons TS, editors. Biology of the Reptilia. Vol. 13. London: Academic Press. pp 273–319.

Brochu CA. 2000. Phylogenetic relationships and divergence timing of *Crocodylus* based on morphology and the fossil record. Copeia 3:657–673.

Brochu CA, Parris DC, Grandstaff BS, Denton Jr RK, Gallagher WB. 2012. A new species of *Borealosuchus* (Crocodyliformes, Eusuchia) from the Late Cretaceous–early Paleogene of New Jersey. J Vertebr Paleontol 32:105–116.

Bronzati M, Chinaglia-Montefeltro F, Langer MC. 2012. A species level supertree of the crocodyliformes. Hist Biol 24:598–606.

Brusatte SL, Benton MJ, Desojo JB, Langer MC. 2010. The higher-level phylogeny of Archosauria (Tetrapoda : Diapsida). J Syst Paleontol 8:3–47.

Buchwitz M, Witzmann F, Voigt S, Golubev V. 2012. Osteoderm microstructure indicates the presence of a crocodylian-like trunk bracing system in a group of armoured basal tetrapods. Acta Zool 93:260–280.

Buffetaut E. 1991. Fossil crocodilians from Tiupampa, (Santa Lucia Formation, Early Paleocene) Bolivia: a preliminary report. Revista Técnica de YPFB, Fosiles y Facies da Bolivia, I. Vertebrados 12:541–544.

Buffetaut E, Marshall LG. 1991. A new crocodilian, *Sebecus querejazus*, nov. sp. (Mesosuchia, Sebecidae) from the Santa Lucia formation (Early Paleocene) at Vila Vila, southcentral Bolivia. Revista Técnica de YPFB, Fosiles y Facies da Bolivia, I. Vertebrados 12:545–557.

Buffrénil V de. 1982. Morphogenesis of bone ornamentation in extant and extinct crocodilians. Zoomorphology 99:155–166.

Buffrénil V de, Rage J-C, Dauphin Y, and Sire J-Y. 2011. An enamel-like tissue, osteodermine, on the osteoderms of a fossil anguid (Glyptosaurine) lizard. CR Palevol 10:427–438.

Buscalioni AD, Piras P, Vullo R, Signore M, Barbera C. 2011. Early Eusuchia Crocodylomorpha from the vertebrate-rich Plattenkalk of Pietraroia (Lower Albian, Southern Appenines, Italy). Zool J Linn Soc 163:S199–S227.

Bystrow AP. 1935. Morphologische Untersuchungen der Deckknochen des Schädels der Wirbeltiere. I. Mitteilung—Schädel der Stegocephalen. Acta zool Stockh 16:65–141.

Castanet J. 1982. Recherches sur la croissance du tissu osseux des reptiles. Application : la méthode squelettochronologique. PhD thesis, University Paris 7, Paris (France), June 1982.

Castanet J, Naulleau G. 1974. Données expérimentales sur la valeur des marques squelettiques comme indicateur de l'âge chez *Vipera aspis* (L.) (Ophidia, Viperidae). Zool Scripta 3: 201–208.

Cerda IA, Powell JE. 2010. Dermal armor histology of *Saltasaurus loricatus*, an Upper Cretaceous sauropod dinosaur from Northwest Argentina. Acta Palaeontol Polonica 55:389–398.

Clack JA. 2002. The dermal skull roof of *Acanthostega gunnari*, an early tetrapod from the Late Devonian. Trans R Soc Edinburgh Earth Sci 93:17–33.

Currey JD. 2002. Bones. Structure and mechanics. Princeton: Princeton University Press. 436 p.

deBraga M, Reisz RR. 1995. A new diapsid reptile from the uppermost Carboniferous (Stephanian) of Kansas. Palaeontology 38:199–212.

Delfino M, Smith T. 2009. A reassessment of the morphology and taxonomic status of '*Crocodylus' depressifrons* Blainville, 1855 (Crocodylia, Crocodyloidea) based on the Early Eocene remains from Belgium. Zool J Linn Soc 156:140–167.

Daeschler EB, Shubin NH, Jenkins FA. 2006. A Devonian tetrapod-like fish and the evolution of the tetrapod body plan. Nature 440: 757–763.

Enlow DH. 1963. Principles of Bone Remodeling. Springfield, IL: Charles C. Thomas. 131 p.

Ferguson MW. 1985. Reproductive biology and embryology of the crocodilians. In: Gans C, BIllet F, Maderson PFA (Eds.), Biology of the Reptilia. Academic Press, New York, pp 329–491.

Ferguson M. 1987. Post-laying stages of embryonic development for crocodilians. In: Webb GJW, Manolis C, Whitehead PJ (Eds.), Wildlife management: crocodiles and alligators. Surrey Beatty and Sons, Sydney, pp 427–444.

Francillon-Vieillot H, Buffrénil V de, Castanet J, Géraudie J, Meunier FJ, Sire J-Y, Zylberberg L, Ricqlès A de. 1990. Microstructure and mineraliszation of vertebrate skeletal tissues. In: Carter JG, editor. Skeletal Biomineralization: Patterns, Processes and Evolutionary Trends. Vol.1. New York: Van Nostrand Reinhold. pp 471–530.

Giles S, Rücklin M, Donogue PCJ. 2013. Histology of « Placoderm » dermal skeletons: Implication for the nature of the ancestral gnathostome. J Morphol 274:627–644.

Georgi JA, Krause DW. 2010. Postcranial axial skeleton of *Simosuchus clarki* (Crocodyliformes: Notosuchia) from the Late Cretaceous of Madagascar. J Vertebr Paleontol 30 (suppl. to issue 6):99–121.

Gradstein FM, Ogg JG, Schmitz M, Ogg G, editors. 2012. The Geologic Time Scale 2012. Amsterdam: Elsevier, 1176 pp.

Grande L, Bemis WE. 1998. A comprehensive phylogenetic study of amiid fishes (Amiidae) based on comparative skeletal anatomy. An empirical search for interconnected patterns of natural history. J Vertebr Paleontol 18 (Memoir 4, suppl. to issue 1): 688 p.

Haines RW, Mohuiddin A. 1968. Metaplastic bone. J Anat 103: 527–538.

Hall BK. 2005. Bones and cartilage: developmental and evolutionary skeletal biology. Amsterdam: Academic Press.

Hancox NM. 1956. The osteoclast. In: Bourne GH, editor. The Biochemistry and Physiology of Bone. New York: Academic Press. pp 213–250.

Hancox NM. 1972a. Biology of Bone. In: Harrison RJ, McMinn RMH, editors. Biological structure and function. Cambridge: Cambridge University Press. 199 p.

Hancox NM. 1972b. The osteoclast. In: Bourne GH, editor. The Biochemistry and Physiology of Bone, 2nd ed. Vol. 1: Structure. New York: Academic Press. pp 45–67.

Hill RV. 2006. Comparative anatomy and histology of xenarthran osteoderms. J Morphol 267: 1441–1460.

Hill RV. 2010. Osteoderms of *Simosuchus clarki* (Crocodyliformes: Nothosuchia) from the Late Cretaceous of Madagascar. J Vertebr Paleontol 30 (suppl. to issue 6):154–176.

Hoffstetter R. 1955. Squamates de type moderne. In: Piveteau J, editor. Traité de Paléontologie. Vol. 5: Squamates de type moderne. Paris: Masson et C^{ie}. pp 604–664.

Janvier P, Martin M. 1979. Les vertébrés Dévoniens de l'Iran central. II—Coelacanthiformes, Struniiformes, Ostéolépiformes. Geobios 12:497–511.

Josse S, Moreau T, Laurin M. 2006. Stratigraphic tools for Mesquite. Available at: http://mesquiteproject.org/packages/stratigraphicTools/.

Kälin J. 1955. Crocodilia. In: Piveteau J, editor. Traité de Paléontologie. Vol. 5. Paris: Masson et C^{ie}. pp 695–784.

Karaplis AC. 2008. Embryonic development of bone and regulation of intramembranous and endochondral bone formation. In: Belezikian JP, Raisz G, Martin TJ, editors. Principles of Bone Biology. Vol. 1. Amsterdam: Academic Press. pp 53–84.

Kley NJ, Sertich JW, Turner AH, Krause DW, O'Connor PM, Georgi JA. 2010. Craniofacial morphology of *Simosuchus clarki* (Crocodyliformes: Nothosuchia) from the Late Cretaceous of Madagascar. J Vertebr Paleontol 30 (suppl 1):13–98.

Krstic RV. 1988. Atlas d'histologie générale. Paris: Masson. 404 p.

Landmann L. 1986. Chapter 9: Epidermis and dermis. In: Bereiter-Hahn J, Matoltsy AG, Richards KS, editors. Biology of the Integument. Vol. 2: Vertebrates. Part IV: The skin of reptiles. Berlin: Springer-Verlag. pp 150–187.

Laurin M. 1993. Anatomy and relationships of *Haptodus garnettensis*, a Pennsylvanian synapsid from Kansas. J Vertebr Paleontol 13:200–229.

Laurin M. 1994. Re-evaluation of *Cutleria wilmarthi*, an Early Permian synapsid from Colorado. J Vertebr Paleontol 14(1): 134–138.

Laurin M, Soler-Gijón R. 2006. The oldest known stegocephalian (Sarcopterygii: Temnospondyli) from Spain. J Vertebr Paleontol 26:284–299.

Lehman J-P. 1955. Rachitomi. In: Piveteau J., editor. Traité de Paléontologie. Vol. 5: Amphibien Reptiles, Oiseaux. Paris: Masson et C^{ie}. pp 67–125.

Levrat-Calviac V. 1986. Etude comparée des ostéodermes de *Tarentola mauritanica* et de *T. neglecta* (Gekkonidae, Squamata). Arch Anat Microsc Morphol Exp 75:29–43.

Levrat-Calviac V, Zylberberg L. 1986. The structure of the osteoderms in the gekko: *Tarentola mauritanica*. Am J Anat 176:437–446.

Levrat-Calviac V, Castanet J, Zylberberg L. 1986. The structure of the osteoderms in two lizards: *Tarentola mauritanica* and *Anguis fragilis*. In: Roček Z., editor. Studies in Herpetology. Prague. pp 341–344.

Lingham-Soliar T. 2014. The Vertebrate Integument. Heidelberg: Springer. 268 pp.
Maddison WP, Maddison DR. 2014. Mesquite: A modular system for evolutionary analysis. Version 3.0. Available at: http://mesquiteproject.org.
Märss T. 2006. Exoskeletal ultrasculpture of early vertebrates. J Vertebr Paleontol 26:235–252.
Martin JE, Smith T, de Lapparent de Broin F, Escuillié F, Delfino M. 2014. Late Paleocene eusuchian remains from Mont de Berru, France and the origin of the alligatoroid *Diplocynodon*. Zool J Linn Soc 172:867–891.
Nesbitt SJ. 2011. The early evolution of archosaurs: relationships and the origin of major clades. Bull Am Mus Nat Hist 352:1–292.
Novitskaya L. 1971. Les amphiaspides (Heterostraci) du Dévonien de la Sibérie. In: Lehman JP, editor. Cahiers de paléontologie Paris: Centre National de la Recherche Scientifique. 130 p.
Padian K. 1984. Pterosaur remains from the Kayenta formation (?Early Jurassic) of Arizona. Palaeontology 27:407–413.
Padian K, Lamm E-T. 2013. Bone Histology of Fossil Tetrapods. Berkeley: University of California Press. 285 p.
Piveteau J, Deschaseaux C. 1955a. Trematosauria. In: Piveteau J, editor. Traité de Paléontologie. Vol. 5: Amphibien Reptiles, Oiseaux. Paris: Masson et C^{ie}. pp 126–135.
Piveteau J, Deschaseaux C. 1955b. Stereospondyli. In: Piveteau J, editor. Traité de Paléontologie. Vol. 5: Amphibien Reptiles, Oiseaux. Paris: Masson et C^{ie}. pp 136–172.
Reisz RR. 1981. A diapsid reptile from the Pennsylvanian of Kansas. Univ Kans Publs Mus nat Hist 7:1–74.
Ricqlès A de, Meunier FJ, Castanet J, Francillon-Vieillot H. 1991. Comparative microstructure of bone. In: Hall BK, editor. Bone. London: CRC Press. pp 1–78.
Ricqlès A de, Pereda-Suberbiola X, Gasparini Z, Olivero E. 2001. Histology of dermal ossifications in an ankylosaurian dinosaur from the Late Cretaceous of Antarctica. Assoc Paleontol Argentina. Publ espec. 7:171–174.
Ross, P, Buffrénil V de, Ramos R. 1994. CITES crocodile survey of Zapata swamp, Cuba: current status of *Crocodylus rhombifer*, the Cuban crocodile. Genève: Secrétariat de la CITES. 26 pp.
Scheyer TM, Desojo JB. 2011. Palaeohistology and external microanatomy of Rauisuchian osteoderms (Archosauria: Pseudosuchia). Palaeontology 54:1289–1302.
Scheyer TM, Sander PM. 2009. Bone microstructure and mode of skeletogenesis in osteoderms of three pareiasaur taxa from the Permian of South Africa. J Evol Biol 22:1153–1162.
Scheyer TM, Mörs T, Einarsson E. 2012. First record of softshelled turtle (Cryptodira: Trionychidae) from the late cretaceous of Europe. J Vertebr Paleontol 32:1027–1032.
Scheyer TM, Desojo JB, Cerda IA. 2014. Bone histology of phytosaur, aetosaur, and other archosauriform osteoderms (Eureptilia, Archosauromorpha). Anat Rec 297:240–260.
Schultze H-P, Arsenault M. 1985. The panderichthyid fish *Elpistostege*: A close relative of tetrapods? Palaeontology 28: 293–309.
Sereno PC. 1991. *Lesothosaurus*, "fabrosaurids," and the early evolution of Ornithischia. J Vertebr Paleontol 11:168–197.
Vickaryous MK, Hall BK. 2006. Osteoderm morphology and development in the nine-banded armadillo, *Dasypus novemcinctus* (Mammalia, Xenarthra, Cingulata). J Morphol 267: 1273–1283.
Vickaryous MK, Hall BK. 2008. Development of the dermal skeleton in *Alligator mississippiensis* (Archosauria, Crocodilia) with comments on the homology of osteoderms. J Morphol 269:398–422.
Vorobyeva EI, Schultze H-P. 1991. Description and systematics of panderichthyid fishes with comments on their relationship to tetrapods. In Schultze H-P, Trueb L, editors. Origins of Higher Groups of Tetrapods. Ithaca: Comstock Publishing Associates. pp 68–109.
Wilberg EW. 2012. Phylogenetic and morphometric assessment of the evolution of the longirostrine crocodylomorphs [PhD]: University of Iowa. 250 p.
Wellnhofer P. 1987. New crested pterosaurs from the lower cretaceous of Brazil. Mitt Bayer Staatsslg Paläont Hist Geol 27: 175–186.
Witzmann F, Soler-Gijón R. 2010. The bone histology of osteoderms in temnospondyl amphibians and in the chroniosuchian *Bystrowiella*. Acta Zool (Stockh.) 91:96–114.
Witzmann F, Scholz H, Müller J, Kardjilov N. 2010. Sculpture and vascularization of dermal bones, and the implications for the physiology of basal tetrapods. Zool J Linn Soc 160:302–340.
Young GC. 2009. An Ordovician vertebrate from western New South Wales, with comments on Cambro-Ordovician vertebrate distribution patterns. Alcheringa 33:79–89.
Zylberberg L, Castanet J. 1985. New data on the structure and the growth of the osteoderms in the reptile *Anguis fragilis* L. (Anguidae, Squamata). J Morphol 186:327–342.
Zylberberg L, Meunier FJ, Laurin M. 2010. A microanatomical and histological study of the postcranial dermal skeleton in the Devonian sarcopterygian *Eusthenopteron foordi*. Acta Palaeont Pol 55:459–470.

JOURNAL OF MORPHOLOGY 277:634–670 (2016)

Comparative Data on the Differentiation and Growth of Bone Ornamentation in Gnathostomes (Chordata: Vertebrata)

Vivian de Buffrénil,[1] François Clarac,[2] Aurore Canoville,[3]* and Michel Laurin[1]

[1]*CR2P (UMR 7207), CNRS/MNHN/UPMC, Département Histoire de la Terre, Muséum National d'histoire Naturelle, Bâtiment de Géologie CC 48, 57 Rue Cuvier F-75231, Paris, Cedex 05, France*
[2]*UPMC Université Paris 06, UMR 7193, Institut des Sciences de la Terre Paris (ISTeP), Sorbonne Universités, 4 Place Jussieu, BC 19, F-75005, Paris, France*
[3]*Steinmann Institute for Geology, Mineralogy and Paleontology, Bonn University, Nußallee 8, Bonn 53115, Germany*

ABSTRACT Bone ornamentation, in the form of rounded pits framed by a network of ridges, is a frequent feature among a great diversity of gnathostome taxa. However, the basic osteogenic processes controlling the differentiation and development of these reliefs remain controversial. The present study is a broad comparative survey of this question with the classical methods used in hard tissue histology and paleohistology. Distinct processes, unevenly distributed among taxa, are involved in the creation and growth of pits and ridges. The simplest one is mere differential growth between pit bottom (slow growth) and ridge top (faster growth). The involvement of several complex remodeling processes, with the local succession of resorption and reconstruction cycles, is frequent and occurs in all major gnathostome clades. Some broad, inclusive clades (e.g., Temnospondyli) display consistency in the mechanisms controlling ornamentation, whereas other clades (e.g., Actinopterygii) are characterized by the diversity of the mechanisms involved. If osteogenic mechanisms are taken into account, bone ornamentation should be considered as a character extremely prone to homoplasy. Maximum likelihood (ML) optimizations reveal that the plesiomorphic mechanism creating ornamentation is differential apposition rate over pits (slow growth) and ridges (faster growth). In some taxas e.g., temnospondyls vs lissamphibians or pseudosuchians, bone ornamentation is likely to be a homoplastic feature due to a convergence process driven by similar selective pressures. ML models of character evolution suggest that the presence of resorption in the development of ornamentation may be selectively advantageous, although support for this conclusion is only moderate. J. Morphol. 277:634–670, 2016. © 2016 Wiley Periodicals, Inc.

KEY WORDS: dermal bone; pits; ridges; histology; bone accretion; bone remodeling

INTRODUCTION

The occurrence of ornamentation (also called sculpture) on the outer surface of the skull roof, mandible, osteoderms and dermal elements of the pectoral girdle, is a common feature in vertebrates (e.g., Vickaryous and Sire, 2009; Witzmann, 2009). It can display diverse aspects, the most common of which, observed in a considerable series of forms, from the Devonian arthrodire placoderms (Miles, 1967; Downs and Donoghue, 2009) to extant archosaurs (Buffrénil et al., 2015), is a pattern of densely-packed pits separated by a network of ridges. These reliefs then form a repetitive motif showing either a honeycomb-like pattern, e.g., the postorbital part of skull roof in crocodiles (Clarac et al., 2015) and the carapace of some turtles, or a partly radiating structure formed by both pits and sub-parallel or slightly divergent grooves framed by ridges, like on the dermal bones of actinopterygians (Lehmann, 1966) and temnospondyls (Bystrow, 1935; Schoch and Milner, 2000, 2014; Witzmann et al., 2010). Considering its striking morphological consistency through time and taxa, this particular type of ornamentation could be viewed as the typical example of a plesiomorphic trait, highly conservative in its morphology. However, the osteogenic mechanisms from which it results seem to be different at least in two groups: the temnospondyls and the pseudosuchians. In the former, ornamentation is supposed to be due to preferential bone accretion on top of the crests (Witzmann, 2009; Witzmann and Soler-Gijón, 2010), a situation shared by the placoderms according to the illustrations found in Downs and Donoghue (2009) and Giles et al. (2013). Conversely, in pseudosuchians, it is mainly created by the excavation of the pits through local bone resorption (Buffrénil et al., 2015; Cerda et al., 2015a). This discrepancy suggests an obvious hypothesis: beyond a superficial phenotypic similarity, ornamentation may not be homologous in all taxa because it involves distinct processes, and might

*Correspondence to: Aurore Canoville; Steinmann Institute for Geology, Mineralogy and Paleontology, Bonn University, Nußallee 8, Bonn 53115, Germany. E-mail: canoville.aurore08@gmail.com

Received 10 December 2015; Revised 10 February 2016;
Accepted 12 February 2016.

Published online 10 March 2016 in
Wiley Online Library (wileyonlinelibrary.com).
DOI 10.1002/jmor.20525

have appeared several times in the gnathostomes, through independent, but convergent, evolutionary processes, and under similar selective pressures. This possibility raises the question of the function of bone ornamentation.

In terms of ontogenetic development and growth, the remodeling process involved in the Sphenosuchia as interpreted by Buffrénil (1982) and Buffrénil et al. (2015) is flexible, and prone to quickly adjust pit and ridge dimensions and positions to the overall size of the bones or to any other morphological requirement. Geometrically, this process is submitted to few constraints because of its capacity to erase existing reliefs (either by resorption of crests or by complete filling of depressions) and replace them by new ones. Preferential apposition on ridges looks a priori more constrained in its potentialities because the transformation of bone ornamentation during growth must necessarily be based on, and thus respect, the topography and geometry of pre-existing reliefs. Up to now, very few studies considered this puzzling question specifically, and mentions of it remain anecdotal (e.g., Witzmann and Soler-Gijón, 2010).

This study is intended to present a broad comparative review (based on both original and previously published data) about the osteogenic mechanisms involved in the creation and growth of the reliefs that constitute the pit-and-ridge type of bone ornamentation in gnathostomes. In reference to the results obtained on this topic (and to similar data available in literature and substantiated by clear photographs), the aim is to assess which mechanism produced bone ornamentation in early gnathostomes, especially in actinopterygians, dipnomorphs, and stegocephalians (defined in Laurin [1998], i.e. the largest clade that includes temnospondyls but not panderichthyids; this includes all limbed vertebrates, and possibly a few vertebrates that may have retained paired fins), and how that mechanism changed over time. We also try to determine if one mechanism appears to have a selective advantage over the other. To a lesser extent, our findings have implications about the homology (or lack thereof) of the ornamentation found in various taxa.

MATERIAL AND METHODS

Biological Sample

The biological sample (Table 1) consists of 39 bone samples representing 33 species (12 are nonidentified), distributed in 32 identified genera, 27 families and 12 orders of gnathostomes, according to most recent works that used rank-based nomenclature (we are aware of the subjective nature of these ranks: e.g., Laurin, 2008). Due to sample accessibility, some taxa displaying the pit and ridge ornamentation are not represented in the sample (e.g., early gnathostomes such as the placoderms are lacking). We nevertheless consider that the phylogenetic structure of this sample is an acceptable approximation of the taxonomic diversity of the pit and ridge ornamentation in osteichthyans. Figure 1 shows the ornamental patterns displayed by most of the taxa included in the sample. Collected bones include elements from the skull roof and shoulder girdle, and thus represent typical membrane bones, as well as osteoderms. Both are considered equivalent for the study of the osteogenic processes controlling ornamentation. Bone histology in some of the taxa used in this study has already been described by other authors, especially Florian Witzmann (2009; see also Witzmann and Soler-Gijòn, 2010) for the temnospondyls and Torsten Scheyer (e.g., Scheyer et al., 2012) for the turtles. We nevertheless present additional observations on these taxa since our attention was focussed on very specific details presented according to a relatively standardized framework.

Sample Processing and Histological Observations

For preparing the samples (extant or fossil) into thin sections, the classical techniques used in comparative bone histology (e.g., Lamm, 2013) were employed. Bones from extant taxa were dehydrated in progressive alcohol baths (70 to 100 degrees) and defatted in acetone, while the fossils where simply cleared of sediments when necessary. After photography, all bone samples were embedded in a polyester resin and cut into slices 1 to 3 mm thick. The latter were polished on one side and glued on glass slides to be finally ground into sections 100 μm (± 20 μm) thick. Several sections with varying orientations (e.g., transversal, sagittal) were performed for each bone according to its morphology, in order to assess structural details that depend on sectional orientation such as the morphology of osteocyte lacunae or the refringence properties of the bone matrix in polarized light. Observations were made with a Zeiss Axioskop 40 microscope, equipped for polarization. Measurements of bone compactness (i.e., actual area occupied by bone tissue expressed as a percent of total sectional area) were performed on digitized images of the sections with the software ImageJ (National Institute of the Health, USA). All the sections are presently housed and numbered in the HISTOS collection of the Muséum National d'Histoire Naturelle, Paris, France.

Basic Clues for Interpreting Relative Bone Growth Rates

The interpretations developed in this study are based on an assessment, at least in relative terms, of the rate of local bone accretion from the fine structure of the osseous tissue. For this purpose we refer, on the one hand, to the typology and nomenclature of bone tissues proposed by Francillon-Vieillot et al. (1990) and, on the other hand, to the results of experimental studies on the relationships between growth rate and bone structure (e.g., Amprino, 1947; Castanet et al., 1996, 2000; Margerie et al., 2002, 2004; Cubo et al., 2012; Kolb et al., 2015), which are broadly acknowledged, as shown by the fact that they have been used to infer growth rates in extinct taxa (e.g., Padian, 2013; Amson et al., 2015). In brief, apposition rate positively influences the three following features of bone tissue, and is grossly correlated with them:

1. Degree of birefringence of the intercellular collagenous matrix. Low birefringence, or *a fortiori* complete monorefringence, reveals a poorly structured collagen meshwork, that is, the "woven-fibered" matrix. This is a typical trait of fast-growing periosteal cortices (growth speed: 15–170 μm/day, according to Castanet et al., 1996, 2000; Margerie et al., 2002, 2004). When growth rate decreases, bone matrix progressively turns into the "parallel-fibered" organization that provokes a "mass birefringence" in polarized light, and corresponds to growth speeds of 2–20 μm/day (Margerie et al., 2002). With further decrease in growth speed, bone matrix becomes "lamellar", with a subdivision into strata of some 3–5 μm in thickness that appear alternatively dark and illuminated in polarized light. Each stratum is composed of parallel-fibered tissue, but the directions of the fibres in adjacent strata are approximately orthogonal. Corresponding growth rates are 0.2–2.5 μm/day (Margerie et al., 2002).

TABLE 1. Biological and paleontological samples used in this study

Higher taxon	Family	Genus	Species	Bone	Geol. age	Coll. number
ACTINOPTERYGII						
Acipenseriformes	Acipenseridae	*Acipenser*	*sturio*	Opercular	Extant	UPMC-JYS. A.s. 2
Neopterygii						
Siluriformes	Pimelodidae	*Phractocephalus*	*hemioliopterus*	Opercular	Extant	MAE-USP. PN 13-831-4
Siluriformes	Ariidae	*Sciades*	*proops*	Opercular	Extant	MNHN-AC/ET. 0018
Osteoglossiformes	Osteoglossidae	*Arapaima*	*gigas*	Opercular	Extant	MNHN-AC/ET. 0034
SARCOPTERYGII						
Porolepiformes	Holoptychidae	*Holoptychius*	*quebecensis*	Scute	U. Dev.	MNHN-F. no number
Stegocephali						
Temnospondyli	Eryopidae	*Eryops*	*megacephalus*	Indet. skull bone	E. Perm.	UPMC-AR.I1/b35
Temnospondyli	Trimerorachidae	*Trimerorachis*	*insignis*	Indet. skull bone	E. Perm.	UPMC-AR.I1/b2
Temnospondyli	Peltobatrachidae	*Peltobatrachus*	sp.	Osteoderm	U. Perm.	MNHN-F. no number
Temnospondyli	Archegosauridae	*Platyoposaurus*	sp.	Indet. skull bone	U. Perm.	UPMC-AR.I2/b11
Temnospondyli	Benthosuchidae	*Benthosuchus*	*sushkini*	Indet. skull bones	E. Trias.	UPMC-AR. I2/b12
Temnospondyli	Metoposauridae	*Dutuitosaurus*	*ouazzoui*	Jug., interclav.	U. Trias.	MNHN-F. AZA 395
Temnospondyli	Metoposauridae	Indet.	sp.	Indet. skull bone	U. Trias.	UPMC-AR. I2/b3
Temnospondyli	Capitosauridae?	*Kupferzellia*	sp.	Postpar.	M. Trias.	SMNS 54673
Temnospondyli	Mastodonsauridae	*Mastodonsaurus*	sp.	Par.	M. Trias.	SMNS 81063
Temnospondyli	Mastodonsauridae	*Parotosuchus*	sp.	Indet. skull bone	E. Trias.	MNHN-F. R13.Z16
Temnospondyli	Plagiosauridae	*Plagiosternum*	sp.	Interclav.	M. Trias.	SMNS No number
Temnospondyli	Plagiosauridae	*Plagiosuchus*	sp.	Postpar.	M. Trias.	SMNS 91040
Temnospondyli	Capitosauridae	*Stanocephalosaurus*	sp.	Indet. skull bones	M. Trias.	MNHN-F. Zar. 41, 59, 63
Embolomeri	Archeriidae	*Archeria*	sp.	Osteoderm	E. Perm.	UPMC-R. I1/b30
Chroniosuchia	Bystrowianidae	*Bystrowiana*	cf. *permiria*	Indet. skull bone	U. Perm.	UPMC-AR. I2/b18
Nectridea	Keraterpetontidae	*Diplocaulus*	sp.	Indet. skull bones	E. Perm.	UPMC-AR. I1/b20-22
Anura	Ceratophryidae	*Ceratophrys*	*cornuta*	Skull roof	Extant	MNHN-F.GR 21
Anura	Natatanura	*Thomastosaurus*.	*gezei*	Max., Fr-Par., Sq.	U. Eoc.	MNHN-F. MALP.1-3
Anura	Alytidae	*Latonia*	*gigantea*	Fr-par., max.	M. Mioc.	MNHN-F. Sa 23489, 23468
Amniota						
Sauropsida	Captorhinidae	*Captorhinus*	*aguti*	Indet. skull bones	E. Perm.	UPMC-AR. I4/b6
Testudines	Trionychidae	*Amyda*	*cartilaginea*	Carapace plate	Extant	MHNL 50.000.1357
Testudines	Trionychidae	*Trionyx*	*triunguis*	Carapace plate	Extant	MNHN-AC.1889.384
Testudines	Trionychidae	*Trionyx*	*triunguis* foss.	Carapace plate	Pleist.	MNHN-F. MN 16
Testudines	Trionychidae	*Aspideretoides*	cf. *riabinini*	Carapace plate	U. Cret.	MNHN-F. no number
Testudines	Trionychidae	*Cyclanorbis*	*senegalensis*	Carapace plate	Extant	MNHN-F. AR 76
Testudines	Emydidae	*Pseudemys*	*rubriventris*	Carapace plate	Extant	MNHN-F. no number
Testudines	Araripemydidae	*Araripemys*	*barretoi*	Carapace plate	E. Cret.	MNHN-F. no number
Squamata	Necrosauridae	*Necrosaurus*	*cayluxensis*	Osteoderms	Eoc.	MNHN-F. QUER.4
Synapsida	Edaphosauridae	*Lupeosaurus*	*kayi*	Indet. skull bone	E. Perm.	UPMC-AR. I7/b8

Meaning of the abbreviations: MAE-USP. PN: Museo de Arqueologia de Universidade de São Paulo – Paraná; MHNL: musée des Confluences, centre de conservation et d'étude des collections, Lyon, France; MNHN-AC, or F: Collections of comparative anatomy (AC) or vertebrate paleontology (F) of the Muséum National d'Histoire Naturelle (Paris, France); SMNS: Staatlisches Museum Naturkunde Stuttgart (Germany); UPMC-AR: Armand de Ricqlès' collections in Université Pierre et Marie Curie (Paris, France); UPMC-JYS: Jean-Yves Sire's collection in Université Pierre et Marie Curie (Paris, France). Abbreviations for geological ages: Dev.: Devonian; E: Early; Eoc.: Eocene; M: Middle; Mioc.: Miocene; Perm.: Permian, Pleist.: Pleistocene; Trias.: Triassic, and U: Upper. Abbreviations for bones sampled: Fr-Par.: fronto-parietal; Interclav.: interclavicle; Jug.: jugal; Max.: maxillary; Par.: parietal; Postpar.: postparietal; Sq.: squamosal; Indet.: undetermined.
Some of our material was labeled as "*Cricotus* sp.," but we follow Holmes (1989) in considering *Cricotus* as a synonym of *Archeria*. Similarly, one of our turtle specimens was registered as *Palaeotrionyx*, a name now considered synonym of *Aspideretoides* cf. *riabinini* (Danilov and Vitek, 2013).

Matrix structure changes gradually from the woven-fibered to the lamellar types when bone depositional rate decreases.
2. Aspect of cell lacunae. Globular or multipolar cell lacunae that may display abundant canaliculi (but this condition is not mandatory) are associated with woven-fibered matrices and thus indicative of fast-growing cortical bone. Conversely, spindle-like or flat cell lacunae (with variable canalicular development) are typically encountered in parallel-fibered or lamellar tissues, and therefore reveal relatively slow growing bone.
3. The density of vascular canals is positively correlated with appositional rate, and can reflect localized acceleration or deceleration of periosteal accretion (Castanet et al., 1996; Margerie et al., 2002, 2004). Moreover, the orientation of the canals (longitudinal, oblique, radial, etc.) is also linked to bone growth rates, but with apparently more complex, and still incompletely elucidated, interactions (cf. Margerie et al., 2002); this is why this last feature (canal orientation) will not be considered in this study. Morphologically, simple vascular canals, when cut transversely, are easily distinguished from cell lacunae, or other possible "holes" contained in bone matrix, by their diameter that is most often larger than 10 μm and their sharp and smooth contour. When cut obliquely or longitudinally, they appear like sharply defined tubes that cannot be confused with anything else.

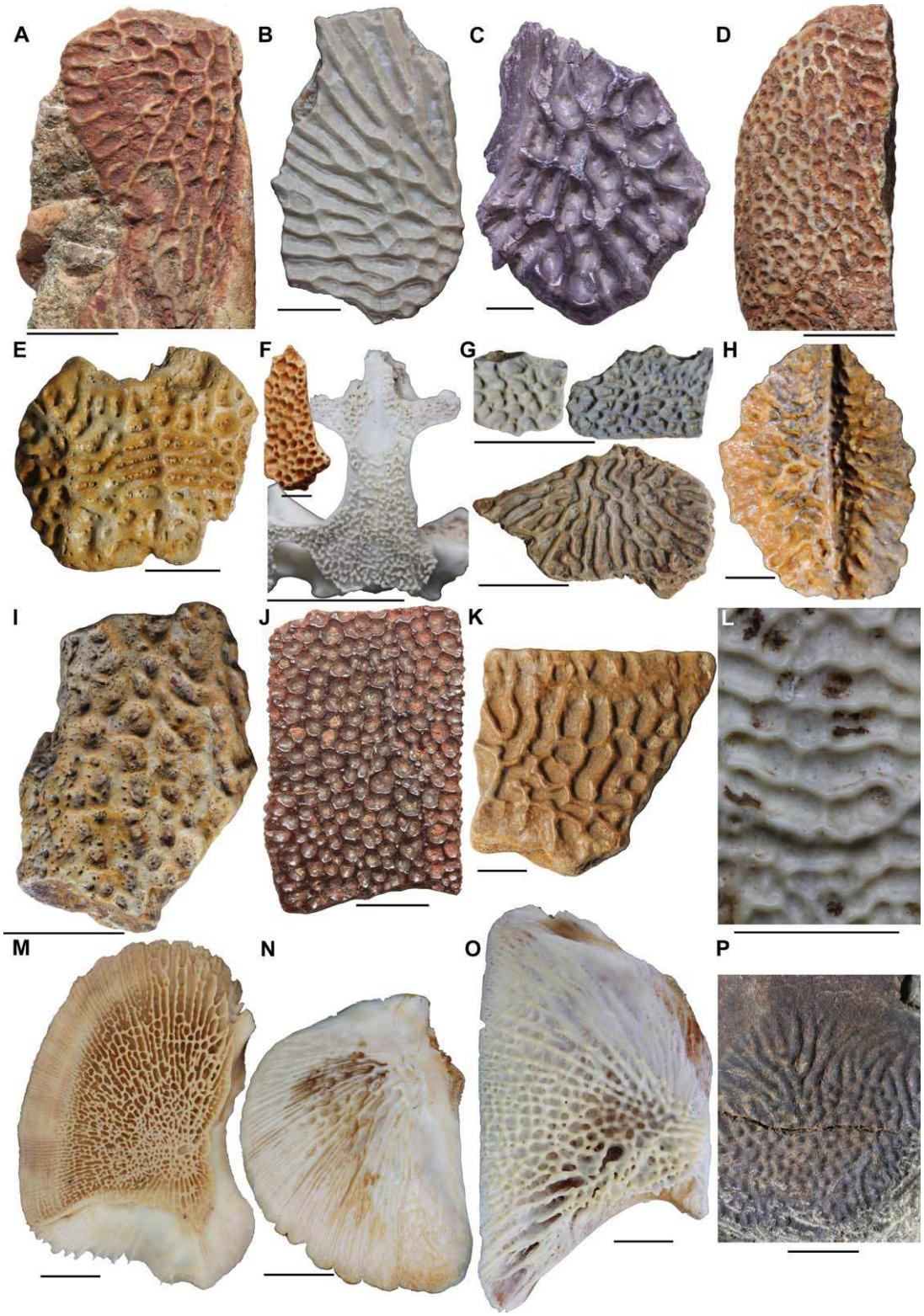

Fig. 1. Morphology of the pit and ridge ornamentation type in the biological sample. **A**: Undetermined skull bone of the Early Triassic *Benthosuchus sushkini* (Temnospondyli). **B**: Undetermined skull bone of the Early Triassic *Stanocephalosaurus* (Temnospondyli). **C**: Fragment of postparietal of the Middle Triassic (Ladinian) *Kupferzellia* (Temnospondyli). **D**: Undetermined skull bone of the Early Permian *Diplocaulus* sp. (Nectridea). **E**: Osteoderm of the Late Permian *Bystrowiana* cf. *permiria* (Chroniosuchia). **F**: Calvarium of the extant *Ceratophrys cornuta* (Anura), with detail of the fronto-parietal of the Eocene *Thaumastosaurus* from the Quercy Phosphorites. **G**: Fragments of undetermined skull bones of the Early Permian amniote *Captorhinus aguti* (upper half) and osteoderm of the Early Permian embolomere *Archeria* (lower half). **H**: Osteoderm of an undetermined Eocene *Necrosaurus* (Squamata) from the Quercy Phosphorites. **I**: Undetermined skull bone of the Early Permian synapsid *Lupeosaurus kayi* (Edaphosauridae, Eupelycosauria). **J**: Carapace fragment of the Early Cretaceous *Araripemys barretoi* (Testudines). **K**: Carapace fragment of the Paleocene *Palaeotrionyx sp*. (Testudines). **L**: Detail of the plate from the carapace of the extant *Amyda cartilaginea* (Testudines). **M**: Opercular of the extant *Acipenser sturio* (Actinopterygii: Acipenseriformes). **N**: Opercular of the extant *Arapaima gigas* (Actinopterygii: Osteoglossiformes). **O**: Opercular of the extant *Sciades proops* (Actinopterygii: Siluriformes). **P**: Scale of the Devonian *Holoptychius* cf. *quebecensis* (Sarcopterygii: Porolepiformes). Scale bars: 1 cm, except for H = 1 mm; M, N = 2 cm.

Reference Phylogeny

A reference phylogeny was compiled from the literature. It attempts to capture the current consensus about topology and divergence times, although some controversies make this exercise difficult. This is especially true of the position of turtles. Therefore, all evolutionary analyses reported below are based on two trees: one in which turtles are located outside Diapsida, as several paleontological studies have suggested (Laurin and Reisz, 1995; Lee, 2001; Lyson et al., 2010), and another in which they are located in Diapsida, as basal archosauromorphs, as suggested by several recent molecular studies (e.g., Hugall et al., 2007; Chiari et al., 2012). Several recent paleontological studies have also placed turtles within diapsids, typically among lepidosauromorphs (e.g., Rieppel and Reisz, 1999; Schoch and Sues, 2015), but an archosauromorph placement is apparently not too unparsimonious from a morphological point of view (Lee, 2013). And to complicate things further, some molecular studies placed turtles among lepidosauromorphs (e.g., Lyson et al., 2012), but we believe that the two selected reference trees summarize well the bulk of the literature on this topic.

Most other taxa were far easier to place, including those within turtles, for which the topologies follow Guillon et al. (2012) for extant taxa, and Sterli et al. (2013) for extinct ones. Stegocephalian phylogeny follows Vallin and Laurin (2004), except for the position of chroniosuchians, which follows Schoch et al. (2010). The phylogeny of temnospondyls follows Schoch (2008, 2013), except for *Peltobatrachus*, which was placed following Eltink and Langer (2014).

The position of lissamphibians (the smallest clade that includes all extant amphibians) is controversial. For most of the 20th century, most authors have considered them to be nested within temnospondyls (e.g., Bolt, 1969; Ruta and Coates, 2007; Sigurdsen and Green, 2011), but several analyses involving one of us (M.L.) have recently supported a position in lepospondyls instead (e.g., Laurin, 1998; Vallin and Laurin, 2004; Marjanović and Laurin, 2013), a result also obtained by Pawley (2006) in one of her analyses. However, this controversy has very little impact on our study because under all recently published phylogenies, their sister-group among the sampled taxa lack remodeling in the process leading to dermal ornamentation. Thus, to avoid complicating needlessly the analyses we placed lissamphibians (represented only by anurans, in our sample) among "lepospondyls" (here represented solely by *Diplocaulus*).

The tree was time-scaled using the Stratigraphic Tools (Josse et al., 2006) of Mesquite (Maddison and Maddison, 2014) using both paleontological (stratigraphic age) and molecular divergence dates, many of which were obtained from Kumar and Hedges (2011).

Evolutionary Analyses

To assess the ancestral condition for gnathostomes, stegocephalians, sauropsids and other clades present in our tree, as well as to reconstruct character history, we performed maximum likelihood (ML) optimizations. This has a few advantages compared with the maximum parsimony (MP) optimizations. First, the ML optimization (Pagel, 1999) uses branch lengths, which are approximately known in the case of paleontological trees because fossils bear temporal information. MP (Swofford and Maddison, 1987) typically neglects branch length information. Second, ML optimization can yield probabilities that each state was present at a given node, rather than a single most parsimonious state, or a set of equally parsimonious states. In both cases, the parsimony solution is suboptimal because even if a single most parsimonious solution exists for a given node, it is not necessarily the actual condition that existed in the last common ancestor (Oakley and Cunningham, 2000; Webster and Purvis, 2002; Bollback, 2006; Germain and Laurin, 2009). Moreover, when a set of equally parsimonious states exists, each state comprised in the set is probably not equally well-supported. Third, ML analysis can reveal asymmetries in transition rates (between states 0 and 1) better than MP analysis because it assesses these through evolutionary models to yield best estimates of both (forward and backward) rates. By contrast, MP often yields ambiguous optimizations on part of the tree, which complicate assessment of transition rates (e.g., Smith et al., 2013).

Support for each ML model was assessed by converting their log-likelihood into AIC weights, using formulae given in Wagenmakers and Farrell (2004) and that involve computing AICc (for small samples) as an intermediate step. This is generally preferable to using the older log-likelihood ratio test because the number of estimated parameters often differs between the compared models (as is the case here), and this complicates interpretation of the log-likelihood ratio test (Wagenmakers and Farrell, 2004). The two usual models (a one-rate and a two-rate model) were assessed in Mesquite 3.04 (Maddison and Maddison, 2014). Below, we report results from each model, as well as a weighted average of values (probabilities of each state at selected nodes) yielded by both models. These are weighted by the AIC weights of each model. This is done for both reference phylogenies (differing in the position of turtles).

For two nodes and characters that appeared particularly relevant (Sauropsida and Actinopterygii), we have calculated model-averaged probabilities of the states. These nodes were selected because their condition is particularly uncertain (the exercise would have been trivial in most other cases because the probability of the most likely state exceeded 99.9%). This was done under two topologies (differing by the position of turtles, inside or outside diapsids).

RESULTS

Stegocephali

Temnospondyli, Lepospondyli (*Diplocaulus*), and Chronosuchia (*Bystrowiana*).

General structural features of ornamented bones. The general micro-anatomic and histological structure of temnospondyl ornamented bones shows substantial variability between taxa, but some general characteristics (and a few atypical situations) can be distinguished, at least in the taxa for which the quality of preservation of the fossils allows detailed observations. These characteristics are shared with the nectridean (lepospondyl) *Diplocaulus* and the chroniosuchian *Bystrowiana*; these taxa are thus included in the following description.

Most bones have a gross diploe architecture, with two compact periosteal cortices framing a cancellous core (Fig. 2A–H). However, the compactness of the core region is extremely variable between specimens, and the resulting global compactness of the sampled bones ranges from 69.6% for the bone of *Trimerorachis* (Fig. 2E) to 87.7% for the interclavicle of *Plagiosternum* (Fig. 2C). When present, the basal cortex is made of variably birefringent parallel-fibered bone. Vascularization is generally sparse in this tissue, but several exceptions exist, mainly the parietal of *Mastodonsaurus* that displays abundant primary osteons organized in parallel strata, the interclavicle of *Plagiosternum*, the postparietal of *Plagiosuchus* and, to a lesser extent, the bone of *Eryops*. The core region, be it of high or low compactness, is always heavily remodeled (Fig. 2I,J), and the local spongiosa is thus secondary (at least for most of its volume). Remodeling is so intense in most specimens that no trace of the primary tissue once present locally persists. In

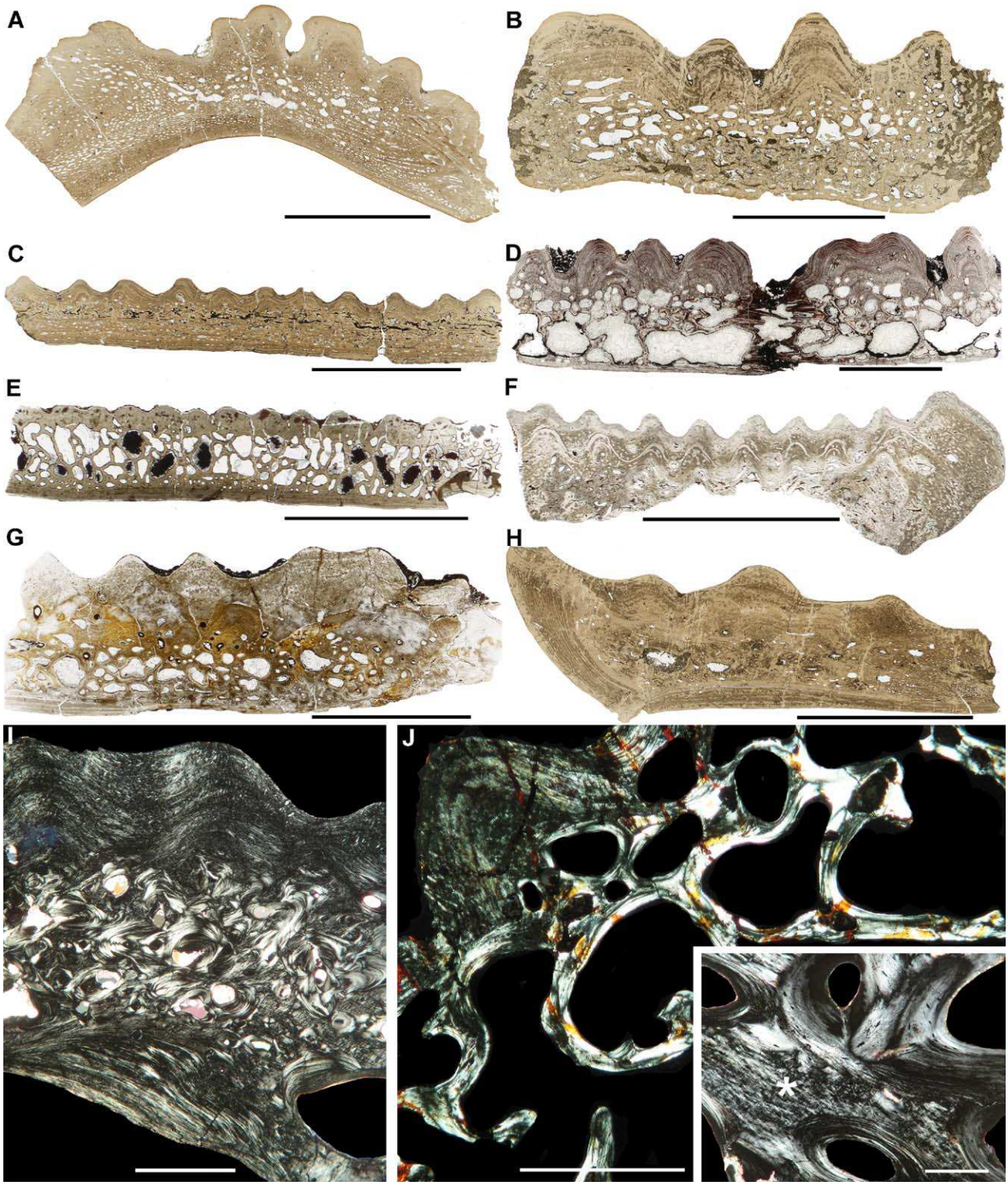

Fig. 2. General structure of ornamented bones in the Temnospondyli (cross sections). **A**: Postparietal of a Middle Triassic *Plagiosuchus* sp. **B**: Postparietal of a Middle Triassic *Kupferzellia* sp. **C**: Interclavicle of a Middle Triassic *Plagiosternum* sp. **D**: Interclavicle of the Late Triassic *Dutuitosaurus ouazzoui*. **E**: Undetermined skull bone of an Early Permian *Trimerorachis* sp. **F**: Skull bone of the Middle Triassic *Stanocephalosaurus*. **G**: Skull bone of an undetermined Late Triassic metoposaur. **H**: Parietal of a Middle Triassic *Mastodonsaurus* sp. **I**: General structure of an undetermined bone of *Platyoposaurus*, viewed in transmitted polarized light. The superficial (ornamented), and basal cortices are made of parallel-fibered tissue; the core of the bone is a tight spongiosa intensely remodeled. **J**: Loose, remodeled central spongiosa in a Late Permian *Peltobatrachus* osteoderm. Insert: Primary woven-fibered-like tissue (asterisk) persisting in the remodeled central spongiosa of a Middle Triassic *Kupferzellia* postparietal. Scale bars: 1 cm, except for I, J (main frame) = 1 mm; J (insert) = 0.2 mm.

the specimens of *Kupferzellia* (Fig. 2J, insert), *Plagiosuchus*, *Parotosaurus*, *Platyoposaurus*, and *Stanocephalosaurus*, the remnants of this tissue, less eroded by remodeling and better preserved by fossilization than in other specimens, display histological features intermediary between parallel-fibered bone (birefringence of bone matrix, though faint and irregular) and woven-fibered bone (multipolar cell lacunae randomly oriented).

The superficial, ornamented cortex also shows structural consistency between taxa but, again, a few peculiar conditions exist. In most specimens, the bottom of the pits is covered by a layer of parallel-fibered bone tissue, comprising spindle-like osteocyte lacunae, oriented parallel to the bone surface, and a birefringent matrix (Fig. 3A,B). Depending on the taxa, this tissue may (in e.g., the *Stanocephalosaurus* bone shown in Fig. 3C or the osteoderm of *Bystrowiana*), or may not (e.g., *Diplocaulus*: Fig. 3B,D) extend into the core of the ridges framing the pits. It is often devoid of vascularization (Fig. 3A,B), but this situation is far from being general, and simple vascular canals or primary osteons (Fig. 3C,E) may occur. Similarly, Sharpey's fibers can occasionally be present in the layers forming the bottom of the pits. Ridges often display a stratified structure characterized by the alternation of well-vascularized (by simple canals or primary osteons) monorefringent or poorly birefringent strata, and avascular birefringent ones similar to *annuli*, as exemplified by *Kupferzellia* (Fig. 3F) or *Mastodonsaurus*. The bone layers located at the base or in the core of the ridges display relatively dense vascularization that decreases toward the cortical periphery (Fig. 3G). Sharpey's fibers are frequent in the apices of the ridges (e.g., Fig. 3B). The main exception to this general pattern is represented by two skull bones (one is from a small specimen, and the other from a much larger one) of *Benthosuchus sushkini* (Fig. 3H) that display ridges made of a poorly birefringent tissue devoid of cyclic growth marks and densely vascularized by a reticular network of simple vascular canals.

All temnospondyl sections share an important common feature: the superficial bone layers located either in the floor of the pits or in the walls of the ridges never contain reversion lines, discordant bone deposits or superficial traces of resorption such as Howship's lacunae. These bone layers are thus entirely made of primary tissues in continuity with, though eventually different in structure from, subjacent bone strata. There is no superficial remodeling (resorption and reconstruction cycles) in temnospondyl ornamented bones, as well as in the bones of *Diplocaulus* and *Bystrowiana* used in this study.

Dynamic processes in superficial cortices Superficial cortices of temnospondyl (and other basal stegocephalians) ornamented bones show evidence of an active modeling process that typically excludes a previous resorption stage. Ornamentation growth can be observed only in relatively peripheral layers because deep cortical strata are generally submitted to extensive resorption and reconstruction, as mentioned above. The pattern and spacing of cyclical growth marks, along with the distribution and density of vascular canals and the refringence characteristics of bone matrix in polarized light, suggest that the overall geometry of bone ornamentation (i.e., pit and ridge shapes and dimensions), is exclusively influenced during growth by local differences in apposition rate and slight shifts in the direction of bone deposits. Six main situations, which may occur simultaneously on a single bone, are frequently observed:

1. Simple, local piling of bone reliefs during growth (Figs. 2B,D,F, 3C, and 4A). This situation may occur in all taxa, and was most clearly observed in a cranial bone of *Stanocephalosaurus* (Fig. 3C), in a *Dutuitosaurus* supratemporal (Fig. 4A), and in the middle region of an osteoderm of *Bystrowiana*. Periosteal bone accretion results in a mere superposition of bone reliefs, with no significant modification in the width or position of pits and ridges from one growth stage to the following one. The apices of the ridges, as well as the center of the pits, do not present any significant drift; therefore, the absolute diameter of individual pits remains constant during growth. Conversely, in relative terms, pit widths tend to decrease as compared to the augmenting size of the bones that bear them. The bottom of the pits may rise in pace with the top of the ridges (e.g., Fig. 3C), or at a slower rate (Fig. 4A). In the first case, pit shape remains unchanged during growth, whereas in the second case, pits tend to become relatively deeper and narrower.
2. Symmetric ridge drift (Fig. 4B). The apices of the ridges that frame an individual pit tend to diverge symmetrically from each other during growth, as a consequence of a lateral off-centering of periosteal deposits on top of the ridges. Opposite to the simple, centered piling described above, this process results in a progressive increase in pit diameter. However, it also tends to constrain the diameters of neighboring pits, and contributes to the *total ridge drift* described below. This growth pattern was observed on the supratemporal of *Dutuitosaurus*, the interclavicle of *Plagiosternum*, the postparietal of *Plagiosuchus*, and the skull bones of *Eryops* (Fig. 4B) and *Stanocephalosaurus*.
3. Total ridge drift (Fig. 4C). The ridges around a given pit migrate in the same direction (i.e., toward the lateral margins of the bone), as a result of similar and parallel off-centering of periosteal bone accretion. Slight differences in the rates of these processes can result in some local widening of the pits during growth (as shown on Fig. 4C), but potentially also in some

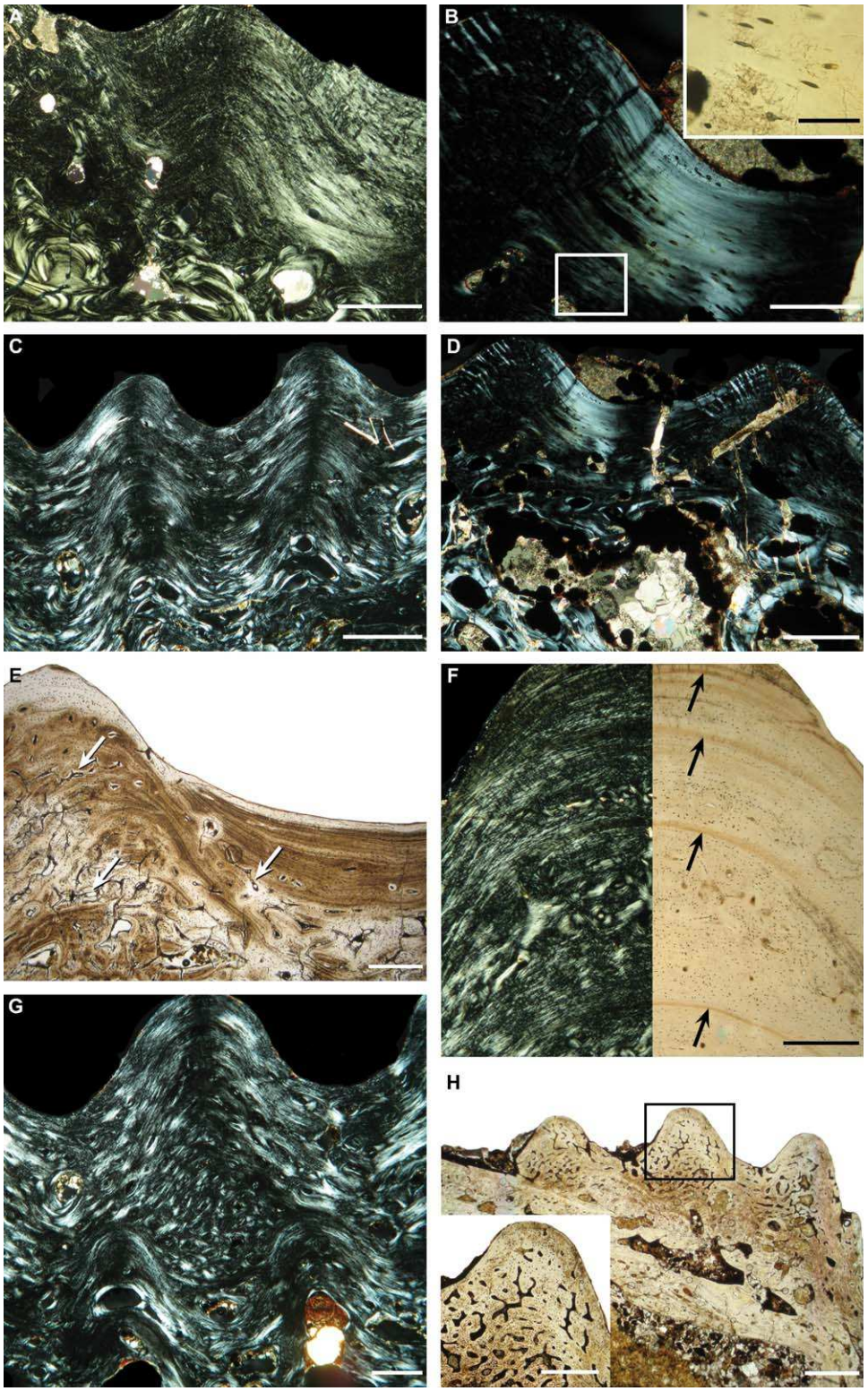

Fig. 3. Histological features of the superficial cortex in the temnospondyls, and in *Diplocaulus* and *Bystrowiana* ornamented bones. **A**: Parallel-fibered bone of variable birefringence in the skull bone of *Platyoposaurus* (polarized light). **B**: Parallel-fibered bone of variable birefringence in an undetermined skull bone of a Late Permian *Diplocaulus* (polarized light). The insert shows the difference in the morphology of cell lacunae between the woven-fibered-like tissue occupying the core of the bone, and the parallel-fibered tissue located in the floor of the pits. **C**: Skull bone of a Middle Triassic *Stanocephalosaurus* (polarized light). Bone deposits are regular and continuous, with no reversion line, from the depth up to the surface of the cortex. **D**: Skull bone of *Diplocaulus* (polarized light). The cores of the ridges are quasi-monorefringent. **E**: Skull bone of *Stanocephalosaurus*. Vascular canals (arrows) occur in the ridge and, to a lesser extent, in the floor of the pit. **F**: Histology of a ridge in a Middle Triassic *Kupferzellia* postparietal. Left half: polarized light; right half: natural, transmitted light. Vascular canals are unevenly distributed, according to the conspicuous cyclical growth marks (arrows). **G**: Vascular proliferation at the base of a ridge, just above a filled pit, in *Stanocephalosaurus* (polarized transmitted light). H: Unusual tissue displaying reticular vascularization (framed field and insert) in the ornamented cortex of a skull bone from the Late Triassic *Benthosuchus sushkini*. Scale bars: C, H = 1 mm; A, D, E-G, H insert = 500 μm; B main frame = 200 μm; B insert = 50 μm.

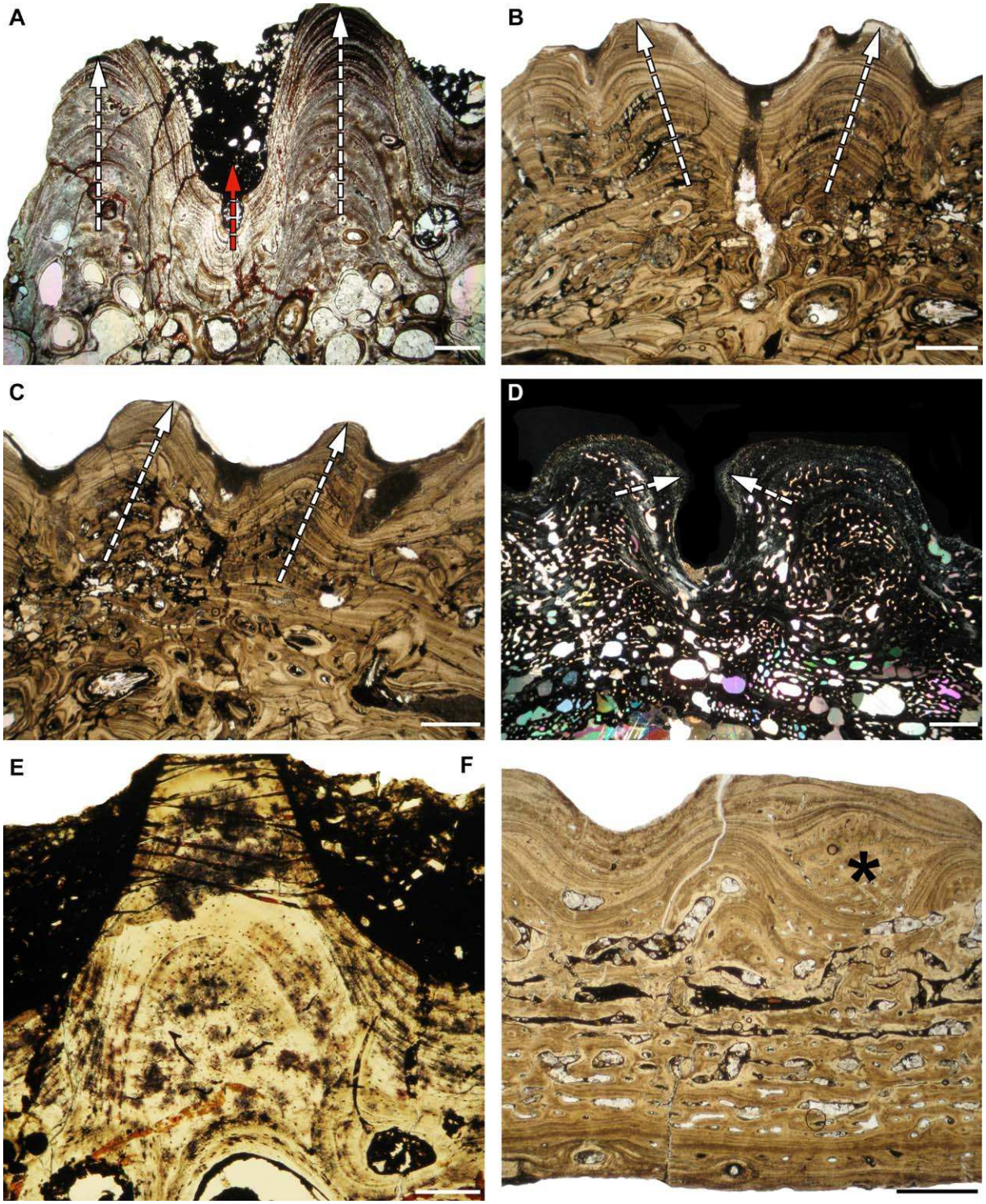

Fig. 4. Dynamic processes in the ornamented cortices of temnospondyls. **A**: Straight, simple centered piling growth of the ridges of the interclavicle of the Late Triassic *Dutuitosaurus*. The pit remains narrow and its depth increases. The dashed arrows indicate the direction of growth over the ridges (white arrows) and pit floor (red arrow). **B**: Symmetric divergence of the ridges during growth. Skull bone of the Early Permian *Eryops megacephalus*. Same symbols as for A. **C**: Sub-parallel ridge drift in the bone of *Eryops megacephalus*. **D**: Convergent ridge drift in the postparietal of the Middle Triassic *Plagiosuchus* (polarized light). **E**: Decrease in ridge width during growth in a Late Permian *Peltobatrachus* osteoderm. **F**: Pit filling (asterisk) in the interclavicle of *Plagiosternum*. Scale bars: A-D, F = 1 mm; E = 250 μm.

narrowing. This situation is frequent (if not general), and was observed in all specimens, except *Benthosuchus*, *Diplocaulus*, *Plagiosuchus*, and one of the *Stanocephalosaurus* specimens.

4. Convergent ridge drift (Fig. 4D). In this case, the ridges surrounding a pit present off-centered periosteal accretion, but this process occurs centripetally toward pit central axis, thus provoking a gradual narrowing of pit diameter, and creating a trend toward local pit closure. This rare process was observed only in the postparietal of *Plagiosuchus*.
5. Reduction of ridge width (Fig. 4E). Periosteal bone accretion can be much faster on the tip of a ridge than on its lateral sides. This process results in a fast increase in ridge height, accompanied with a relative decrease of ridge width (Fig. 4E). Ridges then tend to become sharper during growth and the pits that they border turn proportionally wider and deeper. This rare case was mainly observed in *Peltobatrachus*.
6. Pit filling and relief inversion (Figs. 3G, 4F). Pits can be entirely filled, and disappear to be replaced in situ by ridges. This process relies on a steep acceleration of bone accretion on pit floor, as typically evidenced on bone sections by a local increase in the spatial density of vascular canals (e.g., Fig. 3G). Growth acceleration proceeds until a protruding relief, which actually represents the base of a newly formed ridge, is created. The ridge is then submitted to one or several of the five other morphogenetic processes described above. This relief inversion is relatively frequent; it was observed in *Dutuitosaurus*, *Mastodonsaurus*, *Plagiosternum* and *Stanocephalosaurus*.

Embolomeri (*Archeria*).

General histological features. The bone of *Archeria* examined here is a diploe of medium compactness (88.7%), with avascular and compact cortices (Fig. 5A). The very intense remodeling activity that occurred in the core region of the bone (Fig. 5B) left only scarce remnants of primary bone tissue. The latter has the same gross histological structure as the superficial, ornamented layer that actually represents its upward extension. The superficial layer is composed of a tissue close to the parallel-fibered type, exhibiting poor birefringence in the ridges, and brighter birefringence in the layers forming the floor of the pits (Fig. 5C). Osteocyte lacunae have a rounded shape, an aspect possibly due to their orientation relative to the section plane (their true morphology might thus be spindle-like). This tissue is integrally subdivided into parallel layers by cyclic growth marks, represented by lines of arrested growth, or LAGs (Fig. 5D). All of them are split (they appear as double lines), suggesting that the animal's ecology was characterized by a short period of activity resumption between two yearly diapause phases. The superficial layer is devoid of any sign of resorption or remodeling, and is in mere continuation with the deeper osseous strata located in the core of the bone; however the spacing of the LAGs is wide in the ridges, and narrower in the floor of the pits, thus indicating pronounced differences in local growth rates (Fig. 5D). The basal layer of the bone is made of an avascular, lamellar bone tissue displaying short bundles of Sharpey's fibers, but where cyclic growth marks do not occur (Fig. 5C).

Interpretation of growth patterns. Since parallel-fibered bone tissue is considered to result from faster accretion than lamellar tissue (Castanet et al., 1996, 2000; Margerie et al., 2002, 2004; see also Francillon-Vieillot et al., 1990; Ricqlès et al., 1991), bone growth must have been more active over the ornamented surface than over the basal cortex. The differences observed in both the refringence properties of the bone and the spacing of the LAGs suggest that the ornamental reliefs were produced, as in the temnospondyls, by local contrasts in growth rates between the top of the ridges (fast accretion) and the bottom of the pits (slow accretion). Ridge growth involved no significant drift that could have resulted in pit widening, displacing or entire filling. Pit widening thus appears to have been dependent on a single possible (though not evidenced on the sections) mechanism during growth: a decrease in ridge width.

Lissamphibia (*Ceratophrys*, *Latonia*, and *Thaumastosaurus*).

General histological features. The microanatomical organization of *Ceratophrys* and, to a lesser extent, *Latonia* fronto-parietals is that of a typical diploe, with highly compact cortices framing a loose, central spongiosa (Fig. 6A). The fronto-parietal of *Thaumastosaurus*, like the maxillaries of the three taxa, does not have a diploe structure, although broad resorption bays occur in their central region. Bone tissue in our *Thaumastosaurus* specimen is too degraded to allow detailed observations. In the other two taxa, the most central region of the bones displays a thin (some 50–60μm in maximal thickness in *Ceratophrys*; 70-90 μm in *Latonia*) layer of a monorefringent tissue (Fig. 6A,B) whose general characteristics (morphology and spatial density of cell lacunae: Fig. 6C,D) correspond to the woven-fibered tissue type. This bone layer contains few simple vascular canals (Fig. 6B,D), but these have a wide lumen (up to 50 μm) because of the resorption, followed or not by partial, secondary reconstruction, which occurs on their walls. The deep (basal) cortices are avascular, nonremodeled, and made of parallel-fibered tissue (mass birefringence, spindle-like cell lacunae oriented parallel to bone layers: Fig. 6A,B).

In *Ceratophrys*, the superficial, ornamented cortex has a complex histological structure. Its deep part, in contact with the woven-fibered layer, consists of typical parallel-fibered tissue housing wide

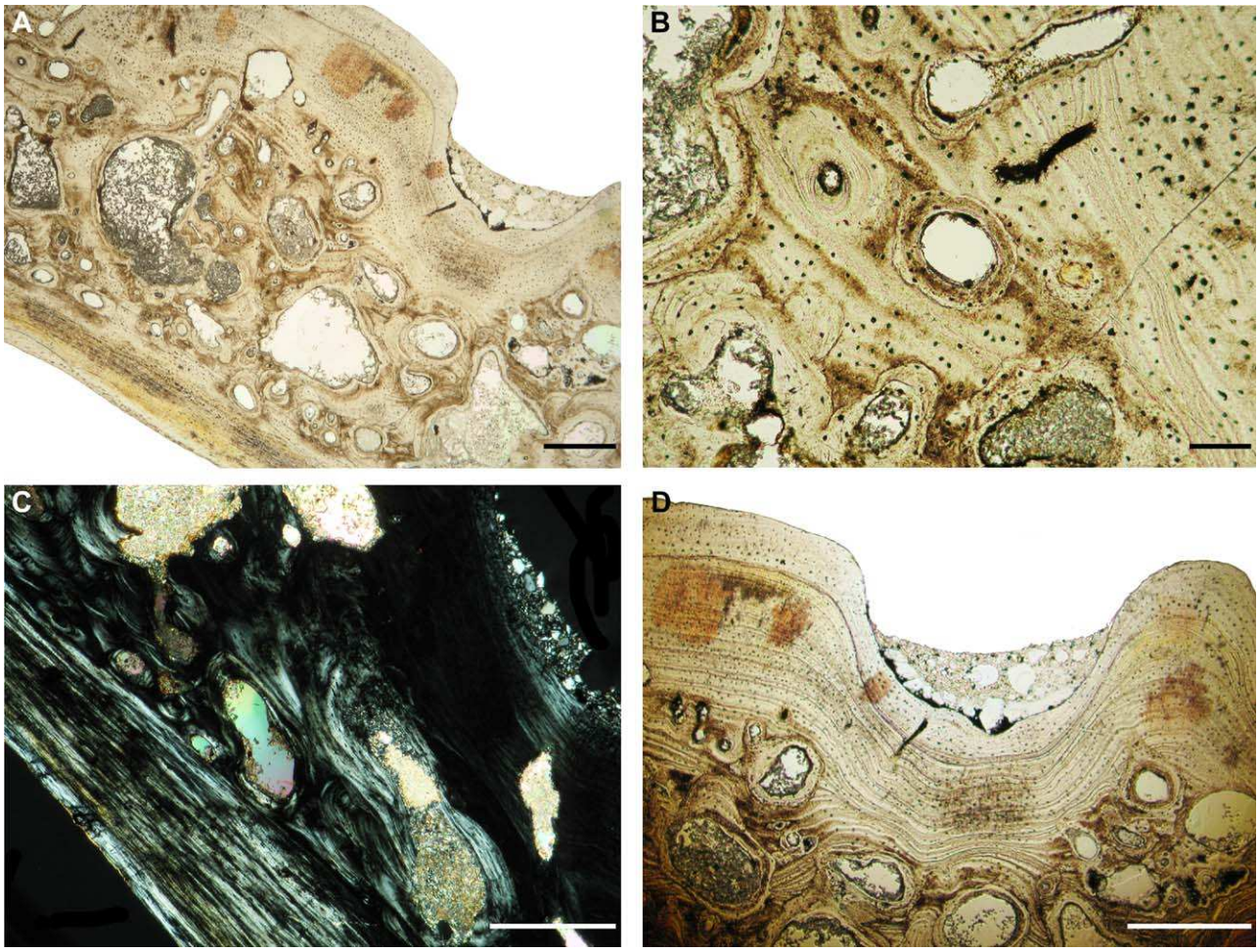

Fig. 5. General histology of ornamented bones in *Archeria*. **A**: General view of the diploe architecture of an Early Permian *Archeria* bone. **B**: Closer view at the intensely remodeled tissue forming the core of the same *Archeria* bone. **C**: Aspect of the basal and superficial cortices of the same *Archeria* bone (polarized light). The basal cortex is made of lamellar tissue, whereas the superficial cortex is of a parallel-fibered type, more birefringent in the floor of the pits than in the core of the ridges. **D**: Cyclical growth marks in the superficial cortex of the same *Archeria* bone. Marks are more tightly spaced in the pit floor. There is no discontinuity or reversion line between the superficial, ornamented layer and the subjacent, remodeled tissue located in the core of the bone. Scale bars: A, C, D = 500 μm; B = 100 μm.

vascular canals that may locally turn into broad erosion bays (Fig. 6C–E). The ornamentation ridges situated upon this layer can display two very distinct patterns in their histological structure: a few are made of the same parallel-fibered tissue as observed in the subjacent layer, of which they merely represent a superficial excrescence displaying signs of inner remodeling (Fig. 6E). However, most of the ridges are made of an avascular tissue that shows a very conspicuous and regular stratification appearing in polarized light in the form of alternatively bright and dark strata of even thickness (Fig. 6C,F,G). Considering the individual thickness of the strata (8–12 μm for the dark ones; 7–8 μm for the light ones), this tissue is unlikely to be true lamellar bone because the thickness of bone lamellae (from 2 to 6 μm, at most) seldom exceeds 5 μm (Currey, 2002); moreover, the regularity of the strata (as also their position within the cortex: see below) precludes the possibility that they represent yearly growth marks. This stratified layer rather represents a peculiar tissue undescribed hitherto in the skull bones of lissamphibians. Its pattern is strongly reminiscent of the "plywood-like structure" described in the carapace of the Trionychidae (soft-shelled turtles) by Scheyer et al. (2007, 2012), and it will tentatively be referred to this tissue, though it lacks the "vertically oriented plies" exhibited by the turtle bones (see also below: "Testudines"). Interestingly, a similar tissue (with slightly thicker lamellae of about 15–18 μm) has also been mentioned in the osteoderms of the Dissorophidae (in *Aspidosaurus* and *Platyhystrix*), a Permian temnospondyl taxon from which several (but not all) authors think that lissamphibians arose (Witzmann and Soler-Gijón, 2010). In *Ceratophrys*, the stratified, plywood-like tissue can be covered, on the apex of the ridges, by a layer of avascular poorly birefringent

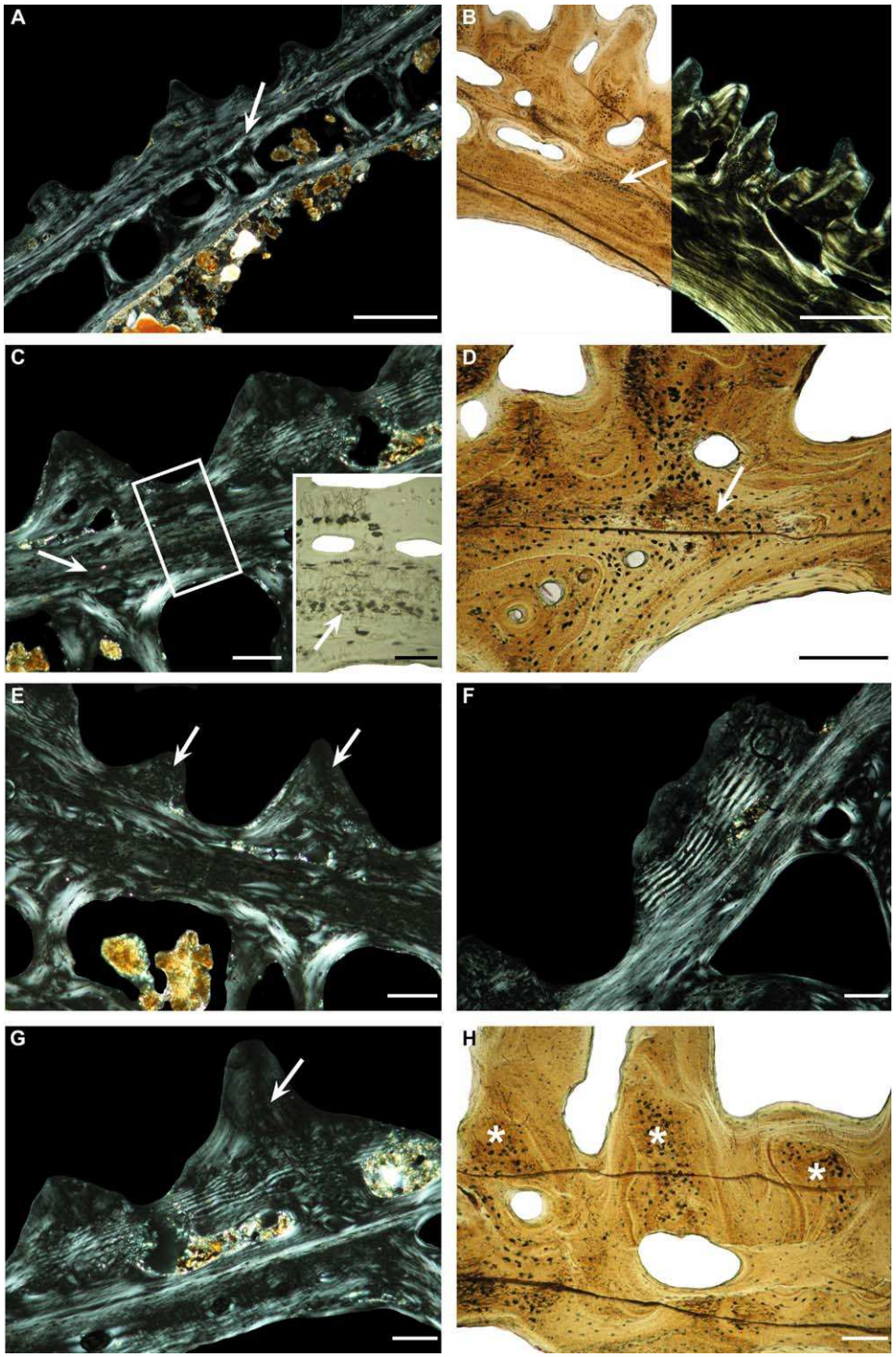

Fig. 6. General histology of ornamented bones in lissamphibians (extant, unless specified otherwise). **A**: Cross section in the fronto-parietal of *Ceratophrys* (polarized light). The general structure is that of a diploe. The arrow points to the thin sheet of monorefringent tissue in the center of the bone. **B**: Cross section in the fronto-parietal of the mid-Miocene *Latonia gigantea* (left half: natural transmitted light; right half: transmitted polarized light). Same symbol as for part A. **C**: Closer view at the central monorefringent bone layer (arrow) in *Ceratophrys* (main frame: polarized light; insert: natural light). **D**: Closer view at the central monorefringent tissue (arrow) in the maxillary of *Latonia*. **E**: Ornamented layer in *Ceratophrys* frontoparietal, with ridges made of remodeled parallel-fibered tissue (arrow) (polarized light). **F**: Superficial layer of plywood-like tissue in the fronto-parietal of *Ceratophrys* (polarized light). **G**: Other view at the plywood-like superficial tissue in the ridges of *Ceratophrys* frontoparietal (polarized light). The apex of the ridge is capped by a poorly-birefringent parallel-fibered tissue with few cell lacunae (arrows). **H**: Ridge structure in *Latonia* fronto-parietal. Deep woven-fibered tissue (asterisks) protrudes into the core of the ridges. Scale bars: A, B = 500 μm; D = 200 μm; C main frame, E-H = 100 μm; C insert = 50 μm.

parallel-fibered bone containing few cell lacunae (Fig. 6A,C,F,G).

In *Latonia*, the superficial, ornamented cortex is basically made of a brightly birefringent and intensely remodeled, parallel-fibered tissue (Fig. 6B,H). However, the core of the ridges comprises an excrescence of the subjacent woven-fibered layer (Fig. 6D,H).

In the three lissamphibian taxa, the superficial, ornamented cortex shows obvious signs of an intense remodeling activity in the form of extensive resorption (unambiguously evidenced by Howship's lacunae; cf. Fig. 7A), followed by partial reconstruction. In *Ceratophrys*, the resorption extends to the whole superficial cortex, though it is actually subdivided into punctual spots (Figs. 6A and 7A,B). It tends to erode both the layer of primary stratified tissue, in which it excavates very sharp and clear-cut pits (e.g., Figs. 6F,G, and 7B), and the subjacent parallel-fibered layer (Fig. 7A–C). The subsequent phase of partial reconstruction (that can itself be followed by a new resorption phase: Fig. 7F,G) sets thin layers of lamellar bone on the bottom and walls of the pits. These reconstructive deposits often show the same asymmetry between the medial and lateral sides of the ridges (e.g., Fig. 7D,F,H) as that previously described in crocodilians by Buffrénil et al. (2015). In *Ceratophrys*, there is apparently no other mechanism for the differentiation of ornamental reliefs than the double process of extensive (but patchy), superficial resorption and partial reconstruction. The same mechanism is likely to have occurred also in *Thaumastosaurus* because ornamented cortices in this taxon show a similar remodeling pattern as that observed in *Ceratophrys* bones (Fig. 7D). In *Latonia*, the situation might have been more complex. The excrescences of woven-fibered bone that protrude in the core of the ridges suggest that the initial stage of ridge differentiation in this taxon was a local and temporary acceleration of bone accretion. Subsequently, an intense remodeling activity involving several resorption and reconstruction cycles occurred on cortical surface (Fig. 7E–G). It was topographically related to the course of the vascular canals running inside the bones, and their outcrop on the bone surface in the middle of pit floors (Fig. 7F,G,I). This remodeling process resulted in a steep deepening of the pits, whose bottoms were reconstructed but very partially. Such a remodeling pattern is fairly different from that observed in *Ceratophrys* and *Thaumastosaurus*, and created a distinct morphology of bone ornamentation: tall, columnar ridges framing deep and narrow well-like pits. In addition, off-centering and topographic drift processes occurred during crest growth in the fronto-parietal and maxillaries of *Thaumastosaurus* (Fig. 7H) and *Latonia* (Fig. 7I).

Amniota

Captorhinidae (*Captorhinus aguti*).

General histological features. The skull roof fragment of *Captorhinus aguti* has a classical diploe architecture (compactness 91.3%). All the cavities located in the core of the bone are former erosion bays whose walls were partly reconstructed by secondary, endosteal deposits of lamellar tissue (Fig. 8A). Between these cavities, abundant remnants of the primary bone deposited at early growth stages remain visible. In polarized transmitted light, this tissue shows a poor and irregular, though detectable, birefringence (Fig. 8B). Local osteocyte lacunae have abundant canaliculi, and a spheroid, multipolar or spindle-like shape; this morphological variability is indicative of their uneven orientation within the bone matrix (Fig. 8B, insert). Considered together, these histological traits suggest the occurrence of a woven-fibered bone tissue type with an atypical intercellular matrix turning into the parallel-fibered type (incipient birefringence). Local vascularization is mainly composed of primary osteons (lumen 25–40 μm in diameter), though few simple vascular canals 10–18 μm in diameter may occur in some areas. The basal cortex of the bone is composed of primary bone tissue (remodeling is very limited) displaying histological features similar to those of the core region. However, in the basal region, birefringence is more pronounced, and vascular canals are mainly simple canals.

The tissue forming the core of the bone extends with no significant modification toward the ornamented, superficial layer, where it constitutes most of the volume of the ridges (Fig. 8C). The outermost ridge strata, over a thickness of some 50–60 μm, as well as the thicker (100–120 μm) bone layer forming the bottom of the pits, are composed of a brightly birefringent parallel-fibered tissue with flat cell lacunae oriented parallel to the general direction of bone layers (Fig. 8C,D). This layer is avascular but may display Sharpey's fibers as dense bundles perpendicular to the surface of the bone. The *Captorhinus* bone examined here displays no cyclic growth marks.

Dynamic processes in superficial cortices. Histological evidence clearly rules out any involvement of superficial remodeling in the development of bone ornamentation in *Captorhinus*. The osseous tissue occurring in ridges is basically similar in structure to that located in the core of the bone, and differs very little from the tissue forming the basal layer. Considering the general, well-established, relationships between bone structure and appositional rate, as reviewed above (cf. chapter "material and methods"), ridges are unlikely to have resulted from local acceleration of periosteal accretion. Conversely, the parallel-fibered bone located on the bottom and walls of the pits is known to grow more slowly than the woven-fibered-like tissue in the ridges. The differentiation of bone sculpture would thus result

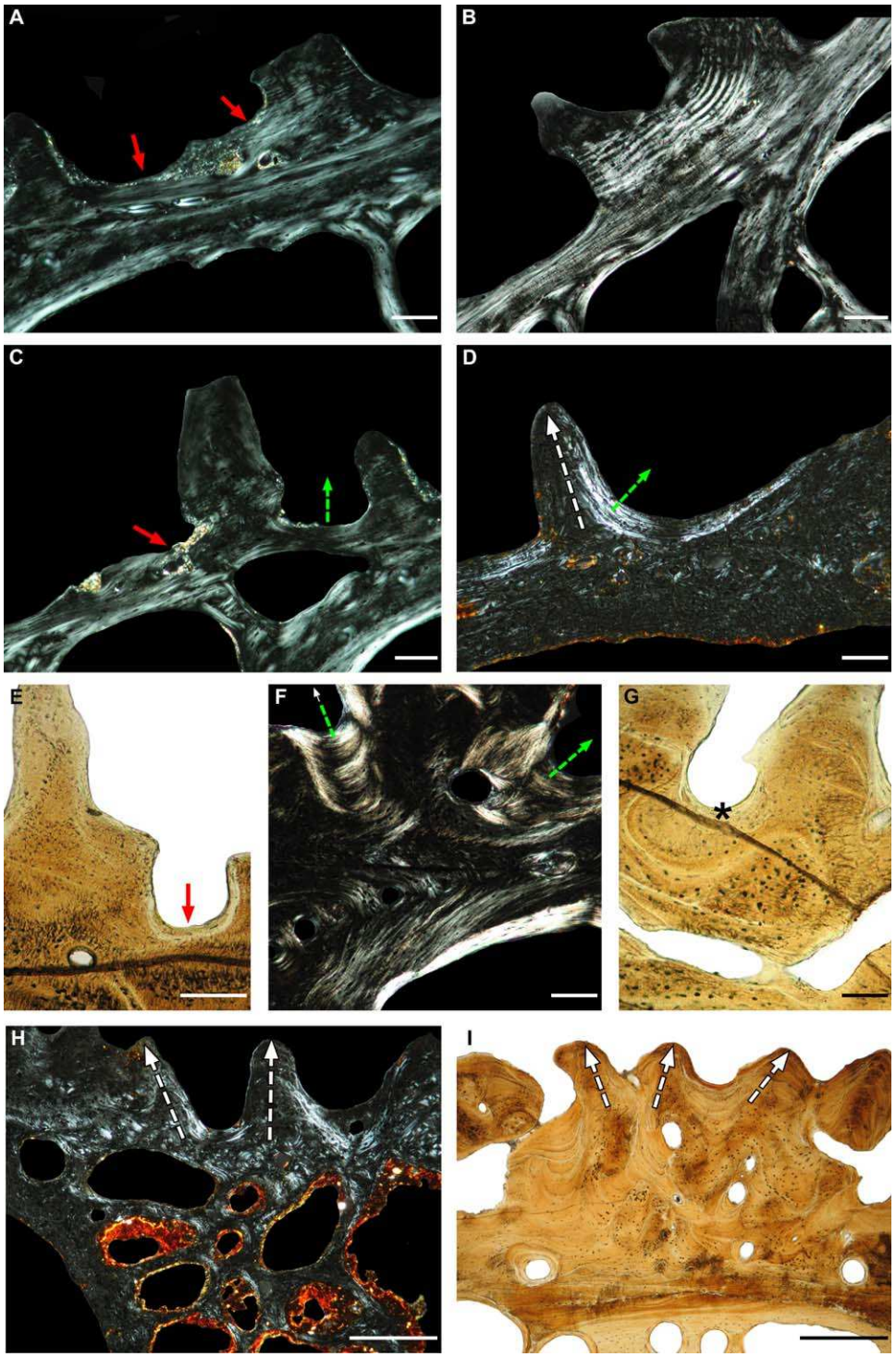

Fig. 7. Remodeling of the ornamented layer in lissamphibians (taxa are extant, unless specified otherwise). **A**: Active resorption (red arrows) in the frontoparietal of *Ceratophrys* (polarized light). **B**: Detail of the clear-cut resorption of the superficial plywood-like layer in the frontoparietal of *Ceratophrys* (polarized light). **C**: Intense resorption process (red arrow) reaching the deep layers of the cortex in *Ceratophrys* frontoparietal (polarized light). The floor of the next pit is under reconstruction (green dashed arrow) (polarized light). **D**: Asymmetric resorption and reconstruction (green dashed arrow) on the frontoparietal of the Eocene *Thaumastosaurus* (polarized light). **E**: Local resorption (red arrow) in the frontoparietal of the mid-Miocene *Latonia*. **F**: Remodeling through asymmetric resorption and reconstruction (arrows) in the frontoparietal of *Latonia* (polarized light). **G**: Remodeling in the vicinity of vascular canals (asterisk) that outcrop on pit floor in *Latonia* frontoparietal. H: Lateral ridge drift (dashed arrows) in the frontoparietal of *Thaumastosaurus* (polarized light). **I**: Divergent and lateral ridge drifts (dashed arrows) in the maxillary of *Latonia*. Scale bars: H, I = 500 μm; E = 200 μm; A–D, F, G = 100 μm.

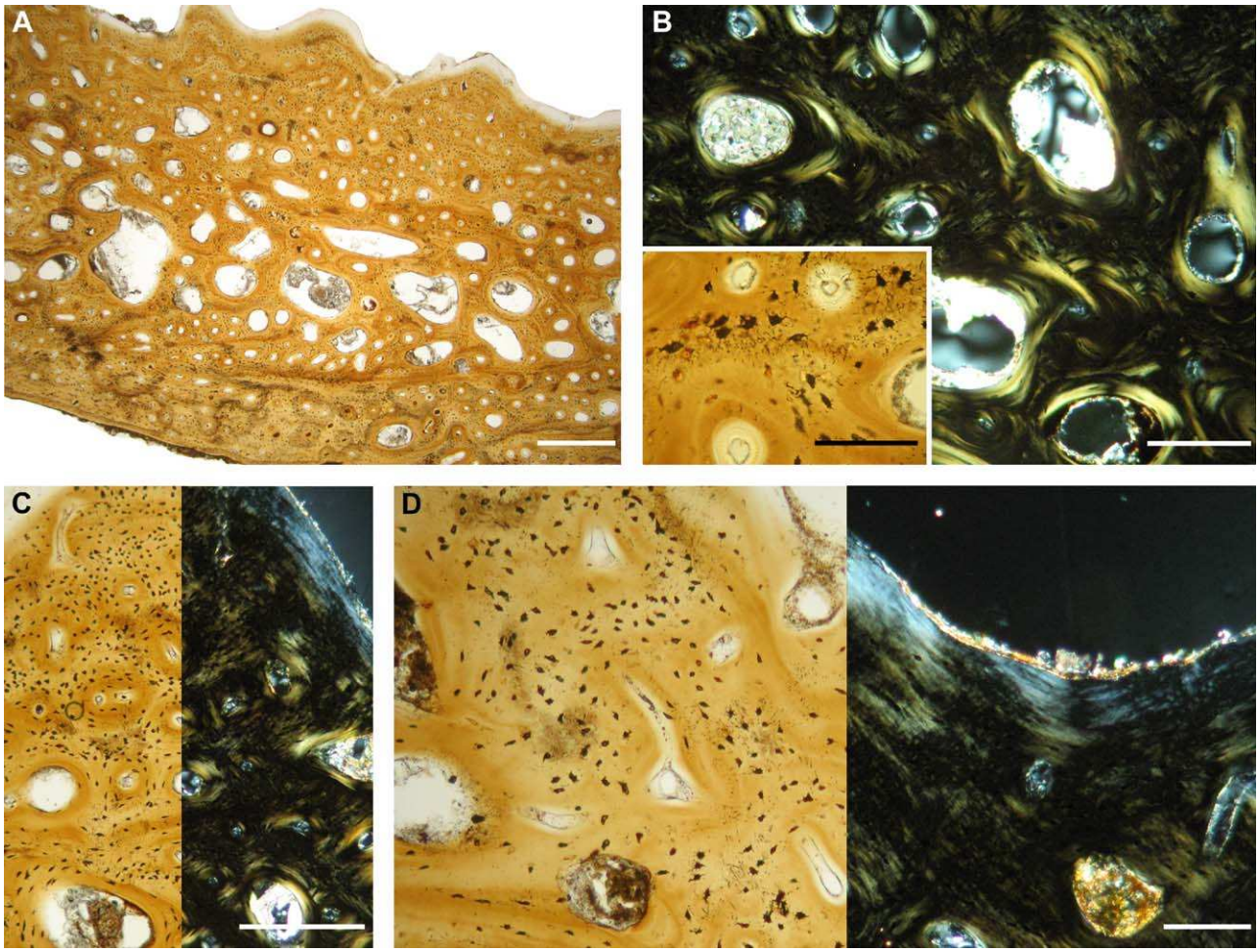

Fig. 8. General histology of ornamented bones in *Captorhinus*. **A**: General diploe-like architecture of an Early Permian *Captorhinus* bone. **B**: Poor birefringence of the remodeled tissue located in the core of that bone (polarized light). The insert shows the multipolar cell lacunae enclosed in the remnants of primary tissue that persist between secondary osteons. **C**: Tissue forming the bulk of the ridges (left half: natural transmitted light; right half: transmitted polarized light). **D**: Birefringent layer covering the sides of ridges and the bottom of pits in the superficial cortex (left half: natural transmitted light; right half: transmitted polarized light). Scale bars: A = 500 μm; C = 250 μm; B main fame, D = 100 μm; B insert = 50 μm.

from the simple mechanism also encountered in temnospondyls and *Archeria*: a discrepancy in accretion rate between the bottom of the pits, where growth was slow, and the top of the ridges, where growth proceeded at the same rate as that occurring on the other parts of the bone surface (except pit bottom and walls). Pit differentiation would have resulted from this local contrast in growth rates. Moreover, there is no indication of spatial drift or off-centering in ridge growth. This general growth pattern offers few possibilities for pit enlargement during growth, with exception for the "decrease in ridge width" mentioned above.

Testudines (Trionychidae, Emydidae, Araripemidae).

General histological features. Ornamented bones in the six chelonian taxa studied here have a typical diploe structure, but strong differences in bone compactness exist between samples (from 82.9% in *Trionyx triunguis* to 96.4% in *Araripemys barretoi*). The basic traits of their histological structure are also comparable (Fig. 9A): their basal cortex consists of a homogeneous and brightly birefringent layer of parallel-fibered tissue that turns, toward the bone periphery, into lamellar tissue. Local vascularization, represented by scarce simple vascular canals, is uneven between taxa. The core of the bones is occupied by monorefringent woven-fibered tissue displaying thick, randomly oriented fiber bundles (i.e. the "interwoven-structural collagenous fiber bundles" of Scheyer and Sánchez-Villagra, 2007) (Fig. 9A, left insert). This region is submitted to intense remodeling through which the deep, compact strata of the cortex are progressively made cancellous (Fig. 9A, right insert). The superficial, ornamented cortex is a thick layer of variably birefringent parallel-fibered tissue. The parts of this layer forming the floor of the pits are always more birefringent, and closer to the lamellar tissue type, than those forming the

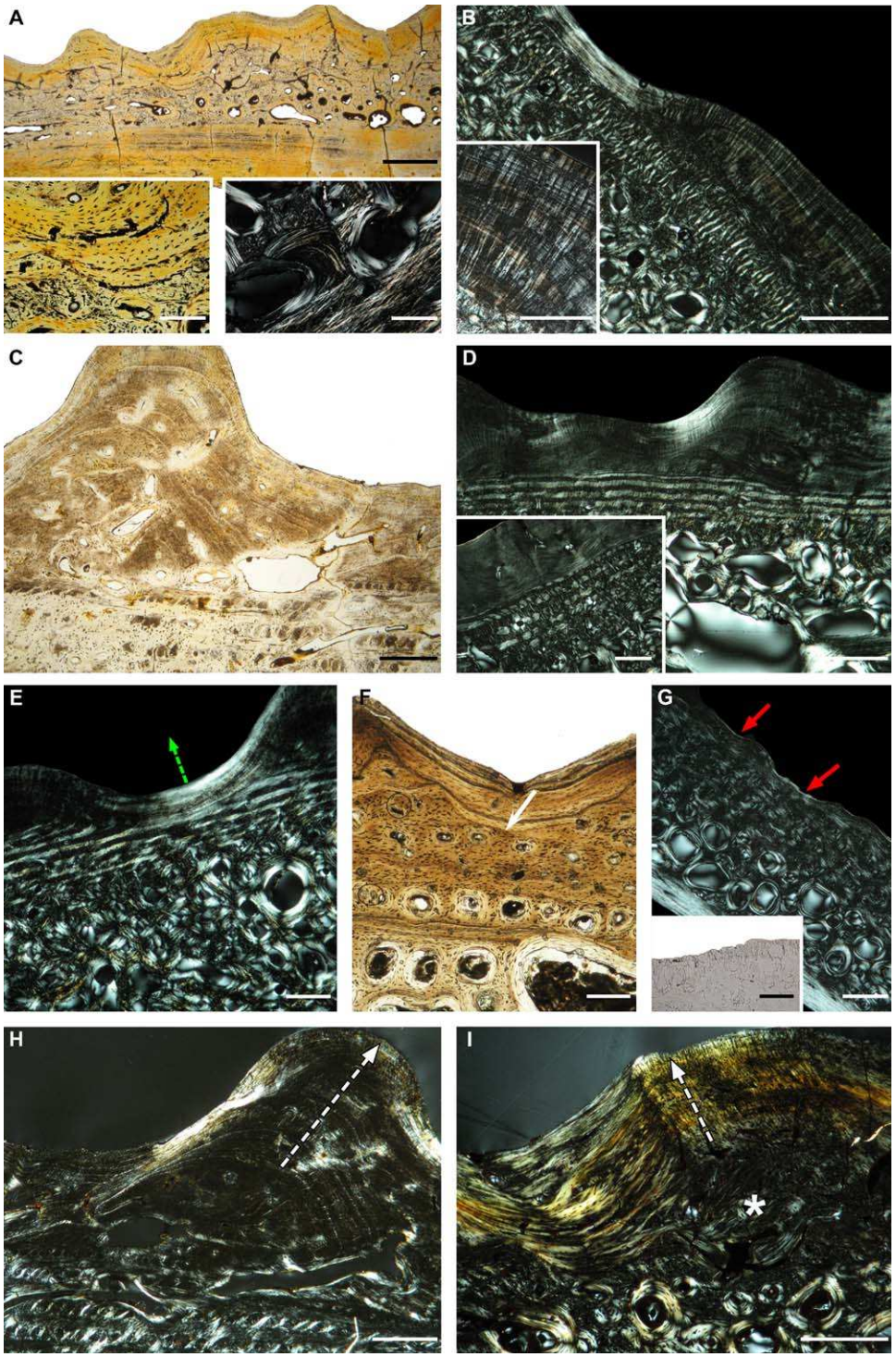

Fig. 9. Histology of carapace plates in Testudines. **A**: General histology of a carapace plate of the Early Cretaceous *Araripemys*. The left insert shows the difference between the woven-fibered tissue located in the core of the plates, and the parallel-fibered cortices. The insert on the right shows the intense remodeling of the core region (polarized light). **B**: Parallel-fibered tissue in the superficial cortex of the extant *Trionyx triunguis*. Abundant bundles of Sharpey's fibers located preferentially within the ridges cross the cortex (main frame and insert in polarized light). **C**: Annuli and simple vascular canals in the superficial cortex of a Late Cretaceous *Aspideretoides* carapace plate. **D**: Plywood-like bone layer encountered in the carapace of the extant trionychids (main frame and insert in polarized light). **E**: Resorption and subsequent reconstruction (green dashed arrow) of the superficial cortex in the extant *Amyda cartilaginea* (polarized light). **F**: Wavy contour of the resorption line (arrow) that marks the limit of a former resorption field in *Araripemys*. **G**: Howship's lacunae (red arrows) on bone surface in the extant *Pseudemys* (main frame: polarized light; insert: Howship's lacunae viewed in ordinary transmitted light). **H**: Lateral ridge drift (dashed arrow) in *Aspideretoides* (polarized light). **I**: Ridge drift (dashed arrow) with multiple resorption/reconstruction cycles, along with pit filling (asterisk) in *Araripemys* (polarized light). Scale bars: A main frame = 1 mm; B main frame, C, D main frame, G-I = 500 μm; A inserts, B insert, D insert, E, F = 250 μm; G insert = 50 μm.

ridges (Fig. 9B). Abundant, vertically oriented bundles of Sharpey's fibers cross the whole thickness of the superficial layer, with a characteristic discrepancy between the pits that have few or no fiber bundles, and the ridges in which most of the fiber bundles occur (Fig. 9B). Like the basal cortex, the superficial, ornamented layer may, or may not, display simple vascular canals and cyclical growth marks in the form of annuli (Fig. 9B,C). The main difference between taxa is the occurrence or the absence of a plywood-like bone layer (a tissue described by Scheyer et al., 2007, 2012; see also Landmann, 1986) consisting of alternatively birefringent and monorefringent strata (an aspect due to the orthogonal orientation of fibers between adjacent strata), linked by strong vertical fiber piles (Fig. 9D–E). This layer is located just under the parallel-fibered bone that bears ornamentation, and occurs exclusively in the trionychids (here: *Amyda cartilaginea*, *Cyclanorbis sp*., *Trionyx triunguis*, and *Aspideretoides*), as already mentioned by Scheyer et al. (2007).

Remodeling of the ornamented layer. In all the specimens examined here (be they trionychids, or araripemyds), except the emydid *Pseudemys*, the superficial, ornamented layer is separated from the subjacent bone strata (woven-fibered bone or plywood-like layer) by a reversion line, with discordant bone deposits above and under this line (Fig. 9D–F,I). Bone deposits situated above the line are thus secondary, reconstructive deposits that can extend continuously over the whole bone surface, or be interrupted by outcrops of the subjacent primary tissue, set to surface by the resorption process. The reversion line is often straight in a part of its course (Fig. 9D) and wavy in other parts, according to the local contour of bone ornamentation (Fig. 9E,F). There is no resorption line in the superficial cortex of the *Pseudemys* specimen examined here. However, in several spots corresponding to the floor of shallow pits, the surface of the bone displays slight depressions bordered by well-characterized Howship's lacunae (Fig. 9G) that unambiguously indicate that a superficial resorption process was active by the time the animal died. This apparent exception finally confirms the general pattern observed in the other taxa. Histological sections also reveal that bone ornamentation in the Testudines experiences the same processes of lateral ridge drift (Fig. 9C,H) or pit filling (Fig. 9I) as those observed in most other taxa described above.

Histological observations suggest that the mode of formation of bone ornamentation on turtle carapace plates relies on osteogenic processes reminiscent of those previously observed in crocodilians (Buffrénil et al., 2015), or described above about lissamphibians. The main peculiarity that distinguishes the turtles from these taxa is the occurrence of an extensive resorption field able to level the preexisting surface of the bone before the accretion of the ornamented surface. According to the local contour, straight or sinuous, of the resorption line, two slightly distinct modalities for the development of bone ornamentation can take place: 1) Local bone surface has been made flat by resorption; ornamental reliefs would then result from slight differences in bone accretion rates between the top of the ridges (faster growth forming poorly birefringent parallel-fibered tissue), and the floor of the pits (slower growth forming a tissue between the parallel-fibered and the lamellar types). This case is illustrated on Fig. 9D. 2) Resorption did not flatten entirely the surface of the bone; then, subsequent accretion of future bone layers further enhances the preexisting reliefs (illustrated on Fig. 9F). In all cases, the development of the ridges seems to be topographically related to, and perhaps facilitated by, the insertion of particularly strong Sharpey's fiber bundles into the bone cortex, a hypothesis already considered by Witzmann (2009) for early stegocephalians. During further growth, the control of pit depth and diameter mainly relies on symmetric or asymmetric ridge drift. Multiple resorption and reconstruction cycles, similar to those described above in the lissamphibians (and general in the pseudosuchians: Buffrénil et al., 2015), are seldom observed in the turtles; however, they may nevertheless occur, as exemplified by the carapace plate of *Araripemys* (Fig. 9I).

Squamata (*Necrosaurus*).

General histology. Though the two necrosaur osteoderms are different in morphology (one has a strong median keel, while the other is nearly flat), they show similar microanatomical and histological organizations, though one of them is more compact than the other (93.7% vs 82%), but contain broad, central cavities due to resorption (occurrence of Howship's lacunae), whose walls are partly reconstructed by endosteal, lamellar deposits (Fig. 10A–C). The core of each osteoderm is occupied by a monorefringent tissue that nevertheless displays numerous thick birefringent fiber bundles (Fig. 10C). Local osteocyte lacunae are ovoid or multipolar with few canaliculi. This tissue can be classified as a form of woven-fibered bone tissue. It is covered on its superficial and basal sides by thick layers of brightly birefringent parallel-fibered bone (Fig. 10A–D) containing Sharpey's fibers. These layers are histologically homogenous, and display only a faint indication of cyclic growth (Fig. 10D). The superficial, ornamented layer lacks any obvious sign of local acceleration or deceleration of growth. It lays in continuity with the subjacent monorefringent tissue, and no reversion line delimits these two tissues. In the design of its inner stratification, as also in its surface reliefs, the ornamented layer, especially that of the keeled osteoderm, follows slight undulations already displayed by the monorefringent tissue over which it develops. Moreover, the bottom of the ornamental pits exhibits clear evidence of bone resorption, in the form of Howship's lacunae (Fig. 10D). This process is

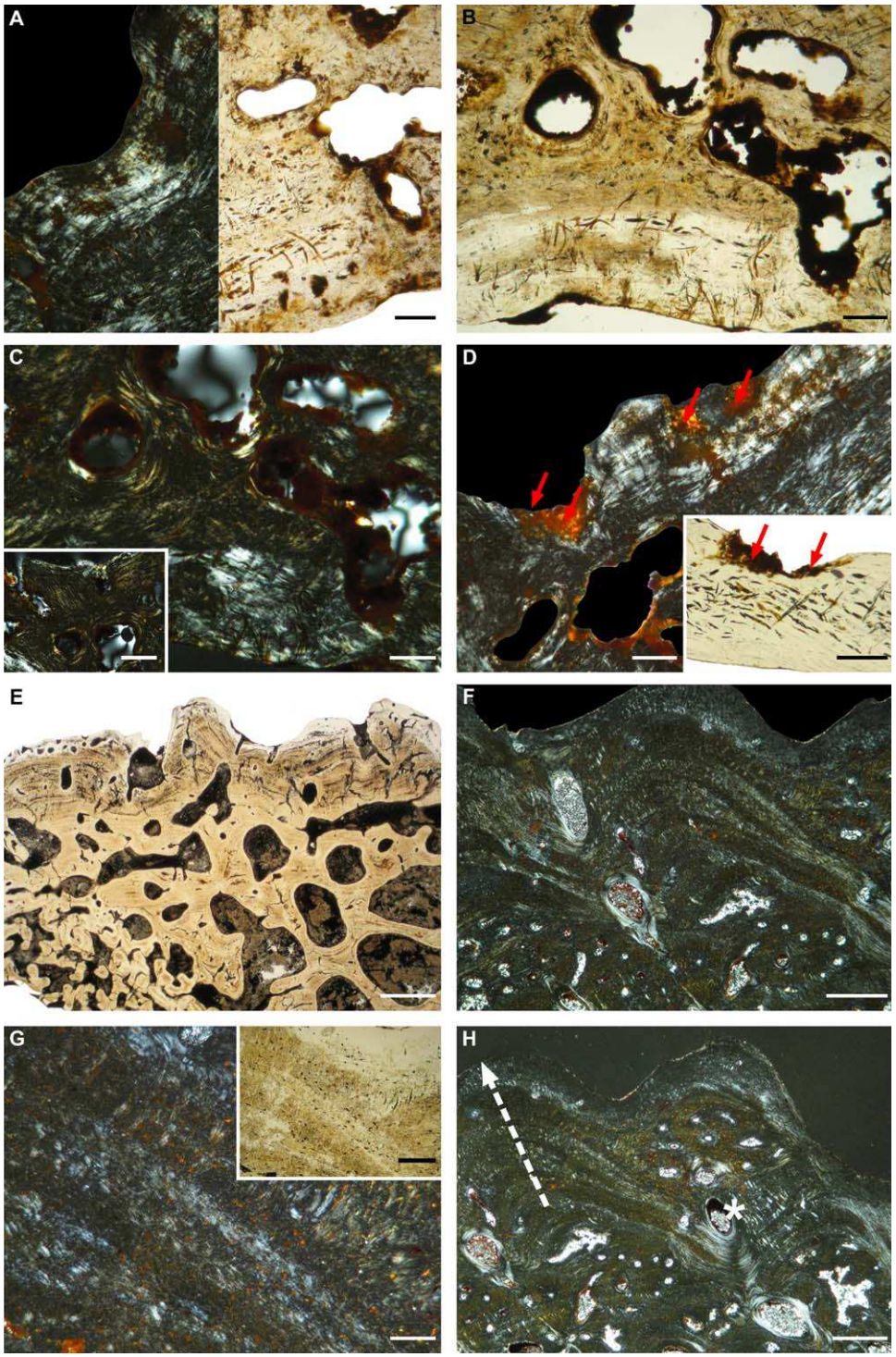

Fig. 10. General histology of ornamented bones in *Necrosaurus* and *Lupeosaurus*. **A**: General structure of an Eocene *Necrosaurus* osteoderm, with birefringent superficial and basal cortices framing a monorefringent core (left half: polarized light; right half: normal light). **B**: Broad central cavities in a *Necrosaurus* osteoderm. **C**: Tissue akin to woven-fibered bone in the core of a *Necrosaurus* osteoderm, with a small part of the subjacent birefringent basal cortex. The insert shows the abundant Sharpey's fibers in the basal cortex (main frame and insert in polarized light). **D**: Superficial resorption (red arrows) not followed by reconstruction in a *Necrosaurus* osteoderm (main frame: polarized light). **E**: General view of an Early Permian *Lupeosaurus* bone. **F**: Avascular cortex made of a poorly birefringent parallel-fibered-like tissue in the bone of *Lupeosaurus*. This bone displays broad annuli that tend to fuse with each other in the floors of the pits (polarized light). **G**: Detail of the histological structure of the tissue forming the ridges. The insert shows that osteocyte lacunae show great differences in canaliculi development between dark, opaque layers and translucent layers (main frame: polarized light). **H**: Lateral ridge drift (white dashed arrow) and pit filling (asterisk) in the ornamented cortex of *Lupeosaurus* bone (polarized light). Scale bars: E = 1 mm; F, H = 500 μm; C insert = 200 μm; G insert = 150 μm; A-D, G main frame = 100 μm.

topographically related to the course of large inner vascular canals whose superficial outcrops were widened by the local resorption. In no case was resorption followed by reconstruction.

Growth pattern of the osteoderm and its ornamentation. In reference to data available about the development of squamate osteoderms (e.g., Buffrénil et al., 2011), the histological observations presented above suggest that necrosaur osteoderms were produced by a double osteogenic process: i) initial dermo-osseous metaplasia that created the woven-fibered tissue of the core region; ii) later in ontogeny, typical osteoblastic accretion of bone that produced the outer, parallel-fibered birefringent layers. The former occurrence of osteoblasts around the osteoderm is evidenced by the endosteal deposits covering the walls of inner cavities: endosteal osteoblasts are known to derive from periosteal osteoblasts that penetrate the core of a bone along its vascular canals (Krstic, 1985; Karaplis, 2008). Ornamentation pits seem to have resulted from a double process. For a limited part (and especially in the keeled osteoderm), they were the mere repercussion on the surface of deeper reliefs borne by the bone forming the core of the osteoderms. For another part, they resulted from an increase of these faint initial reliefs through local resorption in the vicinity of vascular pits. This additional process is likely to have occurred at a relatively late stage of osteoderm growth, when the superficial layer had reached an advanced stage of development. No reconstructive phase, and thus no remodeling in the proper sense, was involved.

Synapsida: Edaphosauridae (*Lupeosaurus*).

General histological features. The *Lupeosaurus* bone fragment is not truly organized as a diploe. It displays a few broad, sub-circular central cavities surrounded by numerous smaller, partly reconstructed resorption bays that colonize also the basal cortex (Fig. 10E). The superficial, ornamented cortex is compact with few, small-diameter primary osteons and simple vascular canals (Fig. 10E,F), along with thick bundles of Sharpey's fibers. Primary bone deposits, be they located in the core of the bone or in the superficial and basal cortices, are characterized by the succession of thick bone layers (thickness of 150–200 μm), alternatively monorefringent with high opacity, and birefringent with low opacity (Fig. 10F,G). Differences in opacity between the layers result from discrepancies in the density of the osteocyte lacunae (less numerous in the light layers), the morphology of their soma, and the abundance of their canaliculi, particularly well-developed in the darker layers (Fig. 10G). This histological structure is indicative of a cyclic growth, with the darker layers featuring "zones" laid down during episodes of fast growth, and the lighter layers representing *annuli*, formed during phases of slower growth. The superficial layer displays neither reversion lines separating discordant bone layers, nor any trace of superficial bone resorption or remodeling.

The spacing of the cyclic growth marks indicates higher growth rates at the level of the ridges than in the pits (Fig. 10F,H): pit floor is made of tightly packed annuli, with nearly no zone inserted between them. Therefore, the differentiation of bone ornamentation in *Lupeosaurus* was mainly a result of local differences in accretion rate, as it was observed above in many other taxa. Moreover, the development of bone ornamentation during growth in *Lupeosaurus* was submitted to the same dynamic trends as those described in the temnospondyls: total ridge drift (Fig. 10F,H), pit filling, and inversion of local reliefs (a ridge replacing a pit: Fig. 10H). In the latter case, the characteristic increase in bone vascularization at the base of the new ridge that was observed in several other taxa, such as the temnospondyls *Stanocephalosaurus* (cf. Fig. 3G) or *Plagiosternum* (Fig. 4F), also occurs in *Lupeosaurus*.

Actinopterygii

Acipenseriformes (*Acipenser sturio*). The opercular of *Acipenser sturio* is not a diploe; it is formed by the junction of two compact cortices: the basal one has a smooth surface; the superficial one displays deep well-like pits separated by vertical ridges (Fig. 11A). Both cortices are made of parallel-fibered bone. This tissue is less brightly birefringent in the superficial cortex than in the basal one. Birefringence is particularly faint in the core of the ridges; conversely, ridge sides are made of strongly birefringent lamellar bone (Fig. 11B). Cell lacunae are typical of parallel-fibered bone (they are flat, without canaliculi) except in the core of the ridges, where they show a multipolar shape and long canaliculi forming a dense network (Fig. 11C,D). Between the two cortices, a thin (thickness 70–120 μm) discontinuous blade of a more opaque tissue displaying multipolar cell lacunae with canaliculi appears locally. The opercular of *Acipenser* is avascular, and displays faint cyclical growth marks. These marks are broadly spaced in the core of the ridges and tightly in their lateral layers (Fig. 11B). Short Sharpey's fibers occur as dense bundles in the core of the ridges. The *Acipenser* opercular shows no sign of inner or outer remodeling by the typical process of resorption followed by reconstruction. However, broad erosion bays perforate the superficial cortex in all parts, and result either in the differentiation of ridges through the erosion of vertical bone blades, or to a general reshaping of the ridges (Fig. 11A,E). This resorption process occurs inside the ornamented cortex, not on its surface.

Histological observations suggest that the creation and growth of ornamental reliefs on the *Acipenser* opercular mainly depends on the development of the ridges. The latter result from local acceleration of bone accretion, as evidenced by both the basic histological

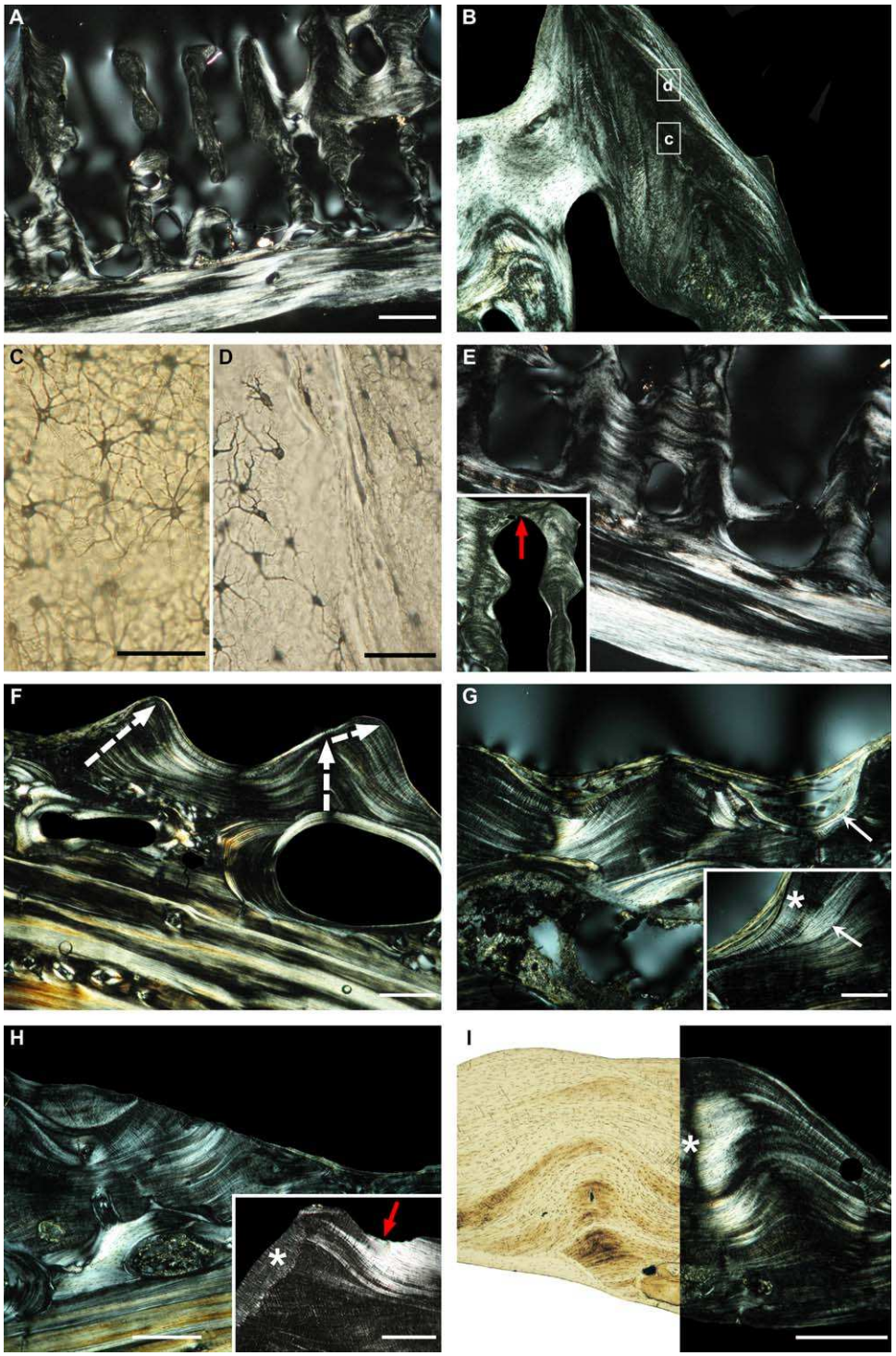

Fig. 11. General histology of ornamented bones in the extant actinopterygians *Acipenser sturio* (**A–E**) and *Arapaima gigas* (**F–I**). **A**: General microstructural organization of an *Acipenser* opercular (polarized light). **B**: Histological structure of a ridge. The core of the ridge is poorly birefringent, while its sides display bright birefringence. The closer fields shown in figures C and D are indicated (polarized light). **C**: Multipolar osteocyte lacunae with long canaliculi in the core of a ridge. **D**: Spindle-like osteocyte lacunae devoid of canaliculi in the lateral sides of a ridge. **E**: Inner resorption in the superficial cortex (the basal one is not resorbed). Insert: reshaping of a ridge by inner resorption (arrow) (polarized light). **F**: General structure of an *Arapaima* opercular (polarized light). Both cortices are birefringent. Ridges are drifting during growth (dashed arrows). **G**: Superficial process of resorption and reconstruction in the ornamented layer. Reversion lines (arrows) and secondary reconstruction deposits (asterisk) are obvious. **H**: Active resorption (by the time the animal died) in an *Arapaima* opercular (main frame). The insert shows Howship's lacunae created by active resorption (red arrow) on top of a ridge, along with reconstruction deposit (asterisk) on the side of the same ridge (polarized light). **I**: Filling of a pit (asterisk) in an *Arapaima* opercular (right frame in polarized light). Scale bars: A = 1 mm; B, E main frame, F, H main frame, I = 500 μm; G main frame and insert, H insert = 250 μm; C, D = 50 μm.

traits of the tissue in the core of the ridges (as compared to the basal cortex and ridge sides), and the spacing of growth marks. In addition to this basal process, a strong activity of inner resorption, not followed by reconstruction, modifies the whole geometry of the ridge network, and makes the pits deeper by eroding their floors from inside.

Osteoglossiformes (*Arapaima gigas*). The opercular of *Arapaima gigas* has a diploe architecture, and a simple histological structure: it comprises two (basal and superficial) cortices made of the same kind of osseous tissue. The latter is a brightly birefringent avascular parallel-fibered bone displaying cyclic growth marks in the form of faint annuli (Fig. 11F). The annuli and the bone strata forming the floor of the pits have histological traits close to those of the lamellar bone tissue. Conversely, the ridge core comprises a less birefringent tissue (Fig. 11F,G). Both cortices house abundant, short Sharpey's fibers. Active remodeling occurs in the central part of the opercular, transforming the deep strata of the cortices into a loose spongiosa (Fig. 11F). The superficial, ornamented cortex displays evidence of extensive remodeling, in the form of reversion lines separating discordant bone deposits (Fig. 11G), along with Howship's lacunae (Fig. 11H). The whole surface of the ornamented cortex is involved and (as described above in turtles) reconstructive bone deposits extend to both the floor of the pits, where they constitute secondary deposits, and the top of the ridges, where they can either represent secondary or primary bone deposits. Several subsequent resorption/reconstruction cycles occur in some areas (Fig. 11H).

According to these histological observations, differentiation and growth of ornamental reliefs in *Arapaima* opercular result from a double mechanism: 1) the commonly-observed discrepancy in accretion rate between pit bottom (slow accretion) and ridge top (faster accretion); 2) an extensive, patchy remodeling of ornamented surfaces by cycles of resorption and subsequent reconstruction. Additionally, the common processes of ridge drift (Fig. 11F) and pit filling (Fig. 11I) observed in most taxa occur also in *Arapaima*.

Siluriformes (*Phractocephalus hemioliopterus* and *Sciades proops*)

The *Phractocephalus* opercular features a typical diploe (Fig. 12A) of relatively low compactness (78.8%). The general histological structure of this bone closely resembles that observed in most temnospondyl bones: the whole basal cortex, the parts of the superficial cortex forming the floor of the pits, and the lateral sides of the ridges are made of birefringent parallel-fibered tissue (Fig. 12A,C,E). This tissue is basically avascular and non-remodeled; however, limited Haversian remodeling occurs in the floor of some pits (Fig. 12C). The core of the ridges is made of a poorly birefringent tissue structurally halfway between the parallel-fibered and the woven-fibered types (Fig. 12C,D). Annuli, more broadly spaced in the axial region of the ridges than in the floor of the pits, occur in both the superficial and basal cortices (Fig. 12D,E). Vascular canals (primary osteons and simple canals) mainly occupy the base of the ridges, and can be ramified. The central spongiosa of the opercular, made of a coarse woven-fibered tissue that tends to stretch into the core of the ridges, is intensely remodeled. With the exception for some secondary osteons located in the floor of some pits, the ornamented layer displays no trace of remodeling, and lacks deep or superficial resorption traces such as reversion lines or Howship's lacunae. The superficial cortex is in continuity with subjacent bone layers, and gradually merges with them (Fig. 12C,D).

The histological characteristics of the opercular (primary bone deposits, spacing of growth marks) suggest that bone accretion rate is more elevated on top of the ridges than on the floor of the pits. This sole difference suffices to explain the creation and growth of ornamental reliefs. During growth, the ridges are subject to the same processes of lateral drift (Fig. 12A) or width reduction (Fig. 12D) as those observed in the temnospondyls. Moreover, pits can be filled up and replaced in situ by ridges, a process resulting from a steep increase in local accretion rate, as suggested by vascular proliferation at those spots (Fig. 12E).

The opercular of the second siluriform species, *Sciades proops*, has a simple structure with two cortices (basal and superficial ornamented) framing a central cancellous region (Fig. 12F). The basal cortex is made of well-characterized lamellar bone tissue, whereas the superficial one is made of both poorly birefringent parallel-fibered bone in the core of the ridges, and brightly birefringent lamellar tissue in the floor of the pits (Fig. 12F,G). Cyclical growth marks in the form of lines of arrested growth are conspicuous in the core of the ridges (Fig. 12G). Their spacing clearly reveals that accretion rate was maximal on the top of the ridges and minimal on their sides. The central spongiosa results from a complex resorption process that creates broad erosion bays in the deep strata of the ornamented cortex, especially in the floor of the pits (Fig. 12F,H). Two additional differences distinguish the basal and the superficial cortices: 1) the basal cortex lacks Sharpey's fibers whereas the superficial one is entirely colonized by very dense bundles of long fibers with a fan-like arrangement, especially in ridges (Fig. 12G insert); 2) the basal cortex shows no sign of remodeling; conversely, the ornamented cortex is extensively and intensively remodeled. Bone remodeling, characteristically evidenced by resorption lines and discordant bone deposits, takes place

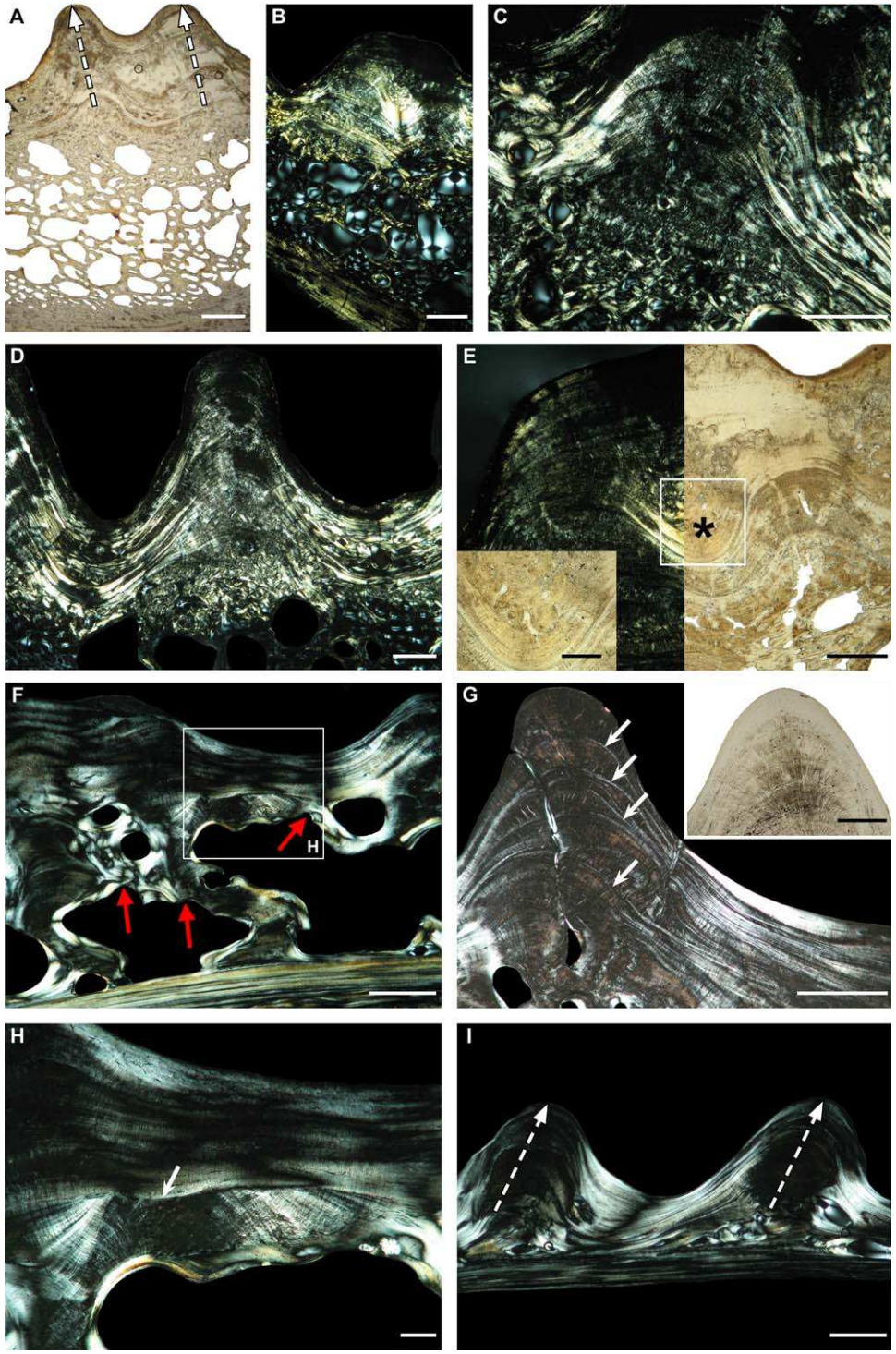

Fig. 12. General histology of ornamented bones in the extant teleosts *Phractocephalus hemioliopterus* (**A–E**) and *Sciades proops* (**F–I**). **A**: general diploe structure of a *Phractocephalus* opercular. Dashed arrows point to the sub-parallel drift of ridges during growth. **B**: General structure of the same bone in polarized light. Both the basal and superficial cortices are birefringent. **C**: Basic bone histology in ridge and pit (transmitted polarized light). Birefringence is poor in the core of the ridge, and there is no reversion line or discordant bone deposits between the superficial and the deeper layers. **D**: Decrease in ridge width during growth (polarized light). **E**: Pit filling during growth. Local vascular density is increased (insert showing enlargement of the framed field), which suggests that pit filling (asterisk) is due to acceleration in accretion (right half and insert: ordinary transmitted light; left frame: polarized light). **F**: General inner architecture of a *Sciades* opercular. The deep strata of the superficial cortex are submitted to intense and extensive remodeling initiated by resorption (red arrows) (polarized light). **G**: Bone histology in a ridge of the same bone (main frame: polarized light; insert: natural transmitted light). The core of the ridges is made of a poorly birefringent tissue displaying cyclical lines of arrested growth (arrows). The view in the insert shows the abundance of Sharpey's fibers in this bone. **H**: Reversion line (arrow) and discordant bone deposits in the superficial layer (polarized light). **I**: Sub-parallel lateral drift of two ridges (dashed arrows) (polarized light). Scale bars: A, B = 1 mm; C-F, I = 500 μm; E insert, G main frame = 250 μm; G insert = 200 μm; H = 100 μm.

on the surface of the ornamental reliefs as well as in the depth of the cortex, especially in the floor of the pits (Fig. 12H). This process spreads over the whole surface of the ornamented layer.

Histological observations suggest that the differentiation and growth of bone ornamentation on the opercular of *Sciades proops* results from the combination of three processes: 1) faster growth on top of the ridges; 2) resorption of pit bottom provoking an increase in pit depth; 3) extensive remodeling of the ornamented surface through resorption and reconstruction. Additionally, the common processes of ridge drift (Fig. 12I), and pit filling occur also in *Sciades* opercular.

Dipnomorpha

Porolepiformes (*Holoptychius*). The scale of *Holoptychius* is not a diploe but a compact (95–97%) solid bone organized in two very distinct layers: a totally avascular basal stratum some 1.8 mm in mean thickness and a superficial layer of variable thickness (0.5–1 mm) densely vascularized by a reticular-like network of wide (diameter *ca*. 50 μm) vascular canals (Fig. 13A). Scale ornamentation is displayed by this second layer. The basal layer is made of typical orthogonal (though slightly irregular) osseous plywood displaying 10–20 bone strata (depending on the area) alternatively light and dark in transmitted polarized light. The dark strata are 100–120 μm in thickness and display big clusters (some 10–12 μm in diameter) of fibers sectioned transversely. The light strata (80–90 μm in thickness) are made of a homogeneous, strongly birefringent tissue (Fig. 13B). Osteocyte lacunae are visible neither in the dark nor in the light strata. Both kinds of strata are actually made of the same type of osseous tissue, pure parallel-fibered bone; the different aspects that they show in polarized light are due to their orthogonal orientation. This description is in agreement with that of the "non-stabilized orthogonal" plywood in the basal layer of elasmoid scales described by Meunier and Castanet (1982; see also Meunier, 1984; Francillon-Vieillot et al., 1990).

The transition between the basal plywood layer and the superficial, densely vascularized layer is very steep and clear-cut; however these layers are separated by no discontinuity such as a reversion line or any trace of a resorption process that could have occurred before the deposit of the superficial layer (Fig. 13C). The ornamented layer mainly consists of a complex assemblage of unevenly oriented big primary osteons (Fig. 13C–E). Traces of primary periosteal tissue between the osteons are extremely sparse and of uncertain interpretation. Bone structure in some regions of the sections suggests that this tissue could be of the same kind as that composing the dark strata of the plywood layer, that is, parallel-fibered bone with fiber bundles oriented perpendicular to the sectional plane. Bone ornamentation does not correspond to any precise histological detail in the structure of the superficial layer, with exception for a slight difference in the density of the vascular canals in the ridges, where canal density is high, and the bottom of the pits, where it is lower (Fig. 13A). This difference suggests that ornamental reliefs result from a slight difference in accretion rate between the top of the ridges and the bottom of the pits. Apparently, no other osteogenic process was involved in the differentiation and growth of *Holoptychius* ornamentation; in particular, the scale displays no evidence of superficial remodeling, ridge drift or pit filling. Among the various taxa examined hitherto in this study, only the ornamented cortex of *Benthosuchus* skull bone displays similar histological features as those observed in the *Holoptychius* scale.

Synthesis of Results: Basic Osteogenic Mechanisms Controlling Ornamentation Growth

The entire set of histological observations presented above allows the distinction of six main mechanisms involved in the differentiation and growth of bone ornamentation. These mechanisms are briefly described below, and sketched in Figure 14, with indication of the basic osteogenic processes (given here in the sequence of their occurrence) from which they result, as listed in Table 2.

1. Neither resorption nor remodeling are involved (Fig. 14A)
   i. Simple difference in accretion rate between ridges (high rate) and pit floor (low rate). This basic process of differential growth (Fig. 14A1) does not necessarily imply that bone accretion is accelerated on top of the ridges, as compared to the basal cortex of the bones, but that growth in pits is slower. Differential growth is compatible with various primary bone tissue types, and often associated with the various other processes listed below. When it is the sole active process, then pit enlargement during growth is limited, depending mainly on divergent ridge drift, or reduction in ridge width. Pit filling is frequent.
   ii. Acceleration of bone accretion on the ridges. In this process (Fig. 14A2), growth is faster, in absolute terms, on top of the ridges than elsewhere on a bone. It is revealed by the histological structure of osseous strata in the core of the ridges, as compared to those occurring in both the floor of the pits and the basal cortex of the bone. Pit enlargement is then controlled by the same mechanisms as those mentioned for the preceding case. This process is very widespread, and was observed in several taxa, but with great local variations.

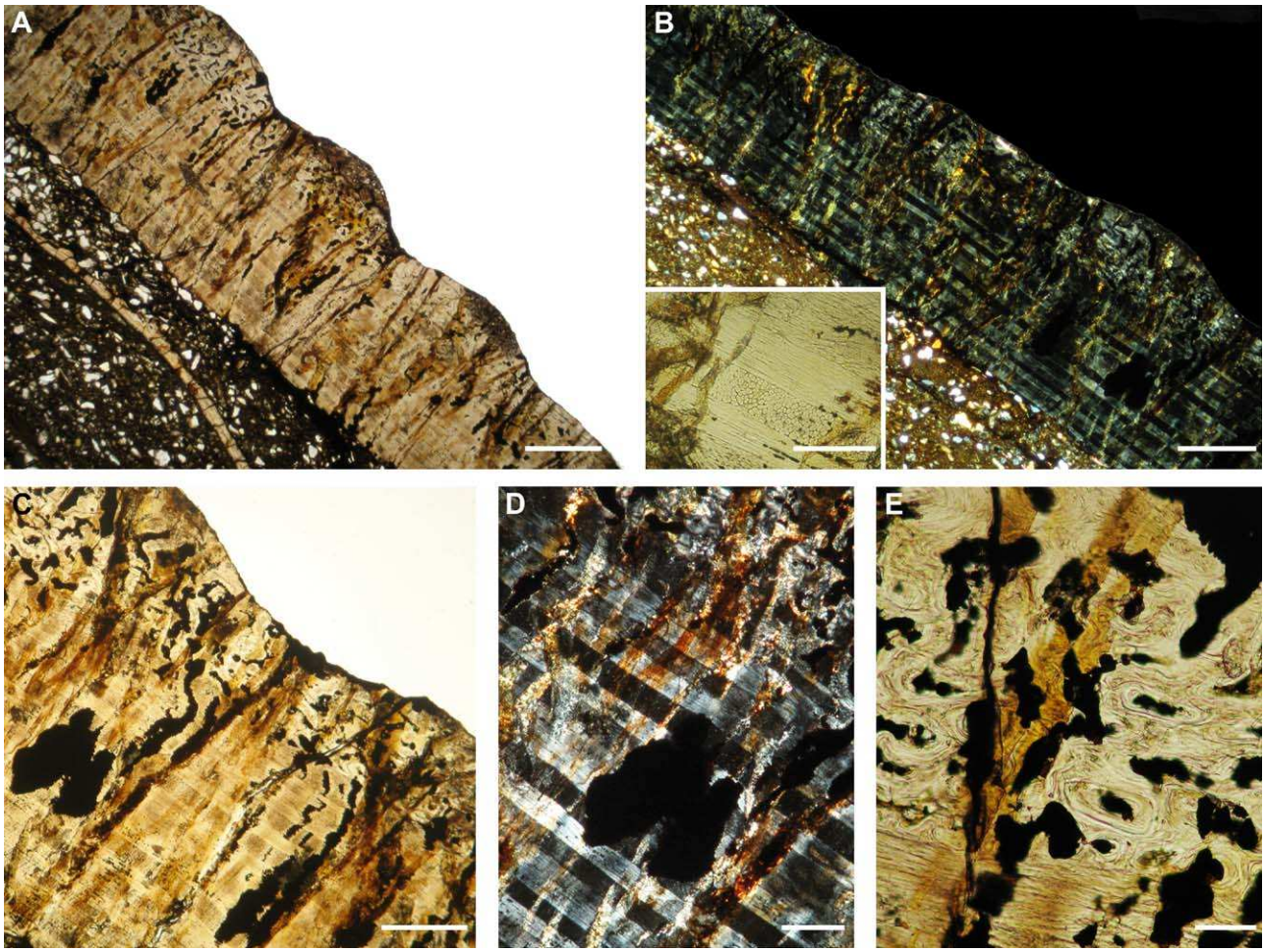

Fig. 13. Histology of the scale of the Late Devonian sarcopterygian *Holoptychius*. **A**: General structure of the scale. Two layers are visible: basal avascular plywood; densely vascularized superficial (ornamented) layer. **B**: Histological structure of the scale in polarized light (main frame), with detail of the plywood structure in natural light (insert). **C**: Detail of the transition zone between the basal plywood and the superficial vascularized layer. There is no discontinuity (e.g., reversion line) between this layer and the subjacent plywood. **D**: Closer view at the transition zone (polarized light). Again, no discontinuity separates the plywood from the superficial layer. **E**: Complex, histological organization of the superficial ornamented layer. Scale bars: A, B main frame = 1 mm; C = 500 μm; D = 250 μm; B insert = 200 μm; E = 100 μm.

2. Resorption or remodeling are involved (Fig. 14B–F)
   i. Extensive, continuous resorption of bone surface prior to the development of a secondary layer that bears ornamentation (Fig. 14B,C). The resorption process may result either in entire flattening of the bone surface (so called "flat integral resorption" hereafter; Fig. 14B) before the accretion of the ornamented layer (as exemplified by *Amyda cartilaginea*), or in the formation of initial reliefs that shall be further amplified (called below "curvy integral resorption"; Fig. 14C) by subsequent bone deposits. In both cases, the secondary, ornamented layer is of the parallel-fibered type and the creation (or amplification) of the ornamental reliefs is due to one of the two processes defined above, i.e. differential growth with (Fig. 14B2,C2) or without (Fig. 14B1,C1) acceleration on top of the ridges.
   ii. Creation of pits by isolated resorption spots (patchy resorption) on bone surface, with subsequent local (patchy) reconstruction (Fig. 14D). In the present sample, this typical remodeling process is well-represented by the actinopterygian *Arapaima*, the lissamphibians *Ceratophrys* and *Thaumastosaurus*, and the turtle *Araripemys*. It allows permanent and flexible modification (reshaping) of bone ornamentation at both local (e.g., one single pit or ridge) and general (the whole set of pits on a bone surface) scales. This process thus makes a fine dimensional accommodation of bone ornamentation to global skeletal growth possible (in addition to contributing to calcium and phosphorus recycling; cf. Dacke, 1979). Bone accretion on the ridges can be accelerated (Fig. 14D2) or not (Fig. 14D1).

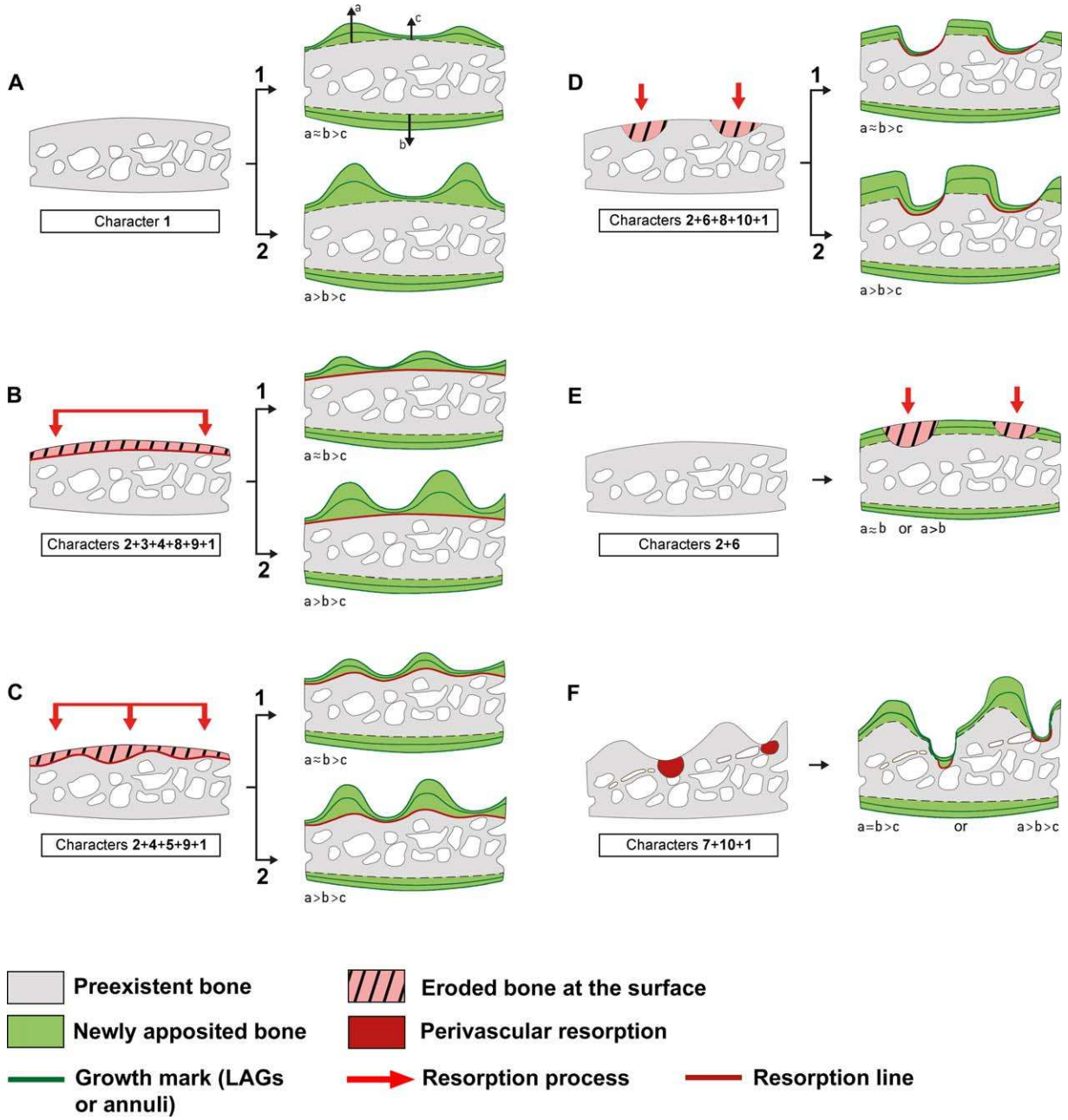

Fig. 14. Schematic representations of the six main mechanisms controlling the differentiation and growth of bone ornamentation, as observed in the sample. For each of these mechanisms, the numbers given in the rectangles refer to the basic osteogenic processes, indicated in Table 2 as "characters", which are sequentially involved in ornamentation morphogenesis. **A1**: Ornamentation is created by simple differential growth. Apposition rate during two growth cycles (green surfaces and green lines) on the ridges (a) is equal to that on the basal cortex (b), and higher to that on pit floor (c). **A2**: Ridge elevation through acceleration of bone apposition ($a > b > c$). **B**: Extensive resorption creating a flat surface prior to the formation of ornamental reliefs. The resorption process sets in place a resorption line (red line). The subsequent bone deposit on the superficial cortex may create ridges through simple differential growth (**B1**) or acceleration (**B2**). **C**: Extensive resorption creates a first outline of ornamental reliefs that is further enhanced in subsequent growth by simple differential growth (**C1**) or acceleration on the ridge (**C2**). **D**: Superficial remodeling of the ornamented cortex. Patchy, discontinuous resorption creates initial pits. Subsequent bone deposits without (**D1**) or with (**D2**) acceleration on ridges create ridges and reconstruct the eroded part of pit floors. In this case, resorption lines and secondary deposits are limited to pit floor. **E**: Pits are created by simple resorption of the superficial cortex, with no subsequent reconstruction. This process is likely to take place at the end of the growth period. F: Intra-cortical erosion of pit floor, with limited, subsequent reconstruction. This process is mainly perivascular. Various configurations may occur for the rate of bone deposition on top of the ridges.

TABLE 2. Character states (numbers in brackets) representing the basic osteogenic processes responsible for the differentiation of the pit and ridge type of bone ornamentation in Vertebrates

	Taxon	Differential Growth (1)	Resorption (2)	Integral Resorption (3)	Flat integral Resorption (4)	Curvy integral Resorption (5)	Patchy superf. Resorption (6)	Inner Resorption (7)	Reconstruction (8)	Continuous Reconstruction (9)	Patchy Reconstruction (10)	Source
Placodermi												
Arthrodira	*Incisoscutum* sp.	1	0	0	0	0	0	0	0	0	0	1
	Bothriolepis canadensis	1	0	0	0	0	0	0	0	0	0	2
Actinopterygii												
Acipenseriformes	*Acipenser sturio*	1	1	0	0	0	0	1	0	0	0	PS
Neopterygii	*Phractocephalus hemioliopterus*	1	0	0	0	0	0	0	0	0	0	PS
	Sciades proops	1	1	1	0	1	0	1	1	1	0	PS
	Arapaima gigas	1	1	0	0	0	1	0	1	0	1	PS
Sarcopterygii	*Holoptychius* sp.	1	0	0	0	0	0	0	0	0	0	PS
Stegocephali												
Temnospondyli	*Eryops megacephalus*	1	0	0	0	0	0	0	0	0	0	PS
	Kupferzellia sp.	1	0	0	0	0	0	0	0	0	0	PS
	Mastodonsaurus sp.	1	0	0	0	0	0	0	0	0	0	PS
	Parotosuchus sp.	1	0	0	0	0	0	0	0	0	0	PS
	Peltobatrachus sp.	1	0	0	0	0	0	0	0	0	0	PS
	Platyoposaurus sp.	1	0	0	0	0	0	0	0	0	0	0
	Plagiosternum sp.	1	0	0	0	0	0	0	0	0	0	PS
	Trimerorachis insignis	1	0	0	0	0	0	0	0	0	0	PS
	Benthosuchus sushkini	1	0	0	0	0	0	0	0	0	0	PS
	Metoposaurus diagnosticus	1	0	0	0	0	0	0	0	0	0	3
	Dutuitosaurus ouazzoui	1	0	0	0	0	0	0	0	0	0	PS
	Indet. sp.	1	0	0	0	0	0	0	0	0	0	PS
	Stanocephalosaurus sp.	1	0	0	0	0	0	0	0	0	0	PS
Embolomeri	*Archeria* sp.	1	0	0	0	0	0	0	0	0	0	PS
Chroniosuchia	*Chroniosaurus dongusensis*	?	1	0	0	0	1	0	1	0	1	4
	Uralerpeton tverdochlebovae	1	0	0	0	0	0	0	0	0	0	5
	Bystrowiana cf. permiria	1	0	0	0	0	0	0	0	0	0	PS
Nectridea	*Diplocaulus* sp.	1	0	0	0	0	0	0	0	0	0	PS
Lissamphibia	*Ceratophrys* sp.	1	1	0	0	0	1	0	1	0	1	PS
	Indet. cf. *Thaumastosaurus*	1	1	0	0	0	1	0	1	0	1	PS
	Latonia gigantea	1	1	0	0	0	1	1	1	0	1	PS
Amniota	*Captorhinus aguti*	1	0	0	0	0	0	0	0	0	0	PS
	Condorchelys antiqua	1	1	0	0	0	1	0	1	0	1	5
	Aspideretoides sp.	1	1	1	1	0	0	0	1	1	0	PS, 6
	Glyptops plicatulus	1	0	0	0	0	0	0	0	0	0	7
	Stupendemys geographicus	?	1	0	0	0	1	0	1	0	1	8
	Amyda cartilaginea	1	1	1	1	0	0	0	1	1	0	PS
	Trionyx triunguis	1	1	1	1	0	0	0	1	1	0	PS
	Trionyx triunguis foss.	1	1	1	1	0	0	0	1	1	0	PS
	Cyclanorbis senegalensis	1	1	1	0	1	0	0	1	1	0	PS
	Pseudemys rubriventris	1	1	0	0	0	1	0	0	0	0	PS

Table 2. (continued).

Taxon	Differential Growth (1)	Resorption (2)	Integral Resorption (3)	Flat integral Resorption (4)	Curvy integral Resorption (5)	Patchy superf. Resorption (6)	Inner Resorption (7)	Reconstruction (8)	Continuous Reconstruction (9)	Patchy Reconstruction (10)	Source
Araripemys barretoi	1	1	0	0	0	1	0	0	0	1	PS
Necrosaurus cayluxensis	0	1	0	0	0	1	0	0	0	0	PS
Crocodyliformes (all taxa)	1	1	0	0	0	1	0	1	0	1	9
Phytosauria	1	1	0	0	0	1	0	1	0	1	9, 10
Doswelliidae	1	1	0	0	0	1	0	1	0	1	11
Aetosauria	1	1	0	0	0	1	0	1	0	1	12, 10
Revueltosaurus callenderi	1	1	0	0	0	1	0	1	0	1	10
Jaxtasuchus salomoni	1	1	0	0	0	1	0	1	0	1	10
Lupeosaurus kayi	1	0	0	0	0	0	0	0	0	0	PS

Score 0: character absent; score 1: character present. The basic information for building this table originates from the present study (PS), or from published studies referenced by the following numbers: 1-Giles et al. (2013); 2-Downs and Donoghue (2009); 3-Witzmann (2009); 4-Buchwitz et al. (2012); 5-Cerda et al. (2015b); 6-Scheyer et al. (2012); 7-Scheyer and Anquetin (2008); 8-Scheyer and Sánchez-Villagra (2007); 9-Buffrénil et al. (2015); 10-Scheyer et al. (2014); 11-Cerda et al. (2015a); 12-Cerda and Desojo (2010).

iii. Creation or deepening of pits by isolated resorption spots on bone surface, with no subsequent reconstruction (Fig. 14E). This simple situation, mainly observed in the necrosaur specimens (and, to a lesser extent, the turtle *Pseudemys*), offers only two possibilities for pit growth during ontogeny: i) increase in diameter through additional resorption on pit periphery; ii) increase in depth through either resorption of pit floor or elevation of ridges. In the necrosaur osteoderms, simple pit excavation was the only mechanism that created ornamentation in flat osteoderms but, in keeled ones, it contributed to the accentuation of pre-existing bone reliefs. It seems likely (though more data are needed) that simple excavation of pits occurs by the end of somatic development in taxa that have limited growth, as exemplified here by the squamate taxon Necrosauridae. Theoretically, acceleration of bone accretion on top of the ridges is possible.

iv. Deep intraosseous resorption of pit floor (Fig. 14F). This process complements other basic morphogenetic mechanism such as differential growth. It involves a resorption activity, often linked to the course of vascular canals, occurring inside the bones, not on their surface. It allows deepening of the pits through the inner erosion and final opening of their floor. Partial reconstruction locally follows the resorption phase. This process, as all the others described above, can be associated or not with accelerated ridge growth. Morphologically, it results in deep, well-like pits, as exemplified by the chondrostean *Acipenser* or the anuran *Latonia*.

In order to have a synthetic view of the taxonomic distribution of these various morphogenetic mechanisms, considered through the basic osteogenic process from which they result, all the histological data about the differentiation and growth of the pit and ridge type of ornamentation, be they derived from the present study or from articles previously published by other authors, were collected and organized into Table 2 that was used to conduct the ML optimization study presented below. Of course, among the data obtained from literature, only those relative to the pit and ridge ornamentation type, and based on clear, unquestionable descriptions accompanied by sharp, explicit illustrations were retained.

Evolutionary Analyses

Evolutionary models can be used, to some extent, to test hypotheses. Our hypothesis is that resorption is selectively advantageous in the development of dermal ornamentation; therefore, forward rates should be higher than backward rates for characters reflecting this phenomenon. Assessing support

for evolutionary models is also a prerequisite to tracing character history, so results about models are presented before optimizations.

The ML analyses of the presence of resorption (character 2 in Table 2) on both topologies (Fig. 15) indicate that the two-rate model is better-supported than the single-rate model, though the difference in support between both models is greater when turtles are placed outside diapsids than among them (Table 3). In both cases, the forward rate is about 3–4 times greater than the backward rate. The occurrence of resorption probably displays the most reliable rates because it is the most variable in our sample; hence, there are more data to estimate the model parameters. This reflects the complexity of the evolutionary pattern of the character (Fig. 15), which appears to display four gains and one loss in stegocephalians, and a pattern more difficult to interpret in actinopterygians (but involving at least two events, possibly including a loss).

Limited additional support for our hypothesis can be gathered from other characters. For instance, for characters 6 (patchy superficial resorption) and 8 (reconstruction), the forward rate is also higher than the backward rate in the two-rate model, though little weight can be attached to this because the one-rate model is better supported, in both cases (Table 3).

A few characters seem to show greater backward than forward rates, but these estimates are probably not reliable. For instance, integral resorption (character 3) has forward and backward rates of 6.21 E-4 and 3.34 E-3 respectively, but these rates cannot be well-constrained because the character appears to display only two gains and no losses (Fig. 16A), and for this character, support for the one-rate model is nearly as great as for the two-rate model (Table 3). An even more instructive case is flat integral resorption (character 4), for which support for the two-rate model is about four times greater than for the one-rate model. For this character, the forward rate (3.81 E-4) is much smaller than the backward rate (6.61 E-3), but this appears to be also unreliable because the model infers the gain two nodes deeper than the most parsimonious position. This situation is presubably due to the short branches linking these nodes, and this forces two losses in the cryptodire turtles *Cyclanorbis* and *Pseudemys* (Fig. 16B). Curvy integral resorption (character 5) also has a greater backward than forward rate according to the two-rate model, but support for that model is less than for the one-rate model (Table 3), and only two gains (and no losses) can be inferred (Fig. 16C). Inner resorption (character 7) similarly shows a greater backward than forward rate according to the two-rate model, but support for that model is only half that for the one-rate model (Table 3), and only three gains (and no losses) can be inferred (Fig. 16D). Continuous reconstruction (character 9) has backward rates about five times greater than forward rates, but support for one- and two-parameter models is about equal (Table 3), and history of the character could be explained by two gains and no losses (Fig. 16F). Finally, for patchy reconstruction (character 10), the backward rate is greater than the forward rate, but the one-rate model has nearly three times more support than the two-rate model, so these estimates cannot be reliable (Table 3).

The ML optimizations (always illustrated and shown using the model with best support) show clearly that resorption (character 2) was absent in the development of ornamentation in the first gnathostomes (Fig. 15). Indeed, resorption is found only in a few clades; it appeared among actinopterygians (perhaps more often than parsimony suggests), among some chroniosuchians (in the Late Permian), among lissamphibians (it appears to prevail at least among anurans), and in most sauropsids. The details of this history are uncertain, as shown by the probabilities of the states at various nodes. The most uncertain part of this history is found among actinopterygians. At the base of the clade, both models under both topologies suggest that the probability that resorption was absent is around 0.73–0.75 (Fig. 15; Table 4). Higher up that clade, the probability that early teleosts lacked resorption decreases, a result consistent with the fact that two out of the three sampled teleosts show resorption (Fig. 15). By contrast, the condition at the base of sauropsids is relatively clear, with both models under both topologies yielding probabilities of resorption being absent in the process responsible for dermal sculpturing around 0.96–0.99 (Table 4). However, the uncertainty in the position of turtles results in substantial uncertainty about the condition in the first crown-reptiles. If turtles are diapsids (Fig. 15B), that ancestor probably used resorption in the development of dermal ornamentation; if turtles are outside diapsids, that ancestor (which then coincides with the basalmost node in Sauropsida) probably lacked resorption, a result partly attributable to the fact that the early eureptile *Captorhinus aguti* lacked such resorption, and partly because of the much greater age of the ancestor, under that topology (Fig. 15A).

The evolution of patchy resorption (character 6) follows a similar pattern, but given that patchy resorption is a special case of the presence of resorption, it has a less inclusive taxonomic distribution. Thus, this character is present only in *Arapaima*, among the sampled actinopterygians, so the character was probably ($0.9 < P < 0.96$) absent at the base of Actinopterygii (Table 4) and of Teleostei. The character was similarly absent at the base of Sauropsida ($0.98 < P < 1.00$), as expected (Table 4). However, within turtles, it either appeared three

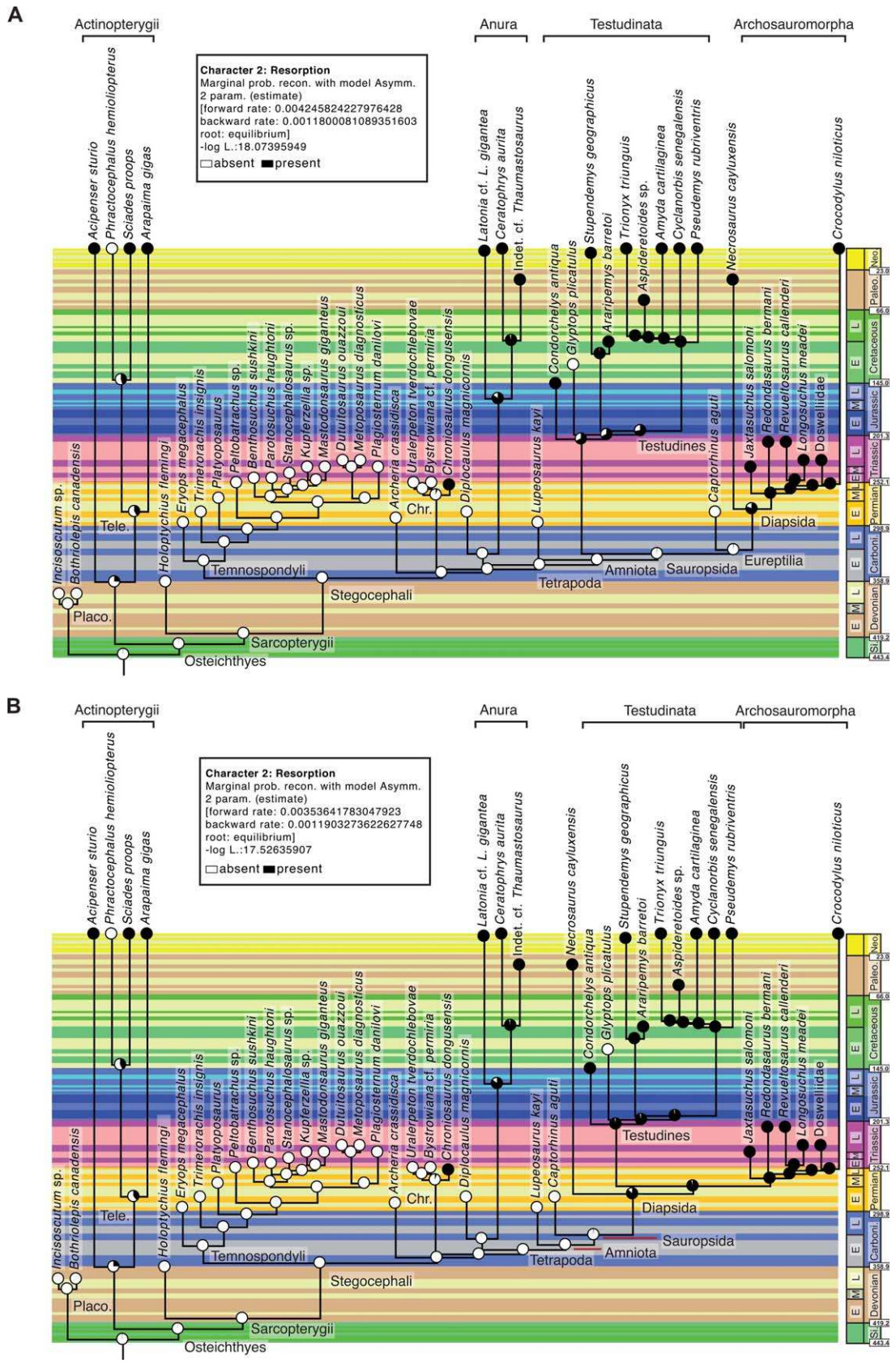

Fig. 15. Evolutionary pattern of the presence of resorption (character 2) in the developmental mechanism responsible for dermal ornamentation in gnathostomes. Maximum likelihood (ML) optimization performed in Mesquite 3.04. The relative extent of the black and white areas in the circles at the nodes indicate the probabilities of each state at that node (black: resorption; white: no resorption), according to the two-rate model of evolution, which is the best-supported model (Table 3). This graphic convention was introduced by Schluter et al. (1997). Two topologies are shown, one (A) with turtles outside Diapsida, and one (B) with turtles in diapsids, among archosauromorphs. Each horizontal colored band represents a geological stage from a recent time scale (Gradstein et al., 2012), though the names of these stages cannot appear on the figure for lack of space. Abbreviations for the names of the clades: Chr.: Chroniosuchia; Placo.: Placodermi; Tele.: Teleostei. Abbreviations for the geologic time scale: Carboni.: Carboniferous; E.: Early; L.: Late; M.: Middle; Neo: Neogene; Paleo.: Paleogene; Si.: Silurian.

TABLE 3. Assessment of evolutionary models of histological characters involved in the development of dermal ornamentation

Char.	Topology	Model	V	-log L.	Rate(s)	AIC	AICc	AICc weights
2, Res.	Test. (Lepi. Archo.)	Mk 1 rate	1	19.991	2.615 E-3	41.982	42.075	0.3056
		Mk 2 rates	2	18.074	F: 4.246 E-3; B: 1.180 E-3	40.148	40.434	0.6944
	Lepi. (Test. Archo.)	Mk 1 rate	1	18.872	2.157 E-3	39.745	39.838	0.4379
		Mk 2 rates	2	17.526	F: 3.536 E-3; B: 1.190 E-3	39.053	39.338	0.5621
3, Int. Res.	Lepi. (Test. Archo.)	Mk 1 rate	1	10.734	6.894 E-3	23.468	23.561	0.4883
		Mk 2 rates	2	9.591	F: 6.211 E-4; B: 3.338 E-3	23.182	23.467	0.5117
4, Flat Res.	Lepi. (Test. Archo.)	Mk 1 rate	1	9.915	3.244 E-4	21.831	21.924	0.2031
		Mk 2 rates	2	7.452	F: 3.813 E-4; B: 6.605 E-3	18.904	19.189	0.7969
5, Curv. Res.	Lepi. (Test. Archo.)	Mk 1 rate	1	8.425	5.075	18.839	18.942	0.5417
		Mk 2 rates	2	7.496	F: 7.006 E-4; B: 6.817 E-3	18.991	19.277	0.4583
6, Pat. Res.	Test. (Lepi. Archo.)	Mk 1 rate	1	20.885	2.559 E-3	43.770	43.863	0.6869
		Mk 2 rates	2	20.574	F: 2.631 E-3; B: 1.3086 E-3	45.148	45.434	0.3131
	Lepi. (Test. Archo.)	Mk 1 rate	1	20.593	2.414 E-3	43.185	43.278	0.7478
		Mk 2 rates	2	20.583	F: 2.482 E-3; B: 2.265 E-3	45.166	45.452	0.2522
7, Inner Res.	Lepi. (Test. Archo.)	Mk 1 rate	1	9.323	8.087 E-4	20.647	20.740	0.6460
		Mk 2 rates	2	8.829	F: 8.313 E-4; B: 3.021 E-3	21.657	21.943	0.3540
8, Rec.	Lepi. (Test. Archo.)	Mk 1 rate	1	22.299	3.656 E-3	46.599	46.692	0.7453
		Mk 2 rates	2	22.277	F: 3.846 E-3; B: 3.432 E-3	48.553	48.839	0.2547
9, Cont. Rec.	Lepi. (Test. Archo.)	Mk 1 rate	1	10.734	6.894 E-4	23.468	23.561	0.4883
		Mk 2 rates	2	9.591	F: 6.211 E-4; B: 3.338 E-3	23.181	23.467	0.5117
10, Pat. Rec.	Lepi. (Test. Archo.)	Mk 1 rate	1	19.587	2.166 E-3	41.173	41.266	0.7186
		Mk 2 rates	2	19.428	F: 1.936 E-3; B: 2.847 E-3	42.856	43.142	0.2814

In all cases, the sample size (n) is 45 taxa. Character 1 is invariable, so it is not shown. Only two characters (2 and 6) of particular relevance are analyzed on both trees.

Abbreviations: AIC: Akaike Information Criterion; AICc: Akaike Information Criterion corrected for small sample size; AICc weights: relative support for each model indicated by AICc; Archo.: Archosauria; B: backward transition rate; Char.: character; Con. Rec.: continuous reconstruction; Curv. Res.: curvy integral resorption; F: forward transition rate; Flat Res.: flat integral resorption; Inner Res.: inner resorption; Int. Res.: integral resorption; Lepi.: Lepidosauria; Mk 1 rate: Markov model with a single evolutionary rate; Mk 2 rates: Markov model with two evolutionary rates (a forward and a backward rate); Pat. Rec.: patchy reconstruction; Pat. Res.: patchy superficial resorption; Rec.: reconstruction; Res.: resorption; Test.: Testudinata; V: number of estimated parameters.

times convergently (and once in diapsids), if turtles are placed outside the Diapsida (Fig. 17A,B), or it appeared at the base of Sauropsida and was lost twice within turtles, if turtles are considered as diapsids (Fig. 17C,D). The evolutionary model (one or two parameters) affects the probabilities of ancestral states in that part of the tree, but much less than topology and branch lengths combined.

The evolution of other characters can be evoked briefly. Integral resorption (character 3) occurs only in the teleost *Sciades* and in most cryptodires (Fig. 16A), and flat integral resorption (character 4) occurs only in some cryptodires (Fig. 16B). Curvy integral resorption occurs only in one teleost and one cryptodire (Fig. 16C). Inner resorption (which starts within the bone, rather than at its surface) is also fairly uncommon; it occurs only in two teleosts and one anuran, which probably represent three independent acquisitions of this character (Fig. 16D). Reconstruction (character 8) occurs in most (but not all) taxa that have resorption (Fig. 16E). The exceptions concern the actinopterygian *Acipenser*, the squamate *Necrosaurus*, and the turtles *Araripemys* and *Pseudemys*. Thus, both character histories differ mostly by more losses in reconstruction (3.66 E-3, in the one-rate model, which has greatest AICc weight, and 3.43 E-3 in the two-rate model) than in resorption (1.18 E-3 in the two-rate model, which has greatest AICc weigth, and 2.16 E-3 in the one-rate model; both according to the topology with turtles in diapsids). Continuous reconstruction (character 9) is much rarer; it occurs in one teleost and most cryptodire turtles sampled here (Fig. 16F). Finally, patchy reconstruction (character 10) occurs in one teleost, one chroniosuchian, the sampled anurans, and most archosauromorphs (which include turtles, in the tree shown); this distribution suggests four appearances and a few reversals, which occur only within crown reptiles (Fig. 16G).

DISCUSSION

Comparative Overview

The new data presented above, as well as previously-published data show that bone ornamentation in most Paleozoic stegocephalians is produced by preferential apposition. Several descriptions of the histological structure of bones displaying the pit and ridge type of ornamentation have already been published, especially for Paleozoic stegocephalians (Bystrow, 1935; Witzmann, 2009; Witzmann and Soler-Gijón, 2010; Witzmann et al., 2010), turtles (Scheyer and Anquetin, 2008; Scheyer and Sánchez-Villagra, 2007; Scheyer et al., 2007), archosaurs (Cerda and Desojo, 2010; Scheyer et al., 2014; Buffrénil et al., 2015; Cerda et al., 2015a), and some other gnathostomes including placoderms (Downs

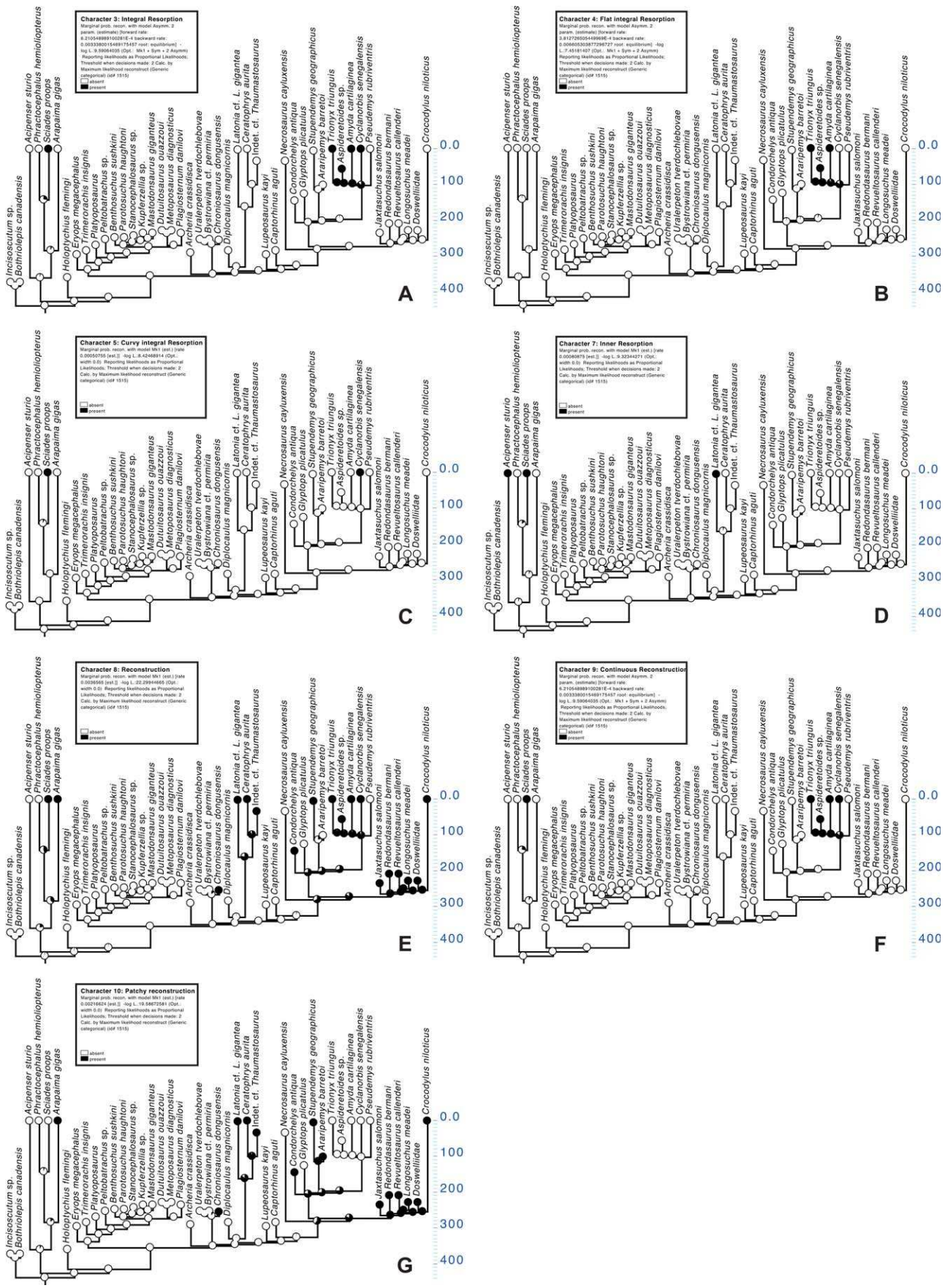

Fig. 16. Evolutionary pattern of the other histological characters linked with the development of dermal ornamentation. To save space, a single topology (with turtles in diapsids) is shown, and only the model with the greatest AICc weight is used to infer character history. For more information, see legend of Figure 15. **A**: Integral resorption (character 3), 2-rate model. **B**: Flat integral resorption (character 4), two-rate model. **C**: Curvy integral resorption (character 5), one-rate model. **D**: Inner resorption (character 7), one-rate model. **E**: Reconstruction (character 8), one-rate model. **F**: Continuous reconstruction (character 9), two-rate model. **G**: Patchy reconstruction (character 10), one-rate model.

TABLE 4. Ancestral states for two characters at selected nodes

Node	Character	Topology	P_0 Mk 1 rate	P_0 Mk 2 rates	P_0, model-averaged	P_1, model-averaged
Sauropsida	2. Resorption	Test. (Lepi. Archo.)	0.9598	0.9882	0.9795	0.0205
	2. Resorption	Lepi. (Test. Archo.)	0.9800	0.9883	0.9847	0.0153
	6. Patchy superficial resorption	Test. (Lepi. Archo.)	0.9809	0.9947	0.9852	0.0148
	6. Patchy superficial resorption	Lepi. (Test. Archo.)	0.9786	0.9800	0.9790	0.0210
Actinopterygii	2. Resorption	Test. (Lepi. Archo.)	0.7480	0.7389	0.7417	0.2583
	2. Resorption	Lepi. (Test. Archo.)	0.7391	0.7513	0.7460	0.2540
	6. Patchy superficial resorption	Test. (Lepi. Archo.)	0.9065	0.9530	0.9210	0.0790
	6. Patchy superficial resorption	Lepi. (Test. Archo.)	0.9157	0.9183	0.9164	0.0836

Abbreviations: Archo.: Archosauria; Lepi.: Lepidosauria; Mk 1 rate: Markov model with a single evolutionary rate; Mk 2 rates: Markov model with two rates (forward and backward); P_0: probability that state 0 was present, according to a given model; P_1: probability that state 1 was present, according to a given model; Test.: Testudinata.

and Donoghue, 2009; Giles et al., 2013). As a consequence, histological studies of dermal bones in most of the temnospondyl, lepospondyl and a few amniote taxa used in the present work are already available in the literature. A detailed comparison between our observations and those previously published would be of limited interest because the details of bone structure (e.g., nature, density and orientation of vascular canals, characteristics of cell lacunae, etc.) are prone to substantial variation between conspecific specimens, bones of a single skeleton, and even the parts of a section. Assessing the importance of this variability in all the taxa that we used is beyond the scope of this study, and would require a much broader sample to be performed. This is why the information that we consider most significant for our purpose are the gross osteogenic events unambiguously displayed by bone sections, that is, the occurrence or absence of superficial bone resorption (followed or not by reconstruction), as well as the nature of local bone tissues (woven-fibered, parallel-fibered, or true lamellar bone) and their vascular supply. The latter features are considered together, in the particular context of each section, as a set of clues revealing local trends in appositional rates, as exposed above (see "Basic clues for interpreting relative bone growth rates" in the Material and Methods section).

For Paleozoic stegocephalians, the histological descriptions presented here generally agree with published data regarding the most relevant question: the creation and growth of ornamental reliefs is basically due to preferential growth on top of the ridges, and excludes significant contribution of superficial resorption, as clearly settled by Witzmann and Soler-Gijón (2010; also see Bystrow, 1935, 1947 and Vickaryous and Hall, 2008). The only exception is relative to some Paleozoic stegocephalians (chroniosuchians) that have been considered either stem-tetrapods (Laurin, 2000; Vallin and Laurin, 2004), as our reference tree shows, or reptiliomorphs (Clack and Klembara, 2009; Schoch et al., 2010), and which are considered in more detail below.

This study further documents the mechanisms contributing to ornamentation growth in basal tetrapods by substantiating the concept of "preferential growth". The latter does not necessarily mean that absolute growth rate is increased on the ridges, as compared to the basal cortex, but that there is a local difference of speed (that difference can be pronounced or slight) between bone apposition on ridge top and on pit floor. Rather than "preferential" growth, the actual process involved is thus "differential" growth, although a real acceleration in local accretion may occasionally occur, especially when a pit is filled up and replaced *in situ* by a ridge.

Because Sharpey's fibers are generally much more abundant in ridges than in pit floors, they have been suspected to induce this differential growth process through traction on bone surface (Witzmann and Soler-Gijón, 2010). The results of the present study confirm that anchorage fibers are unevenly distributed within ornamented cortices; however, their role in the development of ornamental reliefs remains to be ascertained. For the present, this hypothesis indeed fails to explain why ornamentation appears only on the superficial (often dorsal) side of osteoderms, while both sides can be firmly bound to the dermis by thick bundles of Sharpey's fibers (e.g., Moss, 1969; Levrat-Calviac, 1986). It also fails to explain why ornamented bones in some taxa, such as most of the pseudosuchians (cf. Buffrénil et al., 2015), contain far less Sharpey's fibers than the bones of other taxa, like several turtles (this study), whereas they can display much sharper ornamental reliefs. At last, this interpretation does not address the question why ornamentation occurs in certain taxa and not in others, thus differing even between closely related taxa (e.g., among turtles, anurans, etc.), whereas there is no definite argument to settle that skin attachment on bone differs between them.

Beyond basal tetrapods, bone ornamentation has been shown in this study to be mainly caused by differential growth in a broad and diverse sample of gnathostome taxa, including actinopterygians (e.g., *Phractocephalus*), the finned sarcopterygian *Holoptychius*, the embolomere *Archeria,* and the Permian amniotes *Captorhinus* and *Lupeosaurus*. The involvement of this process was also reported

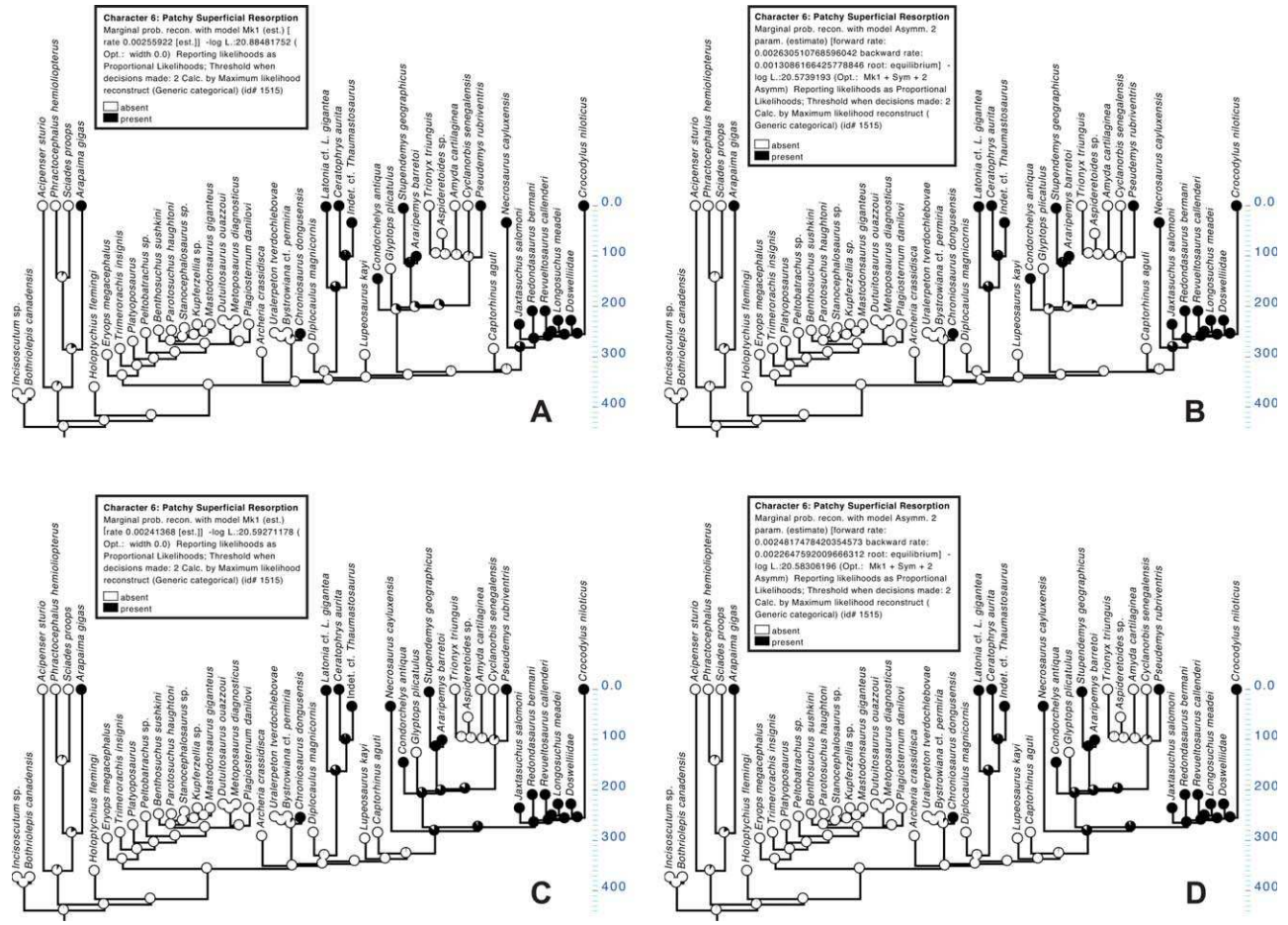

Fig. 17. Evolutionary pattern of the presence of patchy superficial resorption (character 6) in the developmental mechanism responsible for dermal ornamentation in gnathostomes. To make the tree more legible, the stratigraphic scale is omitted and is replaced by a simple absolute time scale. For more information, see legend of Figure 15. Optimization with turtles outside diapsids and a one-rate (**A**) and a two-rate (**B**) model, and with turtles in diapsids with a one-rate (**C**) and a two-rate (**D**) model.

in Devonian stem-gnathostomes, the placoderms, by Giles et al. (2013, see also Downs and Donoghue, 2009).

Turtle ornamentation involves local remodeling, whose interpretation has been problematic. Detailed histological studies of ornamented carapaces in various extant and extinct turtle taxa (e.g., stem-turtles, Trionychidae, Pelomedusidae, Podocnemidae, etc.) were recently conducted by Scheyer and Sánchez-Villagra (2007), Scheyer et al. (2007, 2012), and Cerda et al. (2015b). The occurrence of local remodeling, in the form of resorption and reconstruction topographically related to ornamentation, was mentioned and clearly illustrated in the trionychid *Aspideretoides* (Scheyer et al., 2012), the podocnemyd *Podocnemys erythrocephala*, the bothremydid (an extinct taxon) *Bothremys barbieri* (Scheyer et al., 2007), and the Jurassic stem turtle *Condorchelys antiqua* (Cerda et al., 2015b). However, an interpretation referring to pathological disorders was given to that observation: superficial carapace remodeling would reflect "a reaction to incipient osteomyelitis or *shell rot*" (Scheyer and Sanchez-Villagra, 2007). This interpretation, though in obvious contradiction with the highly organized geometrical pattern created by ornamentation, was later extended by Witzmann (2009) to the scarce phenomena of superficial resorption displayed by ornamented bones in basal tetrapods. This view explicitly refers (*op. cit*. p. 261) to the postulate that true (nonpathologic) bone ornamentation, whenever present, is mandatorily due to "preferential apposition" on ridges and, as such, represents a plesiomorphic character of tetrapods, deeply rooted within finned tetrapodomorphs. We concur that primitively in gnathostomes, resorption was apparently not involved in the development of dermal ornamentation, but not with the interpretation of a pathological nature of resorption (see below).

The process of preferential apposition on ridges is far from being the sole non-pathological mechanism susceptible to create ornamentation. The observations presented above reveal that superficial bone resorption, followed or not by secondary

reconstruction, is involved in 12 (including 6 turtles) of the 33 genera (one of which is not identified) sampled in this study. In addition, this process is a general feature of the pseudosuchians (Buffrénil et al., 2015), including the phytosaurs (Scheyer et al., 2014; Buffrénil et al., 2015), the aetosaurs (Cerda and Desojo, 2010), and the Dosweliidae (a taxon of Triassic archosauriformes: Cerda et al., 2015a). Moreover, the photographs of sections in the osteoderms of the chroniosuchians *Chroniosuchus dongusensis* and *Bystrowiella schumanni* published in Buchwitz et al. (2012) and Witzmann and Soler-Gijòn (2010) suggest that ornamentation in these taxa could also be due, at least partly, to superficial remodeling. It is noteworthy that the specimen of *Bystrowiana* used in the present study does not show evidence of a resorption process, as is also the case for the chroniosuchian *Uralerpeton tvedoschlebovae* described by Buchwitz et al. (2012). This question deserves further investigation. If the various contradictory observations relative to these taxa are confirmed by additional data, they would demonstrate that closely related forms can develop ornamentation through different mechanisms, a situation that precisely matches the observations presented above about the siluriforms *Phractocephalus* (in which only differential growth is involved) and *Sciades* (in which superficial bone remodeling occurs).

The discrepancies observed between various chroniosuchians could possibly reflect individual differences in calcium and phosphorus recycling (a process based on bone resorption), but this hypothesis is unlikely because the core of ornamented bones, which stocks much greater mineral reserves than their superficial layers for an obvious volumetric reason, is itself remodeled and already susceptible to contribute to calcium and phosphorus release. Thus, resorption involved in ornamentation development is unlikely to have appeared as a result of selective pressures to recycle mineral reserves. Finally, as properly pointed out by Cerda et al. (2015a), the formation of bone ornamentation "appears to be more complex than expected" and may respond to distinct immediate determinisms in the taxa that display it.

Our observations show a far more complex evolutionary pattern of the mechanisms responsible for the development of dermal sculpturing than we recently suggested (Buffrénil et al., 2015) based on a sample of Crurotarsi (Pseudosuchia). That study had suggested that the ornamentation found in Crurotarsi might not be homologous with that of most other gnathostomes because, contrary to the latter (represented only by a turtle and a temnospondyl, in our previous study), ornamentation of all sampled Crurotarsi (34 terminal taxa) involves resorption. However, we do confirm the primitive nature of the development of dermal sculpturing through differential apposition.

If the developmental mechanism is a guide to homology, our study identifies at least one other case in which ornamentation may not be homologous. Namely, the three sampled anurans have ornamentation associated with resorption. Given that most lissamphibian and many lepospondyl dermal bones lack ornamentation (Carroll and Gaskill, 1978; Laurin, 1998 [see character 3 in appendices 1 and 2 of that paper]), the occurrence of ornamentation in *Latonia*, *Ceratophrys*, and *Thaumastosaurus* may well result from one or several reappearances of ornamentation from ancestors with smooth dermal bones.

The other cases in which resorption appeared (Fig. 15) may not necessarily suggest that ornamentation in these taxa reappeared from unornamented ancestors because in teleosts and chroniosuchians dermal ornamentation is much more common. However, a comparative study with a much greater taxonomic sampling encompassing many unornamented taxa is needed to settle this question of historical (secondary) homology.

Functional Remarks

The role of bone ornamentation remains unclear. Since Bystrow's pioneer works (1935, 1947), at least five hypotheses have been proposed to explain the functional significance of this character. In brief, bone ornamentation could be involved in: a) reinforcement of skin anchorage onto bone (Witzmann, 2009; Witzmann et al., 2010), b) improvement of cutaneous respiration (Bystrow, 1947), c) prevention of blood acidosis (Janis et al., 2012), d)mechanical strengthening of the bones (Coldiron, 1974, Rinehart and Lucas, 2013) and, e) improvement of thermoregulation (Seidel, 1979; Clarac et al., 2015). Criticizing each of these hypotheses is beyond the scope of this article (see critical synthesis in Clarac et al. 2015). Recent studies by Rinehart and Lucas (2013) and Clarac et al. (2015) pointed out that most of these functional interpretations rely on the assumption that ornamentation was selected to increase the area of dermal bones; this increase can easily be quantified (Clarac et al., 2015). Therefore, the mechanisms controlling the size and geometric features of ornamental reliefs during growth, and thus the resulting gain in area of bone surface at every growth stage, represent key elements on which the results of the present study can yield some relevant information.

The two main processes creating bone ornamentation, i.e. differential growth (with or without absolute acceleration of bone apposition on ridges) and remodeling (resorption and re-deposition on the superficial cortex), have deep consequences on the general growth pattern of bone ornamentation, its consistency with the overall growth of the

bones, and the capacity of ornamental reliefs to be modified during ontogeny, at least regarding pit extension, shape and depth. A detailed study of crocodilian ornamentation (Buffrénil et al., 2015) shows that the initial creation of ornamental reliefs by local cortical resorption, and their subsequent growth by remodeling, are submitted to no geometric constraint since the global geometry of the ornamental pattern can be entirely modified through various processes. The ornamental pattern can indeed be altered by the excavation of new pits (resorption), rising or drifting of ridges (differential apposition) or entire filling of pits, independently of the anatomical limits of the bones, their shape, the level of their growth activity and, to some extent, the detailed characteristics of pre-existing reliefs. Conversely, ornamentation development resulting exclusively from differential growth is directly constrained by existing reliefs. Pits can then increase their individual dimensions (e.g., coping with growth of the entire body) only through the processes described above: divergent drift of ridges, or reduction of ridge width. An increase in pit size resulting from these processes is severely limited for two reasons: on the one hand, a divergent drift of the ridges framing an individual pit necessarily precludes the same phenomenon around the neighboring pits (competition for growth of neighboring pits); on the other hand, a pronounced reduction in ridge width should result, in a first time, in drastic thinning and, *in fine*, in stopping the increase in height of the ridges since width reduction cannot be indefinite.

Convergent models for explaining the geometric pattern of pit development on temnospondyl bones have been proposed by Witzmann et al. (2010) and Morkovin (2015). According to these models ornamentation initially consists of grooves delimited by long radial or sagittal ridges, depending on the shape of the bones. The grooves subsequently form pits by the development of short transverse ridges that transform a system of sub-parallel furrows into a honeycomb-like assemblage of roughly polygonal pits. The present study has shown that once the pits are set in place in temnospondyls, they can modify their size, shape or reciprocal position in limited proportions only with the sole mechanisms of ridge narrowing or drifting and, to a lesser extent, pit filling. In addition, this process is likely to be much slower than resorption-based mechanisms because, for a given volume of bone, the destructive action of osteoclasts is much faster than the constructive action of osteoblasts (e.g., Krstic, 1985). Both processes thus differ sharply in their capacities to control the morphological plasticity and the accommodation capabilities of bone ornamentation.

These considerations lead us to hypothesize that the mechanism that creates bone ornamentation through resorption and remodeling is more advantageous (if ornamentation must adjust through ontogeny to perform whatever its function may be) than the process that produces ornamentation solely by differential apposition. If this is correct, then the presence of the latter in some taxa must be a primitive character, whereas the former must be a more derived condition. We tested this hypothesis by verifying if the process based on resorption and remodeling appeared later than preferential apposition, and if there was a trend toward more resorption and remodeling over time.

Observation of the patterns on the timetrees (Figs. 15–17) is coherent with this hypothesis, with the absence of resorption and reconstruction being clearly the primitive condition, from the root of the tree (Gnathostomata) and well into Amniota, under both topologies and both evolutionary (one- and two rates) models used, for the nine variable characters analyzed here (Figs. 15–17). Furthermore, the ML models that presumably have the most reliable estimates further confirm this interpretation, with forward rates for these characters (numbers 2 and, to a lesser extent, 6) being greater than backward rates. However, our study cannot assess which selective advantages may be conferred by the presence of resorption in the development of dermal ornamentation. This topic would be best investigated using other approaches, such as experimentation.

ACKNOWLEDGMENTS

The authors are extremely grateful to all the colleagues who generously accepted to give or facilitate access to extant or fossil bone samples for this study: Salvador Bailon, Georges Bearez, Gaël Clément, France de Lapparent de Broin, François Meunier, Gabriella Prestes-Carneiro (all in the MNHN, Paris, France), Jean-Sébastien Steyer (CNRS/MNHN, Paris, France), Armand de Ricqlès (UPMC, Paris, France), Rainer Schoch (SMNS, Stuttgart, Germany), and Jean-Yves Sire (CNRS/UPMC, Paris, France). The authors also thank Vincent Rommevaux and Sophie Fernandez (MNHN, Paris, France) for their technical collaboration. The authors are grateful to two anonymous reviewers for their helpful comments and suggestions that improved this manuscript. The authors also thank the editor, Matthias Starck, for his efficient handling of the draft.

LITERATURE CITED

Amprino R. 1947. La structure du tissu osseux envisagée comme expression de différences dans la vitesse de l'accroissement. Arch Biol 58:315–330.

Amson E, Kolb C, Scheyer TM, Sánchez-Villagra MR. 2015. Growth and life history of middle Miocene deer (Mammalia, Cervidae) based on bone histology. C R Palevol 14:637–645.

Bollback JP. 2006. SIMMAP: Stochastic character mapping of discrete traits on phylogenies. BMC Bioinform 7:88.
Bolt JR. 1969. Lissamphibian origins: Possible protolissamphibian from the Lower Permian of Oklahoma. Science 166:888–891.
Buffrénil V de 1982. Morphogenesis of bone ornamentation in extant and extinct crocodilians. Zoomorphology 99:155–166.
Buffrénil V de, Rage J-C, Dauphin Y, Sire J-Y. 2011. An enamel-like tissue, osteodermine, on the osteoderms of a fossil anguid (Glyptosaurinae) lizard. C R Pale 10:427–438.
Buffrénil V de, Clarac F, Fau M, Martin S, Martin B, Pellé E, Laurin M. 2015. Differentiation and growth of bone ornamentation in vertebrates: A comparative histological study among the Crocodylomorpha. J Morphol 276:425–445.
Buchwitz M, Foth C, Kogan I, Voigt S. 2012. On the use of osteoderm features in a phylogenetic approach on the internal relationships of the Chroniosuchia (Tetrapoda: Reptiliomorpha). Palaeontology 55:623–640.
Bystrow AP. 1935. Morphologische Untersuchungen der Deckknochen des Schädels der Wirbeltiere. I. Mitteilung—Schädel der Stegocephalen. Acta Zool 16:65–141.
Bystrow AP. 1947. Hydrophilous and xerophilous labyrinthodonts. Acta Zool 28:137–164.
Carroll RL, Gaskill P. 1978. The Order Microsauria. Philadelphia: American Philosophical Society. 211 p.
Castanet J, Grandin A, Abourachid A, de Ricqlès A. 1996. Expression de la dynamique de croissance dans la structure de l'os périostique chez *Anas platyrhynchos*. C R Acad Sci III 319:301–308.
Castanet J, Rogers KC, Cubo J, Boisard J-J. 2000. Periosteal bone growth rates in extant ratites (ostriche and emu). Implications for assessing growth in dinosaurs. C R Acad Sci III 323:543–550.
Cerda IA, Desojo JB. 2010. Dermal armour histology of aerosaurs (Archosauria: Pseudosuchia), from the Upper Triassic of Argentina and Brazil. Lethaia 44:417–428.
Cerda IA, Desojo JB, Trotteyn MJ, Scheyer TM. 2015a. Osteoderm histology of *Proterochampsia* and Doswelliidae (Reptilia: Archosauriformes) and their evolutionary and paleobiological implications. J Morphol 276:385–402.
Cerda IA, Sterli J, Scheyer TM. 2015b. Bone shell microstructure of *Condorchelys antiqua* Sterli, 2008, a stem turtle from the Jurassic of Patagonia. C R Palevol 15:133–146.
Chiari Y, Cahais V, Galtier N, Delsuc F. 2012. Phylogenomic analyses support the position of turtles as the sister group of birds and crocodiles (Archosauria). BMC Biol 10:65.
Clack JA, Klembara J. 2009. An articulated specimen of *Chroniosaurus dongusensis* and the morphology and relationships of the chroniosuchids. Spec Pap Palaeontol 81:15–42.
Clarac F, Souter T, Cornette R, Cubo J, Buffrénil V de. 2015. A quantitative assessment of bone area increase due to ornamentation in the Crocodylia. J Morphol 276:1183–1192.
Coldiron RW. 1974. Possible function of ornament in the labyrinthodont amphibians. Occasional papers of the Museum of Natural History, the University of Kansas, Lawrence, Kansas, Vol. 33. pp. 1–19.
Cubo J, Le Roy N, Martinez-Maza C, Montes L. 2012. Paleohistological estimation of bone growth rate in extinct archosaurs. Paleobiology 38:335–349.
Currey JD. 2002. Bones, Structure and Mechanics. Princeton and Oxford: Princeton University Press.
Dacke CG. 1979. Calcium Regulation in Sub-Mammalian Vertebrates. London: Academic Press.
Danilov IG, Vitek NS. 2013. Soft-shelled turtles (Trionychidae) from the Bissekty Formation (Late Cretaceous: late Turonian) of Uzbekistan: Shell-based taxa. Cretac Res 41:55–64.
Downs JP, Donoghue PCJ. 2009. Skeletal histology of *Bothriolepis canadensis* (Placodermi, Antiarchi) and evolution of the skeleton at the origin of jawed vertebrates. J Morphol 270: 1364–1380.
Eltink E, Langer MC. 2014. A new specimen of the temnospondyl *Australerpeton cosgriffi* from the Late Permian of Brazil (Rio Do Rasto Formation, Paraná Basin): Comparative anatomy and phylogenetic relationships. J Vertebr Paleontol 34:524–538.
Francillon-Vieillot H, Buffrénil V de , Castanet J, Géraudie J, Meunier FJ, Sire J-Y, Zylberberg L, Ricqlès A de. 1990. Microstructure and mineralization of vertebrate skeletal tissues. In: Carter JG, editor. Skeletal Biomineralization: Patterns, Processes and Evolutionary Trends, Vol. 1. New York: Van Nostrand Reinhold. pp 471–530.
Germain D, Laurin M. 2009. Evolution of ossification sequences in salamanders and urodele origins assessed through event-pairing and new methods. Evol Dev 11:170–190.
Giles S, Rücklin M, Donoghue PCJ. 2013. Histology of the "placoderm" dermal skeletons: Implications for the nature of the ancestral gnathostome. J Morphol 274:627–644.
Gradstein FM, Ogg JG, Schmitz M, Ogg G, editors. 2012. The Geologic Time Scale 2012. Amsterdam: Elsevier. 1176 p.
Guillon J-M, Guéry L, Hulin V, Girondot M. 2012. A large phylogeny of turtles (Testudines) using molecular data. Contrib Zool 81:147–158.
Holmes R. 1989. The skull and axial skeleton of the Lower Permian anthracosauroid amphibian *Archeria crassidisca* Cope. Palaeontographica 207:161–206.
Hugall AF, Foster R, Lee MSY. 2007. Calibration choice, rate smoothing, and the pattern of tetrapod diversification according to the long nuclear gene RAG-1. Syst Biol 56:543–563.
Janis, CM, Devlin, K, Warren, DE, Witzmann, F. 2012. Dermal bone in early tetrapods: A palaeophysiological hypothesis of adaptation for terrestrial acidosis. Proc Biol Sci 279:3035–3040.
Josse S, Moreau T, Laurin M. 2006. Stratigraphic tools for Mesquite. Version 1.0. Available at http://mesquiteproject.org/packages/stratigraphicTools/
Karaplis AC. 2008. Embryonic development of bone and regulation of intramembranous and endochondral bone formation. In: Belezikian JP, Raisz G, Martin TJ, editors. Principles of Bone Biology, Vol. 1. Amsterdam: Academic Press. pp 53–84.
Kolb C, Scheyer TM, Lister AM, Azorit C, de Vos J, Schlingemann MAJ, Rössner GE, Monaghan NT, Sánchez-Villagra MR. 2015. Growth in fossil and extant deer and implications for body size and life history evolution. BMC Evol Biol 15:19–34.
Krstic RV. 1985. General Histology of the Mammal. Berlin: Springer Verlag.
Kumar S, Hedges SB. 2011. TimeTree2: Species divergence times on the iPhone. Bioinformatics 27:2023–2024.
Lamm E-T. 2013. Preparation and sectioning of specimens. In: Padian K, Lamm ET, editors. Bone Histology of Fossil Tetrapods. Berkeley: University of California Press. pp 55–160.
Landmann L. 1986. Epidermis and dermis. In: Bereiter-Hann J, Matoltsy AG, Richards KS, editors. Biology of the Integument, Vol. 2 Vertebrates. Berlin: Springer-Verlag. pp 150–187.
Laurin M. 1998. The importance of global parsimony and historical bias in understanding tetrapod evolution. Part I. Systematics, middle ear evolution, and jaw suspension. Annales Des Sciences Naturelles, Zoologie, Paris, 13e Série 19:1–42.
Laurin M. 2000. Seymouriamorphs. In: Heatwole H, Carroll RL, editors. Amphibian Biology. Chipping Norton: Surrey Beatty & Sons. pp 1064–1080.
Laurin M. 2008. The splendid isolation of biological nomenclature. Zool Scripta 37:223–233.
Laurin M, Reisz RR. 1995. A reevaluation of early amniote phylogeny. Zool J Linn Soc 113:165–223.
Lee MSY. 2001. Molecules, morphology, and the monophyly of diapsid reptiles. Contrib Zool 70:1–18.
Lee MSY. 2013. Turtle origins: Insights from phylogenetic retrofitting and molecular scaffolds. J Evol Biol 26:2729–2738.
Lehmann J-P. 1966. Actinoptérygiens, Dipneustes, Crossoptérygiens. In: Piveteau J, editor. Traité de Paléontologie, tome IV, Vol. 3. Paris: Masson. pp 1–412.
Levrat-Calviac V. 1986. Etude comparée des ostéodermes de *Tarentola mauritanica* et de *T. neglecta* (Gekkonidae, Squamata). Arch Anat Microsc Morphol Expérim 75:29–43.

Lyson TR, Bever GS, Bhullar B-AS, Joyce WG, Gauthier JA. 2010. Transitional fossils and the origin of turtles. Biol Lett 6:830–833.

Lyson TR, Sperling EA, Heimberg AM, Gauthier JA, King BL, Peterson KJ. 2012. MicroRNAs support a turtle + lizard clade. Biol Lett 8:104–107.

Maddison WP, Maddison DR. 2014. Mesquite: A modular system for evolutionary analysis. Version 3. Available at http://mesquiteproject.org

Margerie E de, Cubo J, Castanet J. 2002. Bone typology and growth rate: Testing and quantifying 'Amprino's rule' in the mallard (*Anas platyrhynchos*). C R Biol 325:221–230.

Margerie E de, Robin J-P, Verrier D, Cubo J, Groscolas R. 2004. Assessing the relationship between bone microstructure and growth rate: A fluorescent labeling study in the king penguin chick (*Aptenodytes patagonicus*). J Exp Biol 207:869–879.

Marjanović D, Laurin M. 2013. The origin(s) of extant amphibians: A review with emphasis on the "lepospondyl hypothesis". Geodiversitas 35:207–272.

Meunier FJ. 1984. Spatial organization and mineralization of the basal plate of elasmoid scales in osteichthyans. Amer Zool 24:953–964.

Meunier FJ, Castanet J. 1982. Organisation des fibres de collagène de la plaque basale des écailles des téléostéens. Zool Scripta 11:141–153.

Miles RS. 1967. Observations on the ptyctodont fish *Rhamphodopsis* Watson. J Linn Soc (Zool) 47:99–120.

Morkovin BI. 2015. On the development of surface ornamentation of skull bones in the ontogeny of Early Triassic Benthosuchids (Amphibia, Temnospondyli). Paleontol J 49:57–69.

Moss ML. 1969. Comparative histology of dermal sclerifications in reptiles. Acta Anat 73:510–533.

Oakley TH, Cunningham CW. 2000. Independent contrasts succeed where ancestor reconstruction fails in a known bacteriophage phylogeny. Evolution 54:397–405.

Padian K. 2013. Why study the bone microstructure of fossil tetrapods? In: Padian K, Lamm E-T, editors. Bone Histology of Fossil Tetrapods. Berkeley: University of California Press. pp 1–11.

Pagel M. 1999. The maximum likelihood approach to reconstructing ancestral character states of discrete characters on phylogenies. Syst Biol 48:612–622.

Pawley K. 2006. The Postcranial Skeleton of Temnospondyls (Tetrapoda: Temnospondyli) [PhD]. Melbourne, Australia: La Trobe University. 442 p.

Ricqlès A de, Meunier FJ, Castanet J, Francillon-Vieillot H. 1991. Comparative microstructure of bone. In: Hall BK, editor. Bone, 3: Bone Matrix and Bone Specific Products. Boca Raton: CRC Press. pp 1–78.

Rieppel O, Reisz RR. 1999. The origin and early evolution of turtles. Annu Rev Ecol Syst 30:1–22.

Rinehart LF, Lucas SG. 2013. The functional morphology of dermal bone ornamentation in temnospondyl amphibians. In: Tanner LH, Spielmann JA, Lucas SG, editors. The Triassic System. New Mexico Museum of Natural History and Science, Bull. 61. pp 524–532.

Ruta M, Coates MI. 2007. Dates, nodes and character conflict: Addressing the lissamphibian origin problem. J Syst Palaeontol 5:69–122.

Scheyer TM, Sánchez-Villagra MR. 2007. Carapace bone histology in the giant pleurodiran turtle *Stupendemys geographicus*: Phylogeny and function. Acta Palaeontol Pol 52:137–154.

Scheyer TM, Anquetin J. 2008. Bone histology of the Middle Jurassic turtle shell remains from Kirtlington, Oxfordshire, England. Lethaia 41:85–96.

Scheyer TM, Sander MP, Joyce WG, Böhme W, Witzel U. 2007. A plywood structure in the shell of fossil and living soft-shelled turtles (Trionychidae) and its evolutionary implications. Org Divers E 7:136–144.

Scheyer TM, Mörs T, Einarsson E. 2012. First record of soft-shelled turtles (Cryptodira, Tryonychidae) from the Late Cretaceous of Europe. J Vert Paleontol 32:1027–1032.

Scheyer TM, Desojo JB, Cerda IA. 2014. Bone histology of phytosaur, aetosaur, and other archosauriform osteoderms (Eureptilia, Archosauromorpha). Anat Rec 297:240–260.

Schluter D, Price T, Mooers AØ, Ludwig D. 1997. Likelihood of ancestor states in adaptive radiation. Evolution 51:1699–1711.

Schoch RR. 2008. The Capitosauria (Amphibia): Characters, phylogeny, and stratigraphy. Palaeodiversity 1:189–226.

Schoch RR. 2013. The evolution of major temnospondyl clades: An inclusive phylogenetic analysis. J Syst Palaeontol 11:673–705.

Schoch RR, Milner AR. 2000. Stereospondyli. Handbuch der Paläoherpetologie, Teil 3B. München: Verlag Dr. Friedrich Pfeil. 203 p.

Schoch RR, Milner AR. 2014. Temnospondyli. In: Sues HD, editor. Handbook of Paleoherpetology, Part 3A2. München: Verlag Dr. Friedrich Pfeil.

Schoch RR, Sues H-D. 2015. A Middle Triassic stem-turtle and the evolution of the turtle body plan. Nature 523:584–587.

Schoch RR, Voigt S, Buchwitz M. 2010. A chroniosuchid from the Triassic of Kyrgyzstan and analysis of chroniosuchian relationships. Zool J Linn Soc 160:515–530.

Seidel, MR. 1979. The osteoderms of the American alligator and their functional significance. Herpetologica 35:375–380.

Sigurdsen T, Green DM. 2011. The origin of modern amphibians: A re-evaluation. Zool J Linn Soc 162:457–469.

Smith HF, Parker WH, Kotzé SH, Laurin M. 2013. Multiple independent appearances of the cecal appendix in mammalian evolution and an investigation of related ecological and anatomical factors. C R Palevol 12:339–354.

Sterli J, Pol D, Laurin M. 2013. Incorporating phylogenetic uncertainty on phylogeny-based paleontological dating and the timing of turtle diversification. Cladistics 29:233–246.

Swofford DL, Maddison WP. 1987. Reconstructing Ancestral character states under Wagner Parsimony. Math Biosci 87: 199–229.

Vallin G, Laurin M. 2004. Cranial morphology and affinities of *Microbrachis*, and a reappraisal of the phylogeny and lifestyle of the first amphibians. J Vert Paleontol 24:56–72.

Vickaryous MK, Hall BK. 2008. Development of the dermal skeleton in *Alligator mississippiensis* (Archosauria, Crocodylia) with comments on the homology of osteoderms. J Morph 269:398–422.

Vickaryous MK, Sire J-Y. 2009. The integumentary skeleton of tetrapods: Origin, evolution and development. J Anat 214: 441–464.

Wagenmakers E-J, Farrell S. 2004. AIC model selection using Akaike weights. Psychon Bull Rev 11:192–196.

Webster AJ, Purvis A. 2002. Testing the accuracy of methods for reconstructing ancestral states of continuous characters. Proc R Soc Lond B 269:143–149.

Witzmann F. 2009. Comparative histology of sculptured dermal bones in basal tetrapods, and the implications for the soft tissue dermis. Paleobiodiversity 2:233–270.

Witzmann F, Soler-Gijón R. 2010. The bone histology of osteoderms in temnospondyl amphibians and in the chroniosuchian *Bystrowiella*. Acta Zool 91:96–114.

Witzmann F, Scholz H, Müller J, Kardjilov N. 2010. Sculpture and vascularization of dermal bones, and the implications for the physiology of basal tetrapods. Zool J Linn Soc 160:302–340.

ABSTRACT

Pseudosuchia is the crocodylian lineage which split up with the dinosaurs since the Early-Triassic (around 250 million years ago). At first probably endothermic and terrestrial, pseudosuchians became secondarily ectothermic and some of them returned to a semi-aquatic lifestyle at the Triassic-Jurassic transition (200 Ma): the neosuchians (still present in current nature) and the teleosaurids (disappeared since the Cretaceous). Like some extinct vertebrate groups (« the stegocephalians »), the pseudosuchians possess a dermal bone ornamentation made of pits and grooves on the skull roof, the mandibles and the osteoderms but with theparticularity to be excavated by resorption. The study of both fossil and dry bones combining 3D-data monitoring and quantitative data-based phylogenetic comparative analyses evidenced that the semi-aquatic forms possess a more excavated bone ornamentation. Further, histological analyses based on living animal sampling have revealed that the ornamentation pits always house a vessel proliferation which may be involved in heat exchanges during emerged and semi-emerged periods as well as acidosis buffering during submerged periods (apnea). Concerning the biomechanical and thermal implications, the finite element analyses performed on 3D-modeled osteoderms have proved that the bone ornamentation does not modify the osteoderm heat conduction nor their mechanical resistance. Consequently, we assess that the functional role of bone ornamentation shall mainly concern physiological implications through the set-up of a blood vessel network on the bone periphery (heat transfers, blood acidosis buffering; as hypothesized by previous authors). Secondarily, bone ornamentation may also be involved in phosphor-calcic homeostasis based on the succession of pit resorption and secondary superficial bone deposit in response to the specimens. life-long changes (eggshedding, diets.).

KEY-WORDS

Pseudosuchians, Bone ornamentation, Dermal bones, Phylogenetic Comparative Analyses, Finite Element Analyses, Histology.

RÉSUMÉ

Les pseudosuchiens représentent l'ensemble de la lignée des crocodiliens qui s'est différentiée de celle des dinosaures à partir du Trias inférieur (il y en a environ 250 Ma). A l'origine probablement endothermes et terrestres, les pseudosuchiens sont par la suite devenus ectothermes et certains d'entre eux sont retournés vers un mode de vie semi-aquatique lors de la transition Trias-Jurassique (200 Ma): les néosuchiens (formes encore représentées dans le nature actuelle) et les téléosauridés (disparus depuis le Crétacé). À l'image de certains taxons fossiles comme les « stégocéphales », les pseudosuchiens présentent une ornementation composée de cupules et de sillons à la surface des os dermiques (toit crânien, mandibules et ostéodermes) qui a la particularité de se former par résorption osseuse au sein de ce groupe. L'étude d'os fossilisés et d'os sec par des techniques d'imagerie 3D combinées à des analyses phylogénétiques basées sur des caractères quantitatifs a montré que les formes amphibies présentent un développement accrue de l'ornementation. Par la suite, nos analyses histologiques à partir de prélèvements sur des crocodiliens vivants ont montré que ces cupules hébergent des bouquets vasculaires qui seraient possiblement impliqués dans les échanges de chaleurs en phase émergée et semi-émergée ainsi que dans le tampon, de l'acidité sanguine pendant les phases émergées (en apnée). Concernant les possible implications biomécaniques de l'ornementation, les analyses en éléments finis que nous avons effectuées à partir d'ostéodermes scannés en 3D ont montré que la présence d'ornementation n.avait pas d'influence ni sur la résistance mécanique des ostéodermes ni sur leur capacité à conduire la chaleur. Par conséquent, le rôle fonctionnel de l'ornementation serait strictement d'ordre physiologique en lien avec la mise en place d'un réseau sanguin péri-osseux qui faciliterait à la fois les transferts de chaleur entre l'organisme et l'environnement en phase d'exposition et le stockage du lactate dans les os dermiques en phase d'apnée. De plus, la mise en place de l'ornementation pourrait permettre le maintien de l'équilibre homéostatique phospho-calcique via la succession de résorption superficielle et de dépôt secondaires en périphérie des os dermiques suivant la trajectoire ontogénétique de chaque individu (phase de ponte, jeun prolongé...)

MOTS-CLÉS

Pseudosuchiens, Ornementation osseuse, Os dermiques, Analyses phylogénétiques, Analyses en éléments finis, Histologie.